PHARMACOKINETIC MODELING OF CNS DISPOSITION OF 5-HT_3 RECEPTOR ANTAGONIST WITH QUANTITATIVE ASSESSMENT OF THE ROLE OF P-GLYCOPROTEIN EFFLUX

By

MANTING CHIANG

A dissertation submitted to the

School of Graduate Studies

Rutgers, The State University of New Jersey

In partial fulfillment of the requirements

For the degree of

Doctor of Philosophy

Graduate Program in Pharmaceutical Sciences

Written under the direction of

Leonid Kagan

And approved by

_____

_____

_____

_____

New Brunswick, New Jersey

January, 2020

ABSTRACT OF THE DISSERTATION

Pharmacokinetic modeling of CNS disposition of 5HT3- receptor antagonist with quantitative assessment of the role of P-glycoprotein efflux

By MANTING CHIANG

Dissertation Director:

Leonid Kagan

Neuropathic pain is a chronic pain condition that affects 7-10% of the general population. The currently available treatments are often unable to provide sufficient pain relief for the patients or are prescribed at doses that produce toxic side effects. Emerging research highlights the potential for serotonin subtype receptor 3 (5-HT_3) antagonists, such as ondansetron, as novel treatment strategies for reducing pain symptoms. However, current clinical reports are conflicting on whether ondansetron truly reduces pain symptoms in patients. One of the driving hypotheses is that there is insufficient drug exposure at the site of action needed to produce sustainable and significant pain relief in patients.

The thesis focused on developing quantitative approaches to evaluate central nervous system (CNS) exposure of the 5-HT_3 antagonist, ondansetron. In the introductory Chapter 1, an overview of neuropathic pain, the serotonergic pathway in pain transmission, 5-HT_3 as a pharmacological target for neuropathic pain treatment, CNS physiology, and general pharmacokinetic (PK) knowledge is provided. In Chapter 2, a pharmacokinetic study was completed in wild-type and P-glycoprotein (Pgp) knock-out male and female rats to evaluate plasma and brain, spinal cord, and CSF concentrations after intravenous administration of ondansetron. The study provided quantitative assessment of the role of Pgp in limiting ondansetron exposure in various regions of the CNS, when comparing WT and Pgp KO rats. Slight differences were observed in ondansetron pharmacokinetics and CNS disposition between

male and female animals. A semi-physiological model was developed and successfully captured the data in all tissues for all experimental groups. Chapter 3 wild-type male and female rats were co-administered tariquidar, a specific Pgp inhibitor, with ondansetron. Plasma and CNS results were compared with the previously obtained results from Chapter 2. Our results showed that tariquidar administration at 7.5 mg/kg resulted in complete inhibition of Pgp efflux of ondansetron in brain and spinal cord. There was also an effect of tariquidar on plasma disposition for ondansetron, which may not be dependent on Pgp inhibition. A semi-physiological model successfully described the pharmacokinetics of ondansetron in animals receiving ondansetron and tariquidar, as well as the wild-type and knock-out animals simultaneously. Proposed modeling framework could serve as the base to further analysis of the potential use of Pgp inhibitors in enhancing delivery of $5HT_3$ receptor antagonists to the CNS. In Chapter 4, a population PK study is presented describing the plasma and cerebrospinal fluid (CSF) disposition of ondansetron in patients. Serial plasma and single CSF samples were collected from 14 patients, in addition to patient demographic information such as creatinine clearance and age. A two-compartmental PK model was built to describe plasma disposition with an additional CSF compartment, describing CSF disposition with a single K_P term. In Chapter 5, ondansetron pharmacokinetics was evaluated using a physiologically based pharmacokinetic model (PBPK) model, as well as an allometric model. A full-body PBPK model was constructed to simulate plasma, brain, and CSF profiles and quantify the impact of Pgp efflux of ondansetron on the BBB. An allometric model was constructed to scale ondansetron disposition across rat, cat, cynomolgus monkey, and human. Collectively, the modeling strategies emphasize the impact of Pgp efflux of ondansetron in CNS disposition, and the opportunity of inhibiting Pgp to explore the therapeutic efficacy of ondansetron for neuropathic pain treatment.

ACKNOWLEDGEMENT

I am extremely thankful to have been a part of the Department of Pharmaceutics at Rutgers University, for all of the wisdom I have gained and the friendships that I will never lose. I hope to first express my gratitude to my advisor Dr. Leonid Kagan for selecting my candidate profile out of the pool and inviting me to join his lab. During my PhD, he has provided tremendous opportunity to grow as a scientist and provided the valuable mentorship that I have needed to become a scientist I am proud to be. I am grateful to have had the opportunity to learn from him and have his scientific process and perspective instilled within my own growth as a scientist. The future fruits of my scientific career will be credited to the many hours he had invested in me during my time in his lab and office sipping espresso.

I would like to thank my committee members, Dr. Arash Hatefi and Dr. Bozena Michniak-Kohn for their continued support and guidance, as well as their scientific insight, comments, and critical review of my dissertation. I would also like to thank Dr. Simon Haroutounian for his continued support of my dissertation work as well as the opportunity to work on such exciting projects with clinical impact.

I want to particularly thank the veterinary staff that trained my technical skillset in animal surgery, animal sampling techniques, and animal handling. Dr. Gregory Voronin and Raymond Rosa have been continual sources of assistance and friendships and I am grateful to have worked with them.

My time in the Kagan Lab has been a continuous emphasis on the value and importance of teamwork and collaboration. I hope to thank and acknowledge past and present Kagan Lab members, Dr. Helene Chapy, Dr. Xiaowei Zang, Dr. Jongbong Lee, Dr. Hyunmoon Back, Dr. Luigi Brunetti, Dr. Katarzyna Kosicka, Andrew Wassef, Grace Chong, Sarah Oh, Tiffany Guo, Simone Girgis, Celine Park, Kiran Deshpande, Xizhe Gao, Yi-Hua Sheng, Si-Jia Yu, and Andrew Shen. I will never forget the warm memories and long days spent in Gordan Road together.

My time within the Department of Pharmaceutics could not have continued as smoothly without the significant support and assistance of the administrate team, Ms. Hui Pung, Fei Han, Sharana Taylor, and Marianne Shen. I also hoped to acknowledge the financial support the Department of Pharmaceutics Ernest Mario School of Pharmacy and Washington University Department of Anesthesiology provided, as well as the grant from the National Institute of Neurological Disorders and Stroke R01 grant (NS104500-01). I was also fortunate to receive the Pre-Doctoral Pharmaceutical Sciences Fellowship from the American Foundation for Pharmaceutical Education for 2017 and 2018, as well as the Achillion Pharmaceuticals Fellowship.

I have been extremely lucky to form lasting friendships while at Rutgers, without whom I my time as a PhD student would have been far bleaker. I would like to particularly thank Xiaowei Zang and her husband Xiang, Hyunmoon Back, Daiyi Back, Jongbong Lee, Uijin Jeong, Obeid Malekshah, Helene Chapy, Andriy Kuzmov, Jinghui Zhang, and Chenchang Liu. I am also thankful for the American Association for Pharmaceutical Sciences Student Chapter for allowing me to grow in my communication, leadership, and networking abilities.

Lastly, I would like to acknowledge my family members. To Maryam, who has carried me from the moment I first learned of what pharmacokinetic analysis was to now. I could not have lived this life without you. To Yuting, Liting, and Daphne, who have provided the continuous support and grounding that I have always needed, and never forgetting to remind me where my academic journey started from. And, to my mom and dad, who met during their own graduate years in the cold of Ohio State University and provided the constant fuel and inspiration to continue on. I am forever grateful for your unconditional love and support.

DEDICATION

To my family, my wife, and my younger unbelieving self

TABLE OF CONTENTS

LIST OF TABLES

LIST OF ILLUSTRATIONS

Chapter 1 Introduction

1.1 Neuropathic pain

Neuropathic pain is defined as pain caused by a lesion or disease-related change of the somatosensory system (1, 2). The painful sensations are understood to involve damage from the small fibers of peripheral nerves and of the spino-thalamocortical system of the CNS (3). Physical lesions may be due to site lesions at the nerves or spinal cord, and underlying disease states such as diabetic neuropathy and multiple sclerosis (3). Currently neuropathic pain is estimated to affect 7-10% of the general population (1, 4). Patients suffering from neuropathy often report symptoms that begin in the extremities such as numbness (pins and needles effect), oversensitivity to touch, stabbing and burning pains. Current treatments are often unable to manage the chronic symptoms patients experience, demonstrating the need for effective treatments.

1.1.1 Epidemiology

The assessment of populations affected by neuropathic pain has been challenging due to the limited availability of simple diagnostic criteria needed for large epidemiological efforts. The prevalence of neuropathic pain has largely relied on information from chronic pain populations, focused on specialized centers with specific pain conductions such as postherpetic neuralgia, diabetic polyneuropathy, postsurgery neuropathic pain, multiple sclerosis, spinal cord injury, stroke, and cancer (5-7). Recently, the development of simple questionnaires specific for neuropathic pain systems that focus on asking the incidence and intensity of pain (burning pain, electric shock, pain evoked by brushing), provided useful estimates for the prevalence of neuropathic pain in the global population.

Overall, 7-10% of the population is affected by chronic neuropathic pain, with the incidence rate varying from country to country (1, 4). In the USA and Canada the rates are consistent with the global estimate, while countries such as Japan (3.2%) and Libya (3.9%) may observe lower incidence rate as observed in Figure 1 (4). While the general incidence of neuropathic pain characteristics is 7-10%, the actual incidence rates of specific conditions may vary. For example, the incidence rate for patients affected by diabetic peripheral neuropathy is overall greater than that observed for general neuropathic pain. In Figure 1.1, the countries highlighted in red provide the estimate rate of the population affected by diabetic peripheral neuropathy and are on average 3-4 fold higher than neuropathic pain. United Arab Emirates (37.1%) and Lebanon (53.9%) are observed to have greater populations affected by diabetic peripheral neuropathy (4).

Indeed, diabetic peripheral neuropathy is seen as one of the most frequent types of neuropathic pain, with 60-70% of diabetics suffering from diabetic peripheral neuropathy (8). However, mononeuropathy of the upper/lower limb, as well as pain resulting from carpal tunnel syndrome have higher incidence rate than diabetic peripheral neuropathy (9). A third of cancer patients receiving chemotherapeutic treatment, following even a single dose, may develop neuropathic pain symptoms. A similar incidence rate is determined for HIV patients, where 1 in 3 HIV patients also suffer from neuropathic pain (9, 10). The incidence of neuropathic pain may also vary based on age and sex. In general, women are found to have a higher incidence of chronic neuropathic pain (8% vs. 5.6% in <49 years of age) (11). In higher ages this increases with 63% increased likelihood women may suffer from neuropathic pain, as compared to men, between the ages of 70-79 (9). Overall, based on a study evaluating the incidence rate between men and women from 1996-2002, women have a consistently and statistically significantly higher incidence rate compared than men (Figure 1.2) (9).

1.1.2 Symptoms

The neuropathic pain symptoms may occur throughout the body. The difference conditions of neuropathic pain may govern the topography of pain distribution. Oftentimes, the common distribution of neuropathic pain is understood as “glove and stocking” where symptoms often begin in the extremities such as the hands and feet. For example, the burning and numbing symptoms may be initiated in the extremities and move up the body. When assessing pain symptoms in patients, many have also reported pain felt in the lower back, lower limbs, neck and upper limbs (11). Indeed, some of the most common causes of chronic neuropathic pain are lumbar and cervical radiculopathies (11). Atypical facial pain and trigeminal neuralgia largely affect the face for a subset of patients (12). Phantom limb pain is a specific neuropathic pain conditions where a limb is amputated, but the patient experiences ongoing painful sensations (13). The underlying neural reorganization is attributed to spinal plasticity where the pain sensation in the spinal cord may be sensitized causing the painful sensations (13).

There is also a variety in the types of pain conditions a patient may experience. In an assessment of >12,000 patients suffering from chronic pain, covering both nociceptive and neuropathic pain types, 40% of patients experienced one or more of the following: burning, numbness and tingling (14). Postherpetic neuralgia is a burning pain of nerve fibers and skin, where the pain may subsist after rash, blisters, or shingles may recede (15). Cervical radiculopathies may be attributed to diseases of a root nerve or pinched nerve and can cause the numbing feelings. Trigeminal neuralgia is a common neuropathic pain symptom occurring in the face which is a rapid shooting electric shock with short onset that is often triggered from a nerve lesion (12). Additionally, patients already suffering from chronic back pain and radiculopathy were showing higher incidence of experience the nociceptive and neuropathic pain types (14).

1.1.3 Neurophysiological changes

The somatosensory system processes information related to the perception of touch, pressure, pain, temperature, position, movement and vibration (1). The source of neuropathic pain may be in the central or the peripheral nervous system. The effect of lesions or disease to the spinal cord and/or brain are attributed to central neuropathic pain, and changes to sensory fibers (A, Aδ, and C) are associated with peripheral neuropathic pain disorders (16, 17). Spinal cord injury, multiple sclerosis, demyelinating disease are examples of central neuropathy while diabetes mellitus and chemotherapy induced neuropathy are examples of peripheral neuropathy (17, 18). Figure 1.3 provides greater detail into the distinction of peripherally and centrally located pain states that translate to the distribution of pain.

At the neural level, neuropathic pain represents changes in normal signaling patterns. Sensory nerves with altered electrical properties translate to an imbalance between the excitatory and inhibitory signaling, whereby ascending and descending control systems become impaired. The combination of electrophysiological changes, in addition with anatomical and molecular alterations, lay the groundwork for persistent functional changes in excitatory and/or inhibitory pathways that overtime, will shift the sensory pathway to a state of hyperexcitability, leading to a chronic neuropathic pain state (1).

Fundamentally, the hyperexcitability associated with neuropathic pain is a product of changes in ion channel expression and function, second-order nociceptive neuronal function, and inhibitory inter-neuronal function (1). Sodium, calcium, and potassium ion channel alterations in neuropathy on the affected nerves and fibers effect multiple spinal and brain sensory signaling. When sodium channel expression and activity are increased, the sensory nerve at the spinal cord terminus demonstrate increased excitability, signal transduction, and neurotransmitter release (1, 19). Similarly, lesions to increased calcium channel function may lead to altered inputs into the spinal cord and enhance excitatory synaptic transmission into the nociceptive pathway (1). Second-order nociceptive neuron major functions convey sensory information to the brain, and

the function of these neurons may change when the surrounding afferent fibers demonstrate enhanced excitability (20, 21). For example, the persistent discharge of peripheral afferent fibers with release of excitatory amino acids and neuropeptide often lead to post-synaptic changes in second-order nociceptive neurons, and these second-order changes are largely attributed to sensitization common in physical allodynia (21, 22) Inhibitor interneurons play an important role in the transmission of pain signals. The dysfunction of inhibitory modulation contributes to the imbalance of descending inhibition and excitation, and in neuropathic pain excitation often dominates (1). An example is the noradrenergic inhibition, where under normal conditions, is active in managing pain modulation. However, under neuropathic pain conditions this pathway is attenuated and serotonin signaling is enhanced through the 5-HT_2 and 5-HT_3 serotonin receptors become dominant (1).

1.1.4 Available treatments and challenges

Neuropathic pain is widely understood as being one of the most difficult pain syndromes to treat and is associated with both increased drug prescriptions and visits to health care providers (23-25). Commonly prescribed therapeutics for pain treatment, such as paracetamol, NSAIDs, or even weak opioids (e.g., codeine) are often not effective (1). Based on meta-analyses of clinical studies evaluating effective therapeutic strategies, the first-line recommended medical interventions are pregabalin (GABA analogue), gabapentin (GABA inhibitor), duloxetine (serotonin-noradrenaline reuptake inhibitor) and amitriptyline (tricyclic antidepressant) as outlined in Table 1.1 (1, 26). These treatments have shown efficacy in both central and peripheral neuropathies. Second-line treatments are also available, although may not be as effective as first-line treatments. Lidocaine, offered as patches (5%) has been shown to be efficacy for focal peripheral postherpetic neuralgia although the gain is modest (27, 28). Capsaicin has also been formulated as a high-concentration patch (8%) and demonstrated sustained efficacy for postherpetic neuralgia and diabetic and non-diabetic painful neuropathies (29-31). An opioid-

agonist and SNRI, tramadol, has shown effective in peripheral neuropathic pain although efficacy is not as established in central neuropathic pain (26). Diabetic peripheral neuropathy has also shown improvement following repeated administration of botulinum toxin A, a potent neurotoxin used for muscle hyperactivity, as a third-line treatment option (32-34). Oxycodone and morphine have been shown to be mildly effective, as opioid agonists, although the issues associated with opioid-related issues overshadow the prescription of such drugs.

Overall, the recommendations that are provided relate to the general treatment of neuropathic pain. There is limited evidence of efficacy for therapeutics for specific conditions of neuropathy. Thus, the clinician and patient must work together to evaluate different treatment options, and combinations to identify any option that may be effective in managing the symptoms of the pain. Furthermore, the presentation of diseases, such as cancer or HIV, may alter the suggested dosing recommendations or therapeutic options a patient may take. The guideline for opioid use may not apply for cancer populations, and/or for patients experience acute pain.

1.2. Serotonergic pathway in pain transmission

1.2.1 Descending pathway under normal conditions

Nociceptive information is carried to the spinal cord by peripheral nerve fibers, where it is integrated, amplified, and modulated in the form of neurotransmitter release and synaptic transmission (1). The spinal cord represents the main site of signal integration, and ascending and descending pathways from various regions of the brain, that modulate spinal processing through excitation and inhibition activity, define the ultimate perception of pain (1). Peripheral afferent fibers may be myelinated or unmyelinated and carry the information into the deep laminae of the dorsal horn which may directly stimulate peripheral neurons or indirectly stimulate these neurons through excitatory or inhibitory interneurons (35, 36). These interactions may occur

through the terminals of the peripheral afferent fibers, peripheral neurons, as well as the terminals of other descending pathways (35-38).

The descending efferent pathways start from the amygdala and hypothalamus and project through the rostroventral medial medulla to the spinal cord (1, 39). Pain facilitating and suppression pathways project from the rostroventral medial medulla to the spinal cord acting as descending controls that modulate spinal processing of nociceptive information (1, 40, 41). The descending serotonergic pathway has been studied and shown to play an influential role in inhibitory control of pain processing at the spinal cord (40, 42, 43).

The inhibitory control the serotonergic pathway plays results from the release of serotonin neurotransmitter and the density and expression of the serotonin receptor types. In recent years, spinal release of serotonin was shown to play both an inhibitory and facilitatory (i.e., pro and antinociceptive) effect on pain transmission (42, 44). The complexity of the serotonergic pathway can be traced to the different classes of 5-HT subtype receptors (7 in total), as well as the localization of each specific receptor type that may inhibit or facilitate nociceptive information (42). As shown in Figure 1.4, the various 5-HT receptor subtypes may impact both descending inhibition and facilitation of nociceptive signaling. The inhibition or facilitation is shown to be coupled with the activity of other neurotransmitters. Co-localization of serotonergic neurons with neurotransmitters such as γ-hydroxy-butyric acid (GABA) and enkephalin (ENK) reveal 5-HT modulating nociceptive processing through the interaction with other classes of neuropeptides (41, 45-47).

1.2.2 Changes in pathway during neuropathy

Neuropathy disrupts the normal signaling between the central and peripheral nervous system, and such imbalances between the excitatory and inhibitory sensory signals may lead to changes in spinal cord dorsal horn neurons. Indeed, neuropathy has been associated with

electrophysiological and anatomical changes that can produce a gain or loss of function. A gain of excitation and facilitation of signaling may be observed as enhanced sensitivity to stimuli, while a loss of inhibition may be translated to a lack of sensitivity to certain stimuli (1). These changes may reveal underlying shifts in the descending and ascending pathways controlling the facilitation or inhibition nociceptive mechanisms.

Under normal conditions, the serotonergic pathway has shown both inhibitory and excitatory activity, however under neuropathic conditions the excitatory role has been shown to increase (48). The excitatory descending serotoninergic control has been linked to the activity of 5-HT_3 receptors (48-50). Furthermore, exposure to both acute and chronic noxious stimuli has been linked to accelerated turnover of 5-HT in the spinal cord (51, 52). This potent facilitatory effect is conducted through the dorsal horn 5-HT_3 receptors, and may originate from small afferent input linked to the activation of neurokinin-1 receptor-bearing neurons in the dorsal horn that project to the periaqueductal grey area (53). These neurons connect to the serotonergic projection in the RVM, whereby following high intensity afferent input stimulates the release of serotonin (54). The presence of 5-HT_3 receptors on the neurons and terminals in the dorsal horn, an area of nociceptive stimuli processing, emphasize the role of 5-HT_3 and spinal serotonin in enhancing nociceptive transmission and excitability. The continued excitation in the spinal cord and loss of inhibitory control in the descending serotonergic pathway may contribute to the persistence of neuropathic pain syndromes.

Table 1.1 Strong and weak recommendations for use, along with total daily dose and dose regimen based on evaluation of clinical reports **(26)**

	Total daily dose and dose regimen	Recommendations
Strong recommendations for use		
Gapabentin	1200–3600 mg, in three divided doses	First line
Gabapentin extended release or enacarbil	1200–3600 mg, in two divided doses	First line
Pregabalin	300–600 mg, in two divided doses	First line
Serotonin-noradrenaline reuptake inhibitors duloxetine or venlafaxine*	60–120 mg, once a day (duloxetine); 150–225 mg, once a day (venlafaxine extended release)	First line
Tricyclic antidepressants	25–150 mg, once a day or in two divided doses	First line†
Weak recommendations for use		
Capsaicin 8% patches	One to four patches to the painful area for 30-60 min every 3 months	Second line (peripheral neuropathic pain)‡
Lidocaine patches	One to three patches to the region of pain once a day for up to 12 h	Second line (peripheral neuropathic pain)
Tramadol	200–400 mg, in two (tramadol extended release) or three divided doses	Second line
Botulinum toxin A (subcutaneously)	50–200 units to the painful area every 3 months	Third line; specialist use (peripheral neuropathic pain)
Strong opioids	Individual titration	Third line§

‡Long-term safety following repeat dosing of high-concentration capsaicin patients has not been clearly established, particularly with degeneration of epidermal nerve fibers.

§Sustained release oxycodone and morphine are the highest studied opioids and long-term use may be associated with abuse, immunological changes, and cognitive impairment.

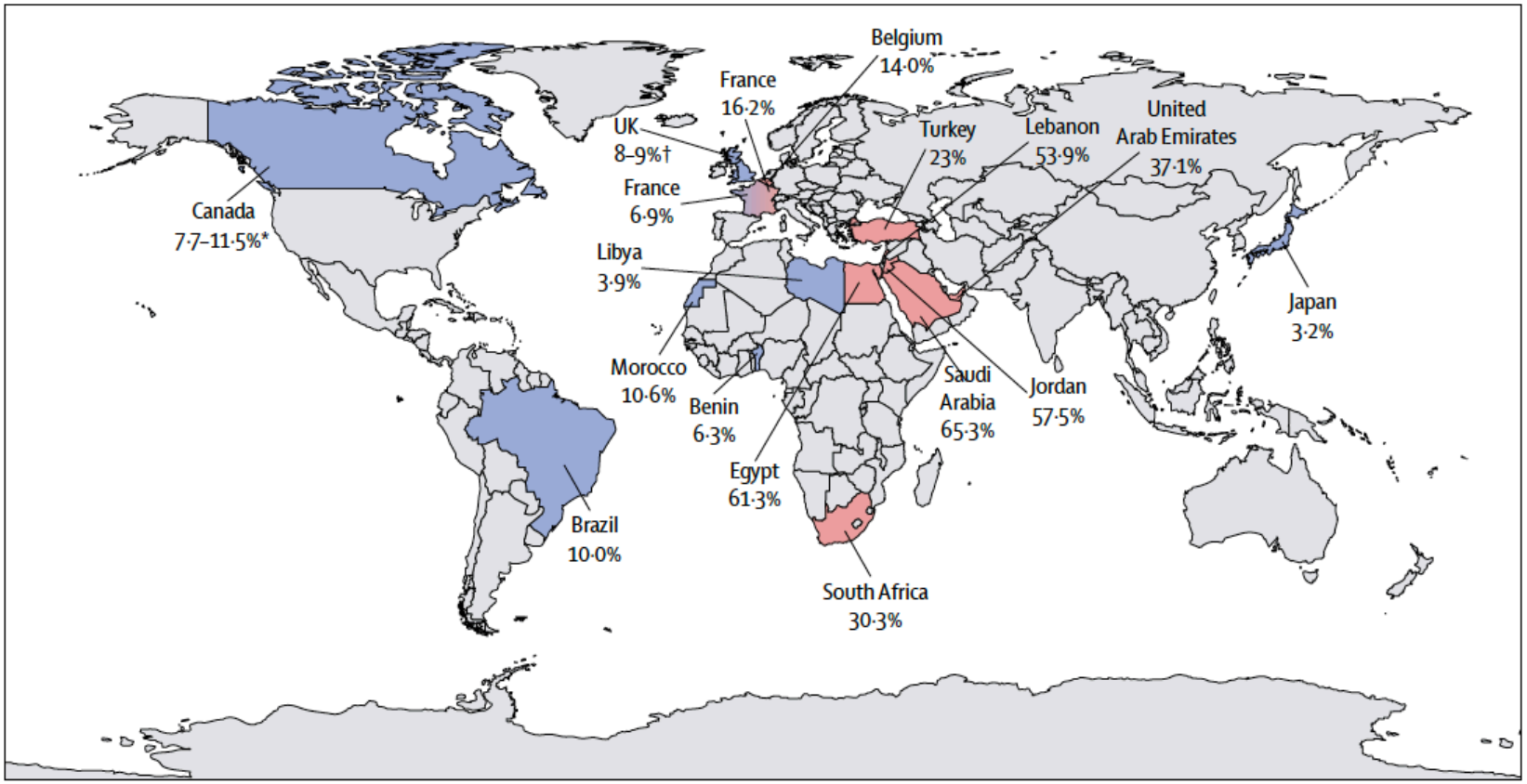

Figure 1.1 Prevalence of neuropathic pain characteristics in general population. General population prevalence estimates are shown in blue, and pink shows specifically diabetic neuropathy estimates. Estimates were based on distinct questionnaires administered to patients **(4).**

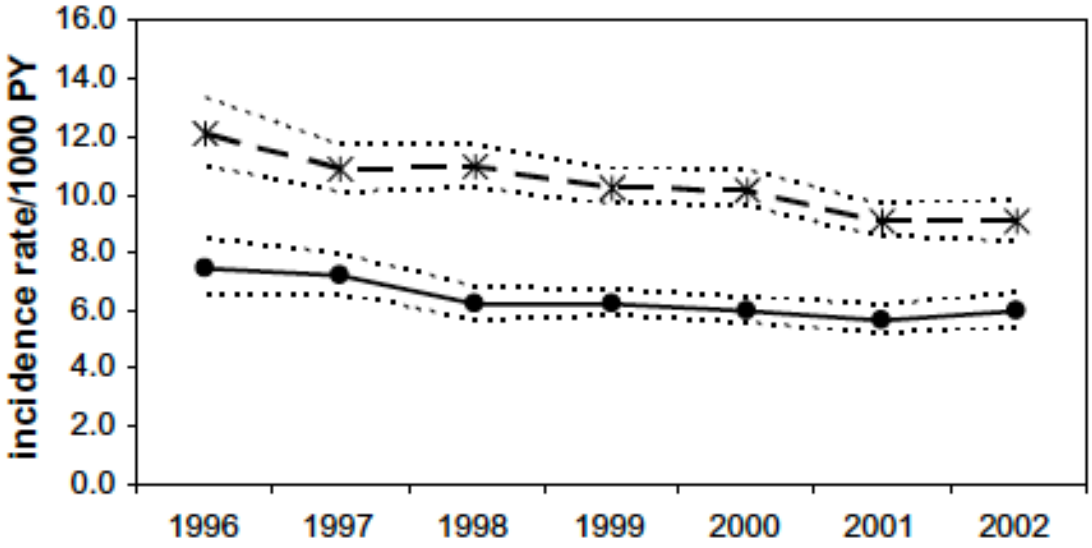

Figure 1.2 Specific incidence rates of neuropathic pain for men (solid line) and women (dotted line) with 95% confidence bands indicated in broken lines. Women demonstrate consistent trend of higher incidence rate per 1000 person years (PY) **(9)**.

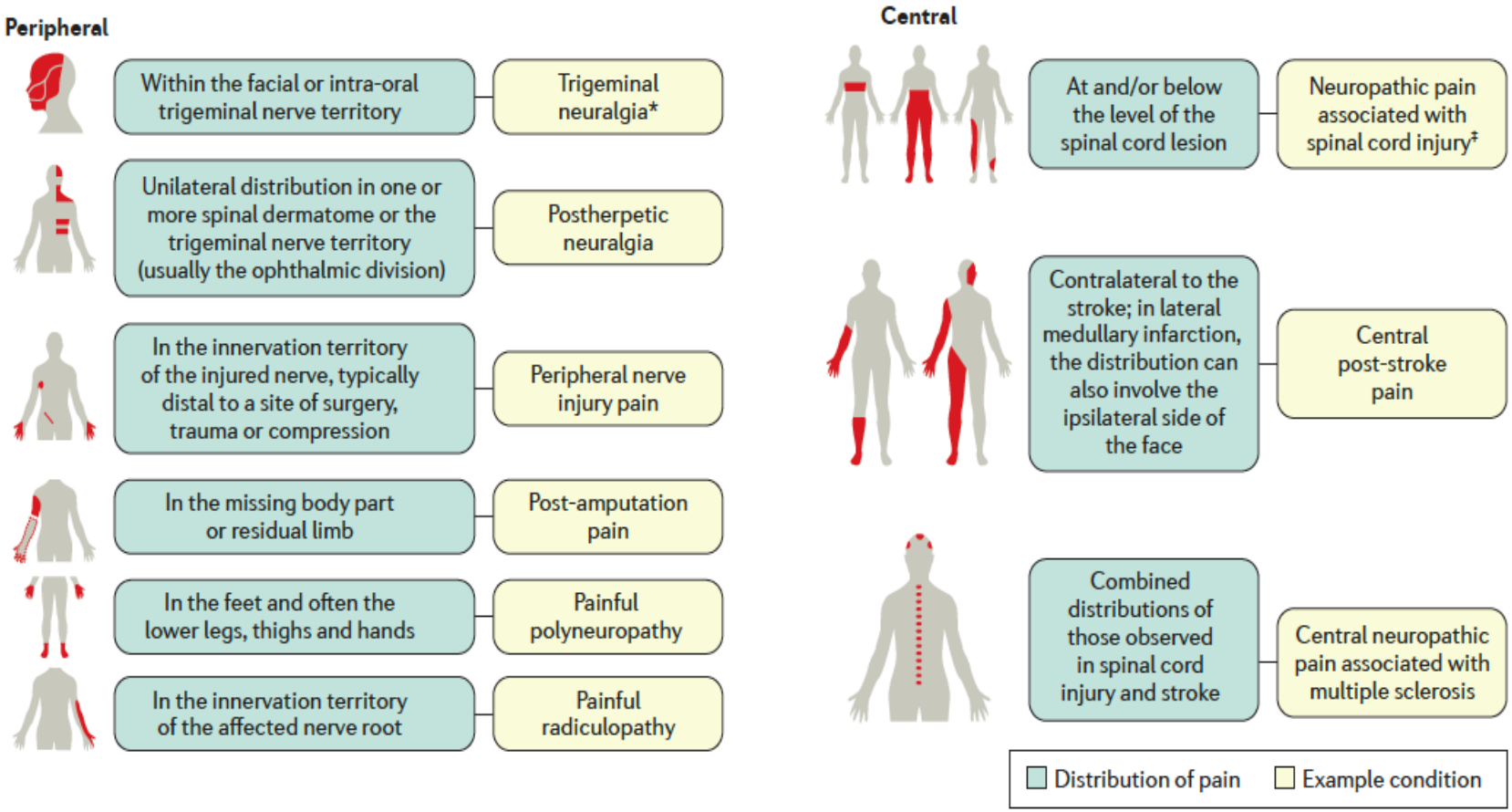

Figure 1.3 Common peripheral and central neuropathic pain conditions and their distribution of pain and sensory signs **(1)**.

*Sometimes associated with central neuropathic pain

‡Sometimes associated with peripheral neuropathic pain

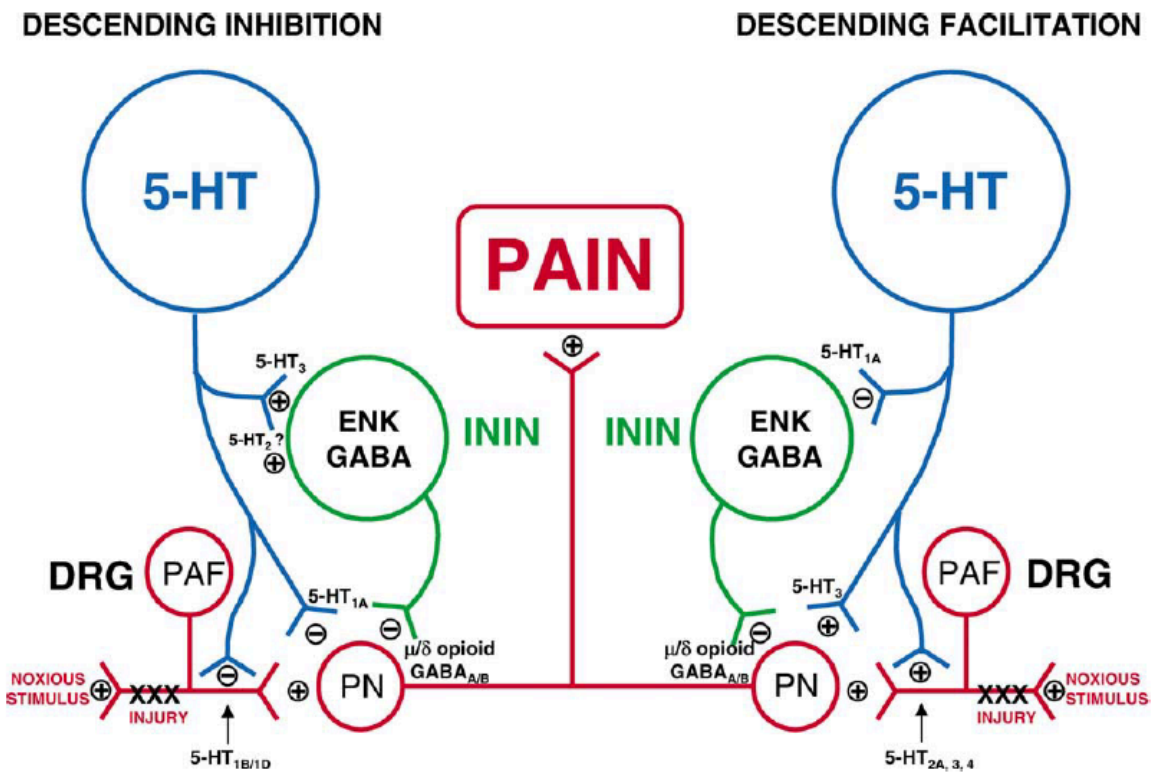

Figure 1.4 Descending inhibition (left) and facilitation (right) are shown through the activity of multiple classes of 5-HT receptors. $5HT_{1A}$, $5HT_{1B/1D}$ receptors are shown to suppress neuronal activity, while $5\text{-}HT_2$, $5\text{-}HT_3$, and $5\text{-}HT_4$ receptors were related to cellular excitability. The receptors are shown to interact with the primary afferent fibers (PAF) that project to the dorsal root ganglion (DRG), as well as the projection neurons (PN) and inhibitory interneurons (ININ) that contribute to nociceptive processing in the spinal cord (35, 42). The related classes of transmitters (enkephalin (ENK), γ-hydroxy-butyric acid (GABA), and μ/δ opioid receptors that contribute to the interaction with ININ are depicted to highlight the antinociceptive input through serotonergic targeting.

1.3 Ondansetron Pharmacokinetics (PK)

1.3.1 Pharmacology

Ondansetron is a highly selective and potent competitive antagonist to the serotonin receptor subtype 3 (5-HT_3R) (55). This receptor is a gated ion channel with selective permeability to sodium, potassium, and calcium ions which contribute to driving the depolarization processes. These receptors are known to be widely distributed across the human body with the highest density of receptors found in the central nervous system (55). In addition to the CNS, 5-HT_3 receptors are also known to exist in lower densities in the peripheral nervous system in the visceral, autonomic, and sensory nerves, such as the vagal nerve terminals (55, 56). The 5-HT_3 receptors have shown involvement in a variety of physiological and pathological processes (1, 42)

1.3.2 Indications approved

Ondansetron is primarily administered for preventing nausea and vomiting commonly associated with highly emetogenic chemotherapeutic regimens, such as cisplatin $\geq$ 50mg/m^2 (56). Following two randomized double-blind monotherapy trials, a 24 mg tablet demonstrated superior efficacy to placebo in preventing emesis associated with the cancer therapy. In the placebo group, 90% of patients receiving a cisplatin $\geq$ 50mg/m^2 dose experienced vomiting without antiemetic treatment. Ondansetron may also be administered following initial and repeated doses of moderately emetogenic cancer therapies to prevent the associated nausea and vomiting episodes (56). In line with previous results obtained from the highly emetogenic chemotherapeutic regimens, in a double-blind study following administration of cyclophosphamide-based chemotherapeutics (e.g., doxorubicin), ondansetron treatment of 8 mg twice a day significantly reduced emesis episodes compared to placebo over a three-day study period. Ondansetron may also be administered for patients receiving radiotherapy following total body irradiation, single high-dose fraction to the abdomen, or daily fractions to the abdomen (56). When evaluating

ondansetron efficacy in radiotherapy-related emesis, ondansetron was compared with metoclopramide in controlling emesis. In a double-blinded trial, patients receiving a single high-dose radiotherapy (800-1,000 cGy) over the anterior or posterior field size of $\geq$ 80cm^2 on the abdomen, patients receiving oral doses three times a day for three days displayed significantly reduced emetic episodes.

1.3.3 Absorption, distribution, metabolism, elimination (ADME)

Ondansetron has been extensively studied in preclinical species, such as rodents, as well as in humans to properly characterize its ADME properties. Ondansetron has been administered as oral tablets, intravenous formulations, and rectal suppositories. Largely the provided information will focus on oral formulations to highlight metabolic pathways as well as intravenous formulations to provide information on ondansetron disposition.

1.3.3.1 Human

The absorption profile of ondansetron following oral tablet shows ondansetron as being well absorbed from the gastrointestinal tract. On average, when ondansetron is administered to healthy subjects as 8mg tablet, the mean bioavailability was approximately 56%. The extent of absorption is considered to be mainly affected by the first-pass metabolism in the liver.

Ondansetron has been determined to be extensively metabolized in humans. Following a radio-labeled dose, only 5% of parent drug was recovered in urine (57). The metabolic elimination pathway for ondansetron has been well characterized showing the primary pathway has hydroxylation of the indole ring followed by subsequent glucuronide and sulfate conjugation as shown in Figure 1 (57).

The human cytochrome P-450 involved in ondansetron metabolism were characterized using in vitro studies as CYP1A1/2, CYP2D6, and CYP3A4 (57). The CYP3A4 isoform was determined to be the primary metabolic pathway for ondansetron, and due to the various

pathways present for ondansetron metabolism it is predicted that any functional loss of one pathway (i.e., genetic polymorphisms) would allow for compensatory mechanisms to demonstrate little change in the eliminating rates of ondansetron. Furthermore, it has been reported that CYP1A1/2 plays the most important role, with CYP2D6 playing a minor role, and CYP3A enzymes relevant at higher concentrations of ondansetron (58).

Ondansetron has also been shown to have a relatively large volume of distribution (~160 L) with a mean distribution volume of 1.9 L/kg, demonstrating that ondansetron is well distributed into tissues outside of the plasma volume (59). Furthermore, ondansetron distributes into erythrocytes with a blood to plasma ratio of 0.83 (57, 59, 60).

The main elimination pathway of ondansetron is via rapid hepatic metabolism. A study evaluating an intravenous, oral, and rectal formulation of ondansetron demonstrated that the half-life following a 24 mg dose was 6.2-6.5 hours for each formulation (61). The calculated elimination rate constant was similarly 0.115-0.118 h^{-1} for the three formulations. Similar results were obtained in a previous report by Hsyu et al., where healthy subjects were administered an 8 mg dose of ondansetron intravenously, orally, to the colon and to the rectum (62). The reported half-life (h) across each formulation was in the range of 4.9-6.9 hours. In this report, the mean residence time (MRT) of ondansetron was also reported at 5.8 h for the intravenous formulation, 6.8 h following oral administration, and 8.8-9.9 h for the rectal and colon administration respectively. Taken altogether, following a single dose of ondansetron, following 48 hours ondansetron will be nearly completely eliminated from the plasma.

1.3.3.2 Rat

Ondansetron pharmacokinetic properties have been evaluated in various preclinical species which has provided the opportunity to scale preclinical research to humans. In Sprague-Dawley rats, ondansetron was intravenously and orally administered in doses from 1 to 20 mg/kg

and determined to have dose-independent pharmacokinetics (63). The extent of absorption following oral doses of ondansetron from 4 to 20 mg/kg was similar to humans, with an absolute bioavailability ranging 40-63% (63).

When ondansetron was orally administered to rats, first-pass metabolism was also observed to play a significant role in eliminating ondansetron. Following absorption from rat gastrointestinal tract, hepatic metabolism was rapid and extensive, metabolizing 94% of the orally administered 8 mg/kg dose (63). Yang et al., also conducted *in vitro* experiments evaluating first-pass effects in the intestine by co-incubating ondansetron with small intestine homogenates and found approximately 18.5% of spike drugs disappeared following a 30 min incubation (63). The possibility of gastric metabolism was also explored, where ondansetron was administered as intragastric and intraduodenal administration and found AUC values to be comparable suggesting gastric metabolism to be negligible in rats. Gastric homogenate studies were conducted to further confirm this finding. The hepatic extraction ratio of ondansetron was also observed, where the AUC following intraportal and intravenous administration of ondansetron was compared. An approximately 64.8% decrease was observed in AUC in intraportal administration compared to intravenous administration, suggesting an extraction ratio of 0.648 (63). These results support the notion that ondansetron is subject to significant hepatic first pass effects. Biliary excretion was also explored for ondansetron elimination, and following 24 h evaluation the cumulative mean value was 0.125% of the dose was identified following intravenous dose, demonstrating the negligible role of the biliary route (63).

The steady-state volume of distribution (V_{ss}) was calculated for 1, 4, 8, and 20 mg/kg following intravenous administration. The values ranged from 496 mL/kg for 1mg/kg, 832 mL/kg for 4mg/kg, 636 mL/kg for 8mg/kg, and 900 mL/kg for the highest dose level of 20mg/kg (63). The estimated plasma volume for male Sprague-Dawley rats is approximately 41.2 mL/kg, supporting the notion that ondansetron is widely distributed in the body (64). Plasma to blood cell partitioning

was also identified (ratios of 1.74-5.31) suggesting that rat blood cell binding does not play a considerable role on distribution kinetics of ondansetron between plasma and blood (63).

1.3.4 Central nervous system penetration of ondansetron

Although the plasma pharmacokinetics of ondansetron is well studied across multiple species, the CNS penetration of ondansetron is not well understood. While direct sampling of CNS tissue is rarely possible in humans, the CSF provides a useful surrogate that can both illuminate exposure in the CNS as well as allow for single or serial measurements. In humans, a single report was published in healthy volunteers comparing plasma and CSF concentrations. Six volunteers were provided five tablet doses of 16 mg taken twice a day two days prior to surgery as well as the day of. Each patient provided a single CSF and blood sample taken at the same time. All of the samples were taken from 1.3-7.7 hours after the last ondansetron dose. The CSF concentrations ranged from 2.6-15.4 ng/mL, with a relatively poor correlation to plasma concentrations ($r = 0.89$, $p = 0.017$) (65).

Overall, the ondansetron exposure in the CSF was approximately 15% of what is seen in the plasma. When considering that ondansetron is approximately 70-76% protein bound, a maximum of 25% of drug is left unbound in plasma for transfer into the CSF (65). Each patient was dosed to approximately steady-state conditions, thereby at the equilibrium dosing with only 15% of the plasma observed in the CSF the extent of penetration is considered to be relatively low.

In 2014, a group also published CSF profile for ondansetron in nonhuman primates to evaluate the utility of CSF as a surrogate for unbound brain concentrations (66). Ondansetron was infused to steady state into the cephalic vein at 0.40 mg/h/kg into eight male cynomolgus monkeys with four blood and CSF samples collected hourly over a 4 hours period. The unbound plasma concentrations on average was 216.8 ng/mL and an average CSF concentration of 99.2 ng/mL. A ratio of CSF concentrations to unbound plasma concentrations was calculated and

reported as $K_{p,uu,CSF}$ and was 0.481±0.109 (mean ± SD) (66). This value was found to be significantly lower than unity ($p<0.05$) demonstrating the significant impact of efflux mechanisms in the CNS limiting CNS penetration of ondansetron (66).

1.3.5 P-glycoprotein transport

Ondansetron has been studied for its interaction with various transporters in the body (Table 1). In 1996, Schinkel et al. published a report detailing the significant impact of a plasma membrane protein that confers drug resistance for its ability to transport drugs out of tumor cells. This multidrug resistance protein (MDR1), also known as P-glycoprotein, was evaluated to transfer a wide variety of compounds with diverse structures and physicochemical proteins. The common features of substrates of Pgp were identified as relatively hydrophobic and amphipathic in nature (67-70). Anticancer agents (e.g., anthracyclines, taxanes), immunosuppressive drugs (cyclosporin A), cardiac drugs (e.g., digoxin), anthelmintic agents (ivermectin) and steroids (hydrocortisone, dexamethasone) were shown as substrates to Pgp (71).

Pgp expression is predominantly in the apical (luminal) membranes of intestinal epithelial cells, bile canalicular membranes, and endothelial cells of cerebral blood capillaries in the brain (71). Previous studies have utilized Pgp knock-out mice to evaluate the tissue specific influence of Pgp on tissue concentrations with the most significant effects observed in the brain (72, 73). The significance of Pgp at the blood-brain barrier is likely due to the density of Pgp at the endothelial cells coupled with the tight-junctions and structure of the brain endothelial cells limiting penetration of particles into the CNS.

The impact of Pgp on ondansetron transport was evaluated using MDR1 (human) transfected pig-kidney epithelial cell line monolayer (LLC-PK1). When comparing amount/percentage ondansetron transported using human MDR1 transfected cell line of apical to basal (A-B) and basal to apical (B-A) over the course of 4 hours, the B-A translocation

demonstrated 16-30% more of ondansetron transport (71). Pgp knock-out mice were also used to evaluate tissue levels of radioactivity of ondansetron, where at 0.2 mg/kg of [^{14}C]ondansetron was administered intravenously and brain levels showed a 4 fold increase in ondansetron exposure (71). These findings are consistent with the notion that Pgp may play a crucial role in affecting CNS penetration and exposure of centrally acting drugs.

1.3.6 Sex differences

The ADME characteristics of a drug may show different PK profiles between male and females due to the differences in the underlying physiology of each sex. Differences in pharmacokinetics due to sex have been shown for ondansetron in both humans and rats following single doses of ondansetron. In both species, females have been observed to have increased exposure following administration of the same dose (74, 75).

When ondansetron was administered as a single oral dose, both the extent and rate of absorption for ondansetron were greater in women than men. The higher absolute bioavailability of ondansetron in woman was also linked to higher plasma concentration levels of ondansetron (56). The greater absolute bioavailability in women was independent of age; at young ages it was 48% and 66%, and at older ages 62% and 75%, for men and women respectively (75). In a study evaluating oral tablet formulations of 8 mg comparing between women and men, a CL/F of 22.7 $\pm$ 0.75 L/hr was determined for women and a significantly higher value (*p-value* < 0.05) was determined in the tablet formulation administered to men at 60.0 $\pm$ 12.7 L/hr (76). The terminal volume V_z/F was also significantly smaller for women, found at 2.58 L/kg compared to men of 3.67 $\pm$ 3.21 L/kg (*p-value* < 0.05) (76). The overall plasma exposure was significantly greater in women than men with an AUC_{inf} of 393.3 $\pm$ 54.7 ng·hr/mL compared to that in men of 167.9 $\pm$ 25.7 (*p-value*< 0.05) (76). The pharmacokinetic differences in the plasma disposition between men and women have largely been attributed to differences in first pass metabolism, which may

then be reflected in the higher absolute bioavailability, reduced clearance and smaller apparently volume of distribution in women compared to men (59, 76).

The trends observed in the clinical evaluation between male and female were also observed in preclinical pharmacokinetic studies in rats. In Sprague-Dawley rats the AUC was 22.6% smaller in males compared to females after intravenous administration of 8 mg/kg of ondansetron (74). Similarly, when rodents were administered 8 mg/kg orally, the male rats also had a 58.8% smaller plasma exposure (AUC) compared to females (74). Yang et al., further investigated any differences in first-pass effect differences between male and female by using hepatic microsomes from each sex and evaluating the intrinsic hepatic clearance (CL_{int}) and total protein levels. Females were found to have a lower CL_{int} of 0.0796 compared to 0.0945 μL/min/mg protein in males and lower total protein levels of 88.9 mg/whole liver in females compared to 127 mg/whole liver for males (74). Overall, male had a 19% higher CL_{int} value compared to females, as well as 42.9% higher protein levels compared to females. A difference in intestinal metabolism between males and females was also shown, where male CL_{int} in the intestine was 17.4% higher than females and males also had 18% greater total protein levels, although these differences were not found to be statistically significant (74).

1.3.7 Clinical examples of ondansetron for neuropathic pain treatment

The pharmacological activity of 5-HT_3R antagonists has been linked to anti-inflammatory, anesthetic, and analgesic effects that may play a role in diminishing pain symptoms (77). The antinociceptive effects of ondansetron may result from central and peripheral activity. It has been demonstrated that 5-HT_3 receptors are present in the central spinal terminal and peripheral afferent fibers (78). The pharmacological efficacy of ondansetron for pain treatment has been linked not only to its activity antagonizing 5-HT_3 receptors but also its ability to block sodium channels in neurons which may produce local anesthetic effects (77, 79). Based on previous efforts, ondansetron administration has been used for two types of pain treatment strategies. The

first is a pre-emptive strategy for acute pain associated with intravenous propofol injection, or surgery related pain (80, 81). The second is for chronic pain, mainly for the treatment of neuropathic pain. In both instances, clinical reports have shown inconclusive results regarding the efficacy of ondansetron for pain treatment.

Ondansetron use in acute pain treatment has been evaluated in a series of clinical studies. In a randomized controlled double-blinded study of 80 subjects, intravenous pretreatment with 4 mg ondansetron was shown to significantly reduce the incidence of pain following propofol injection compared to a saline control (25 vs. 55%, $p < 0.05$) (81). Similarly, a randomized double-blinded study in 60 subjects evaluating pain relief from 4 mg of ondansetron treatment following injection pain from rocuronium and propofol found that ondansetron was effective in reducing pain compared to saline treated placebo ($p < 0.001$) (82). In the same study, a separate group of subjects were treated with lidocaine for pain relief, and when compared with the ondansetron group, lidocaine was identified as significantly more effective in providing pain relief (*p-value < 0.02)* (82). Another study also determined that ondansetron was not as effective in providing pain relief to patients with acute ureteral colic when compared to diclofenac, a non-steroidal anti-inflammatory therapeutic. In a double-blind controlled trial, 64 patients were treated with IV 8 mg ondansetron or 75 mg diclofenac sodium. Although ondansetron demonstrated pain relief as a primary medication in 42.4% of patients (14/33), 19 patients required further pain medication compared to 77.4% of patients who responded with pain relief to diclofenac (24/31) and only 7 patients required additional pain medication (83). Ondansetron demonstrates strong potential for treating acute pain, although conflicting clinical reports may demonstrate that ondansetron efficacy is contingent on disease state and the utility of other pain relief agents.

Neuropathic pain is a chronic pain condition where ondansetron treatment has shown potential for improving management of pain symptoms. A study recruited 26 patients with chronic neuropathic pain who were all unresponsive to the available treatments: opioid analgesics,

nonsteroidal anti-inflammatory drugs, tricyclic antidepressants, and anticonvulsants. Patients were administered a single IV injection of 8 mg ondansetron where baseline and post-treatment pain scores were recorded at 2 hour intervals and compared with placebo (84). The investigators used an 11-point Likert scale to evaluate 5 types of pain associated with neuropathy: burning pain, shooting/lancinating pain, numbness, paresthesia, allodynia. The overall pain scores for patients receiving ondansetron was found to not only change from baseline (-1.17 [95%CI $\pm$ 0.89]) but also significantly improve from those receiving placebo (-1.09 [98% CI $\pm$ 0.79]) *(p* < 0.02) (84). The greatest improvement in pain relief was identified during the first 6 hours, with a maximum effect at 2 hour (84).

A similar study was conducted to confirm previous results however, the investigators found that ondansetron was not an effective therapy to treat peripheral neuropathy. In a randomized double-blind and placebo-controlled study, 15 patients receive an IV infusion of 8 mg ondansetron and used a computerized visual analog scale (VAS) to continuously record patient's intensity and duration of pain (85). Their pain evaluation was focused on dynamic mechanical allodynia, where light strokes of the skin produced sharp pain sensations, and spontaneous ongoing pain associated with peripheral neuropathy. Patients taking strong opioids for treatment were excluded, although the other patients were permitted to continue taking prescribed stable doses of anti-epileptics, antidepressants, tramadol. Overall, the investigators did not identify any improvement in pain for dynamic mechanical allodynia or ongoing pain intensity when treated with 8 mg of ondansetron. The authors indicated that these results may contradict previous reports that over-expression of spinal $5HT_3$ receptors may play a role in dynamic mechanical allodynia (85).

Although conflicting reports are presented for ondansetron efficacy, especially in the neuropathic pain area, the positive reports demonstrate ondansetron treatment may support further investigations to understand with more clarity the role of $5HT_3$ receptors in neuropathic

pain. One of the potential explanations for the conflicting published reports may be related to a PK problem, where the ondansetron exposure at the site of action is insufficient to provide a consistent and clear effect in reducing pain. Increasing the exposure of ondansetron in the CNS, particularly in the spinal tissue, may allow for effective treatment of neuropathic pain symptoms.

1.3.8 Preclinical examples of ondansetron for neuropathic pain

Preclinical animal models provide the unique opportunity to explore the mechanistic basis of ondansetron efficacy in pain treatment, with an emphasis on exploring the underlying neurophysiology. Furthermore, using alternative routes of administration, such as intrathecal injection where drug is administered directly to the spinal cord, a direct link can be made regarding drug exposure and changes in pain response.

Various models have been established to induce neuropathic pain symptoms in rodents and ultimately explore the mechanisms by which serotonergic pathways may be manipulated to produce pain relief. The induction of neuropathic pain symptoms in animals is measured through the changes in nociceptive thresholds by mechanical and/or thermal stimuli. Formalin (50 μL) injection in the paw of a rodent may induce flinching, and the changes in the nociceptive flinching behavior may be recorded to confirm the development of neuropathic pain. In one study, male Sprague-Dawley rats (300-350 g) were subject to formalin-induced flinching and a lumbar intrathecal catheter was used to infuse a total amount of ondansetron at 1 and 3 μg (50). The investigators identified a 30-40% reduction in formalin flinching following ondansetron administration at both doses compared to saline group (p <0.05), demonstrating a significant reduction in pain behavior (50).

A spinal cord injury (SCI) model has also been developed, whereby lesions to the thoracic vertebrae are made and a modified aneurysm clip applied onto the spinal cord, generating a specific force (35 g) for moderate to incomplete SCI (86, 87). This model has demonstrated clinical

relevance in the development of at-level mechanical allodynia and has been used to evaluate intrathecal injections of ondansetron for pain treatment (87, 88). In one report, investigators applied the SCI model to 28 male Wistar rats (220-350g) and administered intrathecal bolus doses of a total ondansetron amount at 1, 10 and 20 μg, where mechanical allodynia was then assessed up to an hour post dose. The investigators found that animals receiving intrathecal injections of ondansetron, across all dose levels, responded with increased pain relief compared to the saline control, and the investigators also observed a dose related response, where increasing doses of ondansetron provided increasing pain relief (87). A similar finding was also observed in another study where 47 male Wistar rats (250-300g) underwent the SCI surgical procedure and were infused with ondansetron intrathecally (2.0 μg/h) for 3 days. At-level mechanical allodynia, neuropathic pain occurring at a sensory transitional zone, was diminished by 40%, and below-level, pain occurring at sites below injury, allodynia by 60% when ondansetron treated animals were compared with the saline treated controls (88). The improvement in pain relief was even sustained for one day following the cessation of drug administration (p-value < 0.05) (88).

Table 1.2 Literature review of ondansetron interaction with various transporters, in both human and mice.

Transporter	Experimental system	Species	Main finding	Citation
P-glycoprotein	LLC-PK1 cells	Human	Ondansetron substrate of Pgp efflux in humans	(71)
		Mouse	Ondansetron is subject to Pgp efflux in mice	(71)
OCT1	HEK293 cells	Human	Ondansetron inhibits OCT1 (IC_{50} = 63.9 μM)	(89)
OCT2	HEK293 cells	Human	Ondansetron inhibits with potency of *Ki* = 3.75 μM	(90)
	HEK293 cells	Mouse	μ Ondansetron inhibits OCT2 with potency of *Ki* = 3.5 μM	(90)
MATE1	HEK-293 cells	Human	Ondansetron inhibits with potency of *Ki* = 0.037 μM	(90)
	HEK-293 cells	Mouse	Ondansetron inhibits OCT2 with potency of *Ki* = 0.07 μM	(90)
MATE-2k	HEK293 cells	Human	Ondansetron inhibits with potency of *Ki* = 0.015 μM	(90)

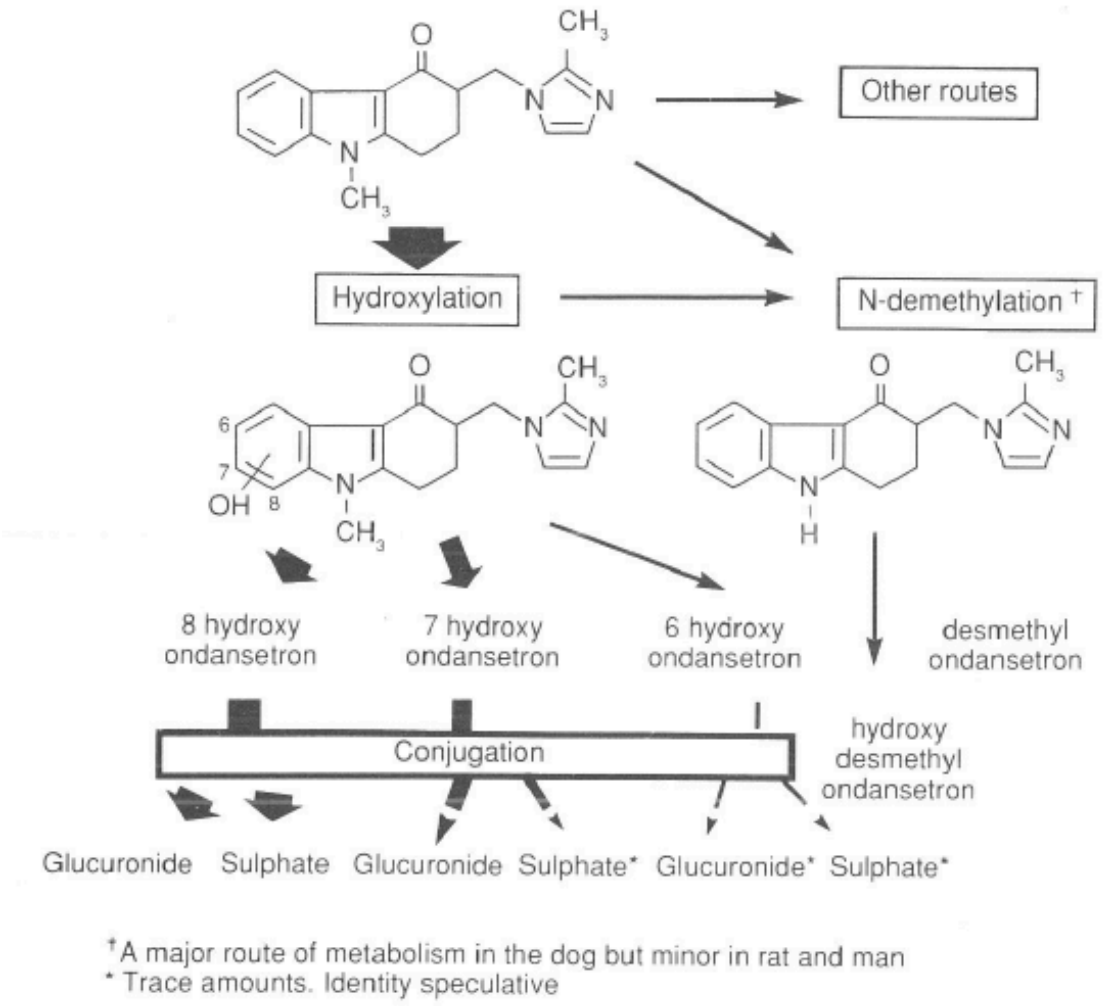

Figure 1.5 Ondansetron metabolism mainly occurs through hydroxylation pathways, with conjugation occurring for select Phase I metabolites (91). The size (width) of the arrows demonstrate the likelihood of metabolism

1.4 CNS Physiology

Drug development to treat diseases affecting the central nervous system still represents a great challenge in the field. The physiology of the CNS provides serious hurdles for drug delivery, as well as for establishing quantitative drug exposure and efficacy relationships (because the sampling from that space is difficult). Understanding factors that govern the rate and extent of drug penetration into the CNS are needed for development of mechanistic models to describe pharmacokinetics and pharmacodynamics in the CNS.

1.4.1 Brain and spinal cord gross anatomy

The central nervous system comprises the brain and the spinal cord. The brain is divided into the cerebrum, containing the left and right hemispheres, the cerebellum, sitting below the cerebrum and the brainstem which connects the cerebrum and cerebellum to the spinal cord (92). Within the brain there are four inter-connected hollow fluid-filled spaces, also known as ventricles, that are linked to cerebrospinal fluid production and distribution (92). The brain is suspended within the skull by a series of membranes that contain spaces for CSF fluid flow as well as blood vessels which support the exchange between blood and CSF (92, 93). Covering the outer cortex of the brain is the pia mater, followed by the arachnoid mater, which is then connected to the dura mater layer located below the skull (94). As drug penetrates through the blood-brain barrier, it travels through the extracellular fluid (ECF) where it may be subject to metabolism, binding to CNS components such as protein or extracellular targets (95-97). Brain ECF concentrations are often considered to rapidly equilibrate with plasma concentrations (98). Bulk flow movement of drug from Brain ECF to CSF has also been demonstrated based on the influence of the distributive forces in the brain (99, 100).

The spinal cord physiology has some key similarities to the brain. Structurally, the spinal cord also is surrounded by the same series of membranes that allow the spinal cord to be anchored within the spinal column. The spinal column is made up of a series of bones, called vertebrae, that protect the spinal cord within it. The spinal column is divided into four main

sections, the cervical (C1-C7 vertebrae), thoracic (T1-T12 vertebrae), lumbar (L1-L5 vertebrae), and sacral sections (S1-S5) as shown in Figure 2 (101). The cervical is considered the “upper” spinal cord section and the “lumbar” the lower sections (101). On either side of the cord, the anterior lateral and posterior lateral fissures are where the ventral and dorsal rootlets exit to form the spinal nerves (101). In a full-grown adult, the spinal cord extends from the cervical region down to L-1/2 vertebrae in the lumbar regions (102). The subarachnoid space within the spinal column extends downward toward the sacrum sections, thus allowing for CSF samples to be taken in the lumbar regions (L3-L5 vertebrae) without damaging the spinal cord itself (102, 103). Few reported studies are published focusing on drug distribution in the spinal cord (104, 105). However, the spinal cord region serves as a critical resource to collect CSF samples, particularly in humans, to reflect the PK of the CNS. Additionally, drug administration via the spinal space (epidural, intrathecal drug administration) are common routes applied in the clinic to improve CNS drug penetration.

1.4.2 Blood brain barrier (BBB)

Therapeutics with target sites in the CNS rely on the extensive vasculature network penetrating through the CNS to deliver the drug. The capillary network is made up of endothelial cells that highly regulate the entry of compounds by three modes: 1) physical barrier consisting of tight junctions limiting paracellular transport, 2) transport barrier where specific expression of membrane transporters, and 3) metabolic barrier where metabolizing enzymes may biotransform molecules in transit (106). Although the BBB is a formidable barrier, there are still a variety of pathways for molecules to enter the CNS depending on drug characteristics, surface area of the barriers as well as specific transport characteristics of the BBB shown in Figure 3. Passive diffusion of lipid-soluble molecules and certain blood gasses is driven by concentration gradient, where the rate of diffusion is both proportional to the differential gradient between blood and tissue, as well as compound size-dependent (106-108). Facilitated diffusion, whereby molecules may rely on a solute carriers (SLCs) to travel along their concentration gradient is also possible

for polar molecules, small peptides, and amino acids among others (109, 110). There are a large number of SLCs expressed on the membrane surface as hydrophilic molecules are unable to diffuse passively, and the tight junctions prevent paracellular transport (111, 112). Fluid phase transport such as pinocytosis, adsorptive-mediated endocytosis, and receptor-mediated endocytosis support the entry of large molecules into the CNS (113-115). The observable endocytic vesicles in the BBB endothelial cells have suggested a relatively limited degree, where one study reported the BBB having 16-20% of the endocytic profile compared to muscle capillary endothelia (116). Active transport based on the expression of membrane transporters on the BBB support both the entry and exit of molecules, shown in Figure 2 (98, 106). This pathway requires energy and may transport compounds against the concentration gradient; and it may be impacted by competitive and noncompetitive inhibitors, as well as influenced by protein kinases that may interfere with protein phosphorylation (98). The active transport mechanism has drawn significant interest in drug discovery and development for both the opportunity of compound entry into the CNS as well as the limited CNS penetration due to efflux transporters. Of particular interest have been the class of ATP-binding cassette (ABC) transporters such as Pgp as well as breast cancer resistance protein (BCRP) which have been shown limit the entry of a wide range of compounds (98, 117). The active efflux pump action limits the entry of lipid soluble compounds which otherwise may have favorable CNS penetration profiles. These transporters, particularly Pgp, are expressed on the luminal membrane demonstrating a clear neuroprotective function transporting compounds from the endothelium to blood (106).

1.4.3 Cerebrospinal fluid (CSF)

The distribution kinetics of drugs in the plasma may not reflect the disposition characteristics of drug in the central nervous system. Preclinical studies evaluating the mechanisms of drug exposure in the CNS supports direct sampling of nervous tissues. However, sampling of the brain and/or spinal cord is rarely possible in humans. The cerebrospinal fluid presents itself as an important surrogate, whereby from its direct interaction with the CNS tissues

and accessibility, enables correlations to be drawn to support drug exposure and effect relationships.

1.4.3.1 CSF production, distribution, absorption

Cerebrospinal fluid is predominantly produced in the ventricles, fluid-filled cavities within the brain. Each ventricle is lined by the choroid plexus which is responsible for producing CSF (93, 94). The choroidal epithelium first passively filters plasma into the choroidal interstitial compartment, and then actively transports components into the ventricular lumen using a variety of carbonic anhydrases and membrane ion carrier proteins (93). CSF is also thought to be derived from extracellular fluid from cerebral capillaries across the BBB and ependymal epithelium, although these are thought to play a minimal role in CSF production (93).

The distribution of CSF typically follows a path that begins in the lateral ventricles, which then flow to the third ventricle (94). Combined with the CSF produced in the third ventricle, it then flows through the cerebral aqueduct to join more CSF produced in the fourth ventricle (94). From the fourth ventricle, CSF can flow through the central canal to the spinal cord as well as follow the subarachnoid space through the median and lateral apertures around the brain (93, 94). The flow path of CSF can also be visualized in Figure 3. In the spinal cord CSF can be reabsorbed in the spinal subarachnoid space and may also circulate back up toward the subarachnoid space in the skull. The absorption of cerebrospinal fluid occurs in arachnoid granulations, which are outpockets of the subarachnoid space protruding into the dural sinuses (94). Arachnoid villi are the endothelium-lined protrusions that support the absorption of CSF into the venous blood system, as shown in Figure 4 (93, 94). The drainage from the cranial arachnoid granulations then pour into the jugular vein, along with the rest of the blood to enter the rest of the circulatory system (93, 94).

1.4.3.2 CSF use as surrogate

The rate and extent of drug exposure in the central nervous system is governed by multiple forces. The target for CNS penetrating drugs is often on the surface or within brain cellular

compartments. Thus, brain extracellular fluid as well as intracellular fluid (ICF) concentrations are the most representative of therapeutic concentrations of drug required to exert a pharmacologic effect. Previous laboratories developed preclinical animal models to quantify the exposure in brain ECF and ICF to correspond to therapeutic effects, however these data are rarely possible to collect in humans. The CSF has been well studied for its use as a surrogate marker to understand exposure in the CNS in animals and humans (118).

One of the basic assumptions driving the use of CSF as a surrogate for CNS exposure is that the CSF and ECF concentrations rapidly equilibrate across the ependymal layer (Nagaya 2016). Furthermore, protein binding is considered negligible, thereby assuming CSF concentrations are already in unbound concentrations

(118, 119). A useful measure used for comparison is calculating the partitioning of unbound drug into the brain ($K_{p,uu,brain}$) with that partitioning observed in CSF ($K_{p,uu,CSF}$) (119, 120). In a previous report, 12 compounds ranging in size and physicochemical properties were administered to male Sprague-Dawley rats and the $K_{p,uu,ECF}$ was compared to the $K_{p,uu,CSF}$ of those compounds (119). The investigators found that for the majority (11/12) compounds, the two partition coefficients were within 3-fold of each other. Importantly, Pgp substrates were evaluated within the study (ondansetron, risperidone, verapamil, quinidine), and while the calculated ratios fell below unity, CSF was still an appropriate surrogate to describe partitioning of drug into brain ECF from plasma (119). The utility of CSF to describe drug partitioning into brain ECF was further confirmed in cynomolgus monkeys, where 12 diverse compounds, that included Pgp substrates, were administered to and $K_{p,uu,ECF}$ and $K_{p,uu,CSF}$ were determined. When comparing $K_{p,uu,CSF}$ and $K_{p,uu,ECF}$, the values fell within 3-fold of each other (66).

Drug concentrations in CSF and various brain compartments have been used to not only describe preclinical CNS PK, but also used to scale to humans through the construction of physiologically-based pharmacokinetic (PBPK) models. Three non-Pgp substrates (acetaminophen, atenolol, remoxipride) and five Pgp substrates (quinidine, paliperidone,

phenytoin, risperidone, morphine) were used to construct a PBPK model containing a central plasma compartments with two peripheral compartments, brain ECF, brain ICF and 4 CSF compartments: lateral ventricle (CSF_{LV}), third ventricle (CSF_{TFV}), cisterna magna (CSF_{CM}), and subarachnoid space (CSF_{SAS}). In rats, the brain ECF, CSF_{LV} and CSF_{CM} were used to construct the model and described the concentration time profile. The model was then scaled according to a simple body weight allometric relationship to humans, where human acetaminophen and morphine data (plasma, lumbar CSF) were also used to support model building. Overall, the generic model structure used demonstrated the ability to translate preclinical findings to describe clinical concentrations, as well as the importance of using CSF as the common factor to draw the relationship from (121).

There are multiple methods to assess CNS exposure and drug penetration in preclinical species, including brain perfusion technique, brain homogenate free fraction method, and brain slice technique (120). However, there is limited opportunity to collect CNS tissue samples in human. CSF sampling remains a valuable method to collect drug concentration information to use for extrapolating preclinical PK into clinical exposure in the CNS. Establishing a framework to correlate CSF concentrations to the brain ECF concentration profile, to then support the extrapolation to the clinic remains a challenging but important endeavor.

1.4.4 Rat and human

Understanding the similarities and differences of the central nervous system is a valuable method to scaling the expected drug distribution properties from preclinical species to humans. The CSF production have shown some similarities between humans and rats. For example, 60-70% of CSF is produced in the ventricles in humans, and similarly 80% of CSF is produced in the ventricles for rats (93, 120). However, the relative turnover of CSF in rats is shown to be higher where the rate of production is 2.2 μL/min with a total volume of 250 μL, showing CSF volume being replaced approximately every 2 hours (122, 123). In humans the total volume replacement is approximately every 6 hours, where the rate of production is 0.4 mL/min, with a total volume of

140-150 mL (93, 120, 124). Rats also have estimated higher replacement of brain extracellular fluid (ECF) compared to humans. The total brain ECF volume in rats is 290 μL, with a production rate of 0.2-0.5 μL/min (99, 125). Compared to humans, where the turnover of total brain ECF volume is every 20-27 hours, with production of 0.15-0.2 mL/min and a total brain ECF volume of 240 mL (126, 127). Table 1 represents information sourced from publications that have highlighted the physiological parameters that represent the CNS, comparing rats to humans.

In addition to the challenge of scaling the physiological processes across species, differences may also remain in evaluating the differences in active transport processes. Pgp transport activity has demonstrated significant differences across multiple species. In a study evaluating Pgp substrate [^{11}C]GR205171 brain distribution in rats, guinea pigs, monkeys, and humans the brain distribution was higher in humans and monkeys, as compared to rats and guinea pigs (128). The ratio of brain to plasma was nearly 9-fold lower in rats when compared to humans (128). When cyclosporin A was administered as a Pgp inhibitor, the species differences still remained, and interestingly the Pgp inhibition appeared higher in rats compared to the other species. Similar differences were also reported for [^{11}C]RWAY, a $5HT_{1A}$ receptor antagonist, that demonstrated low brain uptake in rat and mice, but relatively high exposure when compared to human and monkey brains (129-131). One of the potential explanations for such differences may be species differences in transporter expression levels. In one report comparing guinea pigs to rats, a higher concentration of Pgp inhibitor GF-120918 (elacridar) was needed in the guinea pigs compared to rats to achieve the same increase in brain exposure of a Pgp substrate (132). Although, this was not the case when administered [^{11}C]verapamil in human and rat brain following similar low doses of the cyclosporin A (133). Further experimental work will be required to fully elucidate the similarities and differences in Pgp expression and activity across species to support translational work.

Table 1.3 Central nervous system values for rat and human (134, 135)

	Parameter	Human	Rat
Volumes	BBB	8.25 mL	5. 02 μL
	BCSFB	107.25 mL	37.5 μL
	Brain	1400 g	1.8 g
	Brain vascular space	63.7 mL	0.066 mL
	Brain ECF	240-280 mL	290 μL
	CSF total	130-150 mL	250 μL
	CSF lateral ventricle	20-25 mL	50 μL
	CSF third ventricle	20-25 mL	50 μL
	CSF cisterna magna	7.5 mL	17 μL
	CSF subarachnoid space	90-125 mL	180 μL
Flows	Cerebral blood flow	610-860 mL/min	1.1-1.3 mL/min
	Brain ECF flow	0.15-0.2 mL/min	0.00018-0.00054 mL/min
	CSF Flow	0.3-0.4 mL/min	0.0022 mL/min
Surface Area	Blood brain barrier (BBB)	12-18 m^2	155-263 cm^2
	Brain CSF barrier (BCSFB)	6-9 m^2	25-756 cm^2
	Brain vascular surface	157 cm^2/g brain	150 cm^2/g of brain

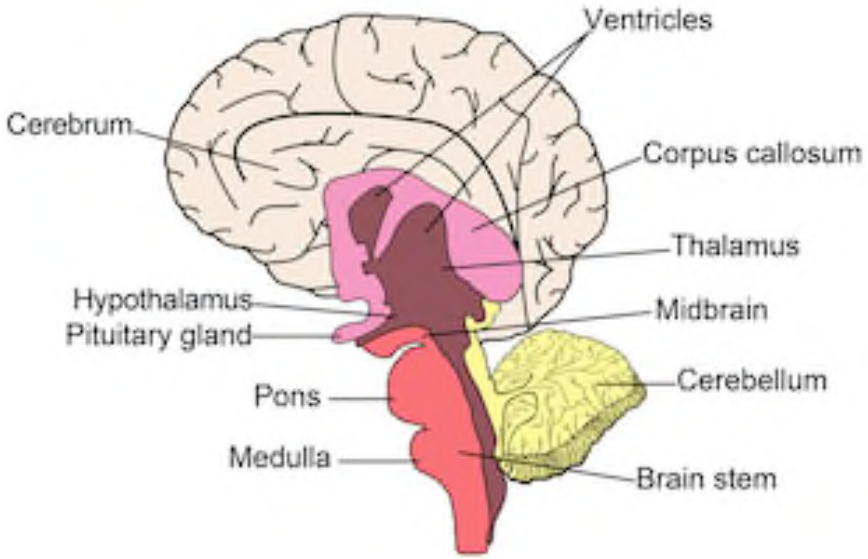

Figure 1.6 Basic anatomy of the brain shown in cross-section. The cerebrum divided into hemispheres (not shown), with ventricles sitting within the brain. Below the cerebrum are the corpus callosum, structure connecting the two hemispheres of the brain, as well as hypothalamus, pituitary gland, and thalamus. Lower section of brain is the midbrain, with the cerebellum and brainstem.

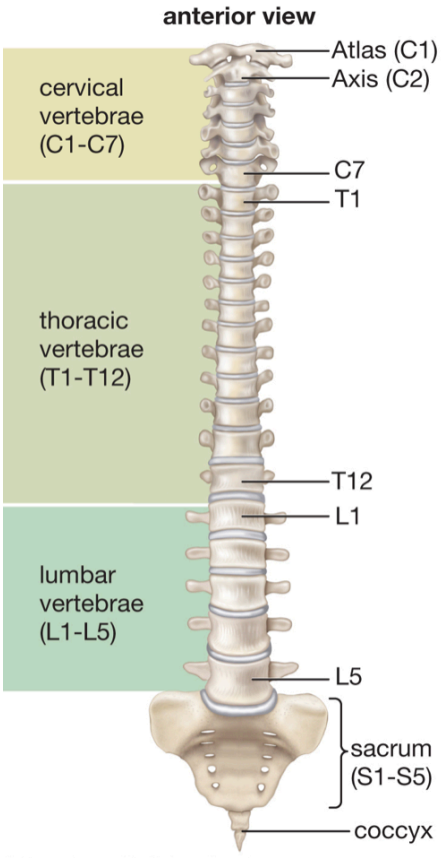

Figure 1.7 A basic schematic of the spinal column, divided by its general areas (cervical, thoracic, lumbar, sacrum) (136).

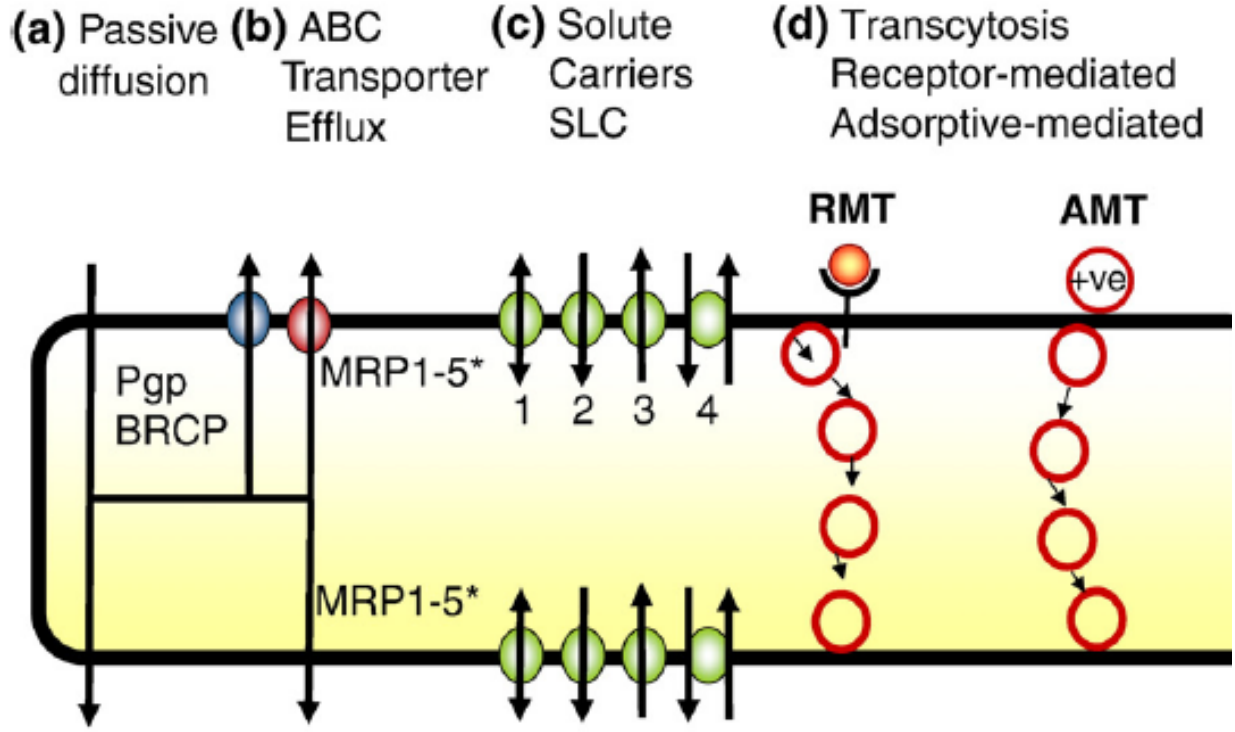

Figure 1.8 A schematic detailing the routes of transport across the blood-brain barrier from the luminal side (bottom) to the tissue (above): (a) Passive diffusion (b) ATP-binding cassette (ABC) transporter efflux (c) Facilitated diffusion by solute carriers (SLC) and (d) transcytosis methods that are receptor- or adsorptive-mediated (RMT, AMT) **(106)**

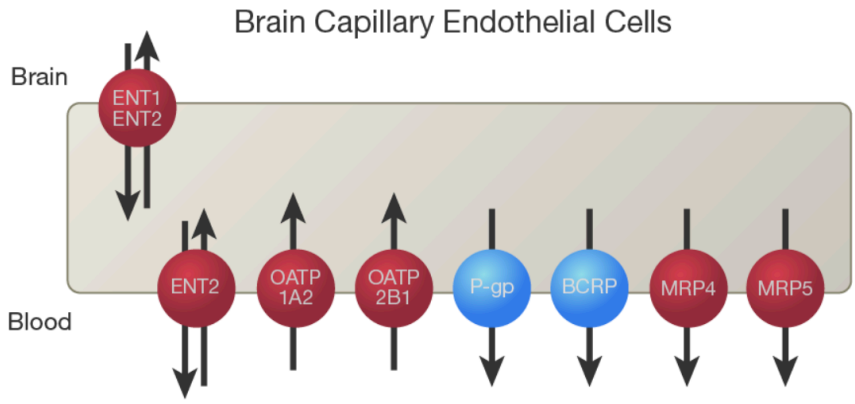

Figure 1.9 Schematic of known active transport systems sitting in the human BBB (120, 137).

Figure 1.10 Basic schematic of CSF flow path from ventricular system to the brain and spinal cord (120).

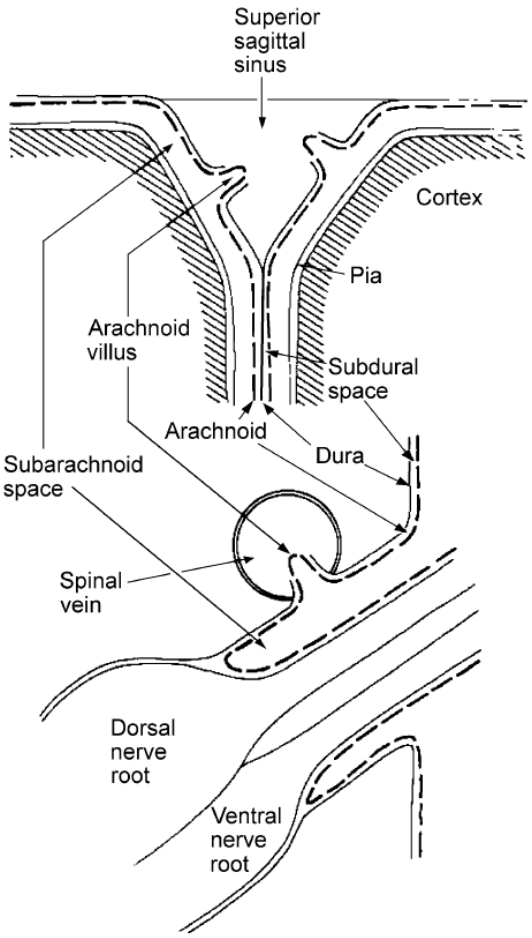

Figure 1.11 CSF absorption in the arachnoid villi of the superior sagittal sinus in the skull as well as the spinal veins on dorsal root nerve **(118)**.

1.5 Pharmacokinetic Modeling

There has been sincere interest to focus pharmacokinetic model development on describing and predicting the PK properties of compounds acting on the CNS to construct an exposure-response relationship for therapeutic development. The range of models span from empirical models, describing the system as a series of compartments with distribution of drug from plasma to the CNS tissues, to physiologically-based models where drug distribution is according to physiological flow rates with fixed tissue volumes to describe the system. Each of the models presented have certain strengths and limitations that dictate its ultimate application in drug development.

1.5.1 Generic multi-compartmental CNS Model

A generic multi-compartmental brain pharmacokinetic model was developed by the de Lange group with the ultimate goal of predicting human brain drug disposition (121). The model was constructed using published (acetaminophen, atenolol, methotrexate, morphine, quinidine, remoxipride) and newly generated data (paliperidone, phenytoin, risperidone) based on rat plasma and brain PK, and externally validated with two additional rat data sets (acetaminophen, remoxipride). The model was then scaled to humans and simulated human plasma and brain PK profiles for acetaminophen and morphine and evaluated for how well the observed data were described by the mode predictions. Active transporter efflux was evaluated by studying tissue disposition with efflux transporter substrates (methotrexate, morphine, quinidine, paliperidone, phenytoin, risperidone) co-administered with a transporter inhibitor (tariquidar, probenecid, GF120918). The details of the dosage, data collected, and additional information on all data sets used to construct the model are presented in Table I.

In the first step, 9 drugs were evaluated for plasma, brain extracellular fluid ($brain_{ECF}$), CSF in cisterna magna (CSF_{CM}) and CSF in lateral ventricle (CSF_{LV}), with transporter substrates co-administered intravenously with inhibitors to evaluate differences in tissue disposition. A microdialysis technique was developed to collect the brain concentration profiles for supporting

the construction of the model, shown in Figure 1. A central compartment with systemic clearance (CL_{PL}) and two additional peripheral distribution compartments with inter-compartmental clearances (Q_{PL_PER1}, Q_{PL_PER2}) were used to describe plasma PK. Drug enters directly into the $brain_{ECF}$ compartment from the plasma, estimated as Q_{PL_ECF}. This directional term is representative of the BBB, quantifying the processes that may limit and/or facilitate drug penetration into the CNS. A drug dispersion term (Q_{DIFF}) was estimated to capture CSF and ECF flow, and turbulence flow (i.e., flow that is not linear and smooth) of drug molecules in the CNS. Physiological volumes for the CNS compartments were fixed in the model.

The preclinical rat datasets used for building the model are shown in Table 1. For the compounds co-administered with a transporter inhibitor: probenecid is a known inhibitor for MRP, OATs, and OATPs, while GF120918 and tariquidar inhibit Pgp. The description of drug efflux adopted a categorical covariate approach, using equation $P = P_{PAT} \cdot (1 + \theta_{COV} \cdot Cov)$ where P represents the parameter, P_{PAT} represents the net transport, and θ_{COV} represents the effect of the transporter, and *Cov* is the effect itself, with 0 fixed to no inhibitor and 1 fixed for the presence of an active transport inhibitor. The effect of drug efflux was estimated on Q_{PL_ECF} and CL_{PL} for compounds co-administered with a transporter inhibitor.

Plasma and brain-related drug-specific parameters were simultaneously estimated for the 9 compounds providing plasma, $brain_{ECF}$ and CSF_{CM} profiles, and the model was then externally validated using 2 additional data sets by simulating profiles and over-laying on the data. Figure 1 depicts the full model schematic, color-coding system- and drug- specific parameters used for model development. Drug-specific parameters were those used for estimating the plasma and CNS PK, such as Q_{PL_ECF}, while system-specific parameters were those that were fixed to describe the physiological attributes of the system (e.g., volume of each CNS compartment). The mean predicted lines, and 95% confidence intervals predicted by the model overall described the observed datasets, providing confidence in the generic brain PK model to describe the disposition across multiple drugs, and accounting for active efflux clearance. The data used for predicting

human brain disposition is defined in Table 2. The ability to predict human brain disposition was evaluated using an acetaminophen and morphine dataset that contained plasma, CSF, and brain tissue ($brain_{ECF}$), replacing physiological volume values for human, estimating plasma-related parameters, and scaling brain-related drug parameters according to equation $P_{human} = P_{rat} \cdot (BW_{human}/BW_{rat})^{0.75}$ where P_{human} is the human parameter to be scaled, P_{rat} represents the value of that parameter estimated in rat, and BW_{human} and BW_{rat} represents the total body weight in human and rat respectively. The human CSF and $brain_{ECF}$ profiles were collected using implanted catheters in patients who suffered brain lesions or severe brain trauma (138, 139). Interestingly, the authors selected the body weight method for developing an allometric method. Alternative methods for scaling PK are also available, such as scaling by brain weight, which may be a highly relevant approach to evaluate in developing physiologically-relevant CNS models. The simulated profiles were able to describe the general trend of brain drug disposition in humans. The acetaminophen profiles demonstrated an under-prediction for the overall variability on CSF variability of the CSF from external-ventricular drainage (CSF_{EVD}) in addition to slightly underpredicting the CSF in subarachnoid space (CSF_{SAS}) profile. The $brain_{ECF}$ profiles in normal patients administered morphine was described well, however in injured patients the $brain_{ECF}$ was largely under-estimated, both in the average profile as well as the 95% CI.

The De Lange model demonstrates the ability to utilize preclinical datasets to predict brain drug disposition in the CNS of humans. Importantly, using simple scaling allometric methods based on body weight, employing known physiological volumes to CNS compartments provides the opportunity to have a quantitative understanding of concentrations in brain tissue, as well as CSF. There is a tremendous advantage to scaling the model based on preclinical studies, as animal studies are often more feasible to run, in addition to being much more cost-effective than clinical studies. Furthermore, the compound selection further demonstrates the opportunity to apply this model for additional compounds that may provide similar accuracy in describing the preclinical and clinical dataset. A significant drawback of this effort is the requirement to use

microdialysis to support preclinical studies. This is a costly and labor-intensive method requiring technical ability to develop a reliable method for sampling drug concentrations at the intended site. In addition, the model itself may limiting in its ability to describe a wider set of compounds with confidence. For example, drug only enters using the Q_{PL_ECF} term, however it is known that drug may also enter the CNS space from the BCSFB, which was not included in the model. In addition, the CNS PK was constructed based only on brain and CSF profiles, where the spinal cord is notably absent. Similarly, the CSF and drug dispersion in the CSF was described across multiple compartments using a single Q_{DIFF} term for each compound. This approach may not have reflected the physiological processes, as oftentimes drug dispersion across multiple tissue spaces is not uniform. Overall, the De Lange model still represents a useful and innovative approach to employing a generic model format to predict human brain disposition.

1.5.1.2 Simcyp 4Brain model

Simcyp is a user-friendly software package that was developed for the main purpose of predicting tissue concentrations in the whole body. Currently, the main use of the software is to predict drug-drug interactions, as well as evaluating concentration profiles in specific populations (e.g., geriatric, Japanese, pediatric). The model utilizes literature values to define each facet of the tissue in the body such as tissue volumes, enzyme expression and density as well as physiological flow rates connecting the full-body PBPK model together. The user is able to develop a drug profile based on its physicochemical and ADME properties and utilize Simcyp to predict the impact on tissue profiles based on different dosing regimens and drug interactions. Simcyp has developed a model for humans, as well as mouse, rat, dog, and monkey. The main pharmacokinetic of drug disposition in each tissue compartment is based on a well-stirred model, whereby the drug entering each compartment is immediately and equally distributed within the whole compartment.

Recently, the Simcyp full-body PBPK model was updated to incorporate multiple compartments within the brain compartment to improve prediction of drug profiles in the CNS

(140). The model framework is shown in Figure 2, whereby the brain compartment was defined as four discrete compartments: brain mass, brain blood, cranial CSF, and spinal CSF. In line with the previous model, physiological flow rates were incorporated to reflect the flow of CSF between each compartment, as well as the water permeation that exists to maintain fluid homeostasis within the brain. The user is able to define the passive permeability terms that would reflect drug diffusing in and out of the brain compartments, as well as any active clearance mechanism that may be present at the BBB or BCSFB.

The model performance was assessed by building a drug profile for acetaminophen and phenytoin, assessing the simulation of concentrations in the brain and lumbar CSF compared with observed. Acetaminophen plasma and CSF profiles were evaluated using three different clinical studies, and phenytoin provided a single clinical study for evaluating plasma and CSF concentrations. Overall, the predicted mean profile and 95^{th} and 5^{th} percentile from Simcyp simulations for both compounds captured not only the mean trend of the data but also the overall spread of the data in both plasma and CSF.

Simcyp provides a useful avenue for predicting human brain disposition for its user-friendly interface, allowing for the bulk of the computational effort to be covered by the software itself. Furthermore, there is a wide latitude of use given that the software itself is capable of accommodating a variety of dosing regimens (i.e., oral, IV, multiple dose, single dose), as well as specific populations (male/female, ethnicity, age) and drugs. Simcyp represents a “bottom-up” approach, where *in vitro* methods are heavily relied on for generating the necessary data to input into the model. For example, the active efflux clearance can be estimated or evaluated using a sensitivity analysis, but to validate the model cell experiments would be needed to identify the required parameters. The inter-lab and general variability of *in vitro* work may mislead the model development process to provide inaccurate simulations of tissue profiles. Furthermore, to utilize the model framework a drug file must be built. However, if the drug was developed many decades ago or is newly generated, much information required for utilizing Simcyp may not be available.

This also illuminates the rigidity of the Simcyp model framework, where much of the model parameters and framework is embedded within the software and is not editable or observable to the user. Although there are notable limitations to the Simcyp software, it has demonstrated an important use for simulating tissue profiles and quantifying drug interactions and transport.

1.5.2 Drug-specific CNS PK models

Empirical models have long been the standard approach for building pharmacokinetic models. The fundamental flexibility in designing empirical models maintains its relevance in both clinical and preclinical spaces. Largely, these models have shown great value in supporting dose selection as well as investigating novel mechanisms that may not be immediately observable based on evaluating the data, or having strict assumptions built into complicated model designs. There is also a capacity of employ various interspecies scaling methods to develop an allometric model. An important utility of the empirical models is the ease to translate pharmacokinetic profiles to pharmacodynamic effect. The limitations of empirical model designs may be in its specificity to the drug that is being studied. Immense validation would be required to utilize the same model for describing the PK of a different dose or drug in a different population. Furthermore, physiological interpretation may also be taken cautiously depending on the assumptions used to construct the model.

1.5.2.1 Empirical CNS Models

Empirical models often simplify the CNS system to only the necessary components needed to describe brain disposition. For example, there are examples of the model development incorporating only plasma compartments with one additional “CNS” compartment, oftentimes representing $brain_{ECF}$. An empirical model was developed to evaluate quinidine PK, estimating parameters describing plasma and $brain_{ECF}$ concentrations using a 3-compartmental model (141). Quinidine systemic distribution was described using 2 compartments, with the $brain_{ECF}$ compartment attached to the central compartment. The model structure is shown in Figure 3. Quinidine is a known substrate of Pgp, and the inhibition of quinidine was evaluated through the

co-administration of tariquidar. The changing tariquidar plasma concentrations was incorporated into the model, whereby the inhibition of Pgp was estimated as a sigmoid inhibitory model in equation $CL_{31Pgp'} = CL_{31Pgp} \cdot \left(1 - \frac{I_{max} \cdot C_{TQR}}{C_{TQR} + IC_{50}}\right)$ where I_{max} represent maximal Pgp inhibition by tariquidar on the BBB (set to 1) and IC_{50} is the plasma concentration of tariquidar needed for half-maximal inhibition. C_{TQR} represents the tariquidar plasma concentration, CL_{31Pgp} is the Pgp mediated efflux clearance from $brain_{ECF}$ to plasma, and $CL_{31Pgp'}$ is the Pgp mediated quinidine efflux clearance in the presence of tariquidar. The ultimate goal of the model was to use a disease specific system (epilepsy) to evaluate the differential expression of Pgp being correlated to the efflux functionality. The model demonstrated the ability to support the ultimate goal by utilizing microdialysis techniques paired with the influence of tariquidar inhibition of Pgp in epilepsy-induced male rats. This model demonstrated the simplicity of using few compartments and terms to describe brain disposition in healthy and disease state animals, as well as using a dynamic method to estimate Pgp inhibition to quantify the limited correlation found between expression and functionality of Pgp on the BBB. The limitation of the model may be that it is constrained to the dosages used in the study, as well as the disease state itself.

There have also been examples of CNS models including CSF compartment in addition to the $brain_{ECF}$ profiles. A report published the brain disposition of L-histidine, modeled as two systemic compartments and an additional brain and CSF compartment (142). This model was also able to include two unique points, 1) including a bulk term to account for the bulk flow from CSF to plasma, which was fixed according to previous reports estimating this flow term and 2) describing the additional capacity limited transport of L-histidine to the brain based on Michaelis-Menten kinetics. This group benefited from obtaining both brain and CSF data, to provide a semi-mechanistic model that may allow for greater quantification of brain disposition. Furthermore, the inclusion of the capacity-limited transport of L-histidine further provides insight into the distribution of L-histidine at the BBB. Developing a semi-mechanistic model such as this utilizes the

advantages from empirical modeling, such as the flexibility of model design and parameter inclusion, as well as that found in physiologically-based modeling where the ultimate translation of the results may give insight into the physiological system.

1.5.3 Minimal physiologically-based pharmacokinetic (mPBPK) model

Minimal physiologically-based pharmacokinetic models were recently developed to provide a physiological perspective on drug disposition in the whole-body, while limiting the complexity and challenge that is often associated with modeling full-body PBPK profiles (143). This approach may limit the number of physiological compartments that is included in the model without losing out on detailed descriptions of drug exposure within specific tissue spaces. The utility of this model has been demonstrated for a wide range of therapeutics, ranging from small molecule drugs such as antibiotics, to large molecule monoclonal antibodies. An additional advantage of this approach is the scalability across species, where the mPBPK model has been shown to scale drug disposition by employing a simple body weight allometric equation. This model framework may support both IV as well as oral dosing of drugs, with oral dosing including an additional compartment representing the hepatic compartment to account for any liver metabolism that may impact drug absorption and distribution.

1.5.3.1 mPBPK model structure and assumptions

The model structure contains a single blood or plasma compartment, that is able to support intravenous administration, that has a fixed plasma volume (V_P) with a central clearance term, as shown in Figure 5. The tissues are assumed to be lumped into few discrete compartments. The flow of drug within the model is dictated by the total cardiac output (Q_{CO}), and each compartment received an estimated fraction (f_{d1}) of the flow. This allows for the flexibility to define drug distribution in tissues that may be lumped together as having flow-permeability or (such as liver, kidney), as well as those which may be permeability-limited in a secondary compartment according to Fick's Law of Perfusion. The partition of drug into each compartment is estimated as K_{P1} into the estimated volume of each lumped compartment (V_1). Importantly, two main

assumptions dictate the use of the model, 1) the total sum of volume terms will be equal to total BW or extracellular fluid volume and 2) the total sum of f_d terms will be less than or equal to 1.

1.5.4 Population PK Model

When constructing models to describe clinical data, a great challenge is the considerable variability in drug concentrations and effect. The population approach to PKPD modeling, known as nonlinear mixed effect modeling, is able to handle the significant variability observed in clinical data as well as define what aspects of the variability may be attributed to physiological effects - such as age, gender, ethnicity – as well as what aspects may be due to variability is residual, as a product of other sources such as bioanalytical error. In addition to describing the variability within a dataset, this approach supports “sparse sampling” which relies on fewer data points from a larger population of patients to contribute to an overall understanding of the mean population profile, as well as predicting and estimating the individual profile for each individual patient. The advantages of developing a population PK model has found applications in preclinical datasets to support the description of animal variability and PK.

1.5.4.1 Model structure and assumptions

There are two main aspects to the nonlinear mixed effect modeling, emphasizing the “mixed effects” portion, which is attributed to the fixed and random effects. The fixed effects define the central tendencies, or “typical values” of the structural parameters of the model for the population. There is then the random effects, which are a set of parameters that quantify the magnitude of variability observed in the model. This variability is divided into inter-individual variability, where covariates such as body weight, sex, and age will be evaluated to identify any influence on the estimated parameters, inter-occasion variability which describes variability specific to difference arising between sampling occasions, and residual variability which is a term lumping in unexplained variability between observed and predicted values. For both fixed and random effects, the effect is assumed to behave as a normal distribution with a mean of 0 (μ=0) and a variance of ω^2. Thus, each parameter follows these two assumptions, with the mean

population value at the center of the distribution, and each individual-specific parameter deviates some value from the mean. The random effect parameters are modeled as specific functions depending on the source of variability. These model structure selected may be attributed to the trends observed in the data, and which model structure may better describe this variability. Covariates (continuous and categorical data) may also be incorporated into the model to describe variability that may be attributed to measurable parameters, such as age and bodyweight. The inclusion of covariates often follows strict statistical guidelines that rely on the overall objective function, criteria for model evaluation, as well as general model diagnostics, to define whether a covariate is truly improving model estimation.

While nonlinear mixed effects modeling adopts a complex statistical framework, the ability to describe sources of variability in the model and estimate both population and individual profiles demonstrate the great strength of this approach. For example, a population based model was published detailing a model describing regional brain distribution of drug in rat CNS, with variability terms estimated on terms distribution drug from plasma to the CNS compartments (120). Additionally, the population approach was used to predict quinidine concentrations in $brain_{ECF}$ following Pgp inhibition by tariquidar and allowed for description of residual error in the data set (141).

1.5.5 Interspecies model

Quantitative relationships have been developed to scale the observed pharmacokinetics in preclinical species to humans. This has allowed for using extensive preclinical characterization to describe human PK, where in the clinical space tissue sampling and/or extensive blood sampling may not be supported or allowed.

1.5.5.1 Allometric relationships

The simplest approach is to scale parameters based on the ratio of body weights of human to the reference preclinical species, as shown in equation $P_{human} = P_{ref} \cdot (BW_{human}/BW_{ref})^b$ where P_{human} represents the scaled parameters in the human, and P_{ref} represents that found in the

reference species, the total bodyweight of human and reference species (BW_{human}, BW_{ref}) respectively, and the allometric exponent “b”. Previous works have established common relationships for PK parameters that have scaled across multiple species, such as plasma clearance across mouse, rat, monkey, dog, and man, where the allometric exponent was defined as 0.75. Similarly, central volume of distribution has been shown to be scaled according to the ratio of bodyweights, with an exponent determined as 1 (144). Additional scaling approaches have also been defined that has shown utility in various studies (145-147). Each of the allometric relationships have demonstrated utility in differing compounds, highlighting the importance of identifying the approach which reasonably describes the relationship of the compound as well as the known relationship across species. Oftentimes the prediction that is shown from interspecies scaling is defined as describing the data within 2- to 3- fold. Although, this range may be quite large when translated to plasma and/or tissue concentrations, and so employing allometric scaling must be evaluated cautiously, while keeping in mind the ultimate goal of the model

Table 1.4 A summary of rat brain distribution data for model development and external validation (121)

Study design	Model development										External validation	
	Published data							Newly produced data			Published data	Newly produced data
	Acetaminophen	Atenolol	Methotrexate	Morphine	Morphine	Quinidine	Remoxipride	Paliperidone	Phenytoin	Risperidone	Acetaminophen	Remoxipride
Species	rat	rat	rat	rat	rat	rat	rat	rat	rat	rat	rat	rat
Nr of animals	16	5	23	65	18	41	29	21	14	16	8	65
Dosage, mg/kg (infusion time, min)	16 (10)	10 (1)	40, 80 (10)	4, 10, 40 (10)	10, 40 (10)	10, 20 (10)	4, 8, 16 (30)	0.5 (20)	20, 30, 40 (10)	2 (20)	200[a] (1)	0.7, 5.2, 14 (10)
Nr of samples (sampling times, min) plasma	67 (0–240)	32 (0–120)	186 (0–300)	825 (0–360)	306 (0–190)	313 (0–360)	189 (0–240)	182 (0–360)	109 (0–480)	124 (0–360)	67 (0–180)	290 (0–240)
dialysate	592 (0–240)	106 (0–120)	1065 (0–300)	238 (0–360)	299 (0–180)	1678 (0–360)	125 (0–240)	660 (0–240)	152 (0–480)	436 (0–240)	72 (0–180)	489 (0–240)
Active transport inhibitor	–	–	probenecid[b]	GF120918[c]	–	tariquidar[c]	–	tariquidar[c]	tariquidar[c], probenecid[b]	tariquidar[c]	–	–
Dosage of active transport inhibitor, mg/kg (infusion time, min)	–	–	150 (10)	6 (cont)[d]	–	15 (10)	–	15 (10)	15 (10) 150 (10)	15 (10)	–	–
Data												
plasma	X	X	X	X	X	X	X	X	X	X	X	X
$brain_{ECF}$	X	X	X	X	X	X	X	X	X	X	X	X
CSF_{LV}	X		X			X						X
CSF_{CM}	X		X			X		X		X		X
References	(6)	(69)	(25)	(70)	(71)	(24)	(26)				(72)	

$brain_{ECF}$ a brain extracellular fluid compartment, *CSF_{LV}* a compartment of cerebrospinal fluid in lateral ventride, *CSF_{CM}* a compartment of cerebrospinal fluid in cisterna magna

[a]; mg, [b]; inhibitor of MRPs, OATs and OATPs, [c]; inhibitor of P-gp, [d]; continuous infusion

Table 1.5 Summary of human acetaminophen and morphine data (121)

Study design		Acetaminophen		Morphine	
		Study 1	Study 2	Study 1	Study 2
Condition of patients		human with traumatic brain injury	human with nerve-root compression pain	human with traumatic brain injury	human with traumatic brain injury
Nr of patients		7	1 (mean values)	2	1
Dosage		1 g, 30 min infusion	2 g (propacetamol), short infusion	10 mg, 10 min infusion	10 mg, 10 min infusion
Nr of samples (sampling time, h)	plasma	38 (0–6 h)	11 (0–12 h)	23 (0–3 h)	11 (0–3 h)
	brain ECF or CSF	54 (0–5.5 h)	11 (0–13 h)	74 (0–3 h)	37 (0–3 h)
data references	Newly generated	(31)	(34)	(33)	
Data					
plasma		X	X	X	X
$brain_{ECF}$				X ("normal" and "injured" brain tissue)	X ("normal" and "injured" brain tissue)
CSF_{EVD}		X			
CSF_{SAS}			X		
f_p [a]		85%	85%	–	–
f_p references		(32)	(32)	(34)	(33)

$brain_{ECF}$ a brain extracellular fluid compartment, *CSF_{EVD}* a compartment of cerebrospinal fluid in EVD, *CSF_{SAS}* a compartment of cerebrospinal fluid in subarachnoid space

[a] free fraction in plasma

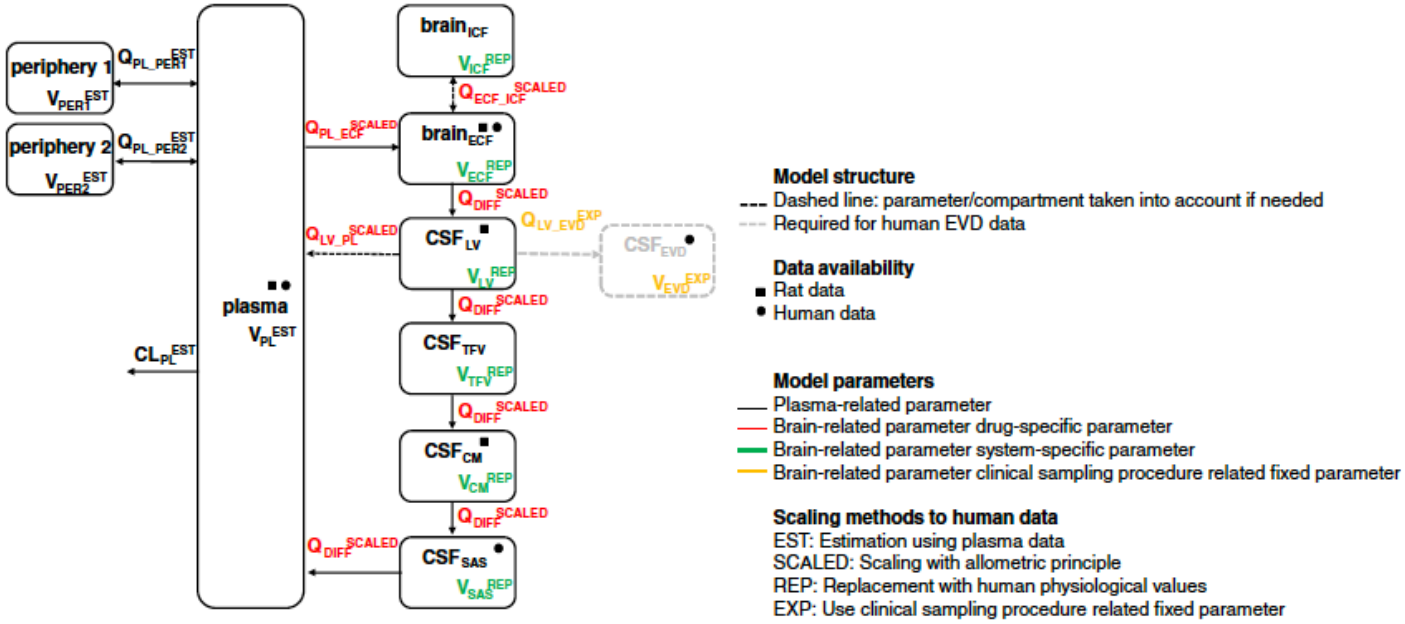

Figure 1.12 Generic brain pharmacokinetic model with central plasma compartment (plasma) and two peripheral plasma compartments (periphery 1, 2). $Brain_{ICF}$, $brain_{ECF}$, CSF_{LV}, CSF_{TFV}, CSF_{CM}, CSF_{SAS} represent the brain compartments with a CSF_{EVD} included for the human study related to clinical sampling (121).

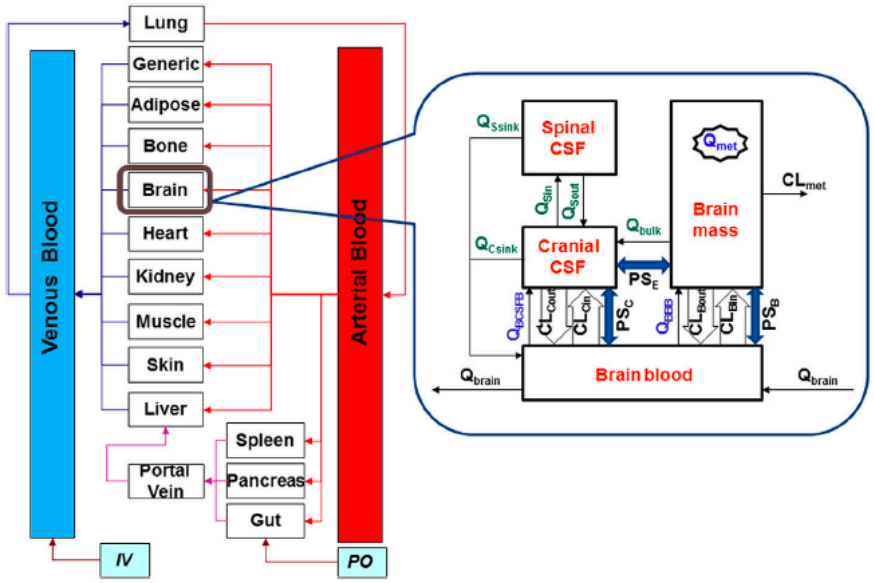

Figure 1.13 The 4-compartmental brain model containing brain mass, brain blood, cranial CSF, and spinal CSF compartments embedded within the "brain" compartment (140). $Q_{Sin\ and}$ Q_{Sout} define CSF flow from cranial to spinal compartment and *vice versa*. Q_{Csink} and Q_{Ssink} denote CSF flow out of cranial and spinal CSF compartments. Q_{BCSFB} defines CSF secretion from choroid plexus, and Q_{bulk} represents bulk flow from brain mass to cranial CSF. Q_{BBB} defines water transfer due to hydrostatic pressure between brain blood and brain mass compartments. Q_{met} represents water permeation from brain blood to brain mass via BBB to maintain fluid balance within the model. CL_{Bin}, CL_{Bout}, CL_{Cin}, CL_{Cout}, are the overall clearance uptake/efflux from active transporters expressed on the BBB and BCSFB. The PS_B, PS_C, PS_E, represent passive permeability surface area products from BBB, BSCFB, and brain-CSF barrier respectively. Metabolic clearance within the brain is accounted for by CL_{met} (L/h). Cerebral blood flow is represented by Q_{brain} which connects the 4brain compartment to the whole-body PBPK model.

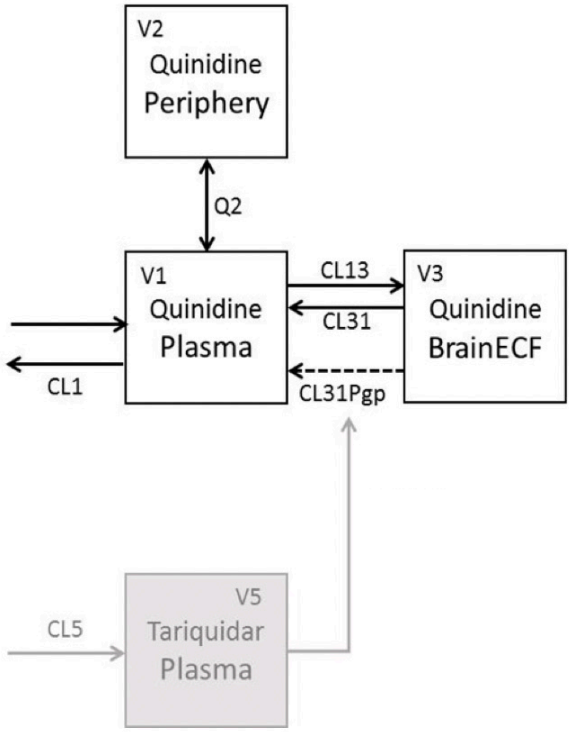

Figure 1.14 Empirical population PK model to describe quinidine Pgp inhibition in plasma and $brain_{ECF}$. Two compartments are used to describe plasma PK with central clearance (CL1). Passive transport into and out of $brain_{ECF}$ defined as CL13 and CL31 respectively (141). CL31Pgp is used to quantify Pgp efflux clearance across BBB from $brain_{ECF}$ compartment. Tariquidar defined as 1 compartment model, with CL5 defining the plasma PK. V1 and V2 were estimated volume for the plasma, while V3 was fixed to 145 μL for the left and right brain ECF (141).

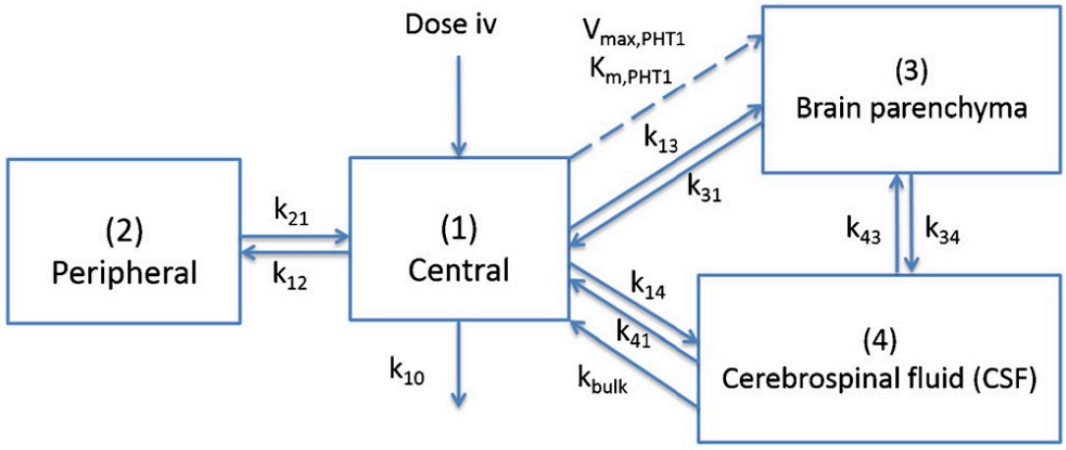

Figure 1.15 Empirical modeling describing L-histidine distribution in plasma and CNS. The system is described with two plasma compartments (central (1) and peripheral (2)), with two additional CNS compartments (brain parenchyma (3) and CSF (4)) (142). Central elimination (k_{10}), inter-plasma distribution (k_{21}, k_{12}) and brain-plasma distribution (k_{13}, k_{31}), plasma-CSF distribution (k_{14}, k_{41}) and brain-CSF (k_{34}, k_{43}) were included in addition to bulk flow of CSF to plasma (k_{bulk}) as well as Michaelis-menten kinetics to describe peptide-histidine transporter 1 (PHT1) of L-histidine from plasma to brain ($V_{max,PHT1}$, $K_{m,PHT1}$) (142)

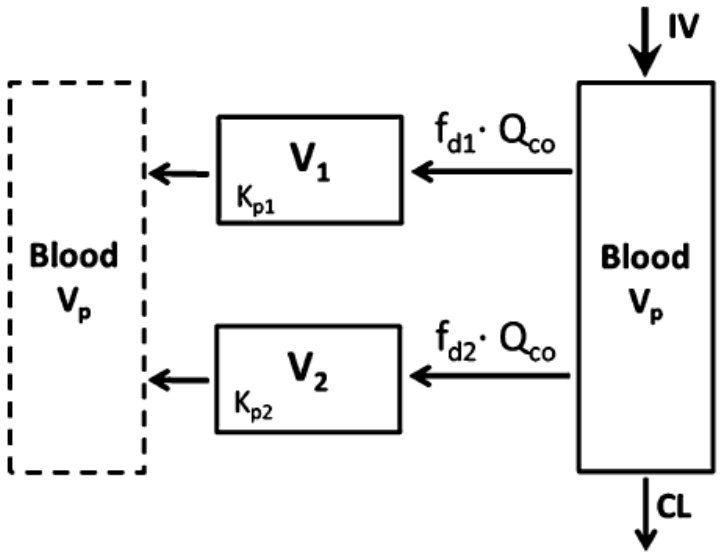

Figure 1.16 A minimal PBPK model that contains two lumped tissue compartments. The blood compartment supports IV administration, with central clearance from blood compartment. Each lumped tissue compartment is defined by fractional flow (f_{d1}) of the total cardiac output (Q_{CO}) into the lumped compartment with volume (V1, V2) and drug partitioning defined as K_{p1} (143) .

1.6 Summary

Neuropathic pain affects nearly 7-10% of the global population. Neuropathic pain arises from a lesion or disease-related change to the somatosensory system. Currently, the available therapies are often unable to provide sufficient pain relief, or the recommended dosages may produce unwanted toxic effects in patients.

The neurophysiological changes are related to changes in normal signaling patters, often those related to the balance of excitatory and inhibitory signaling. The descending serotonergic pathway has been studied for its role in neuropathy, and the expression of 5-HT_3 receptors in the spinal cord has been linked to neuropathic pain. Pre-clinical reports have shown that intrathecal administration of ondansetron, a 5-HT_3 receptor antagonist, is effective in reducing pain symptoms in rats. Clinical reports have been inconclusive in confirming the use of ondansetron for providing pain relief for patients. The inconsistency of clinical reports may be related to the factors affecting the pharmacokinetics of ondansetron in the CNS. Ondansetron, being a Pgp substrate, may have limited distribution into the CNS due to the efflux activity. Furthermore, sex differences in plasma pharmacokinetics have been observed in both clinical and preclinical studies, which may lead to differences CNS exposure.

The CSF is often used as a surrogate for drug penetration since the brain and spinal cord are rarely able to be sampled in the clinic. However, actual tissue concentrations may differ from the CSF. Pharmacokinetic studies supported with modeling efforts may allow for quantification of drug PK in specific tissues. Previous modeling efforts, ranging from empirical to physiologically-based pharmacokinetic models have demonstrated the ability to quantify plasma and CNS disposition. Pgp efflux, as well as sex may be included in model development to quantify the effect on overall drug pharmacokinetics.

1.7 Specific aims

1. To evaluate the role of Pgp-mediated efflux on ondansetron pharmacokinetics and CNS disposition using genetic and chemical knock-out models in an preclinical in-vivo study

2. To evaluate plasma pharmacokinetics and CNS disposition of ondansetron in human volunteers using CSF as biomarker of CNS partitioning

3. To develop translational mechanistic, empirical, and semi-physiological pharmacokinetic models for ondansetron using preclinical and clinical data

Chapter 2 Pharmacokinetic modeling of the impact of P-glycoprotein on ondansetron disposition into the central nervous system

2.1 Introduction

Neuropathic pain is a complex chronic pain condition affecting 7-10% of the general population (23). For example, 60-70% of diabetic patients also suffer from peripheral neuropathy, and 30-40% of cancer patients receiving chemotherapeutic regimens may develop peripheral neuropathic symptoms (4). Available treatment options are often unable to meet the need of the patients, where the therapies either do not achieve sufficient pain relief, or produce intolerable adverse events (148, 149). Previous reports have demonstrated the potential utility of serotonin subtype receptor 3 (5-HT_3) antagonists for the treatment of neuropathic pain (84, 87). For example, in a spinal cord injury model in male Wistar rats a significant pain relief in the rats with increasing doses of intrathecal ondansetron (a 5-HT_3 receptor antagonist) was observed compared to control animals receiving no treatment (87).

Ondansetron is commonly used for treatment of postoperative nausea and vomiting and prevention of nausea/vomiting associated with emetogenic cancer therapies (56). Ondansetron has a strong binding to 5-HT_3 receptor (pK_i = 8.07), acts as a competitive antagonist to 5-HT_3 receptors, and has comparable potency to other 5-HT_3 receptor antagonist antiemetics (55, 150, 151). These drugs exert their pharmacologic effect through binding to the receptors in the chemoreceptor trigger zone in the area postrema, within the fourth ventricle of the brain, as well as peripheral locations such as the gastrointestinal tract (152-154). The blood-brain barrier (BBB) at the chemoreceptor trigger zone is incomplete (154), and therefore does not present a substantial barrier for ondansetron antiemetic action. However, when evaluating the therapeutic potential for ondansetron for neuropathic pain, understanding the factors that may impact achieving therapeutic concentrations at the site of action (in the CNS) becomes critical.

P-glycoprotein (Pgp), is expressed on the luminal membrane of brain endothelial cells, thereby limiting CNS penetration of numerous compounds (71). Using an LLC-PK1 cell culture expressing human MDR1, ondansetron was shown to be subject to Pgp efflux (71). Concentration of ondansetron in the brain of Pgp knock-out mice was 4-fold higher compared to wild type animals 30 minutes following intravenous (IV) injection of 0.2 mg/kg [^{14}C]ondansetron (71).

In humans, ondansetron is administered IV (usually 4-8 mg every 8 hours) and orally (up to 8 mg three times daily) with bioavailability of 50-87%. The volume of distribution in adults was reported as 1.9 L/kg. The drug is metabolized by CYP1A2, CYP2D6, and CYP3A4 enzymes, and the half-life in adults is 3-6 hours and can be prolonged to 20 hours in severe hepatic impairment patients (155). Sex-dependent pharmacokinetics has been reported in humans and rats, with females showing a higher exposure (74-76).

The main goal of this study was to evaluate the role of Pgp in limiting ondansetron exposure at different parts of the CNS (brain, spinal cord, and cerebrospinal fluid) using a genetic knockout rat model. An additional goal was to examine sex-dependent differences in plasma pharmacokinetics and CNS distribution. Mechanism-based pharmacokinetic model was constructed to quantify CNS disposition of ondansetron in all cohorts.

2.2 Materials and Methods

2.2.1 Materials

Ondansetron hydrochloride, *N*-benzylbenzamide, ethylenediaminetetraacetic acid tripotassium (K_3EDTA) were obtained from Sigma-Aldrich (St. Louis, MO, USA). Pooled male rat plasma and cerebrospinal fluid was purchased from BioIVT (Westbury, NY, USA). All solvents were of HPLC or higher grade and were purchased from Fisher Scientific (Fair Lawn, NJ, USA).

2.2.2 Animals

All animal studies were approved and conducted under guidelines of the Institutional Animal Care and Use Committee at Rutgers University. Wild-type Sprague-Dawley rats (WT) and P-glycoprotein knockout (KO) rats (Mdr1a(-/-), SD-Abcb1a^{tm1sage}) were purchased from Horizon Discovery (previously Sage Labs Inc., Boyertown, PA). Male WT and KO rats weighing 300-350 grams (10-12 weeks) and female WT and KO rats weighing 250-280 grams (12-14 weeks) were used in all studies. Animals were maintained in a vivarium with controlled temperatures and 12/12 hour dark and light cycle with free access to food and water. The jugular vein was cannulated to support intravenous drug administration and serial plasma sampling using polyethylene tubing (PE-50, Braintree Scientific, Braintree, MA) under light isoflurane anesthesia. After surgery, animals were allowed to recover for 24 hours and subcutaneous meloxicam and intradermal bupivacaine analgesia was provided.

2.2.3 Experimental design

For initial assessment of the effect of Pgp of plasma pharmacokinetics of ondansetron a single dose study with sequential blood sampling was conducted in male wild-type (WT-M) (n=3) and male Pgp knock-out (KO-M) (n=5) rats. Ondansetron (10 mg/kg, 10 mg/mL in water) was freshly prepared and administered intravenously through the jugular vein cannula followed by a saline flush (0.2 mL). Serial blood samples (300 µL) were collected at 0.25, 0.5, 0.75, 1, 1.5, 2, 2.5, 3, and 4 hours into EDTA tubes. Heparinized saline (20 IU/mL) was used for volume replacement after each sample. Plasma was separated by centrifugation (7 min, 13,000 RPM), transferred to a fresh tube, and stored in -20°C pending analysis.

Assessment of the effect of Pgp on CNS disposition of ondansetron was conducted next in male WT and KO animals. Animals previously used in the plasma pharmacokinetics study were used following a one-week washout period; and additional animals were included to achieve n=4-6 per time point. Freshly prepared ondansetron solution (10 mg/kg) was injected intravenously through the jugular vein cannula or through the tail vein. Animals were sacrificed at predetermined time points (0.16, 0.25, 0.5, 1, 1.5, 2, and 2.5 hours) under isoflurane anesthesia, and terminal

samples were collected including plasma, cerebrospinal fluid (CSF), brain, and spinal cord and stored at -20°C (other tissues were also preserved for future analysis).

The study was expanded to include female rat cohorts (wild-type female (WT-F), Pgp knock-out female (KO-F)) using terminal sampling approach (n=4-6 per time point) as described above.

2.2.4 Sample analysis

The approach for analysis of ondansetron in plasma and CSF was based on our published method (156) that was developed with slight modifications to previously reported assays (63, 157). Briefly, 100 μL of plasma or CSF were mixed with 10 μL of a N-benzylbenzamide (100 μg/mL in acetonitrile - internal standard) and 300 μL of an alkalizing agent (0.1M NaOH for plasma or saturated sodium carbonate solution for CSF). Methyl-*tert*-butyl-ether (3 mL) was used for extraction; samples were vortexed for 10 min and centrifuged for 5 min at 1900g at 4°C (5810R centrifuge, Eppendorf, Hauppauge, NY, USA). Organic layer was transferred into a new test tube, and samples were then evaporated to dryness under nitrogen (TurboVap, Biotage, Charlotte, NC, USA). The residue was reconstituted with 100 μL of acetonitrile in water (3:7, v/v). Samples were vortexed at high speed for 5 min and transferred into HPLC vials.

Tissue homogenization was performed using the Bullet Blender 5E Gold (NextAdvance, Troy, NY, USA). Whole tissues were thawed over ice and washed with phosphate-buffered saline (PBS 1X) three times, or until residual blood was washed off. Tissues were then blotted dry and weighed. PBS 1X solution was added in a 2:1 v/w ratio to the tissues, and the homogenizing beads were added in a 1:1 w/w ratio to tissues. Speed and duration of homogenization cycle was optimized following protocols published by NextAdvance for each tissue (158). Homogenate was transferred to a fresh tube and frozen at -20°C for future analysis.

For extraction of ondansetron from tissue homogenates, Agilent Bond Elut solid phase extraction (SPE) cartridges were used (Agilent Technologies, Santa Clara, CA, USA) with a vacuum manifold. Homogenate (100 μL) was mixed with a 10 μL N-benzylbenzamide (100 μg/mL in acetonitrile - internal standard) and methanol (100 μL) and vortexed for 20s, then centrifuged at 13,000 rpm for 3 minutes. The supernatant was loaded onto SPE cartridges (preconditioned

with 500 μL of methanol and equilibrated with 500 μL water). The column was first washed with 500 μL of 5% methanol in water, and the samples were eluted with two washes of 400 μL of methanol. Samples were evaporated to dryness under a stream of nitrogen gas. The residue was reconstituted with 100 μL of acetonitrile in water (3:7, v/v). Samples were vortexed at high speed for 5 min and transferred into HPLC vials.

Agilent 1260 Infinity HPLC (Santa Clara, CA, USA) equipped with a photodiode array detector was used in the study. The running conditions were based on our previously published method (156). Briefly, separation was achieved with a Phenomenex Gemini Twin Technology C18 column (particle size x length x diameter: 3 μm x 150 mm x 2 mm), protected by a SecurityGuard pre-column (Torrance, CA) maintained at 45°C. The mobile phase consisted of 5 mM ammonium acetate buffer (pH 4 adjusted with glacial acetic acid) and acetonitrile under gradient conditions that were published before (156), and the flow rate 0.6 mL/min. The injection volume was 40 μL. The detection wavelength was 310 nm and 275 nm with a retention time of 2.5 and 8.5 min for ondansetron and N-benzylbenzamide, respectively. The limit of detection was 10 ng/mL for plasma and 50 ng/mL for CNS tissues.

2.2.5 Data analysis

A standard noncompartmental analysis was performed using individual plasma concentration-time profiles in WT-M and KO-M rats. The area under the plasma concentration-time curve from time zero to infinity (AUC_{plasma}), half-life ($t_{1/2,plasma}$), mean residence time (MRT), systemic clearance (CL) and volume of distribution at steady state ($V_{d,ss}$) were calculated for each animal using Phoenix WinNonlin version 8.1 (Certara, Princeton, NJ) and reported as mean ± standard deviation (SD). Pharmacokinetic parameters were compared between WT-M and KO-M groups using t-test, and $p<0.05$ was considered significant.

For plasma profiles in WT-F and KO-F rats and for all tissue samples ondansetron concentration is reported as mean ± SD for each time point; and noncompartmental analysis was

conducted using naïve averaged data. For brain, spinal cord, and CSF the area under the tissue concentration-time curve (AUC_{tissue}) and tissue half-life ($t_{1/2,tissue}$) are reported.

To provide an overall assessment of the effect of Pgp status (WT or KO) on ondansetron exposure, an average fold increase in concentration for each tissue was calculated by taking a ratio between mean concentrations between KO and WT animals at each time point and calculating the mean and SD across all time points. Ondansetron partition coefficient (Kp) for each tissue was calculated using two approaches. The first method was based on the ratio between AUC_{tissue} (for brain, spinal cord, and CSF) and AUC_{plasma} for each of the cohorts (WT-M, KO-M, WT-F, KO-F). However, since the AUC values were based on terminal samples, no statistical comparison among the groups could be performed. To overcome this limitation, Kp for each tissue was also calculated based on a ratio of mean concentrations (between the CNS compartment and plasma) at each individual time points. Under the assumption that partition to the CNS is rapid and Kp remains constant over time, the mean (and SD) of ratios at all time points was computed. Statistical difference among cohorts was evaluated using a two-way ANOVA followed by Bonferroni's *post-hoc* test in Graphpad Prism (version 8, San Diego, CA).

2.2.6 Pharmacokinetic modeling

Semi-physiological pharmacokinetic model for describing ondansetron systemic disposition and distribution into various parts of the CNS was developed. Mean concentration time profiles for plasma, brain, spinal cord, and CSF were used. The model was first developed using data for male rats only and then evaluated for female rats. Initially WT-M and KO-M plasma datasets were used to construct systemic disposition model for ondansetron. Following IV administration ondansetron exhibited polyexponential plasma profiles; therefore, two- and three-compartment systemic disposition model with linear elimination were tested. Two-compartment model was able to satisfactorily describe the data, and inclusion of an additional peripheral compartment did not improve model fits. A semi-physiological CNS distribution model was developed using WT-M and

KO-M data in a step-wise approach beginning with the brain, followed by spinal cord, and CSF compartments. Initially, the parameters estimated for systemic disposition were fixed while CNS model was developed (under the assumption that the total amount of the drug in the CNS is minimal compared to the rest of the body).

Interconnectivity of CNS compartments followed animal physiology, and previously published CNS model were consulted (121, 140, 142). The volume of the brain (V_{brain}) was fixed to a previously reported value of 1.8 mL (159, 160), which was also in agreement with the brain weight measured in this study (**Table 2.1**). The volume of the CSF compartment (V_{CSF}) was fixed to 0.25 mL (160). The volume of the spinal cord (V_{spinal}) in rats has not been reported before and was fixed to 0.6 mL, based on measurements in this study (a density of 1 was assumed for all tissues, **Table 2.1**). Schematic of the final model is presented in **Figure 2.1** and all parameters are described in **Table 2.4**. All CNS compartments were directly connected to the central disposition compartment (with the volume V_1) with first-order rate constants (k_{13}, k_{31}, k_{14}, k_{41}, k_{15}, k_{51}) to describe a bidirectional passive permeability. Physiologically, the CSF and CNS extracellular fluid have areas for nutrient and compound exchange, therefore distributional terms between CSF and the brain, CSF and spinal cord were included (k_{35}, k_{53}, k_{45}, k_{54}) (93, 94). Pgp efflux at the BBB was described using a first-order term (k_{pgp}). Pgp efflux was previously shown to occur at the barrier between the blood and the spinal cord tissue, similar to the BBB; therefore, k_{Pgp} term was also included to describe Pgp efflux of ondansetron from the spinal compartment to plasma (161, 162). The following differential equations were used to describe the model:

$$\frac{dA_1}{dt} = k_{21} \cdot A_2 + k_{31} \cdot A_3 + k_{41} \cdot A_4 + k_{51} \cdot A_5 - (k_{el} + k_{12} + k_{13} + k_{14} + k_{15}) \cdot A_1 + k_{Pgp} \cdot A_3 + \\ + k_{Pgp} \cdot A_4 \quad (1)$$

$$\frac{dA_2}{dt} = k_{12} \cdot A_1 - k_{21} \cdot A_2 \quad (2)$$

$$\frac{dA_3}{dt} = k_{13} \cdot A_1 + k_{53} \cdot A_5 - \left(k_{31} + k_{35} + k_{Pgp}\right) \cdot A_3 \quad (3)$$

$$\frac{dA_4}{dt} = k_{14} \cdot A_1 + k_{54} \cdot A_5 - \left(k_{41} + k_{45} + k_{Pgp}\right) \cdot A_4 \quad (4)$$

$$\frac{dA_5}{dt} = k_{15} \cdot A_1 + k_{35} \cdot A_3 + k_{45} \cdot A_4 - (k_{51} + k_{53} + k_{54}) \cdot A_5 \quad (5)$$

where A1, A2, A3, A4, A5 represent the amount of ondansetron in the central, peripheral, brain, spinal cord, and CSF compartments. All parameters were shared between WT-M and KO-M datasets, except for k_{Pgp} term that was estimated for the WT-M and set equal to zero for the KO-M. During final model runs, all model parameters were estimated simultaneously using WT-M and KO-M data for plasma, brain, spinal cord, and CSF. At the next stage, the final model structure established for male animals was applied for female cohorts (WT-F and KO-F) and a separate set of parameters was estimated.

R (version 3.31) and Rstudio (version 1.2.5001, Boston, MA, USA) with Ubiquity package were used for model development and estimation of the parameters (163). Nelder-Mead Optimization method was used and a variance model was defined as: $VAR_i = \left(\sigma_1 \cdot \Upsilon(\theta, t_i)\right)^2$ where VAR_i is the variance of the *ith* data point, σ_1 is the variance model parameter, and $\Upsilon(\theta, t_i)$ is the *ith* estimated value from the pharmacokinetic model. The model performance was evaluated by visual inspection of the fitted curved, system convergence, Akaike Information Criterion, and objective function value.

2.3 Results

Plasma pharmacokinetics and disposition of ondansetron to various regions of the CNS was investigated in male and female WT and Pgp KO rats after IV administration of a single 10 mg/kg dose. Physiological measurements of the size of the brain and spinal cord was obtained and used

in pharmacokinetic model development (**Table 2.1**). Initially, the concentration of ondansetron in upper and lower parts of the spinal cord in WT-M and KO-M rats was determined separately. Interestingly, the concentrations were not statistically different, and a single concentration measurement was adopted for the rest of the study.

Observed concentration-time profiles of ondansetron in plasma of WT-M and KO-M rats were very similar (**Figure 2.2**). Results of the noncompartmental analysis of individual profiles are presented in **Table 2.2**. While the profiles were almost superimposable, and there was a statistically significant difference in $t_{1/2,plasma}$, and the rest of the parameters were similar. Observed concentration-time profiles of ondansetron in plasma of WT-F and KO-F rats were also superimposable. The results of the noncompartmental analysis of plasma naïve averaged data are presented in **Table 2.2**; and no statistical comparison could be conducted. Due to limitations in the limit of detection for ondansetron in the CNS, plasma pharmacokinetic study in female rats and tissue disposition study in both male and female rats were not conducted beyond 2.5 hours. Comparison of noncompartmental parameters between WT-M and WT-F cohorts showed that $V_{d,ss}$ and CL were higher in female rats, similar to previous reports (74, 75).

CNS tissue disposition study showed that in both male and female rats Pgp genetic knockout resulted in significantly higher concentrations of ondansetron in all tested regions of the CNS at most of the time points (**Figures 2.2 and 2.3**). The mean ratio of the concentrations between KO and WT animals was 2.39-5.48, depending on the region of the CNS (**Table 2.3**). Partition coefficients calculated based on the AUC were less than 1 for brain and spinal cord in WT animals and were increased to 1.38-3.92 in KO rats. Partition coefficient for CSF was lower than partition to the brain or spinal cord.

Kp values calculated based on ratio of AUCs could not be used to evaluate statistical significance of differences among study groups (due to the fact that naïve averaged data were used). Under

the assumption that partition to the CNS is rapid and Kp remains constant over time, mean Kp were also calculated based on ratio of concentrations (between CNS compartments and plasma) at each individual time points (**Table 2.3**). Statistical comparison of these Kp values for all study groups and all CNS compartments in shown in **Figure 2.4**.

Comparison of pharmacokinetic profiles between male and female rats for WT and KO strains is shown in **Figure 2.5**. For plasma, brain and CSF the profiles were similar; however, for the spinal cord the concentrations in males were mostly higher compared to female rats of both strains.

Semi-physiological pharmacokinetic model was successfully developed to simultaneously describe plasma pharmacokinetics and CNS disposition of ondansetron. The final model included two compartments to describe systemic disposition and three physiological CNS compartments (i.e., brain, spinal cord, and CSF) – **Figure 2.1**. All CNS compartments were connected to the central distribution compartment with bidirectional exchange processes. In addition, in WT animals the model included Pgp-mediated efflux from brain and spinal cord compartments. The rest of the parameters were shared between WT and KO strains; and parameter estimation was performed separately for male and female rats. The final model provided good simultaneous description of all 4 tested tissues (plasma, spinal cord, brain, and CSF) in WT and KO strains for male (**Figure 2.2**) and female (**Figure 2.3**) rats. In the final model, for simplicity and to improve the precision of parameter estimated the rate constant for exchange between CSF and brain and CSF and spinal cord compartments were set to be equal ($k_{35}=k_{45}$ and $k_{53}=k_{54}$). All parameters were estimated with sufficient precision (**Table 2.4**).

2.4 Discussion

Neuropathic pain is a debilitating condition affecting a large population and therapeutic options are quite limited. Antagonism of $5HT_3$ receptors is a promising approach for treatment of neuropathy, and direct delivery of $5HT_3$ receptor antagonists to the site of action was shown to

be efficacious (50, 87). However, the results of several small clinical studies were contradictory (84, 85). Pgp is a known factor affecting drug pharmacokinetics and especially permeability to the CNS; furthermore, Pgp genetic polymorphism in humans is known to affect drug efficacy and pharmacokinetics (71, 117, 164). We hypothesized that polymorphism in Pgp expression and the extent of Pgp-mediated efflux from the CNS in various patients may have contributed to contradictory outcomes of clinical trials with $5HT_3$ receptor antagonists. Since a direct assessment of CNS disposition of drugs in humans is rarely feasible, in this preclinical study we performed a mechanistic assessment of the role of Pgp in exposure of various regions of the CNS to ondansetron using a genetic Pgp knockout rat model.

Pharmacokinetics of other Pgp substrates (loperamide, paclitaxel) was previously shown to be altered in these Pgp KO rats (165, 166). Pgp KO mice and rats have been shown to provide comparable results in brain disposition studies (167). The availability of KO rat models offers an important advantage over KO mice by allowing for a significantly larger size of biological specimens, which facilitates bioanalytics. In this study, we found that Pgp KO has not significantly affected plasma pharmacokinetics of ondansetron, as plasma profiles in KO rats overlapped with profiles in both male and female WT animals (**Figures 2.2 and 2.3**). Our findings support a previous report in which no difference was detected in plasma concentrations 30 min after IV administration of 0.2 mg/kg ondansetron in wild-type and mdr1a KO mice (71, 117). In contrast, concentration of ondansetron in all tested CNS regions in Pgp KO rats was increased in average by 2.4-5.5-fold compared with WT animals (**Figures 2.2, 2.3, 2.4 and Table 2.3**). These data are in line with a previously reported 4-fold increase in ondansetron concentration in the brain of Pgp KO mice compared to WT (only a single time point data were available (71).

Differences in plasma pharmacokinetics of ondansetron have been reported between sexes in both rats and humans (74, 75). Plasma AUC was 23% lower in male rats following intravenous dose of 8 mg/kg (p<0.05) (74). In a clinical study, women were observed to have

consistently higher AUC values after dosing of an oral or two suppository formulations ($p < 0.05$) (76). In this study, we found almost no difference in plasma profiles of ondansetron between sexes (**Figure 2.5**); although, there was a slight trend for lower initial concentrations and higher concentrations at later time points. The differences are reflected in noncompartmental parameters (**Table 2.2**). The lack of a more significant differences compared to previously published results may be related to the experimental design (a shorter time frame of sample collection and terminal sampling). From the CNS data, only the spinal cord concentrations were substantially higher in male rats **Figure 2.5**). Overall, all male and female data could not be reliable fitted simultaneously using a shared set of parameters; therefore, parameters estimation was performed separately (**Table 2.4**). Information comparing Pgp expression or other physiological differences at the level of BBB between males and females could not be found in the literature; and sex-dependent differences in CNS disposition of $5HT_3$ receptor antagonists should further investigated in the future.

In this study we evaluated ondansetron disposition into three different regions of the CNS. Partitioning into the spinal cord is usually not considered in pharmacokinetic analysis; and CNS disposition studies and CNS pharmacokinetic modeling (empirical, semi-physiological, or physiologically-based) are primarily focused on the brain and sometimes include the CSF (121, 140, 168). Only a single example including the spinal cord into a population pharmacokinetic model to describe an antisense oligonucleotide in a multi-compartmental CNS model could be found in the literature (104). Ondansetron can bind to $5\text{-}HT_3$ receptors expressed in the brain and the spinal cord; and understanding the exposure in the spinal cord disposition is required to ultimately connect the pharmacokinetics to ondansetron efficacy in neuropathic pain studies. Ondansetron concentrations were showed to be similar in the upper and the lower part of the same spinal cord (to the best of our knowledge, such data have not been reported before). In this study, we showed that total ondansetron exposure (AUC_{tissue}) is different in various CNS matrices

(highest in the brain, and lowest in the CSF). Pgp KO increased ondansetron concentration in all CNS regions; however, the magnitude of the effect was dependent on the region. Importantly, using CSF values for quantitative assessment may underestimate the role of Pgp on drug exposure in the brain or the spinal cord. These findings are important for translational research because CSF samples can often be used as a surrogate matrix to evaluate overall CNS drug disposition in humans (120, 169). CSF can be relatively ease sampled through cisterna magna puncture in preclinical species and through lumbar punctures or catheter implantations in the clinic (169). We have previously reported CSF ondansetron partition coefficient of 0.15 in a population pharmacokinetic analysis in human study ((170), **see chapter 4**), which is similar to a value for CSF partition found in this study (**Table 2.3**).

An important goal of the work was to construct a semi-physiological pharmacokinetic model to quantitatively described the role of Pgp efflux on ondansetron exposure in the CNS. The final model successfully captured the time-course of ondansetron in plasma, brain, spinal cord CSF, and all parameters (except for K_{Pgp}) could be shared between WT and KO animals. Model parameters were estimated with sufficient precision, and separate sets were needed for male and female rats. Alternative structural models were evaluated during data analysis, including models with a unidirectional transfer from the brain to the CSF or division of brain and/or spinal cord into two subcompartment. For example, models that included a “deep-tissue” compartment in the brain had been reported (168, 171). None of these models were able to provide superior data description based on model evaluation criteria. Development of models with additional tissue subcompartment will necessitate data with a higher special resolution (for example, brain microdialysis). While several physiological models focusing on the CNS were published before, they mostly focused on the brain and the CSF (121, 140). The weight of the rat spinal cord is reported in this study (**Table 2.1**). However, another important physiological value required for a

full physiologically-based model – the blood flow for the spinal cord – was not available in the literature, and this should be addressed in future studies.

2.5 Conclusion

In conclusion, the study provided important quantitative information on the role of Pgp in limiting ondansetron exposure in various regions of the CNS using data from WT and Pgp KO rats. Male and female animals demonstrated slight difference in ondansetron plasma pharmacokinetics and CNS disposition. Semi-physiological model was developed and successfully captured the data in all tissues in all study groups. Proposed modeling framework could serve as the base to further analysis of the potential use of Pgp inhibitors in enhancing delivery of $5HT_3$ receptor antagonists to the CNS.

Table 2.1 Weight of brain and spinal cord in male and female wild type and Pgp knockout rats (mean (SD), n=10)

	Brain				**Spinal Cord**			
	WT-M	KO-M	WT-F	KO-F	WT-M	KO-M	WT-F	KO-F
Tissue weight (g)	1.79 (0.17)	1.86 (0.13)	1.59 (0.15)	1.70 (0.13)	0.571 (0.07)	0.583 (0.08)	0.640 (0.06)	0.615 (0.08)

Table 2.2 Noncompartmental plasma pharmacokinetic parameters for ondansetron following IV dosing of 10 mg/kg (mean and (SD), if available)

	Male		Female*	
Parameter	**Wild-type**	**Knock-out**	**Wild-type**	**Knock-out**
$t_{1/2,plasma}$ (h)	0.52 (0.01)	0.65 (0.04)	0.54	0.64
$AUC_{plasma,0-\infty}$ ($h \cdot \mu g \cdot mL^{-1}$)	3.83 (0.64)	3.70 (0.49)	2.52	2.57
MRT (h)	0.47 (0.04)	0.47 (0.10)	0.76	0.72
$V_{d,ss}$ (mL)	417 (98)	422 (124)	802	766
CL ($mL \cdot h^{-1}$)	869 (132)	892 (120)	1050	1029

***** In female rats, concentrations were obtained from terminal sampling; therefore, individual profiles were not available, and SD could not be calculated.

Table 2.3 Noncompartmental pharmacokinetic parameters for ondansetron following IV dosing of 10 mg/kg for brain, spinal cord, and cerebrospinal fluid

	Brain				**Spinal Cord**				**CSF**			
Parameter	WT-M	KO-M	WT-F	KO-F	WT-M	KO-M	WT-F	KO-F	WT-M	KO-M	WT-F	KO-F
$t_{1/2,tissue}$ (h)	0.57	0.44	0.55	0.55	0.65	0.66	0.65	0.62	0.588	0.507	0.777	0.784
$AUC_{tissue,0-\infty}$ ($h \cdot \mu g \cdot mL^{-1}$)	2.64	14.5	2.0	8.89	1.54	6.8	1.18	3.55	0.289	1.31	0.270	0.672
$K_{P,AUC}$	0.689	3.92	0.794	3.46	0.402	1.83	0.468	1.38	0.075	0.354	0.107	0.261
$K_{p,concentration}$, mean (SD)	1.75 (1.2)	5.17 (1.5)	0.761 (0.3)	3.56 (1.1)	1.11 (0.4)	3.62 (1.3)	0.524 (0.3)	2.43 (0.9)	0.273 (0.3)	0.328 (0.1)	0.139 (0.09)	0.283 (0.35)
Average ratio of KO/WT concentrations, mean (SD)	5.48 (1.7)		4.37 (0.6)		4.52 (1.5)		3.61 (1.4)		2.91 (1.3)		2.39 (0.7)	

Table 2.4 Final model estimated parameters for plasma pharmacokinetics and CNS disposition of ondansetron in male and female wild-type and Pgp knock-out rats

			Male		Female		
Parameter	**Parameter Description**	**Unit**	**Estimate**	**CV%**	**Estimate**	**CV%**	
V_1	Central volume of distribution	mL	14.7	10	19.5	6	
k_{el}	Systemic elimination rate constant	h^{-1}	4.88	16	2.42	10	
k_{12}	Distribution rate constants to/from peripheral distribution compartment	h^{-1}	3.23	29	1.22	22	
k_{21}		h^{-1}	2.46	11	1.10	18	
k_{13}	Distribution rate constants to/from brain compartment	h^{-1}	43.5	29	3.94	20	
k_{31}		h^{-1}	75.0	29	14.7	22	
k_{14}	Distribution rate constants to/from spinal cord compartment	h^{-1}	22.7	29	0.941	19	
k_{41}		h^{-1}	131	30	21.1	18	
k_{15}	Distribution rate constants to/from CSF compartment	h^{-1}	0.122	32	0.171	23	
k_{15}		h^{-1}	47.1	61	36.7	63	
$k_{35}=k_{45}$	Rate constant for brain/spinal cord and CSF exchange	h^{-1}	0.450	25	0.814	26	
$k_{53}=k_{54}$		h^{-1}	26.8	42	57.4	13	
k_{Pgp}	Rate constant for Pgp-mediated efflux from the CNS	h^{-1}	168	32	45.0	22	
V_{brain}	Brain volume	mL	1.8*	-	1.8*	-	
V_{spinal}	Spinal volume	mL	0.6*	-	0.6*	-	
V_{CSF}	CSF volume	mL	0.25*	-	0.25*	-	
var_P	Variance		0.05	18	0.03	19	

* Parameters were fixed to physiological values

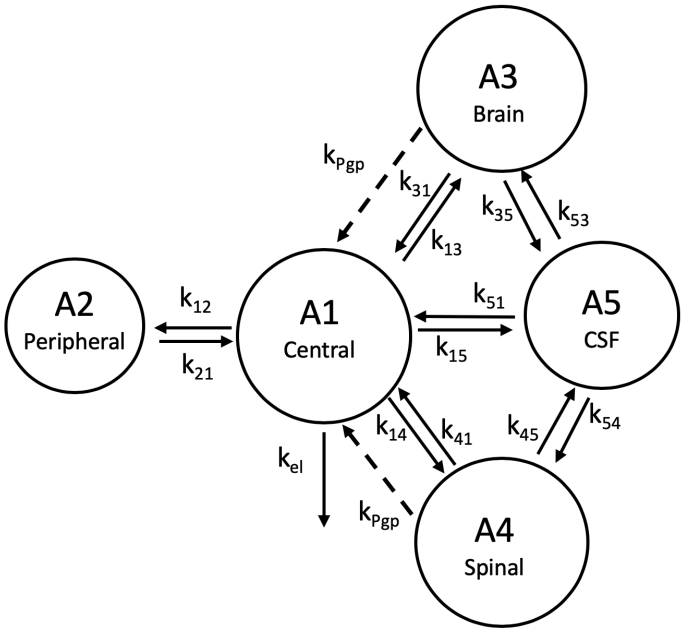

Figure 2.1 Schematic of the semi-physiological pharmacokinetic model used to capture systemic disposition and CNS distribution of ondansetron in male and female wild type and Pgp knockout rats. Model equations and parameters are described in Methods and Table 2.4. k_{Pgp} was included only for wild type animals.

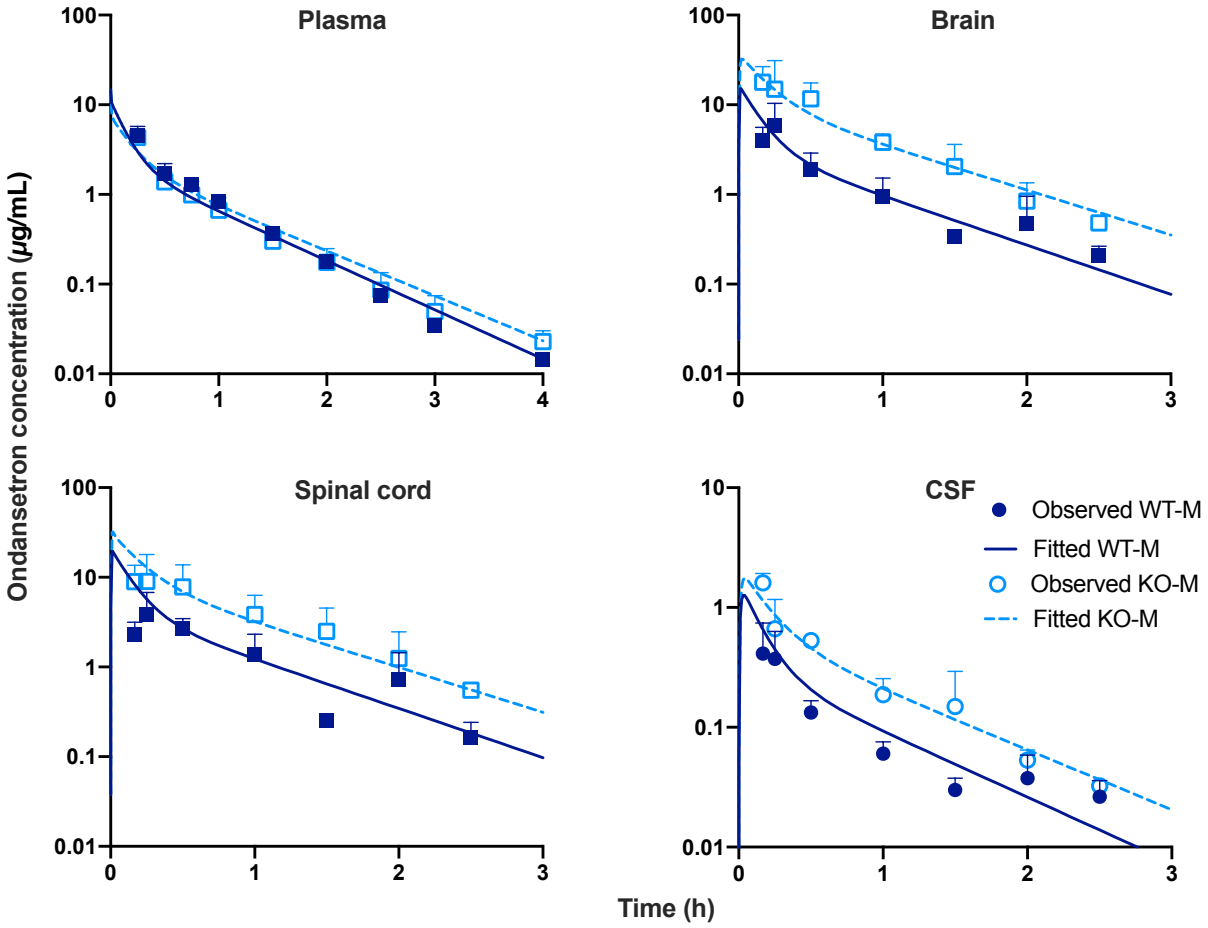

Figure 2.2 The observed and fitted pharmacokinetic profiles for male WT and KO animals following IV bolus 10mg/kg dose of ondansetron. The observed (symbol) for wild-type (filled) and Pgp knock-out (open) are overlaid with the model fitted profile for wild-type (solid line) and Pgp KO (broken line).

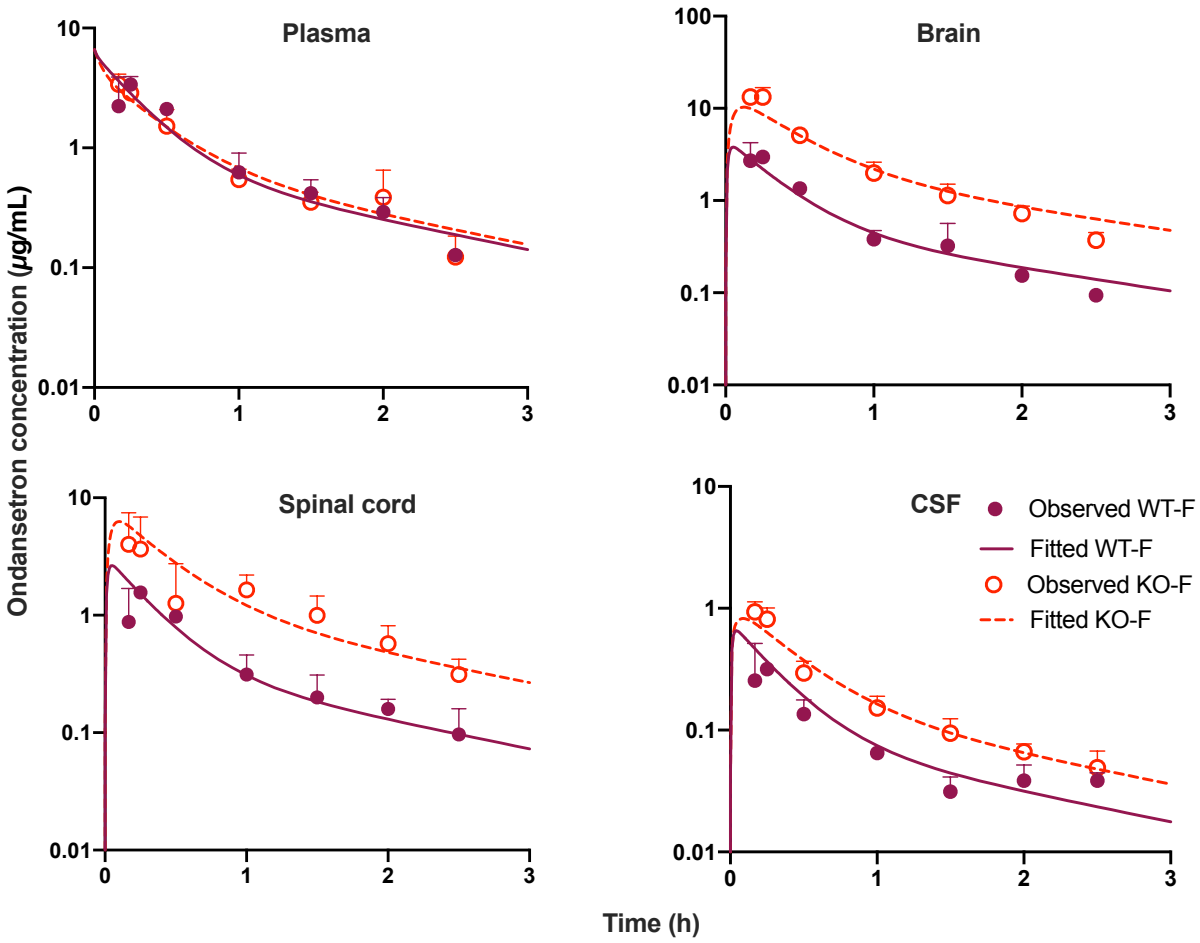

Figure 2.3 The observed and fitted pharmacokinetic profiles for female WT and KO animals following IV bolus 10mg/kg dose of ondansetron. The observed (symbol) for wild-type (filled) and Pgp knock-out (open) are overlaid with the model fitted profile for wild-type (solid line) and Pgp KO (broken line).

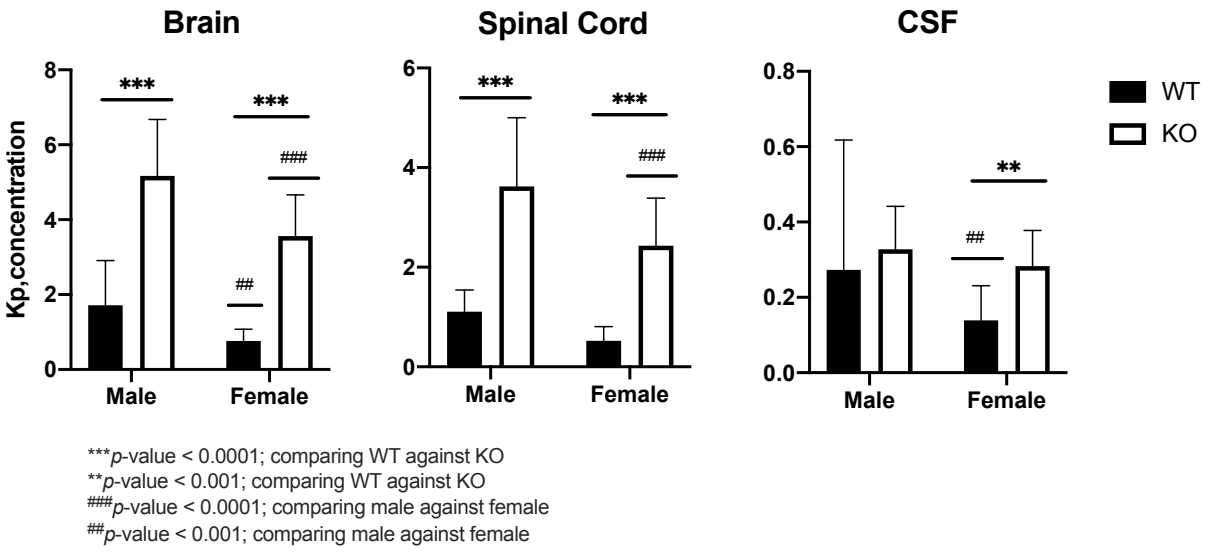

Figure 2.4 The K_P values for brain, spinal cord, and CSF plotted to compare statistical differences amongst the four experimental groups. A 2-way ANOVA with Bonferroni's *post-hoc* test was performed to compare the effect of Pgp and sex on ondansetron partition into different regions of the CNS.

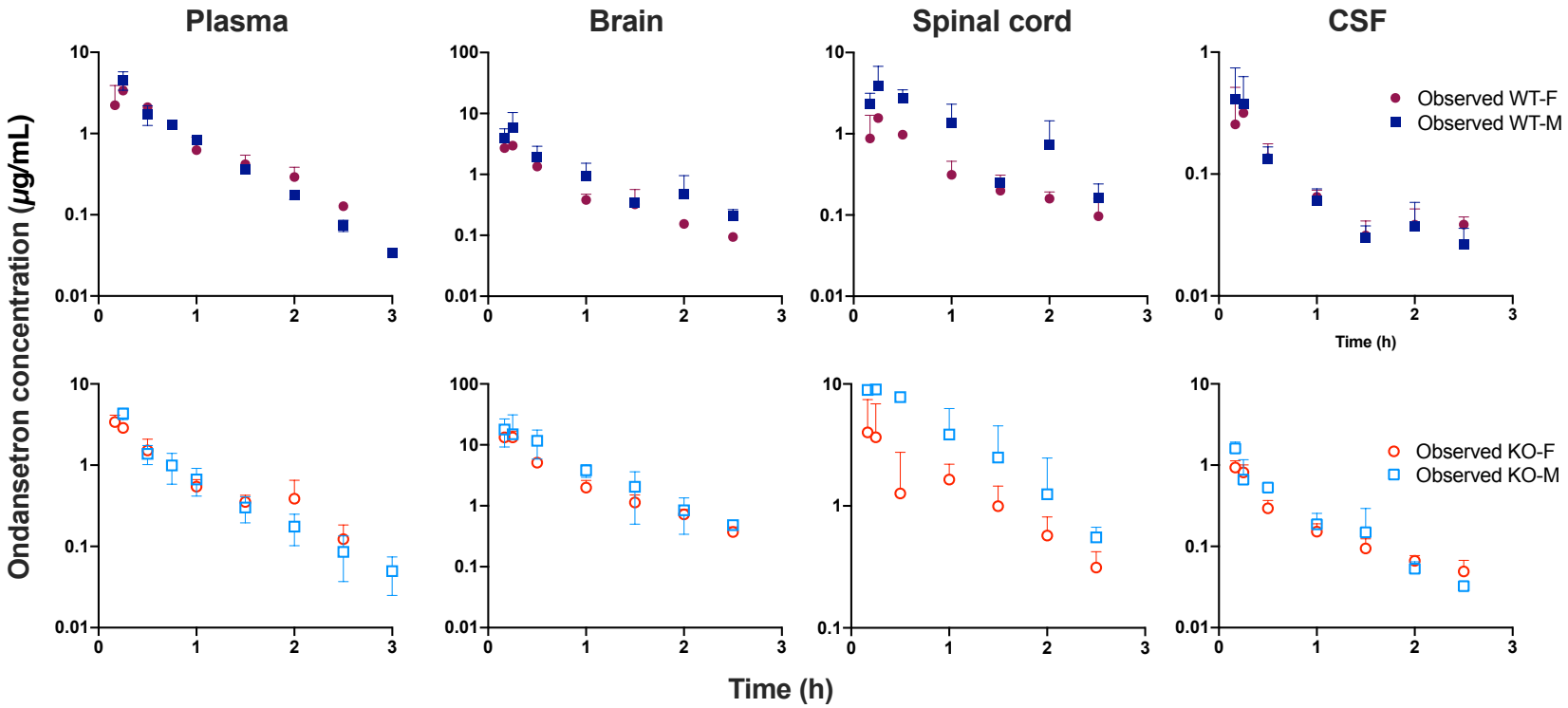

Figure 2.5 The observed pharmacokinetic profiles for WT and KO animals following IV bolus 10mg/kg dose of ondansetron. The observed (symbol) for wild-type (filled) and Pgp knock-out (open) are plotted.

Chapter 3 Pharmacokinetic modeling of the effect of tariquidar on ondansetron disposition into the central nervous system

3.1 Introduction

Neuropathic pain is characterized by a lesion- or disease-related change in nociceptive signal transmission or processing in the nervous system (1). This may affect the central nervous system, with changes to the brain or spinal somatosensory pathways, or the peripheral nervous system where sensory fibers carrying nociceptive information have altered electrical properties (1). The spinal cord acts as the main site of signal integration, where ascending and descending pathways from cortical regions process and modulate the excitation and inhibition activity of incoming signals from peripheral afferent fibers (1). Research has been done to understand how each control mechanism may behave, under normal conditions and in the context of neuropathic pain development (1, 42).

The serotonergic pathway offers a descending control pathway, shown to have both inhibitory and excitatory properties (42). Under neuropathic conditions, an increase in excitatory activity has been shown through the activity of the serotonin receptor subtype 3 (5-HT_3) receptors in the spinal cord (48-50). Additional evidence also links accelerated turnover of serotonin (5-HT) in the spinal cord (51, 52). Interest in the administration of 5-HT_3 receptor antagonists to treat neuropathic pain has grown, with both preclinical and clinical reports investigating the pain relief potential of ondansetron, a 5-HT_3 receptor antagonists commonly used for antiemetic treatment. Intrathecal administration of ondansetron in a neuropathic animal model demonstrated a dose-dependent improvement in pain relief (87). However, previously published clinical reports have been inconclusive, with some studies reporting effective pain relief following a single IV dose of 8mg ondansetron, while others report no pain improvement compared to placebo (84, 85) The

inconclusive clinical reports may be related to insufficient drug exposure at the target (i.e., spinal 5-HT_3 receptors) rather than ineffective pharmacological approach.

Achieving sufficient drug concentrations in the central nervous system (CNS) is crucial for therapeutic efficacy. Active efflux of Pgp at the blood-brain barrier (BBB) has shown a significant impact in limiting CNS exposure to a wide range of compounds (71, 117). Specific inhibitors to Pgp have been evaluated following co-administration to achieve target concentrations at the site of action (172, 173). Tariquidar is a more specific third-generation Pgp inhibitor that has demonstrated potent inhibitory activity (nM IC_{50}) and affinity to Pgp (K_D = 5.1 nM) (174-176).

Ondansetron is subject to P-glycoprotein (Pgp) efflux at BBB, which limits its penetration into the CNS. In our previous study, Pgp knock-out rats demonstrated significantly higher exposure of ondansetron in brain, spinal cord, and cerebrospinal fluid, compared to wild-type rats when administered a single IV bolus dose of ondansetron (10 mg/kg). However, the plasma concentrations did not differ between wild-type and Pgp knock-out rats (**see Chapter 2**). These findings are corroborated by another report (71). Furthermore, differences in plasma pharmacokinetics have been documented for ondansetron, with females displaying increased exposure following oral and intravenous dosing in preclinical and clinical reports (74, 75).

The main goal of this study was to evaluate the impact of tariquidar administration in limiting ondansetron exposure at different regions of the CNS (brain, spinal cord, and cerebrospinal fluid) in a wild-type rat model. The results built upon previously obtained studies using a genetic knockout rat model. An additional goal was to evaluate sex-dependent differences in Pgp inhibition by tariquidar affecting ondansetron plasma pharmacokinetics and CNS disposition. A mechanism-based pharmacokinetic model was developed to quantify plasma and CNS disposition of ondansetron in all cohorts.

3.2 Materials and Methods

3.2.1 Materials

Ondansetron hydrochloride, *N*-benzylbenzamide, ethylenediaminetetraacetic acid tripotassium (K_3EDTA) were obtained from Sigma-Aldrich (St. Louis, MO, USA). Tariquidar was obtained from Azatrius Pharmaceuticals (Mumbai, India). Pooled rat plasma and cerebrospinal fluid (CSF) was purchased from BioIVT (Westbury, NY, USA). All solvents utilized for the experiments were purchased as HPLC grade or higher from Fisher Scientific (Fair Lawn, NJ, USA).

3.2.2 Animals

All animal experiments were approved and conducted under the guidelines of Rutgers University Institutional Animal Care and Use Committee. Wild-type male Sprague Dawley rats (10-12 weeks, 300-350 grams) and wild-type female Sprague Dawley rats (12-14 weeks, 250-280 grams) were purchased from Horizon Discovery (previously Sage Labs Inc., Boyertown, PA). Animals were maintained in a vivarium with controlled temperatures and 12/12 hour dark and light cycle with free access to food and water. The jugular vein was cannulated to support intravenous drug administration using polyethylene tubing (PE-50, Braintree Scientific, Braintree, MA) under light isoflurane anesthesia. After surgery, animals were allowed to recover for 24 hours and subcutaneous meloxicam and intradermal bupivacaine analgesia was provided.

3.2.3 Experimental Design

For initial assessment of the effect of tariquidar on plasma pharmacokinetics of ondansetron, a single dose study with sequential blood sampling was conducted in male (OT-M) (n=2) and female (OT-F) (n=2) rats. Ondansetron (10mg/kg, 10 mg/mL in water) and tariquidar (7.5 mg/kg, 5 mg/mL in 2% aqueous dextran (g/v) solution) were freshly prepared and administered through the jugular vein cannula followed by a saline flush (0.2 mL). Tariquidar formulation preparation and dose selection followed a previous preclinical report (177), and it was administered 30 minutes prior to ondansetron. Following ondansetron drug administration, serial blood samples (250 µL) were collected at 5, 10, 15, 30, 45 min, 1, 1.5, 2, 2.5, 3, and 4 hours into

EDTA tubes. Heparinized saline (20 IU/mL) was used for volume replacement after each sample. Plasma was separated by centrifugation (7 min, 13,000 RPM), transferred to a fresh tube, and stored in -20°C pending analysis.

Assessment of the effect of Pgp inhibition using tariquidar on CNS disposition of ondansetron was conducted in male and female rats. Animals previously used in the plasma pharmacokinetics study were included following a two-week washout period; and additional animals were used to achieve n=4-6 per time point. Tariquidar solution (7.5 mg/kg) followed after 30 minutes by ondansetron solution (10 mg/kg) were injected intravenously through the jugular vein cannula or through the tail vein. Animals were sacrificed at predetermined time points (0.16, 0.25, 0.5, 1, 1.5, 2, and 2.5 hours) under isoflurane anesthesia, and terminal samples were collected including plasma, cerebrospinal fluid (CSF), brain, and spinal cord and stored at -20°C (other tissues were also preserved for future analysis).

3.2.4 Sample Analysis

The approach for analysis of ondansetron and tariquidar in plasma and CSF was based on our published method (178). Briefly, 100 μL of plasma or CSF were mixed with 10 μL of a N-benzylbenzamide (100 μg/mL in acetonitrile - internal standard) and 300 μL of an alkalizing agent (0.1M NaOH for plasma or saturated sodium carbonate solution for CSF). Methyl-*tert*-butyl-ether (3 mL) was used for extraction; samples were vortexed for 10 min and centrifuged for 5 min at 1900g at 4°C (5810R centrifuge, Eppendorf, Hauppauge, NY, USA). Organic layer was transferred into a new test tube, and samples were then evaporated to dryness under nitrogen (TurboVap, Biotage, Charlotte, NC, USA). The residue was reconstituted with 100 μL of acetonitrile in water (3:7, v/v). Samples were vortexed at high speed for 5 min and transferred into HPLC vials.

Tissue homogenization was performed using the Bullet Blender 5E Gold (NextAdvance, Troy, NY, USA). Whole tissues were thawed over ice and washed with phosphate-buffered saline (PBS 1X) three times, or until residual blood was washed off. Tissues were then blotted dry and

weighed. PBS 1X solution was added in a 2:1 v/w ratio to the tissues, and the homogenizing beads were added in a 1:1 w/w ratio to tissues. Speed and duration of homogenization cycle was optimized following protocols published by NextAdvance for each tissue (158). Homogenate was transferred to a fresh tube and frozen at -20°C for future analysis.

For extraction of ondansetron from tissue homogenates, Agilent Bond Elut solid phase extraction (SPE) cartridges were used (Agilent Technologies, Santa Clara, CA, USA) with a vacuum manifold. Homogenate (100 μL) was mixed with a 10 μL N-benzylbenzamide (100 μg/mL in acetonitrile - internal standard) and methanol (100 μL) and vortexed for 20s, then centrifuged at 13,000 rpm for 3 minutes. The supernatant was loaded onto SPE cartridges (preconditioned with 500 μL of methanol and equilibrated with 500 μL water). The column was first washed with 500 μL of 5% methanol in water, and the samples were eluted with two washes of 400 μL of methanol. Samples were evaporated to dryness under a stream of nitrogen gas. The residue was reconstituted with 100 μL of acetonitrile in water (3:7, v/v). Samples were vortexed at high speed for 5 min and transferred into HPLC vials.

Agilent 1260 Infinity HPLC (Santa Clara, CA, USA) equipped with a photodiode array detector was used in the study. The running conditions were based on our previously published method (178). Briefly, separation was achieved with a Phenomenex Gemini Twin Technology C18 column (particle size x length x diameter: 3 μm x 150 mm x 2 mm), protected by a SecurityGuard pre-column (Torrance, CA) maintained at 45°C. The mobile phase consisted of 5 mM ammonium acetate buffer (pH 4 adjusted with glacial acetic acid) and acetonitrile under gradient conditions that were published before (178), and the flow rate 0.6 mL/min. The injection volume was 40 μL. The detection wavelength was 310 nm for ondansetron and 275 nm for N-benzylbenzamide and tariquidar. The retention time was 2.5 min, 8.5, and 9.0 min for ondansetron, N-benzylbenzamide and tariquidar respectively. The limit of detection was for

ondansetron 10 ng/mL for plasma and 50 ng/mL for CNS tissues. The limit of detection for tariquidar was 50 ng/mL for plasma and CSF and 100 ng/mL for brain and spinal cord samples.

3.2.5 Data Analysis

Ondansetron and tariquidar concentrations in plasma and all tissues are reported as mean ± SD for each time point. Data analysis was performed separately for male (OT-M) and female (OT-F) rat groups. Furthermore, ondansetron concentration in plasma and tissues (and corresponding pharmacokinetic parameters) were compared to the results or our previous study, in which ondansetron was administered alone as a 10 mg/kg single intravenous bolus to male and female wild type (WT-M, WT-F) and Pgp knockout (KO-M, KO-F) animals (**see Chapter 2**). A standard noncompartmental analysis was performed using average plasma concentration-time data (samples obtained from sequential and terminal experiments were combined). The area under the plasma concentration-time curve from time zero to infinity (AUC_{plasma}), half-life ($t_{1/2,plasma}$), mean residence time (MRT), systemic clearance (CL) and volume of distribution at steady state ($V_{d,ss}$) were calculated using Phoenix WinNonlin version 8.1 (Certara, Princeton, NJ). For all tissue concentration-time profiles noncompartmental analysis was conducted using naïve averaged data. For brain, spinal cord, and CSF the area under the tissue concentration-time curve (AUC_{tissue}) and tissue half-life ($t_{1/2,tissue}$) are reported.

To provide an overall assessment of the effect of Pgp inhibition on ondansetron exposure, an average fold increase in concentration for each tissue was calculated by taking a ratio between mean concentrations between OT-M/F (from this study) and WT-M/F or KO-M/F (from a previous study) animals at each time point and calculating the mean and SD across all time points. Ondansetron partition coefficient (Kp) for each tissue was calculated using two approaches. The first method was based on the ratio between AUC_{tissue} (for brain, spinal cord, and CSF) and AUC_{plasma} for each of the cohorts (OT-M, OT-F). However, since the AUC values were based on terminal samples, no statistical comparison among the groups could be performed. To overcome

this limitation, Kp for each tissue was also calculated based on a ratio of mean concentrations (between the CNS compartment and plasma) at each individual time points. Under the assumption that partition to the CNS is rapid and Kp remains constant over time, the mean (and SD) of ratios at all time points was computed. Statistical difference among cohorts was evaluated using a standard two-way ANOVA followed by Bonferonni's *post-hoc* test to compare the average $K_{P,concentration}$ of all groups against each other in Graphpad Prism version 8 (San Diego, CA).

3.2.6 Pharmacokinetic modeling

Semi-physiological pharmacokinetic structural model developed previously to describe ondansetron systemic disposition and distribution into various parts of the CNS in wild-type and Pgp knock-out rats was adopted for this analysis (see **Chapter 2**). A schematic of the model is presented in **Figure 3.1** and all parameters are described in **Table 3.3**. In this model, systemic disposition of ondansetron is described by a central (A_1) and peripheral (A_2) distribution compartments and a linear elimination process (k_{el}). Interconnectivity of CNS compartments followed animal physiology, and previously published CNS model were consulted (121, 140, 142). The volume of the brain (V_{brain}) was fixed to a previously determined value of 1.8 mL which was also in agreement with the brain weight measured published in our previous study (159, 160). The volume of the CSF compartment (V_{CSF}) was fixed to 0.25 mL (160). The volume of the spinal cord (V_{spinal}) was measured and reported in our previous study, and was fixed to 0.6 mL. All CNS compartments were directly connected to the central disposition compartment (with the volume V_1) with first-order rate constants (k_{13}, k_{31}, k_{14}, k_{41}, k_{15}, k_{51}) to describe a bidirectional passive permeability, and distributional terms between CSF and the brain, CSF and spinal cord were included (k_{35}, k_{53}, k_{45}, k_{54}). Pgp efflux at the BBB was described using a first-order term (k_{pgp}) and was included for wild type animals only; the term was set to zero in KO rats. The following differential equations (1-5) were used to describe the model:

$$\frac{dA_1}{dt} = k_{21} \cdot A_2 + k_{31} \cdot A_3 + k_{41} \cdot A_4 + k_{51} \cdot A_5 - (k_{el} + k_{12} + k_{13} + k_{14} + k_{15}) \cdot A_1 + k_{Pgp} \cdot A_3 + + k_{Pgp} \cdot A_4 \quad (1)$$

$$\frac{dA_2}{dt} = k_{12} \cdot A_1 - k_{21} \cdot A_2 \quad (2)$$

$$\frac{dA_3}{dt} = k_{13} \cdot A_1 + k_{53} \cdot A_5 - \left(k_{31} + k_{35} + k_{Pgp}\right) \cdot A_3 \quad (3)$$

$$\frac{dA_4}{dt} = k_{14} \cdot A_1 + k_{54} \cdot A_5 - \left(k_{41} + k_{45} + k_{Pgp}\right) \cdot A_4 \quad (4)$$

$$\frac{dA_5}{dt} = k_{15} \cdot A_1 + k_{35} \cdot A_3 + k_{45} \cdot A_4 - (k_{51} + k_{53} + k_{54}) \cdot A_5 \quad (5)$$

where A1, A2, A3, A4, A5 represent the amount of ondansetron in the central, peripheral, brain, spinal cord, and CSF compartments.

The whole dataset included ondansetron profiles of OT-M and OT-F in plasma, brain, spinal cord, and CSF obtained in this study and previous data for male and female WT and KO animals. Mean concentration time profiles for plasma, brain, spinal cord, and CSF were used. The model was first developed using data for male rats only and then evaluated for female rats. Due to changes in the plasma pharmacokinetics of ondansetron following co-administration of tariquidar separate terms for central volume of distribution($V_{1,TQR}$) and elimination rate constant ($k_{el,TQR}$) were required to capture the data. Several functions to describe tariquidar-induced Pgp inhibition were considered. However, due to a long half-life of tariquidar observed in the study there was not enough information in the dataset to capture tariquidar concentration-dependent inhibition. The final model included and a separate term for describing Pgp function in OT groups ($k_{Pgp,TQR}$). The rest of the parameters were shared across WT, KO, and OT models. All model parameters were estimated simultaneously using WT-M, KO-M, and OT-M data for plasma, brain, spinal cord, and CSF. At the next stage, the final model structure established for male animals was applied for female cohorts (WT-F, KO-F, OT-F) and a separate set of parameters was estimated.

Following establishing the final model, simulations were performed to assess the effect of the extent of Pgp inhibition on ondansetron exposure in the CNS. The value of K_{Pgp} was adjusted and the rest of the parameters were kept fixed to the previously estimated values (for either WT or OT groups).

R (version 3.31) and Rstudio (version 1.2.5001, Boston, MA, USA) with Ubiquity package were used for model development and estimation of the parameters (163). Nelder-Mead Optimization method was used and a variance model was defined as: $VAR_i = \left(\sigma_1 \cdot \Upsilon(\theta, t_i)\right)^2$ where VAR_i is the variance of the *ith* data point, σ_1 is the variance model parameter, and $\Upsilon(\theta, t_i)$ is the *ith* estimated value from the pharmacokinetic model. The model performance was evaluated by visual inspection of the fitted curved, system convergence, Akaike Information Criterion, and objective function value.

3.3 Results

The effect of Pgp inhibition following tariquidar administration (7.5 mg/kg) on the plasma and CNS disposition of ondansetron was investigated in wild-type male and female rats after a single ondansetron dose of 10 mg/kg. The observed concentration-time profiles of ondansetron in plasma of OT-M and OT-F were plotted with previously obtained results in WT-M, KO-M and WT-F, KO-F animals. For both OT-M and OT-F, ondansetron plasma concentration was increased when compared to WT and KO animals (**Figures 3.2 and 3.3**). The results of the noncompartmental analysis of plasma data are presented in **Table 3.1**; and no statistical comparison could be conducted. The full PK study was conducted until 2.5 hours due to the limitations of the bioanalytical limit of detection for ondansetron in the CNS. Comparison of noncompartmental parameters between OT-M and OT-F cohorts showed similarities between the two groups with plasma AUC of 6.13 and 5.65 h $\cdot\mu g \cdot mL^{-1}$ respectively. These values were nearly double of what was found in WT-M/KO-M, and WT-F/KOM (**See Table 2.2**).

The CNS tissue disposition study revealed that male and female animals co-administered with tariquidar showed higher concentrations of ondansetron in all tested regions of the CNS across as compared to both WT rat (administered ondansetron alone) and KO strain (**Figure 3.2 and 3.3**). The mean ratio of concentrations comparing OT and WT animals was 4.22-13.4, depending on the region of the CNS (**Table 3.2**). The partition coefficients calculated based on AUC for brain and spinal cord were more than 1, calculated as 2.8-4.15. The calculated partition coefficient for CSF was lower than those found in the brain or spinal cord (**Table 3.2**).

The K_P values calculated by the ratio of AUCs could not be used for evaluating statistical significance or differences among study groups since the values are based on naïve averaged values. The K_P term calculated based on the ratio of concentrations (between CNS tissue and plasma) at each individual time points (**Table 3.2**). This approach assumed that the partitioning of ondansetron into the CNS is rapid, and that the K_P remains constant over time. Statistical comparison of these $K_{P,concentration}$ values for all study groups and all CNS compartments are shown in **Figure 3.4**.

A comparison of pharmacokinetic profiles between male and female rats is shown in **Figure 3.5**. The observed OT-M and OT-F profiles are nearly super-imposed for plasma, brain, spinal cord, and CSF compartments.

Previously developed semi-physiological structural pharmacokinetic model (**Figure 3.1**) was adopted to simultaneously describe plasma pharmacokinetics and CNS disposition of ondansetron in WT, KO, and OT groups. In the model, Pgp-mediated transport was only included as an efflux process from the brain and spinal cord compartments to the central distribution compartment. This model structure was supported by the fact that WT and Pgp KO groups did not show any significant difference in ondansetron plasma pharmacokinetics (**see Chapter 2**). In this study, concentration of ondansetron was higher and the half-life was longer after co-

administration of ondansetron with tariquidar compared to both WT and KO groups (**Figures 3.2 and 3.3**). The reason for these changes is not completely understood; however, it can be hypothesized that they were not related to the effect of tariquidar on Pgp, because in animals lacking Pgp (KO groups) no such change was observed. To overcome this, separate terms for central volume of distribution ($V_{1,TQR}$) and elimination rate constant ($k_{el,TQR}$) were required to capture the data in OT groups. In the final model a separate term for describing Pgp function in OT groups ($k_{Pgp,TQR}$) was estimated; and the value was several orders of magnitude lower compared to WT rats, which indicates an almost complete inhibition of Pgp-mediated transport.

The rest of the parameters were shared between WT, KO, and OT strains; and parameters were estimated separately for male and female rats. The final model provided good simultaneous description of all 4 tested tissues (plasma, spinal cord, brain, and CSF) in WT, KO, and OT groups for male (**Figure 3.2**) and female (**Figure 3.3**) rats, and all parameters were estimated with sufficient precision (**Table 3.3**).

Simulations were conducted to assess the effect of the extent of Pgp inhibition on ondansetron exposure in the CNS. The effect of tariquidar on plasma pharmacokinetics of ondansetron was considered independent of Pgp function. Two sets of simulations were performed using parameters for either WT or OT groups. The value of k_{Pgp} estimated for WT group was decreased by 50% or 90%. **Figure 3.6** shows simulated profiles for ondansetron exposure in brain and spinal cord in male rats: panels A and B – simulations with parameters for WT; and panels C and D simulations with parameters for OT group. Model fits for WT, KO, and OT are shown for comparison. For example, 1 h after ondansetron dose, 50% and 90% of Pgp inhibition would result in 1.5- and 3-fold higher concentration in the brain on male rats; and 1.2- and 2-fold in the spinal cord, respectively.

Tariquidar concentrations were also measured in all collected samples (**Figure 3.7**). Relatively high variability between the animals was observed, and no sex-dependent trends in pharmacokinetics could be identified. Tariquidar could be detected in any of the CSF samples with an established method and the limit of quantification. The half-life of tariquidar in plasma was in 3.1 h male and 2.2 h in female rats; similar long half-lives were observed in the CNS. Concentration in the brain was 2-3-fold higher than in plasma and exposure in the spinal cord was comparable to plasma. Due to the fact that tariquidar concentration did not vary significantly over the time course of ondansetron pharmacokinetic experiment, presence of tariquidar was treated as a categorical covariate in the ondansetron pharmacokinetic model.

3.4 Discussion

In a previous work, we have shown that ondansetron distribution to various parts of the CNS is affected by a genetic knockout of Pgp transporter (**see Chapter 2**). In this work, we evaluated the utility of co-administering ondansetron with tariquidar (a third generation Pgp inhibitor) in wild type animals to enhance exposure of the CNS to ondansetron. In both male and female rats, tariquidar demonstrated effective inhibition of Pgp efflux; and ondansetron disposition to the CNS tissues was significantly increased compared to wild-type animals receiving ondansetron alone (**Figures 3.2 and 3.3**). The extent of tariquidar effect at the level of CNS was comparable to the effect of genetic knock out of the Pgp transporter. Interestingly, the plasma disposition was also altered when ondansetron was co-administered with tariquidar (as discussed below). Semi-physiological model (**Figure 3.1**) successfully captured plasma and all CNS tissue profiles simultaneously in OT groups (from this study) and WT and KO groups (from Chapter 2), and all parameters were estimated with sufficient precision. Observed data and modeling suggest that complete inhibition of Pgp and the CNS was obtained with tariquidar (**Figures 3.2 and 3.3 and Table 3.3**). We also showed that tariquidar concentrations in plasma, brain, and spinal cord do not significantly change during the course of the experiment (**Figure 3.6**); this trend was also observed in our previous

work ((178), see **Appendix 1**). Due to this prolonged half-life of tariquidar, a sigmoid inhibitory function that was originally proposed for describing Pgp inhibition in OT groups or the use of brain/spinal cord tariquidar concentration could not be included in the model; and the final model incorporated tariquidar administration as a categorical covariate. Simulations were performed to assess potential effect of a partial Pgp inhibition on ondansetron partition to the brain and spinal cord (**Figure 3.7**), and this can be further evaluated in future studies.

In this proof of concept study, a relatively high dose of tariquidar was used with a purpose to demonstrate the maximum potential enhancement in CNS distribution of ondansetron in comparison to ondansetron injected alone. Previously, a complete inhibition of Pgp was reported 30 min after intravenous injection of tariquidar doses above 6 mg/kg (177). A dose of 15 mg/kg was used in several preclinical reports evaluating Pgp inhibition by tariquidar; therefore, we initially tried to used a 15 mg/kg dose of tariquidar administered 30 min before ondansetron (10 mg/kg) in our study (141, 177). However, this dose level of tariquidar led to toxicity (fatal seizure-like symptoms) in male and female rats immediately after ondansetron injection. The toxicity was not observed before administration of ondansetron. Decreasing tariquidar dose to 7.5 mg/kg allowed for eliminating this toxicity, and this dose level was selected for future experiments.

Co-administration of ondansetron (10 mg/kg) with tariquidar to wild type rats resulted in almost doubled plasma ondansetron concentration in comparison to ondansetron administered alone to wild-type (and Pgp KO) rats. Previously, we observed a similar phenomenon when administering ondansetron intravenously (5 mg/kg) with tariquidar (15 mg/kg) in which case the plasma concentration of ondansetron was very similar to ondansetron 10 mg/kg injected alone (compare **Figure 2.2** in Chapter 2 and pharmacokinetic figure in **Appendix 1**). Due to the fact that concentrations of ondansetron in OT groups were higher than in KO groups (lacking Pgp), it could be hypothesized that this finding is not directly related to inhibition of Pgp by tariquidar and that some other tariquidar-induced changes are occurring. The effect on plasma disposition of

drugs due to co-administration of tariquidar has been reported before (179-181). For example, significantly higher plasma $AUC_{0-\infty}$ and lower CL was observed for intravenous ciprofloxacin (7 mg/kg) in male Wistar rats co-administered with 15 mg/kg of tariquidar (179). On the other hand, the effect of tariquidar on plasma pharmacokinetics was not observed for loperamide or in another study with ciprofloxacin (182, 183). Another a relatively selective third generation Pgp inhibitor, elacridar, was later shown to affect cytochrome P450 enzymes (184). Separate parameters for ondansetron elimination ($k_{el,TQR}$) and central volume of distribution ($V_{1,TQR}$) were required to capture plasma profiles in OT groups. Overall, experimental results of this study (also supported by modeling) suggest that a higher CNS exposure to ondansetron in OT groups relative to KO groups is potentially related to a higher ondansetron exposure in the plasma that drives partitioning to the CNS.

Previous works reported sex-dependent differences in plasma disposition of ondansetron between males and females, both preclinically and clinically (74, 75). In our previous work (**Chapter 2**), we found some sex-dependent differences in ondansetron pharmacokinetics and CNS disposition in both WT and Pgp KO rats. In this study, a more pronounced difference was observed between OT and WT/KO in female rats in plasma and in CNS profiles. It is currently not clear whether these differences are observed due to Pgp-related or proposed Pgp-not related effects of tariquidar on ondansetron pharmacokinetics.

3.5 Conclusion

In conclusion, the study provided important quantitative information on the role of Pgp in limiting ondansetron exposure in various regions of the CNS using tariquidar (a Pgp inhibitor) in wild type rats. The results showed that tariquidar at 7.5 mg/kg resulted in a complete inhibition of Pgp efflux of ondansetron in brain and spinal cord. Our results also highlighted the effect of tariquidar on plasma disposition for ondansetron, which may not be dependent on Pgp inhibition (this should be further evaluated in future studies). A semi-physiological model successfully captured

pharmacokinetics of ondansetron in wild type and Pgp KO animals receiving the drug alone or in wild type animals receiving ondansetron and tariquidar combination. Our work provides a basis for utilizing tariquidar to evaluate enhanced CNS disposition of ondansetron using Pgp inhibition in the clinic to achieve therapeutic drug concentrations that may provide successful treatment of neuropathic pain.

Table 3.1 Noncompartmental plasma pharmacokinetic parameters for ondansetron following co-administration IV of ondansetron (10 mg/kg) and tariquidar (7.5 mg/kg)

Parameter	OT-M	OT-F
$t_{1/2,plasma}$ (h)	0.638	0.998
$AUC_{\mathbf{plasma},0-\infty}$ (h ·μg·mL^{-1})	6.13	5.65
MRT (h)	0.577	0.919
$V_{d,ss}$ (mL)	302	396
CL (mL·h^{-1})	525	447

Table 3.2 Noncompartmental pharmacokinetic parameters for ondansetron in brain, spinal cord and cerebrospinal fluid following co-administration IV of ondansetron (10 mg/kg) and tariquidar (7.5 mg/kg)

	Brain		**Spinal Cord**		**CSF**	
Parameter	OT-M	OT-F	OT-M	OT-F	OT-M	OT-F
$t_{1/2,tissue}$ (h)	0.580	0.352	0.907	0.596	0.517	0.580
$AUC_{tissue,0-\infty}$ ($h \cdot \mu g \cdot mL^{-1}$)	22.0	19.16	15.0	15.6	1.37	1.49
$K_{P,AUC}$	3.58	3.39	2.44	2.76	0.223	0.263
$K_{P,concentration}$ mean (SD)	5.88 (5.8)	4.08 (2.4)	4.72 (2.8)	4.02 (2.6)	0.363 (0.16)	0.344 (0.27)
Average ratio of OT/WT concentrations Mean (SD)	6.98 (5.6)	7.92 (4.2)	9.82 (3.5)	13.4 (4.9)	4.22 (2.6)	6.07 (2.4)
Average ratio of KO/WT concentrations, mean (SD)	5.48 (1.7)	4.37 (0.6)	4.52 (1.5)	3.61 (1.4)	2.91 (1.3)	2.39 (0.7)

Table 3.3 Final model estimated parameters for plasma pharmacokinetics and CNS disposition of ondansetron male and female wild-type and Pgp knock-out rats following administration of ondansetron alone and male and female wild-type rats following co-administration of ondansetron with tariquidar

			Male		Female	
Parameter	**Parameter Description**	**Unit**	**Estimate**	**CV%**	**Estimate**	**CV%**
V_1	Central volume of distribution	mL	17.5	6	13.3	7
$V_{1,TQR}$	Central volume of distribution	mL	12.7	6	11.3	7
k_{el}	Systemic elimination rate constant	h^{-1}	3.60	9	5.06	11
$k_{el,TQR}$	Systemic elimination rate constant for OT animals	h^{-1}	3.38	9	3.02	11
k_{12}	Distribution rate constants to/from peripheral distribution compartment	h^{-1}	2.14	22	4.37	19
k_{21}		h^{-1}	2.62	9	2.32	10
k_{13}	Distribution rate constants to/from brain compartment	h^{-1}	17.6	16	13.0	14
k_{31}		h^{-1}	39.6	16	25.2	18
k_{14}	Distribution rate constants to/from spinal cord compartment	h^{-1}	9.37	18	3.60	17
k_{41}		h^{-1}	71.0	18	31.5	22
k_{15}	Distribution rate constants to/from CSF compartment	h^{-1}	0.081	29	0.518	17
k_{15}		h^{-1}	6.84	64	47.3	25
$k_{35=45}$	Rate constant for brain/spinal cord and CSF exchange	h^{-1}	0.928	21	0.914	18
$k_{53=54}$		h^{-1}	66.6	16	79.9	15
k_{Pgp}	Rate constant for Pgp-mediated efflux from the CNS	h^{-1}	81.9	16	101	19
$k_{Pgp,TQR}$	Rate constant for Pgp-mediated efflux from the CNS for OT animals	h^{-1}	0.002	11	0.0001	59
V_{brain}	Brain volume	mL	1.8*	-	1.8*	-
V_{spinal}	Spinal volume	mL	0.6*	-	0.6*	-
V_{CSF}	CSF volume	mL	0.25*	-	0.25*	-
var_P	Variance		0.05	18	0.03	19

*: Fixed parameters

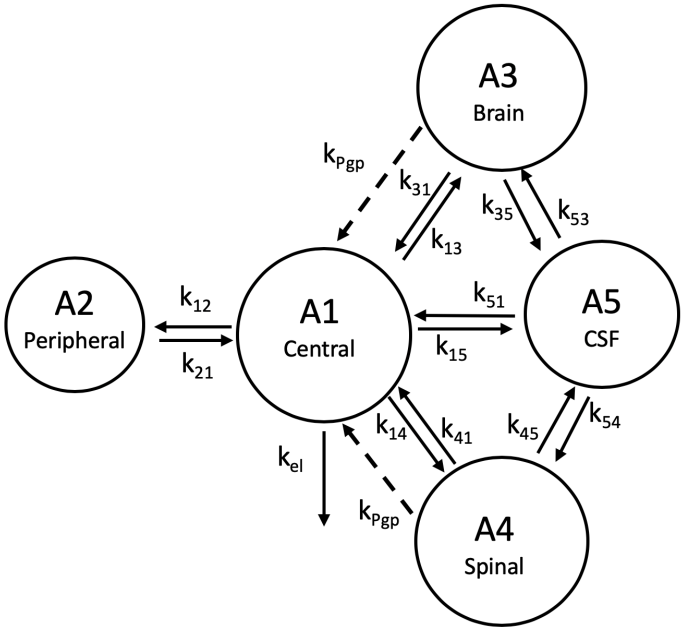

Figure 3.1 Schematic of the semi-physiological pharmacokinetic model used to capture systemic disposition and CNS distribution of ondansetron in male and female wild type and Pgp knockout rats after administration of ondansetron alone and in wild type rats following co-dosing with tariquidar. Model equations and parameters are described in Methods and Table 3.1. k_{Pgp} was included only for wild type animals.

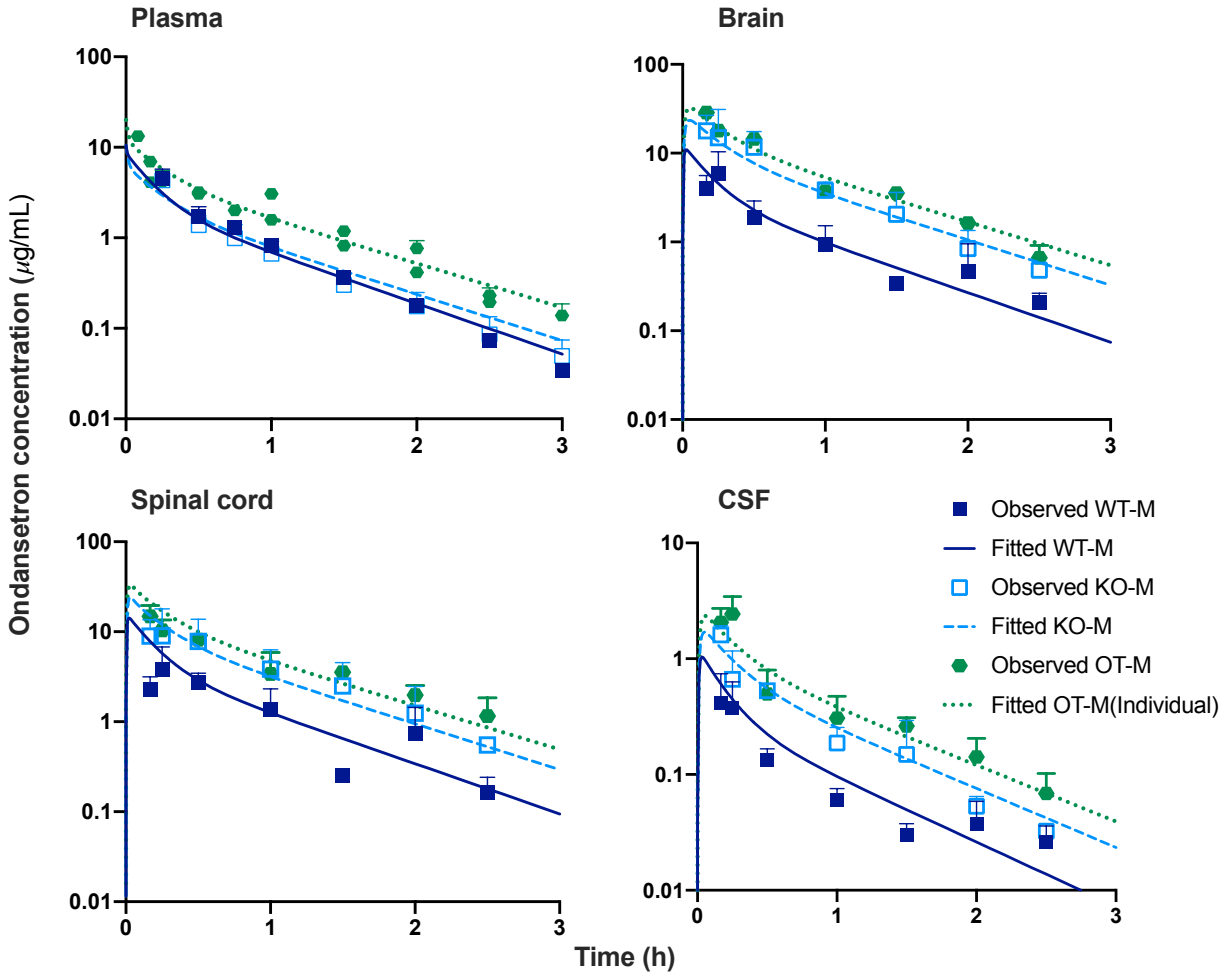

Figure 3.2 The observed (symbol) and fitted (line) pharmacokinetic profiles for male WT (filled square) and KO (open square) animals following IV bolus 10 mg/kg dose of ondansetron and male OT (filled hexagon) animals co-administration of ondansetron (10 mg/kg) and tariquidar (7.5 mg/kg) IV bolus.

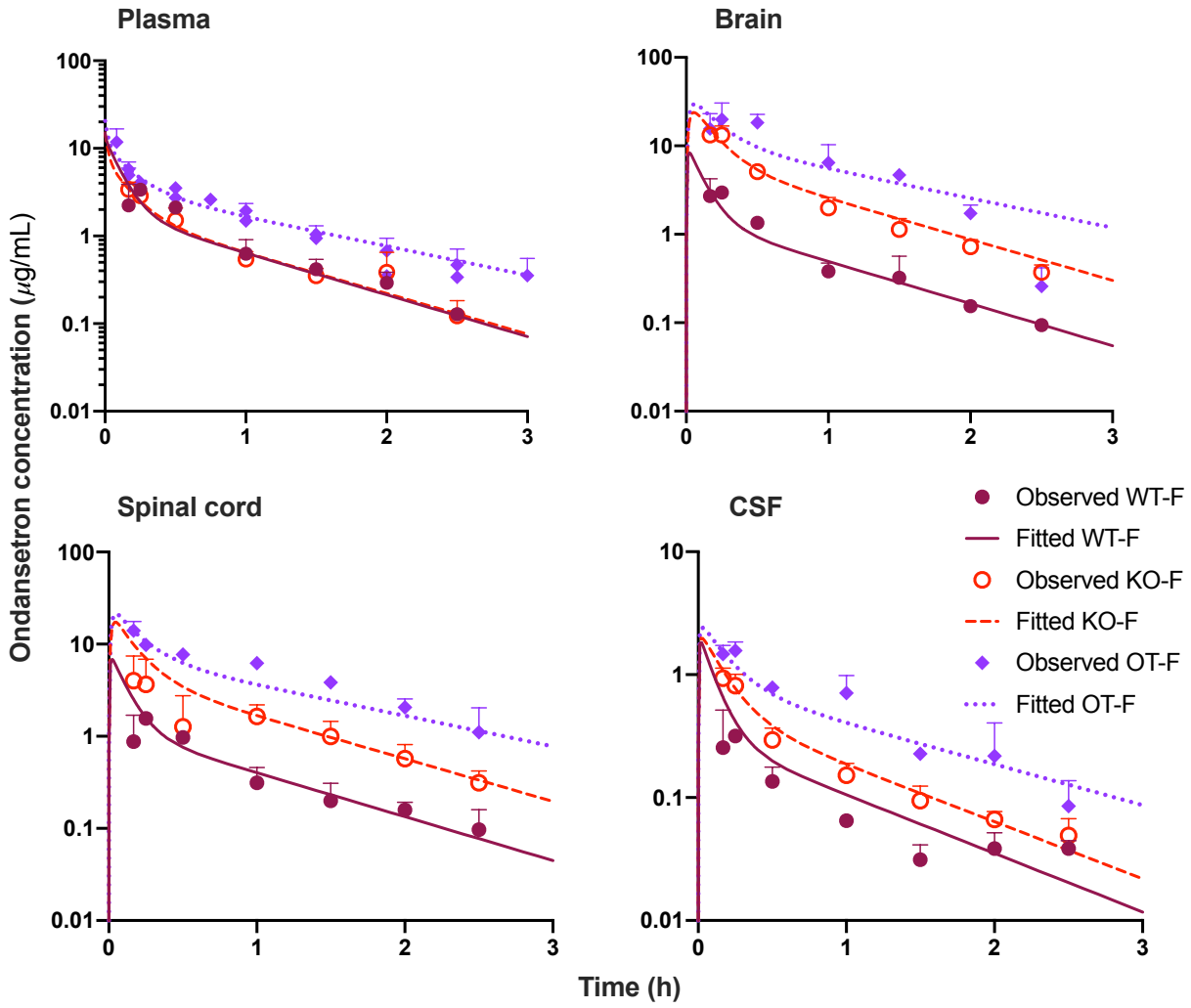

Figure 3.3 The observed (symbol) and fitted (line) pharmacokinetic profiles for female WT (filled circle) and KO (open circle) animals following IV bolus 10 mg/kg dose of ondansetron and female OT (filled diamond) animals co-administration of ondansetron (10 mg/kg) and tariquidar (7.5 mg/kg) IV bolus.

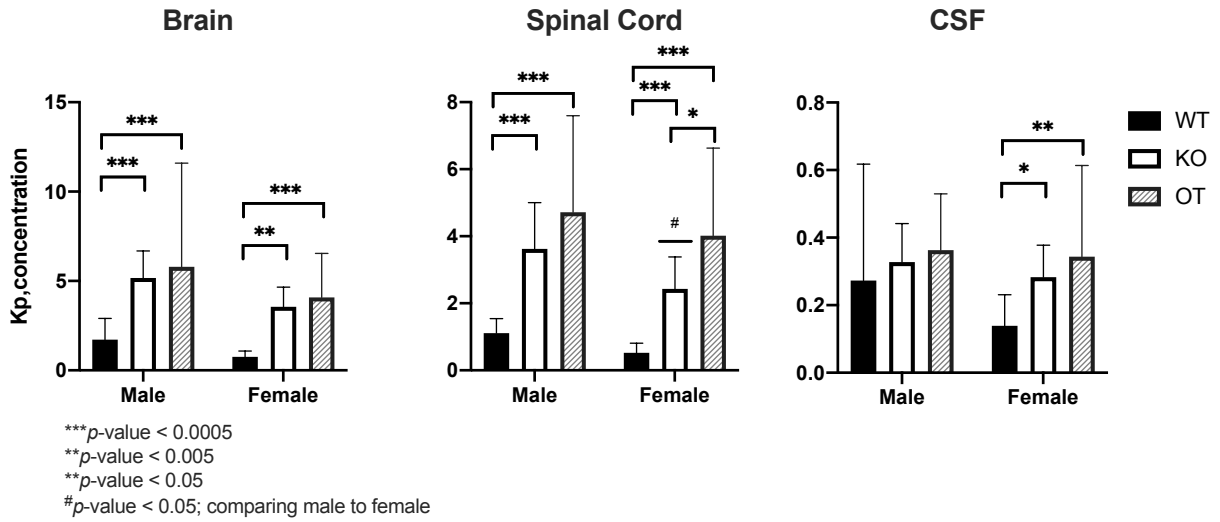

Figure 3.4 The K_P values for brain, spinal cord, and CSF plotted to compare statistical differences amongst the six experimental groups. A 2-way ANOVA with Bonferroni's *post-hoc* test was performed to compare the effect of Pgp and sex on ondansetron partition into different regions of the CNS.

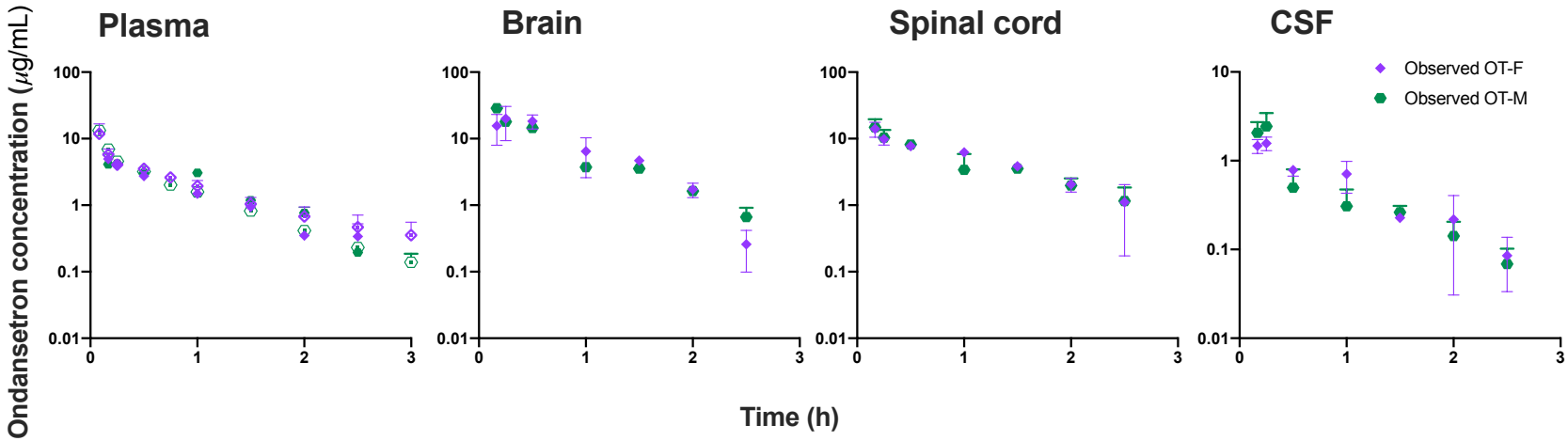

Figure 3.5 The observed pharmacokinetic profiles for OT-M and OT-F animals following IV bolus 10mg/kg dose of ondansetron co-administered with 7.5 mg/kg tariquidar. The observed (symbol) for OT-M (filled hexagon) and OT-F (filled diamond) are overlaid with the plot.

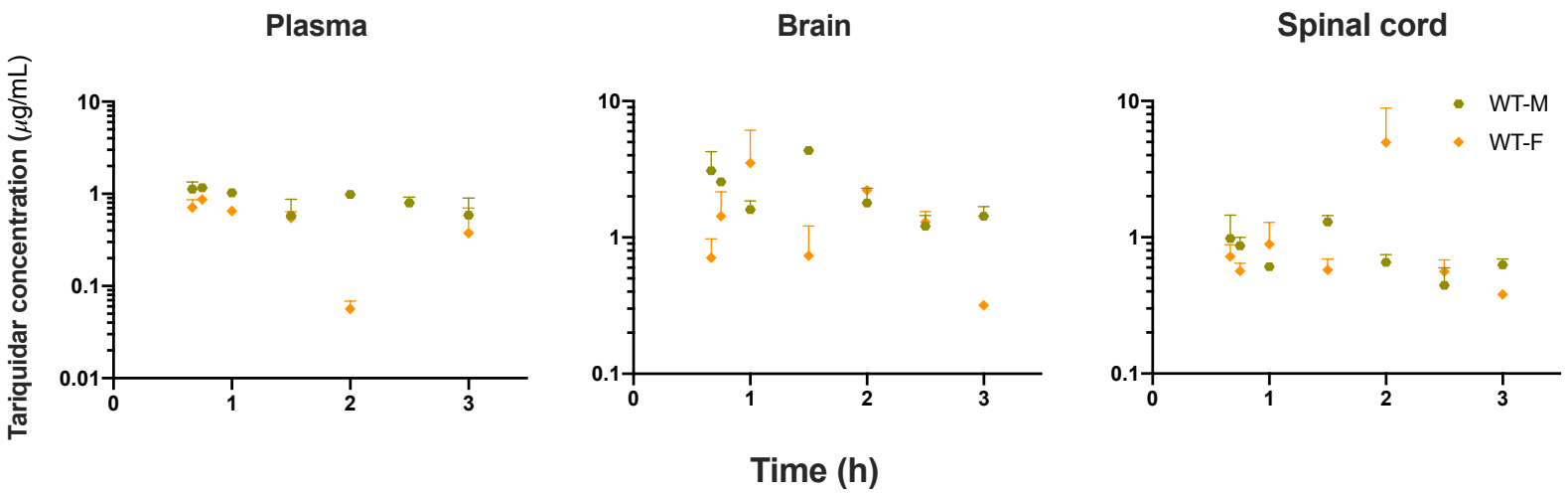

Figure 3.6 Observed tariquidar concentrations in plasma, brain and spinal cord following IV administration of 7.5 mg/kg to OT-M (filled hexagon) and OT-F (filled diamond) rats.

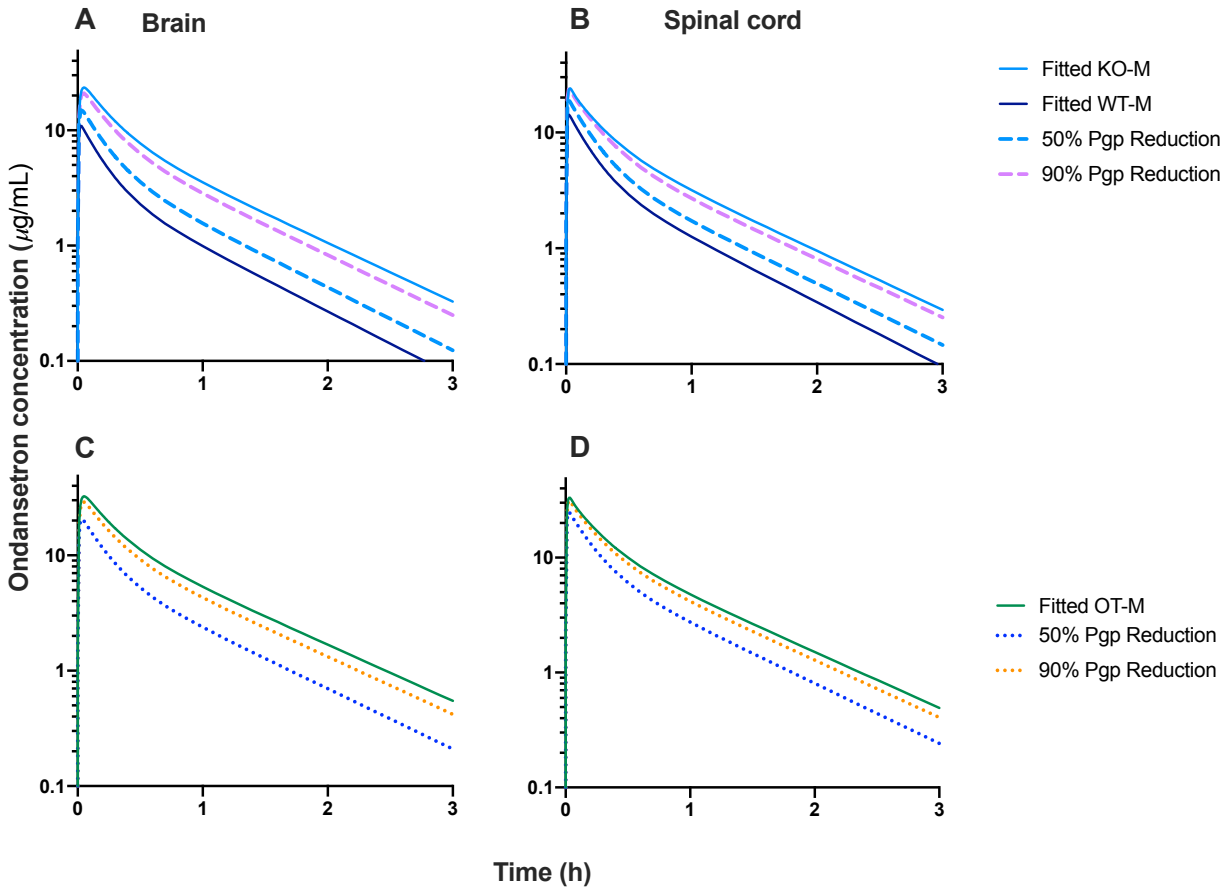

Figure 3.7 Simulations based on k_{Pgp} reduction in WT-M by 50% and 90% were evaluated and overlaid with the fitted profiles for WT-M and KO-M (A, B). Simulations based on k_{Pgp} reduction by 50% and 90% (C, D) were completed in OT-M animals and overlaid with fitted OT-M profile.

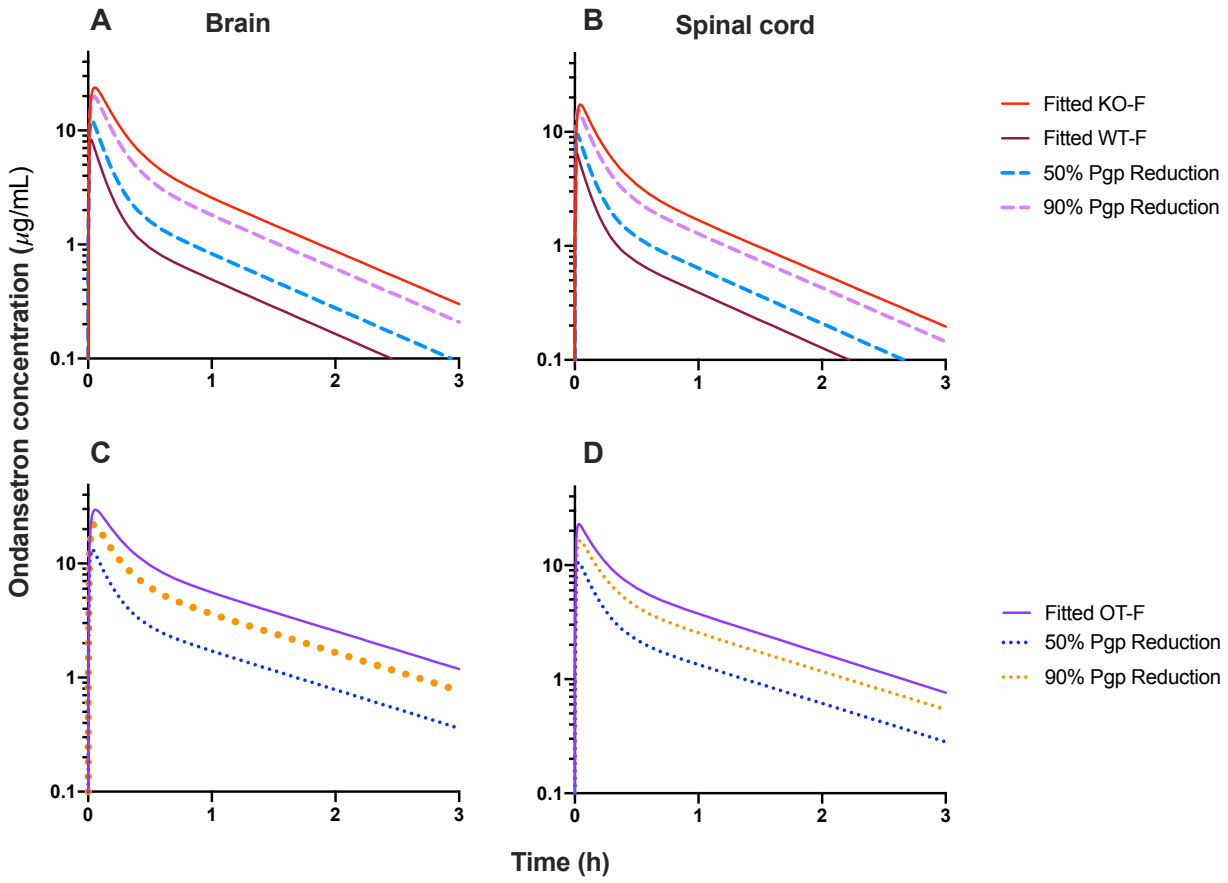

Figure 3.8 Simulations based on k_{Pgp} reduction in WT-M by 50% and 90% were evaluated and overlaid with the fitted profiles for WT-F and KO-F (A, B). Simulations based on k_{Pgp} reduction by 50% and 90% (C, D) were completed in OT-F animals and overlaid with fitted OT-F profile.

Chapter 4 Plasma and cerebrospinal fluid pharmacokinetics of ondansetron in humans[1]

4.1 Introduction

Neuropathic pain affects 7-8% of the adult population worldwide and is particularly challenging to treat (23, 185). More than 30% of neuropathic pain patients continue to suffer despite treatment; and there is clearly an urgent need for new treatment approaches (26). Serotonin is an important contributor to endogenous analgesic mechanisms. Under normal conditions, descending serotonergic neural control from the rostral ventromedial medulla to the spinal cord inhibits neuronal activity and hypersensitivity, and contributes to analgesia (186). This is primarily a result of serotonin activity on 5-HT_1 and 5-HT_7 subtypes of serotonin receptors, which are all G-protein coupled receptors (GPCRs) (187). However, it is suggested that after peripheral nerve damage, the character of serotonergic descending modulation changes from inhibitory to facilitatory through overexpression of 5-HT_3 receptors (5-HT_3Rs) in the spinal cord, as 5-HT_3Rs have excitatory properties, and are the only ion channels among the 5-HT receptor family (188, 189). These findings suggest that 5-HT_3Rs in the central nervous system (CNS), particularly in the spinal cord dorsal horn, could be a promising pharmacological target in neuropathic pain (190, 191). Clinical trials performed with systemically-administered 5-HT_3R antagonists for treating neuropathic pain have yielded mixed results (84, 85). On the other hand, preclinical literature suggests that intrathecal (IT, directly to the cerebrospinal fluid - CSF) administration of 5-HT_3R antagonists such as ondansetron alleviates mechanical and thermal hypersensitivity in animal models of nerve injury (87, 190).

We hypothesized that one of the mechanisms leading to unsuccessful clinical translation of the promising animal data in neuropathic pain models is related to inability to achieve effective ondansetron concentration at the site of action following systemic administration. CNS distribution

[1] Manting D. Chiang, Karen Frey[1], Chris Lee, Evan D. Kharasch, Dani Tallchief, Christopher Sawyer, Jane Blood, Leonid Kagan, and Simon Haroutounian (Under revision at British Journal of Clinical Pharmacology)

of 5-HT_3R antagonists such as ondansetron may depend on the expression level of efflux transporters at the capillaries of the blood-brain barrier (BBB), such as P-glycoprotein (Pgp), which limit CNS exposure (71, 192). The literature on the antiemetic effects of ondansetron (its primary clinical indication) indeed supports enhanced antiemetic effect in patients with single nucleotide polymorphisms (SNPs) in the ABCB1 gene that encodes the P-glycoprotein (193).

There are limited data on CNS penetration of 5-HT_3R antagonists. Direct sampling from the brain or spinal cord is rarely possible in humans, and assessment of the time-course of drug concentrations in the CSF may serve as a more practical approach (194). Furthermore, serial CSF sampling requires either an intrathecal catheter, or serial subarachnoid punctures, the latter of which are undesirable and a safety concern. Considering the challenges associated with performing such studies, population pharmacokinetic (PK) modeling can be utilized for analysis of sparse data (such as a single CSF sample collected at different time points from different subjects) and provides both the mean population trend and between-subject variability. Therefore, the goal of the study was to investigate the CSF distribution of ondansetron after intravenous (iv) administration of clinically-relevant doses and use population-based PK modeling approach to describe ondansetron distribution to the CNS.

4.2 Materials and Methods

4.2.1 Study Design

The study was approved by the Washington University IRB and was registered on clinicaltrials.org (NCT02901054) prior to participant enrollment. Candidates for a surgical total knee or total hip replacement were invited to participate in the study, where a single dose of iv ondansetron was administered in the pre-operative waiting room, followed by serial blood and a single CSF sampling. Patients from this surgical population were selected (*in lieu* of healthy volunteers), as these patients receive intrathecal anesthesia as a standard of care, allowing CSF access. Ondansetron was administered at varying times before the anticipated lumbar puncture,

to achieve a reasonable distribution of sampling intervals to allow a population PK modeling approach.

4.2.2 Inclusion and exclusion criteria

Patient inclusion criteria were: 1) 18 and 70 years old; 2 elective hip or knee arthroplasty with spinal anesthesia; 3) ability to provide informed consent. Exclusion criteria were: 1) history of or current hepatic or renal insufficiency; 2) BMI $\geq$ 33; 3) heart failure or active arrhythmias; 5) Patients with severe systemic disease that is a constant threat to life; 6) contraindication or allergy to ondansetron ; 7) Concurrent use of drugs known to prolong the QT-interval (such as thioridazine or quetiapine), and strong inhibitors of CYP450 enzymes (such as fluconazole or erythromycin); 8) Patients who are pregnant or lactating.

4.2.3 Study drug administration

An intravenous catheter was inserted in an arm for drug administration. Ondansetron was administered in a single 16 mg dose as a 15 min intravenous infusion. A 5-lead continuous electrocardiogram (ECG) monitoring was performed throughout the infusion and for approximately 30 min after the end of the infusion. Intraoperative and postoperative monitoring was performed per standard of care. No changes were made to the routine intraoperative management and hemodynamic physiological monitoring.

4.2.4 Data collection

An intravenous catheter was inserted in the arm opposite to the arm used for drug administration for obtaining blood samples. At baseline, a 5 mL blood sample was collected for pharmacokinetics (PK) and another 5 mL sample for genetic analysis. Six 5 mL serial venous blood samples were obtained from all subjects at 0 (pre-treatment), 15 (end-infusion), 30, 60, 120, and 180 min from the beginning of ondansetron infusion in each patient. The samples were collected into heparinized tubes, put on ice, and centrifuged for 10 min at 5000 RPM. Plasma was then

transferred to two 1.5 mL vials and stored at -80°C until analysis by HPLC-UV. A single CSF sample of 4mL was collected from each patient immediately following spinal needle insertion and before administration of spinal anesthesia. The timing of ondansetron infusions was scheduled to allow for obtaining a single CSF sample 30-90 minutes after the beginning of the infusion. The CSF samples were transferred to 1.5 mL vials and stored at -80°C until analysis.

4.2.5 Plasma and CSF sample preparation and analysis

The plasma and cerebrospinal fluid samples were assayed for ondansetron by high-performance liquid chromatography using Agilent Technologies 1260 Infinity HPLC-UV system by slight modification of reported methods (157, 195). In brief, 100 µL aliquot of plasma sample was used and 10 µL of a 100 µg/mL antipyrine solution added as internal standard. 200 µL of NaOH 1M solution was added as an alkalizing agent for plasma, and 200 µL of cold acetonitrile was added for protein precipitation. Solutions were vortexed at high-speed and extracted with 3mL of ethyl acetate. Samples were then centrifuged at 4ºC 3900 RPM for 7 min, the organic phase was transferred to a fresh tube and evaporated under nitrogen gas. The assay for ondansetron concentration in CSF samples follows the same procedure, however 200 µL saturated sodium carbonate solution was used as the alkalizing agent. The samples were then reconstituted with 70:30 water:methanol mixture and a 50 µL aliquot was injected into the HPLC system. Separation was achieved using a Poroshell EC-C_{18} column (Agilent Technologies, 4.6 x 100 mm, 2.7 µm). The mobile phase, consisted of 10 mM ammonium acetate (pH adjusted to 3.5 with glacial acetic acid) : methanol (80:20), and the flow rate was set to 1.5 mL/min. The detection wavelength was 310 nm. The retention times of ondansetron and antipyrine were approximately 11 min and 4.6 min respectively. The detection limit of ondansetron in plasma and CSF samples were 10 and 5 ng/mL.

4.2.6 Genotyping

The DNA isolation and genotyping included analysis of single nucleotide polymorphisms (SNPs) in P-glycoprotein transporters and Organic Cation Transporter 1 (OCT1), which have been associated with altered response to ondansetron (89, 193, 196) . The following five P-glycoprotein (ABCB1) SNPs: C3435T, C1236T, G2677T, G1199A, and T129C, and four OCT1 (SLC22A1) SNPs: R61C, G456R, G401S, and C88R that have been reported to affect ondansetron pharmacokinetics or clinical antiemetic effect were evaluated. The genotyping was performed at Washington University Genome Technology Access Center. Whole blood samples were extracted using QiIAamp DNA mini Blood kit (QIAGEN). The DNA was quantified and quality controlled using nanodrop and gel readings. The SNPs were interrogated using Taqman probes (Applied Biosystems). Each SNP had its own 20 µL reaction well with a final concentration of 1X Taqman probe mix, 1X Taqman PCR master mix, and 20-40 ng of DNA. The samples were cycled and analyzed on CFX96 Real-time PCR Detection System (Bio-Rad). The collected blood and DNA samples were de-identified and coded to ensure patient confidentiality and HIPPA compliance.

4.2.7 Pharmacokinetic analysis

Given that the CSF samples largely were not obtained at the same time as the plasma sample, an estimated plasma concentration at CSF sampling time was determined. This estimated value was obtained by selecting two observed plasma concentrations: one immediately before the time of CSF sample and one immediately following the time of CSF sample. An exponential regression equation was used to calculate plasma concentration at the time of CSF sample.

A noncompartmental analysis was conducted on the plasma concentration-time profiles for each patient using Phoenix WinNonlin (Pharsight version 7, Certara); volume of distribution at steady state ($V_{d,ss}$), total systemic clearance (CL_T), mean residence time (MRT), the half-life ($t_{1/2}$), and the area under the plasma concentration-time curve ($AUC_{0-\infty}$, from time zero to infinity, using linear trapezoidal rule) were calculated.

4.2.8 Population pharmacokinetic modeling

The plasma and CSF data were analyzed using NONMEM Version VII (ICON Development Solutions, Ellicott City, Maryland, USA). First-order conditional estimation method (FOCE) with interaction and ADVAN6 subroutine were utilized for all model runs. Post-processing was conducted with Pirana and R (R-project, www.rproject.org, version 3.3.1). Standard step-wise approach was used for population PK model building that included 1) construction of a base model for plasma PK based on plasma data only, 2) addition of a CSF compartment and CSF data, 3) assessment of inter-individual variability (IIV) in PK parameters, and 4) assessment of covariate effects for PK parameters. The model fitting process was guided by multiple criteria including successful model convergence, visual inspection of the model fits and standard diagnostic plots, and assessment of precision and accuracy of estimated model parameters.

Visualization of plasma concentration-time profiles for all patients indicated that a multicompartment model was needed to describe plasma data. Two-compartment model with linear elimination provided a good description of the data (and a three-compartmental model did not significantly improve model fit); and the model was parameterized in clearance and volume terms with systemic clearance from the central compartment (CL), inter-compartmental clearance Q, volume of the central compartment (V_C) and volume of the peripheral compartment (V_T). Model schematic and equations (1 and 2) used to describe the model are outlined in Figure 2. Upon establishing the base model for plasma pharmacokinetics, a CSF compartment was included to capture the disposition of ondansetron to the CNS. Two forms of the CSF model were explored: 1) using one or two first-order rate constants to describe the rates with which drug is entering and exiting the CSF compartment, and 2) using an equilibrium partition coefficient (K_P) for modeling distribution of ondansetron to the CSF. The final model used the K_P approach (Figure 2 and equation 3). An exponential form was used for estimating inter-individual variability on the PK parameters (Equation 4). A constant coefficient of variation model was used to describe the

residual random error (Equation 5). Several demographic and clinical covariates were available, including total body weight, height, body mass index (BMI), sex, age, and creatinine clearance (calculated by Cockcroft-Gault equation). All covariates were first screened through exploratory data analysis to visualize potential covariate relationships on PK parameters. Subject sex was not found to be an important variable (through t-test PK parameter differences between males and females) and was excluded from the analysis. Continuous covariates were incorporated into the model using a power function centered to the median value according to Equation 6. Covariates were evaluated using a step-wise procedure based on reduction of objective function and reduction of IIV of PK parameters, goodness of fit plots, successful minimization, and scientific reasoning. A covariate was considered significant during a forward addition step if the objective value function was reduced by at least 3.84 (*p-value* < 0.05, degree of freedom (df) =1). In the backward elimination step an increase greater than 6.35 *(p-value* < 0.01) or more was required for a covariate to be retained in the model.

4.3 Results

Overall, 19 subjects met the study inclusion criteria and signed informed consent (Figure 1 - CONSORT flow diagram). Two subjects were further excluded due to abnormal baseline ECG, and one subject withdrew consent before the study day. In an additional subject, the surgery was cancelled about 30 minutes prior to the scheduled time, due to a previously undetected infected wound. The subject did receive the intravenous ondansetron infusion, but no CSF sample had been obtained as spinal anesthesia was not performed. Participant demographics, including age, sex, BMI, height, weight, and creatinine clearance are depicted in Table 1. Serial plasma samples and a single CSF sample (timing for CSF sample is shown in Table 2) were collected from 15 subjects. Due to technical issues, the samples from one subject (#14) could not be reliably quantified and were therefore excluded from pharmacokinetic analysis. Genotyping data of

subjects for Pgp and OCT1 transporters, as well as the individual CSF to plasma concentration ratios of ondansetron are presented in Table 2.

4.3.1 Population Pharmacokinetic Model

For initial data assessment, noncompartmental analysis of individual plasma concentration-time profiles in all subjects was conducted and the results are presented in Table 3. Calculated parameters in this study are similar to published previously values (62).

Pharmacokinetic data were further analyzed using mixed-effect (population) modeling approach. Two-compartment distribution model with linear elimination was selected to describe plasma concentration-time profiles from 14 subjects. Good description of the experimental data was obtained, and all parameters were estimated with sufficient precision. Expanding the model to three compartments did not improve model fits. Individual and population model fits along with observed plasma data are shown in Figure 3. Final model estimated parameters are shown in Table 4. Inclusion of inter-individual variability improved model fits; and it was estimated to be 47% for CL and 44% for V_C. Inter-individual variability on peripheral volume and intercompartmental clearance could not be reliably estimated. Multiple covariates were evaluated on various model parameters based on criteria specified in the Methods. Inclusion of subject's age as a covariate on V_C and total body weight on V_T was found to significantly improve the model. It was determined that with increasing age, the central volume term decreases, with an estimated exponent of -4.91; and with increasing body weight the peripheral volume term decreased, with an estimated exponent of -2.44 (Table 4). The inclusion of the individual genotype for Pgp (the five tested polymorphisms) or OCT-1 (the four tested polymorphisms) did not improve the model or provide a more accurate determination of the CSF:plasma partition coefficient Kp.

Initially, a model that included a differential equation with one or two rate constants was attempted to describe ondansetron disposition into the CSF. Reasonable description of experimental

observations in the CNS was obtained; however, due to a limited number and time frame of CSF observations, inter-individual variability could not be reliably estimated in such a model. Current data suggest a fast equilibration between plasma and CSF; therefore, it was assumed that concentrations in the CSF could be described using an equilibrium partition coefficient K_P. The population typical value was estimated as 0.147 for K_P (with %RSE of 9.18%), and the inter-individual variability for K_P was estimated to be 27.3% (Table 4). The average CSF:plasma ratio of ondansetron was 0.15 (range 0.08 and 0.26), with individual values presented in Table 2.

No adverse effects were reported during ondansetron infusion or post-administration monitoring. No ECG or vital sign changes had been observed with the continuous monitoring during, and for 30-minutes after the ondansetron infusion. The surgical and postoperative course was normal in all study subjects.

4.4 Discussion

Using population PK approach, we were able to reliably construct individual CSF time-concentration profiles of ondansetron, using a single CSF sample at variable times from each participant. The study demonstrated that after iv administration, CSF to plasma partition coefficient of ondansetron is approximately 0.15.

While intrathecally administered ondansetron has shown antinociceptive effects in animal models of neuropathic pain due to its pharmacologic activity as a 5-HT_3R antagonist, clinical studies have shown mixed results with systemic ondansetron alleviating neuropathic pain in patients (84, 85). Ondansetron is capable of blocking 5-HT_3 receptors *in vitro* in low nanomolar concentrations (197). Most rodent studies have used the administration of 1-2 mg/mL ondansetron solution intrathecally in 25-100 µg doses, potentially creating micromolar local concentration of ondansetron around the spinal cord (188, 198). We hypothesized that the lack of clinical translation from preclinical studies can be, at least in part, attributable to the challenge in achieving target drug concentrations within the CNS following systemic administration. To

quantitatively describe the changing drug concentrations in the CNS, we developed a population PK model, as represented through CSF distribution data alongside plasma concentrations.

Ondansetron plasma pharmacokinetic parameters have been well documented in the literature, however limited information has been published describing CNS disposition, and the quantitative relationship between plasma and CNS disposition. Our measured and modeled results demonstrated approximately 7-fold lower concentration of ondansetron in the CSF compared to plasma, suggesting relatively poor CSF penetration. The CSF concentrations of ondansetron, 1-2 hours after IV administration were around 0.01-0.02 mg/L (i.e. 35-70 nanomole/L). If achieving effective analgesic concentrations of ondansetron in the spinal cord require CSF concentrations in excess of the ~50 nanomolar concentrations observed in the current study (compared with ~350 nanomolar peak plasma concentrations), then the systemic administration of ondansetron might not allow for appropriate testing of its analgesic effects in neuropathic pain.

A two-compartmental model was constructed to describe plasma PK, with inter-individual variability (IIV) terms and covariate descriptors to provide unique PK information for each patient included in the study. The plasma disposition profile was then linked to a CNS compartment using a single partition-coefficient term (K_P). Our modeling efforts demonstrated the ability to describe individual CSF concentration profile, based on a single CSF data point. Providing such a window into CNS disposition is extremely valuable and supports the opportunity to maximize CNS penetration of ondansetron for patients on an individual basis.

Understanding the required therapeutic concentrations to achieve effects within the CNS is challenging, especially given the difficulty of obtaining direct samples for analysis. CSF has been proposed as a surrogate sample to represent the disposition of drugs in the CNS to build a quantitative understanding of drug concentrations in the brain (199, 200). Furthermore, to develop a classic pharmacokinetic model to understand the distribution and elimination of drug in the body,

multiple samples would be required over a full time-course to allow for modeling. This type of modeling would preclude the analysis for CSF distribution, as it often not possible to obtain more than a single CSF sample per patient. Our study demonstrates that the population modeling is a useful approach and allows for sparse sampling across multiple patients to estimate the average pharmacokinetic parameters, as well as predict the individual pharmacokinetic profile for each of the observed patients.

The study has potential limitations. Our cohort was relatively small, and only a single CSF sample was obtained per subject to measure ondansetron concentration. A larger patient pool would enable a more robust understanding for the CSF distribution and elimination and assessment of transporters polymorphism on PK parameters. Furthermore, only a limited time range of CSF sampling was included in the study, and a longer sampling would be required to fully understand the CSF distribution and elimination of ondansetron. Sampling of the CSF at earlier time points may help identify the initial distribution rates and exposure. Only subjects 45-70 years of age and BMI of 21-33 kg/m^2 were enrolled, which may limit the extrapolation of the results to populations with age and BMI outside these ranges. Our study has also notable strengths, including rigorous screening criteria to ensure patient safety, CSF concentration measurement, and population PK modeling. Patients from this surgical population were selected (*in lieu* of healthy volunteers), as these patients receive intrathecal anesthesia as a standard of care, allowing CSF access, which eliminates any potential risks associated with performing a lumbar puncture for CSF collection in healthy volunteers.

4.5 Conclusion

The results suggest relatively limited CSF penetration of ondansetron after a single 16 mg intravenous dose. The population PK modelling that we undertook provides a viable and facile approach that can allow studying a large number of individuals in a high-throughput setting, compared to conventional PK methods. A more detailed investigation with repetitive CSF

collection and pharmacodynamics endpoints will be required for further understanding of CNS distribution kinetics of ondansetron and its potential analgesic effects in humans.

Table 4.1 Subject demographics

Patient ID	*Age*	*Sex*	*BMI (kg/m^2)*	*Height (cm)*	*Total BW (kg)*	*CL_{CR} (mL/min)*
1	54	F	31.6	168	89.1	98.2
3	59	M	27.4	178	86.8	132.0
5	56	M	27.2	180	88.2	84.4
8	63	F	21.4	183	71.8	98.9
9	66	F	27.4	168	77.3	110.7
10	70	M	24.4	183	81.8	74.3
11	59	F	28.1	173	84.1	-
12	60	F	28.5	170	82.3	-
13	45	M	26.2	185	90.0	127.7
14[a]	62	F	26.9	157	66.8	64.0
15	64	M	26.9	175	82.7	87.4
16	49	M	29.1	170	84.1	103.2
17	51	F	32.3	173	96.8	147.4
18	49	M	24.2	178	76.6	115.4
19	58	F	24.5	170	70.9	99.5
Mean (±SD)	**57 (7)**	**M (50%)**	**27.1 (2.9)**	**175.3 (5.9)**	**83.1 (7.2)**	**103.3 (23.5)**
Median	**57**		**27.3**	**174.2**	**83.4**	**99.5**

BMI = body mass index, BW = body weight, CL_{CR} = creatinine clearance, calculated

[a] - Subject 14 was excluded from population pharmacokinetic analysis due to irregular plasma concentration profile

Table 4.2 Individual CSF/plasma concentration ratio data, and Pgp and OCT1 genotype

Patient ID	*CSF sampling after ondanse tron (min)*	*CSF/Plasma ratio (at sampling time)*	**P-glycoprotein SNPs**					**OCT-1 SNPs**			
			C3435T	**C1236T**	**G2677T**	**G1199A**	**T129C**	**R61C**	**G465R**	**G401S**	**C88R**
1	47	0.077	GA	GA	CC	CC	AA	TC	GG	CC	TT
3	80	0.147	AA	AA	N/A	CC	AA	CC	GG	CC	TT
5	65	0.132	GG	GG	CC	CC	AA	CC	GG	CC	TT
8	56	0.170	GA	GA	CC	CC	AA	CC	GG	CC	TT
9	54	0.167	AA	AA	N/A	CC	AA	CC	GG	CC	TT
10	47	0.077	GA	GA	CC	CC	AA	CC	GG	CC	TT
11	58	0.128	GA	GA	CC	CC	AA	CC	GG	CT	TT
12	76	0.138	GA	GA	CC	CC	AA	CC	GG	CC	TT
13	39	0.144	GA	GA	CC	TC	AA	CC	GG	CC	TT
15	83	0.124	GA	GG	TC	CC	AA	CC	GG	CC	TT
16	75	0.212	GA	GA	CC	CC	AA	CC	GG	CC	TT
17	37	0.264	AA	AA	N/A	CC	AA	CC	GG	CC	TT
18	54	0.131	GA	AA	CC	CC	AA	TC	GA	CC	TT
19	59	0.227	GA	GA	CC	CC	AA	CC	GG	CC	TT

Table 4.3 Noncompartmental analysis of human plasma pharmacokinetics for ondansetron (n=14)

Parameter	*Mean (±SD)*
$t_{1/2}$ *(h)*	4.88 (2.3)
MRT *(h)*	6.91 (3.3)
$AUC_{0-\infty}$ *(h·μg/L)*	625 (296)
$V_{d,ss}$ *(L)*	185 (50)
CL *(L/h)*	33.0 (20)

SD – standard deviation; $t_{1/2}$ – half-life; MRT – mean residence time; $AUC0_{-\infty}$- AUC from time 0 to infinity; $V_{d,ss}$ – volume of distribution at steady-state, CL – total clearance

Table 4.4 Final parameter estimates from population pharmacokinetic model for ondansetron human pharmacokinetics

Population Pharmacokinetic Parameters			
Parameter	Description	Estimate	RSE%
CL *(L/h)*	Systemic clearance	23.4	16.6
V_C *(L)*	Volume of the central compartment	72.7	17.2
Q *(L/h)*	Inter-compartmental distribution clearance	218	10.3
V_T *(L)*	Volume of the peripheral tissues compartment	104	7.8
K_P	CSF/Plasma partition coefficient	0.147	9.2
B for ($V_{C, AGE}$)	Exponent for covariate effect of age on V_C	-4.91	18.7
B for ($V_{T,BW}$)	Exponent for covariate effect of total body weight on V_T	-2.44	43.4
Inter-individual Variability (CV%)			
IIV CL		46.8%	52.5
IIV V_C		43.5%	46.3
IIV K_P		27.3%	57.1
Residual Variability (CV%)			
RV_{plasma}	Residual error for plasma concentration	18.4%	29.3
RV_{CSF}	Residual error for CSF concentration	17.3%	-[a]

RSE% - relative standard error in %; CV% - coefficient of variation in %; IIV – estimate for the variance of the inter-individual variability.

[a] - residual variability value was fixed in the final model run to allow for estimation of inter-individual variability for K_P

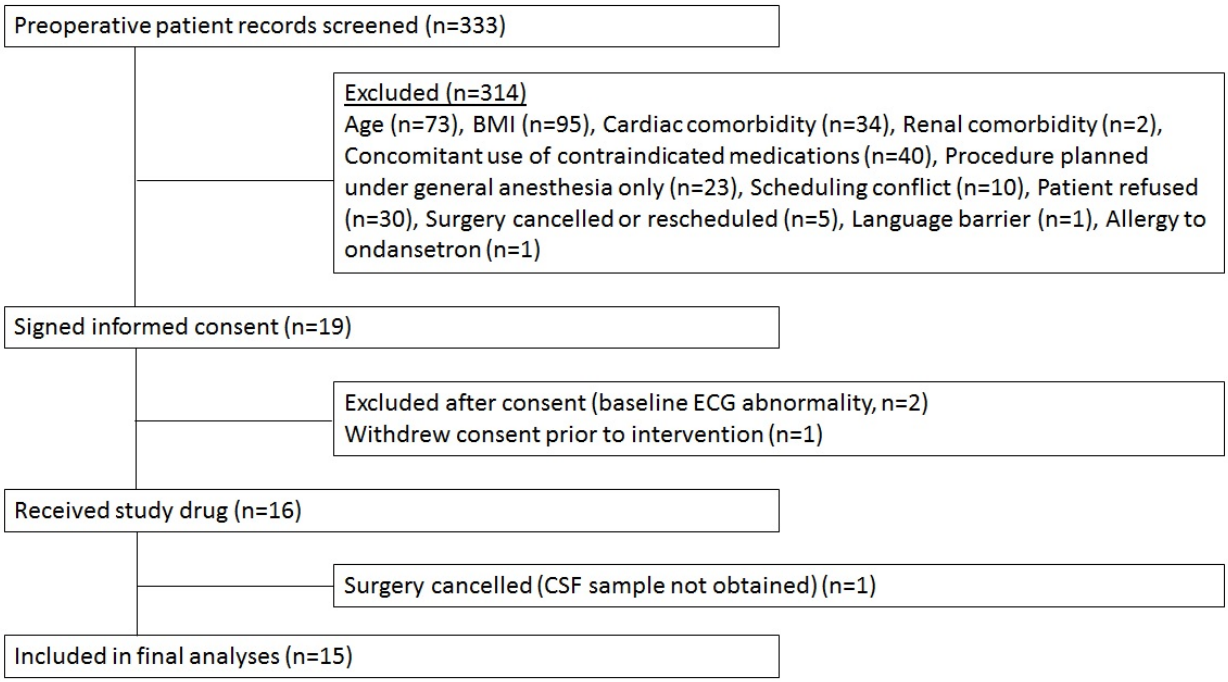

Figure 4.1 Participant flow chart

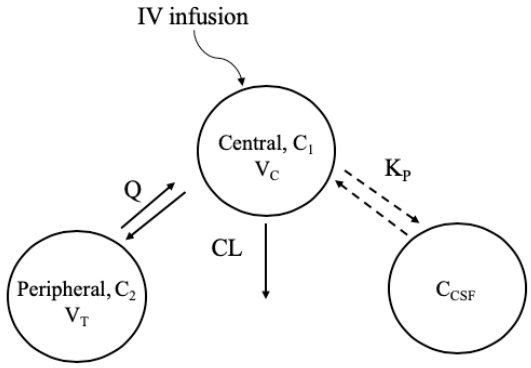

$$\frac{dC_1}{dt} = -\frac{CL}{V_c} \cdot C_1 - \frac{Q}{V_c} \cdot C_1 + \frac{Q}{V_T} \cdot C_2 \quad (1)$$

$$\frac{dC_2}{dt} = \frac{Q}{V_c} \cdot C_1 - \frac{Q}{V_T} \cdot C_2 \quad (2)$$

$$C_{CSF} = K_P \cdot C_1 \quad (3)$$

$$CL_i = CL_{TV} \cdot e^{-\eta_i} \quad (4)$$

$$C_{ij} = C_{pred,ij} \cdot (1 + \varepsilon_{ij}) \quad (5)$$

$$CL_{TV} = A \cdot \left(\frac{COV}{COV_{median}}\right)^B \quad (6)$$

Figure 4.2 Schematic of the population PK model used to capture plasma pharmacokinetics and CSF distribution. Equations 1-3 present a two compartment model that was used to describe systemic disposition, where C_1 and C_2 are drug concentrations in the central and peripheral compartment; and the concentration in the C_{CSF} is described using an equilibrium partition coefficient (K_P). Other structural model parameters are systemic clearance CL, inter-compartmental clearance Q, volume of the central compartment V_C, and volume of the peripheral compartment V_T was used for modeling distribution of ondansetron to the CSF. Equation 4 exemplifies inclusion of inter-individual variability on pharmacokinetic parameters, where CL_i is the value of CL in *i*th subject, CL_{TV} is a typical value of CL in the population, and η_i is the inter-individual random effects for individual *i* for this parameter. Equation 5 describes the residual random error, where C_{ij} and $C_{pred,ij}$ represent the *j*th observed and predicted concentrations for the *i*th individual respectively and ε_{ij} is the residual random effect. Equation 6 exemplifies inclusion of a covariate (COV) effect for a PK parameter, where the coefficient A and exponent B are estimated.

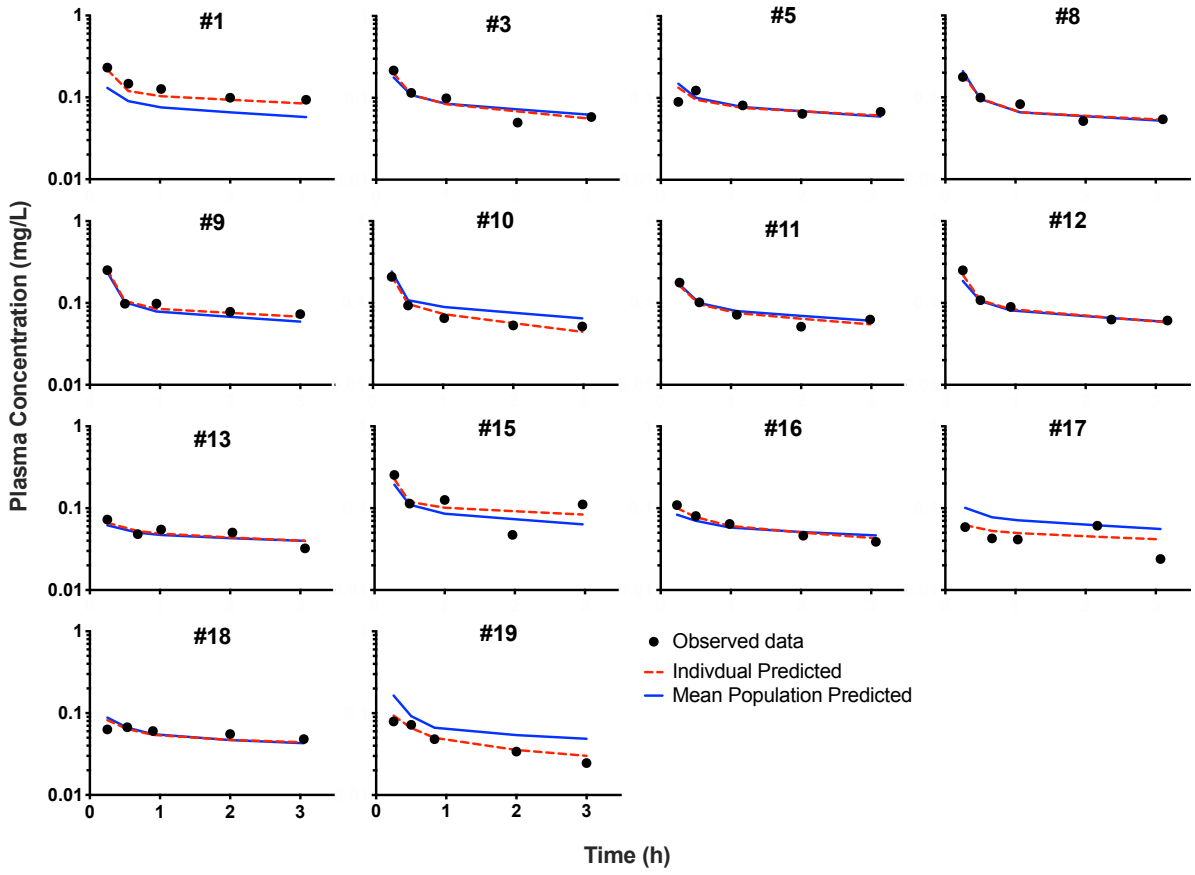

Figure 4.3 Concentration-time profiles of ondansetron in plasma for 14 subjects included in the population pharmacokinetic analysis. The model provided a good description of the experimental data.

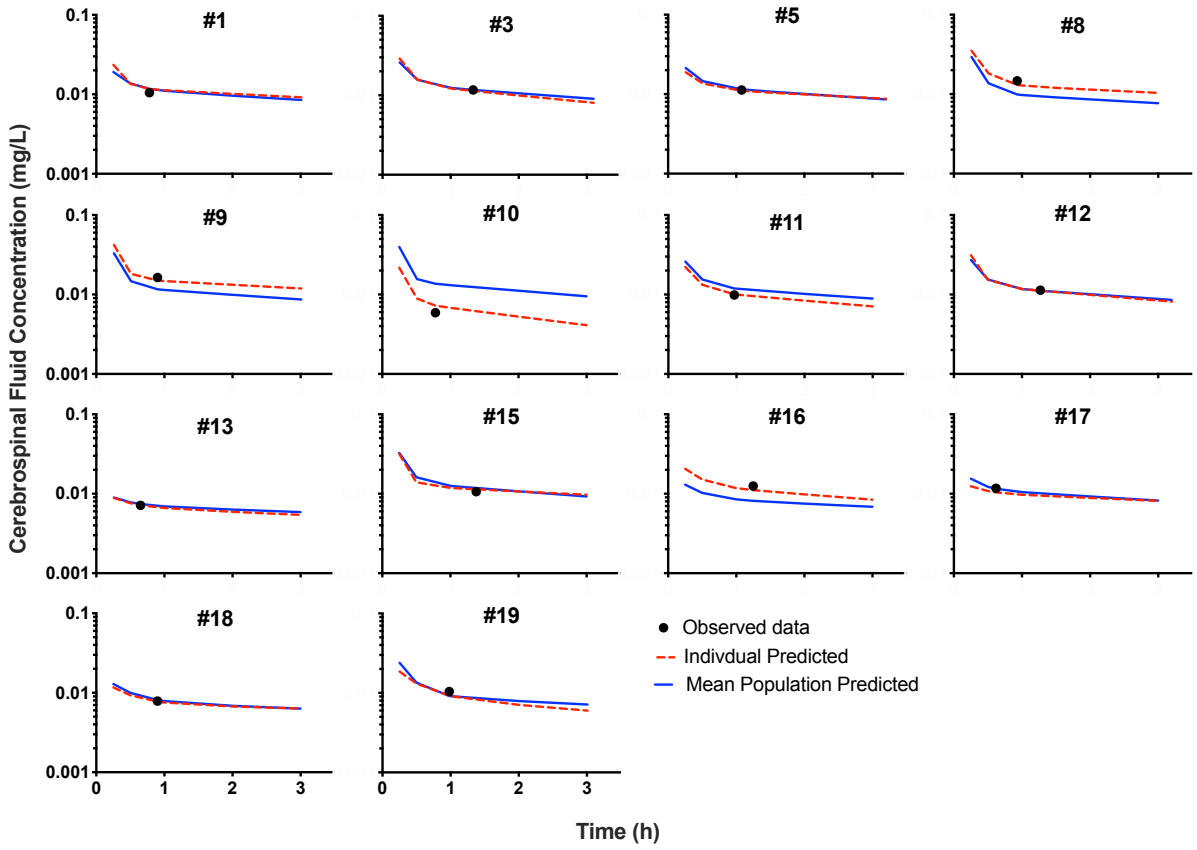

Figure 4.4 Concentration-time profiles of ondansetron in cerebrospinal fluid for 14 subjects included in the population pharmacokinetic analysis. The model provided a good description of the experimental data.

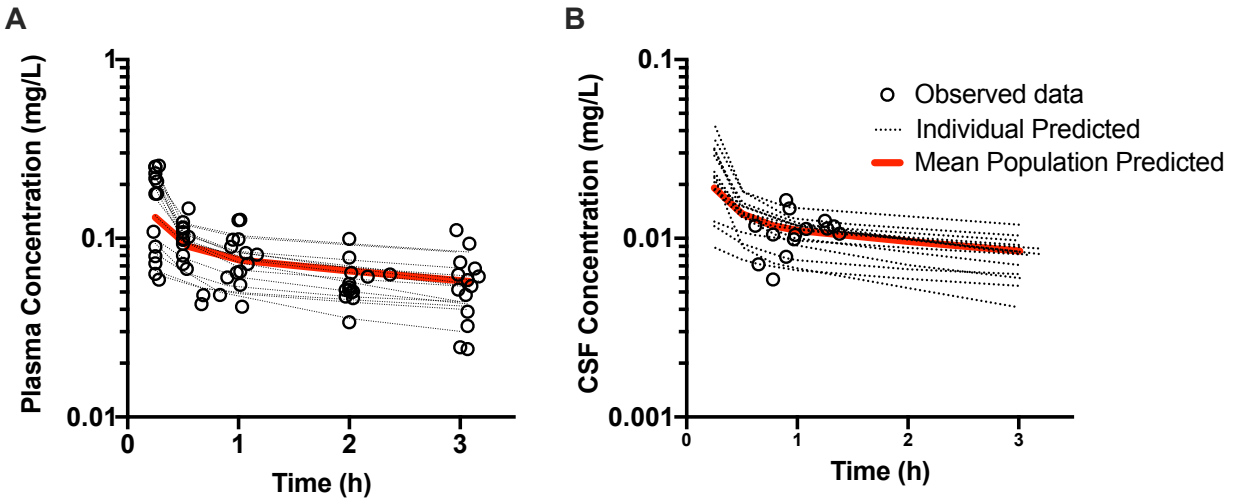

Figure 4.5 Concentration-time profile of ondansetron in plasma for all 14 subjects (open circles) are overlaid with model-based predictions for each individual prediction (black dotted line) and plotted against population predicted (solid red line).

Chapter 5 Pharmacokinetic approaches for describing ondansetron disposition: Physiologically-based modeling to allometric scaling methods

5.1 Introduction

Preclinical evaluation of treatments is the critical foundation supporting development of safe and effective treatments for humans. Pharmacokinetic (PK) modeling is an effective tool to establish the quantitative description of the PK properties and provide reliable estimates of drug exposure in humans based on preclinical studies. Physiologically-based pharmacokinetic (PBPK) models are a useful method to evaluate the tissue specific concentrations. PBPK models include physiological information in the species of interest (organ volumes and blood flow rates) (201, 202). Furthermore, fundamental pharmacokinetic characteristics of a compound, such as absorption, distribution, metabolism and elimination (ADME) may be functionalized by the physiological processes. The specific enzymes and their abundance and isoforms may be incorporated into a model to describe hepatic elimination of various compounds. The partitioning of compounds throughout the body may be dependent on physicochemical properties rather than empirical estimation of a volume of distribution term.

Simcyp is a PBPK modeling package that allows user to construct a drug compound file that details the basic its physicochemical properties (and may include known ADME properties) that may govern its interaction in the body; and it support parameter estimation and whole-body simulations. This software package includes built-in physiological information file for humans and several preclinical species (rat, mouse, dog, cynomolgus monkey) constructed based on literature values to allow the user to evaluate different dosing regimens and predict tissue exposures. A notable advancement in the recent version of Simcyp software is the addition of the “4brain model” (140). The 4brain model opens up prediction of drug distribution in to the CNS and includes four separate compartments: brain mass, brain blood, cranial CSF, and lumbar CSF (140).

Allometric scaling approaches allow for translation of preclinical pharmacokinetics to predict and describe clinical data. There have been various scaling strategies implemented to allow for describing multiple compounds. Most commonly, body weight has been shown to be an effective method of scaling basic pharmacokinetic parameters such as the volume of distribution and systemic clearance across multiple species (144). A method defined as maximum life-span potential has also been developed based on the maximum heart beats expected for each species for scaling pharmacokinetic properties, as well as the brain-weight correction (145, 146). The variety of methods allow for different compound PK to be successfully scaled across species based on specific compound disposition characteristics.

The goal of this work was to evaluate various modeling strategies to explore ondansetron pharmacokinetics including disposition into the CNS and translation of preclinical findings to the clinic. A PBPK model was constructed using the Simcyp software to evaluate tissue disposition, particularly in the brain and CSF. This model was then used to quantitatively evaluate the impact of Pgp on ondansetron efflux from the CNS. The ability to scale ondansetron plasma disposition was also explored by building an allometric pharmacokinetic model.

5.2 Materials and Methods

5.2.1 Data Sources

The whole-body physiological-based model was constructed during our preliminary analysis of ondansetron pharmacokinetics in regions of the central nervous system. The model was constructed using the serial plasma profile collected from the wild-type male (WT-M) and Pgp knock-out male (KO-M), as well as the few terminal brain, and cerebrospinal fluid (CSF) samples collected (n=2-3 per time point). The validation of the PBPK model used values digitized from the literature. A previous report by Yang and colleagues provided serially sampled plasma

profile in males following a single IV bolus administration of ondansetron (8 mg/kg), and provided two time points for the brain (5, 30 min) (63).

To investigate inter-species scaling of ondansetron, pharmacokinetic data was collected from the literature. Only studies evaluating ondansetron administered by the intravenous route was included in the analysis to minimize formulation-dependent or absorption-dependent variability. The mean data of each publication was captured using Plot Digitizer (version 2.6.8). Six publications reporting ondansetron plasma pharmacokinetic profiles following a single intravenous administration to rat, cat, cynomolgus monkey, and human were identified. All publications were selected for the allometric model construction, and were used to construct the allometric model. In rat, 4 dose levels were include, a single dose level for cat and cynomolgus monkey, and two dose levels in human were used (**Table 5.2**). Yang and colleagues reported IV bolus administration profiles of 1, 4, 8, and 20 mg/kg plasma disposition in rat (63). Quimby and colleagues reported ondansetron disposition in cats following an IV bolus dose of 0.4 mg/kg (203). Nagaya and colleagues conducted a pharmacokinetic study in cynomolgus monkey, and administered an IV infusion of ondansetron 0.81 mg/kg (66). Three different publications were collected to model human plasma disposition, with a 5 min infusion of 8 mg, a 15 min infusion of 8 mg, and a 20 min infusion of 24 mg (61, 62, 204).

5.2.2 Physiologically-based pharmacokinetic model development and simulation

Simcyp Animal version 17 (Certara, Princeton NJ) was used to construct a physiologically-based pharmacokinetic model. The Simcyp framework requires input of a drug's physicochemical properties, elimination pathways, and the user is able to select the absorption and distribution models that are programmed into the software. The absorption information was disregarded as all data used were from intravenous administration. The distribution throughout the body was estimated using Method 2 based on a previously published method (205, 206). The values required for input are presented in **Table 5.1**. The dosing regimen was then inputted to reflect

the study design (IV bolus administration, 10 mg/kg) and the simulated plasma profile was then overlaid onto the observed data points. Visual inspection was conducted to evaluate sufficient capture of the *in vivo* data.

Following satisfactory description of the plasma profile for wild-type male SD rats, the rate of Pgp efflux at the blood-brain barrier (BBB) was then included into the model using the 4Brain model (140). Three passive permeability terms are calculated and inputted into the model as shown in **Table 5.1**. The passive permeability surface area product on the BBB (PSB) was calculated as 0.3 mL/min based upon the apparent permeability term obtained from *in vitro* multiplied by the surface area of the rat BBB (207, 208). Based on previous reports, the passive permeability surface area product on the BCSFB (PSC) was best inputted as 50% of the PSB, therefore 0.15 mL/min was inputted. (207, 209). The passive permeability surface area product on the barrier between CSF and brain (PSE) is considered to not be a limiting factor, and through correspondence with Simcyp scientists, they recommended a large value to be entered (80 mL/min) (209).

The Pgp efflux parameter ($CL_{int,Pgp}$) was then identified based on sensitivity analysis. A range of values from 0.0001 to 100 μL/min/fmol was simulated in steps of 10^1 to evaluate how well it could describe the WT-M average brain and CSF profile. After obtaining a reasonable description of the WT-M data, profiles were then simulated for KO-M data. Similarly, a sensitivity analysis was conduct from 0 to 100 in steps of 10^1 to evaluate whether ondansetron efflux in the CNS should be included to describe the KO-M brain and CSF pharmacokinetic profile.

After identifying the best values to describe the plasma, brain, and CSF data for the *in vivo* data for WT-M and KO-M (**Chapter 2**), the Simcyp model was then validated with the external dataset, described above.

5.2.3 Allometric model development and evaluation

R (Ver. 3.31) and Rstudio (Version 1.2.5001, Boston, MA, USA) with Ubiquity package were used for overall model development process and estimation of the parameters (163). Parameter estimation processes utilized Nelder-Mead Optimization method, with a variance model defined as: $VAR_i = \left(\sigma_1 \cdot \Upsilon(\theta, t_i)\right)^2$ where VAR_i is the variance of the *ith* data point, σ_1 the variance model parameter, and $\Upsilon(\theta, t_i)$ is the *ith* predicted value from the pharmacokinetic model. The model performance was evaluated by visual inspection of the observed versus predicted plot, system convergence, Akaike Information Criterion, and objective function value.

The model was first constructed based on the digitized rat data (195). A one-, two-, and three-compartmental model was evaluated. A three-compartmental model with central elimination (k_{el}) and first-order rate constants describing distribution to peripheral plasma compartments (k_{12}, k_{21}, k_{13}, k_{31}) best described the data. A schematic of the final model selected is shown in **Figure 5.1**. Following satisfactory description of the plasma PK profiles for rat, the three other species were then included into the model. The plasma PK parameters were scaled based on a simple allometry method using body-weight. The equation used for scaling is shown in equation : $P = A \cdot \left(\frac{BW_1}{BW_{ref}}\right)^b$ where *P* represents the PK parameter, A represents the allometric coefficient, BW_1 is the body weight of the species (cat, cynomolgus monkey, human) and BW_{ref} representing the body weight of the reference species (rat), and *b* the allometric exponent that was estimated. To reduce overparameterization of the model, the inter-compartmental rate constants (k_{12}, k_{21}, k_{13}, k_{31}) shared a single allometric exponent (k_{all}). Furthermore, previous efforts demonstrated the ability to scale volume of distribution across multiple species with an exponent of 1 (144, 145). Therefore, the exponent for volume (V_1) was fixed to 1. The model rate constants, and exponents for the rate constants were then simultaneously estimated across all four species for each dose level.

5.2.4 Simulation of clinical data based on allometric model

The final allometric model developed was used for generating simulation of ondansetron concentrations in plasma, and CSF to compare with the collected clinical data (**See Chapter 4**). The dosing regimen of the clinical study (16 mg IV infusion over 15 min) was used to generate a simulated plasma profile based on the final model. If the partitioning of ondansetron intro CSF is assumed to be similar across species, and that it is constant over time, a single K_P term may be used to calculate the expected CSF concentration in humans based on preclinical data. Previously calculated K_P term (**See Chapter 2**) was 0.075 (wild-type male Sprague-Dawley rats) and 0.107 (wild-type female Sprague-Dawley rats). These two values were averaged (K_P=0.091), to account for the presence of male and female in the clinical dataset, and then used to calculate the CSF profile.

5.3 Results

5.3.1 PBPK model simulation

The PBPK framework within Simcyp was then used to simulate the expected plasma and tissue profiles following ondansetron intravenous injections. This disposition of ondansetron is informed by the physicochemical properties of the drug, as well as metabolic elimination to describe the whole-body disposition. This model was developed during the early stages of the project (**See Chapter 2**), where few points were collected for each tissue in WT-M and KO-M. This model was used as an initial evaluation to quantify Pgp efflux clearance in the brain, and compare between WT-M and KO-M.

The drug parameters are presented in **Table 5.1**, and the results of the plasma, brain, and CSF simulation are presented in **Figure 5.2**. The simulated plasma profile for WT-M and KO-M was able to sufficiently describe the plasma concentrations. The 4-brain model was then implemented

to identify the rate of Pgp efflux clearance at the BBB (CL_{int}). The CNS simulations identified a CL_{int} of 1 μL/min/fmol was sufficient for describing both brain and CSF disposition for wild-type males (**Figure 5.2**). This was based on a series of simulations with a wide range of values after calculating the passive permeability values for ondansetron brain permeability. The KO-M profiles were then evaluated to identify if a CL_{int} value was needed to describe the brain and CSF disposition. After conducting the sensitivity analyses, a CL_{int} of 0.2 μL/min/fmol was shown to sufficiently describe KO-M ondansetron disposition in the brain and CSF simultaneously (**Figure 5.2**).

An external validation was then conducted to evaluate how well this model was able to describe dataset that was sourced from the literature. The Simcyp model that was developed for the WT-M data was then applied for the Yang data set, where the only changes were made to the dosing regimen to reflect the published report. The CL_{int} of Pgp efflux, obtained for WT-M profiles was capable of describing the two points in the brain (**Figure 5.3**).

5.3.2 Allometric plasma PK model

An interspecies model was developed to describe plasma disposition across four species. This model is empirical in nature, and used first-order rate constants and simple body-weight allometric equation to fit the plasma concentrations across each species. This model was completed during the early stages of the project working only on digitized data. The main interest was the ability to predict human pharmacokinetics using animal data. The three preclinical species used in the model strengthened the ability to scale to humans.

A three compartmental model was identified to best describe the plasma disposition across the four dose levels for rat (1, 4, 8, 20 mg/kg) as shown in **Figure 5.4**. Cat, cynomolgus monkey, and human profiles were then included into the model, with final estimated parameters

presented in **Table 5.3**. The final interspecies model was able to describe plasma disposition across all four species well while estimating the parameter values with sufficient precision.

5.3.3 Plasma and CSF simulation

The allometric plasma pharmacokinetic model was used as the foundation to simulate plasma and CSF concentrations, for comparison with the previously collected clinical data (**Figure 5.5**). Although the initial distribution of ondansetron is over-estimated, the elimination phase of ondansetron is described well. At approximately 1 hour, the simulation is able to describe both the plasma and CSF concentrations collected from the patients.

5.4 Discussion

Our study explored additional pharmacokinetic modeling strategies to describe ondansetron disposition in plasma and the CNS. The PBPK Simcyp model was developed to provide an initial quantitative assessment of Pgp efflux at the BBB using the pilot brain and CSF *in vivo* profiles. An interspecies model was developed to assess the ability to use animal data to describe human pharmacokinetics.

The PBPK Simcyp model demonstrated unique advantages in describing ondansetron disposition. The ease of using a user-friendly model interface with built-in information of the rat physiology allowed for description of Pgp efflux at the BBB, using *in vivo* brain and CSF concentrations. However, the trade-off of the Simcyp model is the inability to access and modify the physiological information that is built-in. The 4brain model within Simcyp allows for physiological description of drug pharmacokinetics in different regions of the CNS, however the spinal cord is absent in the 4brain model (including only brain blood, brain mass, cranial CSF, and spinal CSF). Therefore, while Simcyp was useful to provide an initial quantitative assessment

of Pgp efflux, our efforts led to the development of our own mechanistic model to describe the *in vivo* data.

An interspecies scaling model was also explored to evaluate the ability to describe human pharmacokinetics based on animal data. Based on our model, it can be shown that ondansetron plasma disposition can be successfully described based on animal data, using only a body-weight allometric equation. This model was then applied to develop simulations of plasma and CSF profiles and compared with the collected clinical data. During the allometric model development, there was insufficient data for the initial distribution of ondansetron, and this can be reflected in the overestimation of the initial ondansetron concentrations. However, following approximately 1 hour, the simulation is describing both plasma and CSF concentrations that were collected. This is a promising direction in predicting human CNS disposition based on preclinical studies. This will also be useful for future efforts to expand the model to include CNS disposition across multiple species, where additional allometric approaches can be evaluated. For example, approaches have been established to scale by maximum life-span potential correction, brain weight, as well as including two-term's for the power equation (145-147).

5.5 Conclusion

Additional modeling strategies were employed to describe the disposition of ondansetron in plasma, brain, and CSF. The PBPK Simcyp model assessed the quantitative impact of Pgp efflux at the BBB using brain and CSF profiles. This model was validated using an external dataset with plasma and brain concentrations. An interspecies model was constructed to describe human pharmacokinetics using preclinical plasma profiles. The ability describe plasma disposition lays the foundation to support future work to include scaling of CNS data, such as CSF.

Table 5.1 Simcyp parameter input for ondansetron in Simcyp Animal v17

	Parameter	Unit	Value	Citation
Physico-chemical properties	**Molecular weight**	g/mol	293.4	(56)
	Compound type	-	Monoprotic base	(56)
	Log P	-	2.4	(56)
	pKa	-	7.4	(56)
	B/P	-	0.74	(195)
	f_u	-	0.470	(195)
Elimination	**CYP2D6**	μL/min/pmol of isoform	183.5	(210)
	CYP1A2	μL/min/pmol of isoform	79.5	(210)
	CYP3A4	μL/min/pmol of isoform	57.9	(210)
Transport	**BBB: PSB**	mL/min	0.3	(207, 208)
	BCSFB: PSC	mL/min	0.15	(207)
	CSFBB: PSE	mL/min	80	(209)

Table 5.2 Dosing regimen for four species used in allometric model

Species	Dose(s)	Citation
Rat	1, 4, 8, 20 mg/kg	(195)
Cat	0.4 mg/kg	(203)
Cynomolgus monkey	0.81 mg/kg	(119)
Human	8 mg infusion (5 min) 8 mg infusion (15min) 24 mg infusion (20min)	(204) (62) (61)

Table 5.3 Final parameters obtained from the allometric model scaling across four species. The left-hand side provides the basic parameter estimates used for simultaneous estimation, and on the right are the allometric exponents utilized to describe the plasma PK for all species.

3 CM PK Parameter				**Allometric Exponent**		
Parameter		**Estimate**	**CV%**	**Parameter**	**Estimate**	**CV%**
V_1	(L)	6.43	11.8	V_1	1	fixed
k_{12}	(1/h)	9.44	13.6	k_{all}	-0.436	3.6
k_{21}	(1/h)	0.057	27.0			
k_{13}	(1/h)	24.7	8.0			
k_{31}	(1/h)	3.0	6.4			
k_{el}	(1/h)	51.5	10.4	k_{el}	-0.441	1.5

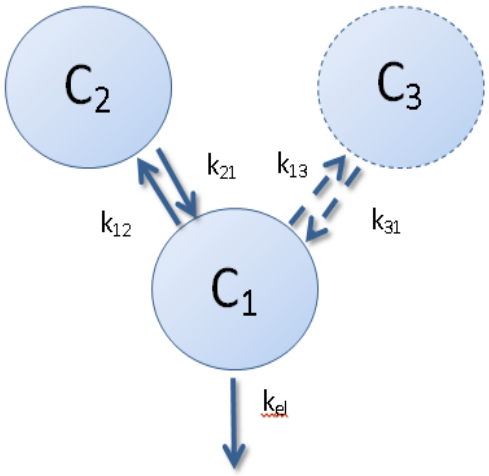

Figure 5.1 A basic schematic of the three compartmental model developed for allometric scaling across four species (rat, cat, cynomolgus monkey, human). The central compartment (C_1) has elimination (k_{el}), with two peripheral compartments (C_2, C_3) and inter-distributional rate constants (k_{12}, k_{21}, and k_{13}, k_{31}).

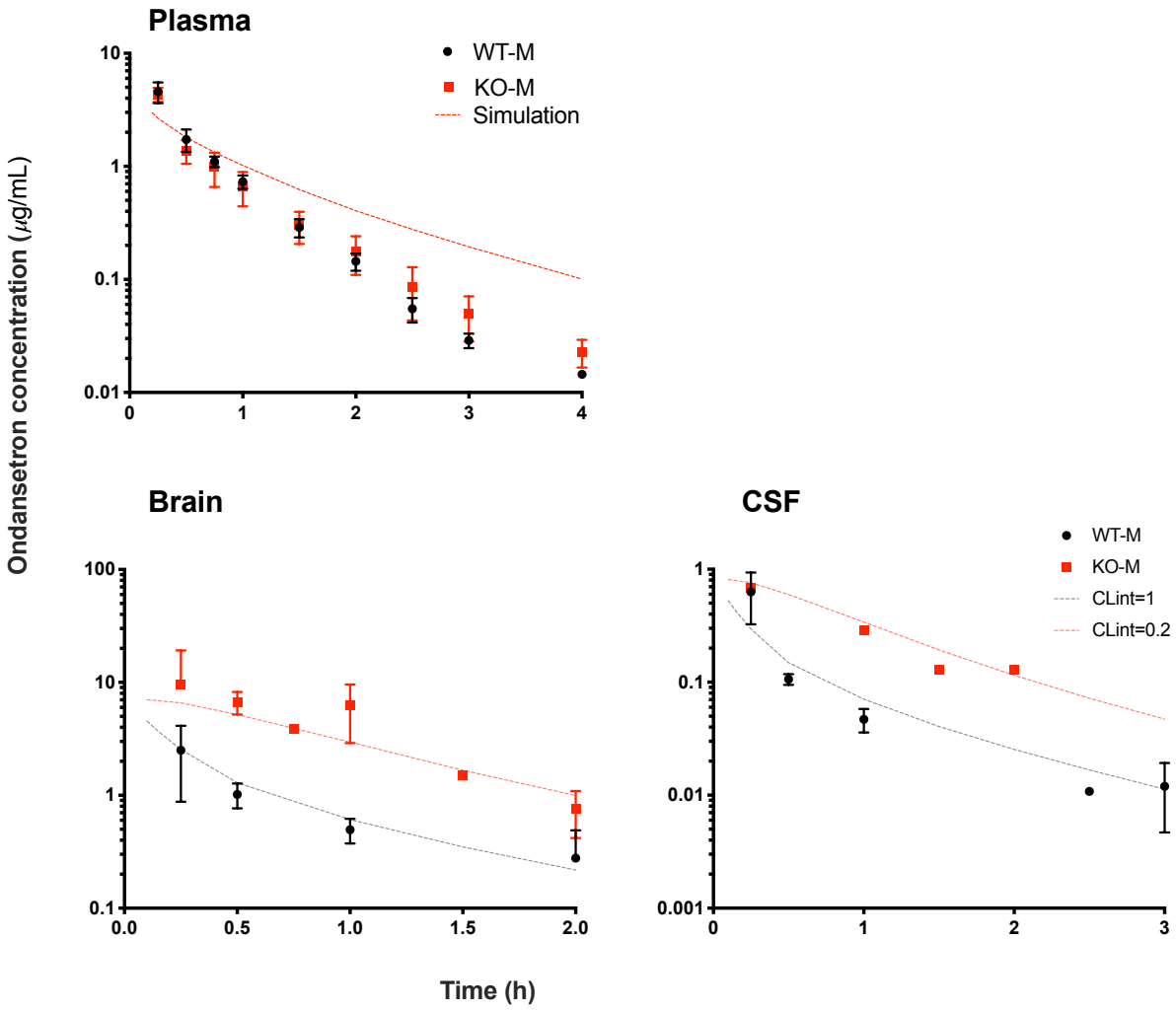

Figure 5.2 The results of the Simcyp simulation overlaid on observed plasma (A), brain (B) and CSF (C) following single intravenous administration of ondansetron (10 mg/kg) to wild-type (WT) and Pgp knockout (Pgp KO) male Sprague-Dawley rats. The WT data is presented as black circles, and Pgp KO in the red squares. The Simcyp simulation is in the dotted line, with black dotted lines reflecting WT simulation and red dotted line reflecting Pgp KO simulation

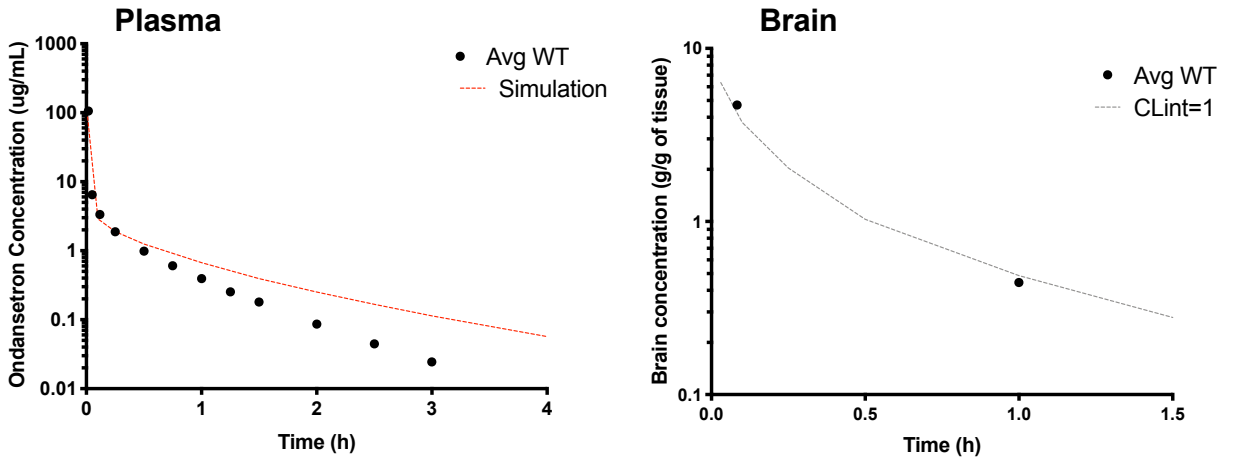

Figure 5.3 The results of the external validation of the Simcyp model using data extracted from Yang et al. The observed data was obtained from male SD rats receiving a single IV bolus administration of 8 mg/kg. The Simcyp model used for simulation reflected the parameters fixed to the wild-type animal, with intrinsic Pgp efflux clearance fixed to 1 μL/min/fmol of protein

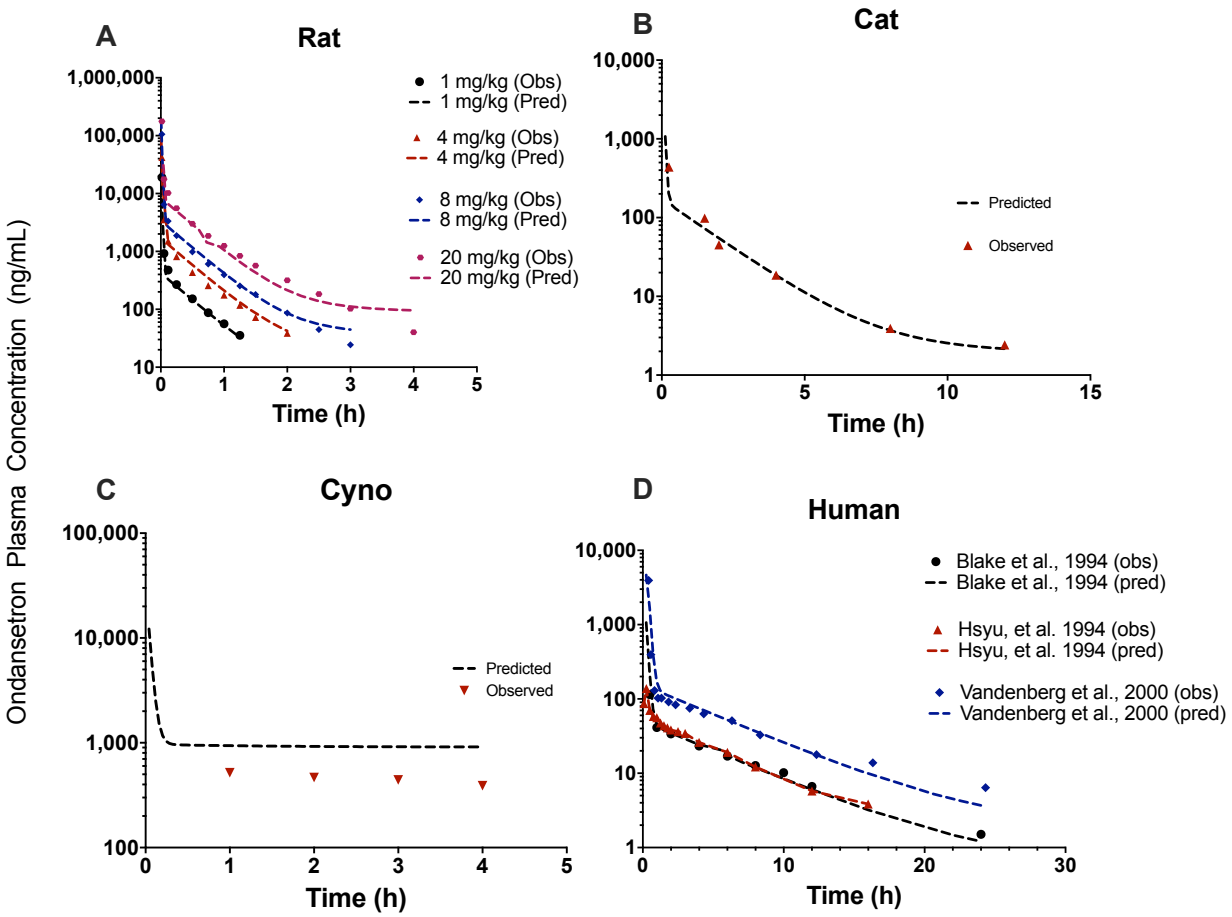

Figure 5.4 The results of the allometric model scaling plasma disposition across rat (A), cat (B), cynomolgus monkey (C), and human (D). The estimated profiles are presented in dotted lines, and the observed data is presented in solid symbols.

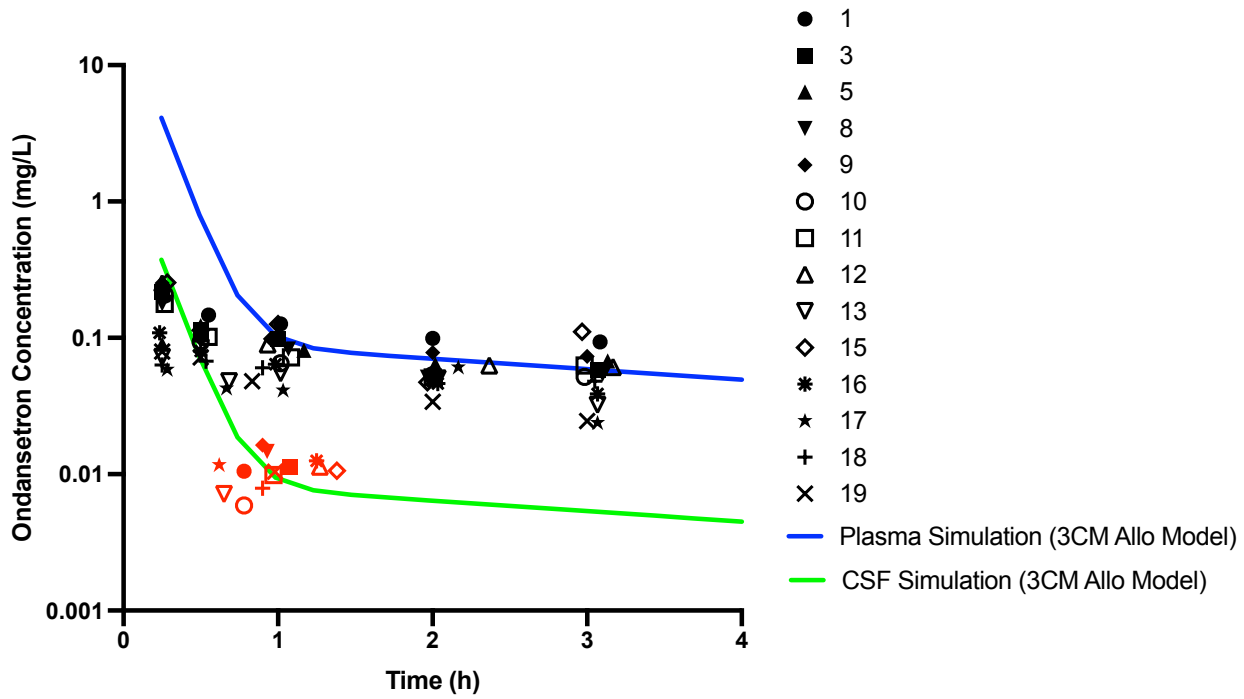

Figure 5.5 Plasma and CSF profiles simulates based on the 3CM interspecies model. Observed human plasma shown in black symbols, and single CSF samples from each patient in red symbols. The solid blue line is the simulated plasma profile, and the green line is the calculated CSF concentrations based on Kp value of 0.091.

Chapter 6 General discussion and future work

6.1 General discussion

In this PhD project, preclinical and clinical pharmacokinetic models were developed to assess the CNS disposition of a 5-HT_3 receptor antagonist. Preclinical pharmacokinetic studies additionally allowed for the quantitative assessment of P-glycoprotein efflux on CNS disposition.

Neuropathic pain is a complex chronic pain condition affecting a large population with limited therapeutic options for patients. Preclinical studies antagonizing spinal 5-HT_3 receptors highlighted a promising treatment option for neuropathic pain (87). However, small clinical studies were inconclusive (84, 85). An important step to bridging the preclinical reports to the clinical inconsistencies is understanding the drug disposition at the site of action, i.e., the CNS. Currently, only a single clinical study reported six CSF concentrations following administration of ondansetron, a 5-HT_3 receptor antagonist (65). Furthermore, preclinical work has largely focused on presenting 2-4 concentration time points following ondansetron administration in CSF or brain (66, 195). The spinal 5-HT_3 receptors are prominent targets for translating drug exposure to therapeutic effect; however, we did not identify any reports citing spinal cord concentrations of ondansetron in animals or humans. This work presents an important step to quantifying CNS disposition of a ondansetron to support future studies evaluating the therapeutic potential of antagonizing 5-HT_3 receptors.

Pgp is a prominent efflux transporter, expressed on the BBB, and has been shown to limit drug exposure in the CNS as well as drug efficacy. Pgp substrates (loperamide, paclitaxel) administered to Pgp KO rats have been shown to have altered pharmacokinetics (165, 166). In our study, Pgp KO rats had significantly enhanced exposure of ondansetron in various regions of the CNS (2.4-5.5-fold). The plasma profiles between WT and KO rats were comparable. Our

findings support a previous report in WT and Pgp KO mice, where ondansetron brain exposure was increased 4-fold in KO mice, but had equivalent plasma exposure (71). Chemical knock-out of Pgp was also explored in our study, through the co-administration of tariquidar, a third-generation Pgp inhibitor. Co-administering tariquidar (7.5 mg/kg) showed complete inhibition of Pgp efflux, and CNS tissue concentrations were significantly increased compared to wild-type animals receiving ondansetron alone.

A relatively high dose of tariquidar used to achieve inhibition of Pgp efflux at the CNS. Previous reports using tariquidar used a dose of 15 mg/kg, demonstrating complete inhibition of Pgp 30 min post-dose (141, 177). The co-administration of ondansetron (10 mg/kg) with this high dose of tariquidar results to fatal seizure-like toxicity in male and female animals. A toxicity assessment was conducted, and our efforts determined that a dose of 7.5 mg/kg allowed for eliminating this fatal toxicity event while still maintaining complete inhibition of Pgp. An additional finding in our tariquidar study was the increased systemic concentrations of ondansetron following co-administration of ondansetron with tariquidar, compared to knock-out animals receiving ondansetron alone. Additional tariquidar-induced changes, that are independent of Pgp inhibition, may be occurring that affect systemic concentrations. A study in male Wistar rats co-administered tariquidar (15 mg/kg) and ciprofloxacin (7 mg/kg) intravenously reported significantly higher plasma exposure and lower systemic clearance in animals receiving tariquidar. However, this effect on systemic concentration is not consistent (182, 183).

The plasma disposition of ondansetron has been reported to have sex-dependent differences in both rat and humans. The plasma AUC in male rats was 23% lower compared to females following intravenous dose of 8 mg/kg (p-value < 0.05) (74). A clinical study reported women to have consistently higher plasma exposure following oral or suppository formulations (p-value < 0.05) (76). Our pharmacokinetic studies also evaluated potential differences between male and females. When administering ondansetron alone to male and female rats (wild-type and

Pgp knock-out), we did not find distinct differences in plasma profiles, although there was a slight trend in the latter points for females to have higher concentrations. In the CNS tissues, only male spinal cord concentrations were higher. We also evaluated sex-dependent difference in animals co-administered with tariquidar. Interestingly, the biggest differences were between animals receiving the co-administration of tariquidar and ondansetron, and the WT and KO animals receiving ondansetron alone. Future work is required to clarify whether these differences are Pgp-related, or due to non-specific action of tariquidar.

A clinical assessment was conducted to evaluate CNS disposition of ondansetron in a small set of patients, using CSF as a biomarker. Our work also evaluated the potential impact of genetic polymorphisms of transporters ondansetron is a substrate of: Pgp and OCT1. The information collected was then used to support the development of a population pharmacokinetic approach. Previously, direct quantitative assessment linking plasma and CSF distribution of ondansetron had not been completed, and influence of polymorphism on ondansetron distribution was also not established. Our measured and fitted model results showed that ondansetron has approximately 7-fold lower concentration in the CSF, compared to plasma. This reflects relatively poor CSF penetration following systemic administration of ondansetron. Future working evaluating the analgesic effect of ondansetron may require other routes of administration. Furthermore, the effect of polymorphisms on transporters did not reveal a significant relationship, likely due to the fact of our relatively small sample size (n=14).

An important advantage to the development of pharmacokinetic models is the ability to describe and predict drug concentrations in other species, or in tissues of interest. A semi-physiological model was developed to provide description of ondansetron disposition in various regions of the CNS. This model adequately described the PK of ondansetron in the absence of Pgp due to genetic or chemical knock-out in male and female rats. Drug portioning into the spinal cord is often neglected in pharmacokinetic analyses, with previous models emphasizing drug

disposition in the brain and CSF (121, 140). Pharmacokinetic modeling also allows for the use of surrogate biomarkers to describe drug partitioning into the CNS. In clinical studies, brain and spinal cord are rarely samples, leaving CSF as a valuable surrogate to evaluate CNS pharmacokinetics. A CSF compartment included into the model allows for the description and prediction of CNS exposure in both preclinical and clinical species.

6.2 Future work

The understanding of 5-HT_3 receptor antagonist distribution within the central nervous system has been limited, based on the scarcity of published reports. A comprehensive and informative full-body physiologically based pharmacokinetic model is needed to expand the current tissue disposition profiles of ondansetron, as well as including more sampling time points to fully capture the early disposition and latter elimination phase. A mechanistic model was used to capture plasma, brain, spinal cord, and CSF where physiological volumes were used for the CNS compartments. In future studies, quantifying ondansetron concentrations in the rest of the body, as well as including physiological flow rates for wild-type and Pgp knock-out models should be completed.

Intrathecal administration of ondansetron in a neuropathic pain animal model has shown increasing pain relief with increasing doses of ondansetron (87). Further studies are needed to explore the effect of increased ondansetron exposure in the CNS due to Pgp inhibition, and link it to a pharmacodynamic effect. The development of a pharmacokinetic-pharmacodynamic model would support the quantitative assessment of a dose-exposure-response relationship. In addition, employing microdialysis techniques would allow for improved assessment for the changing drug concentrations in specific regions of the CNS. Serial sampling would allow for drug concentration time profiles from individual animals, and allow for an understanding for how changing drug concentration may be linked to the pain relief ondansetron may provide.

The pharmacokinetic models presented demonstrate the potential to construct a full translational model, including specific tissue disposition in multiple species. Future studies in the clinical population are needed to expand the clinical data set and strengthen the interspecies scaling relationships. Serial cerebrospinal fluid samples may be collected by the implantation of catheters. Furthermore, the use of Pgp inhibitors in the clinic would also allow for capturing the effect of Pgp inhibition across multiple species.

Appendix 1 Simultaneous quantification of ondansetron and tariquidar in rat and human plasma using HPLC-UV[2]

A.1.1 Introduction

P-glycoprotein (Pgp), also known as ATP-binding cassette sub-family B member 1 (ABCB1) transporter, is a drug efflux pump that actively transports drugs out of cells against the concentration gradient (211). Pgp is mainly expressed in the epithelial cells of kidney, liver, intestine, adrenal gland and the blood-brain barrier (BBB) (211, 212). Due to the active efflux. Drugs that are Pgp substrates may not reach their site of action at sufficient concentrations to exert therapeutic effect and may result in reduced efficacy and drug resistance (117, 213). One example is treatment-resistant depression (TRD) which has been partly attributed to the Pgp efflux at the BBB limiting the distribution of antidepressants to the brain (211). Additionally, Pgp substrates often suffer from poor oral bioavailability by intestinal efflux, which could be enhanced significantly by use of Pgp inhibitors (214). As such, there has been a growing interest in the application of Pgp inhibitors to overcome the efflux mechanism and improve drug pharmacokinetics as well as treatment outcomes (215, 216).

Tariquidar (XR9576) is a potent and selective third-generation Pgp inhibitor that has shown to improve therapeutic efficacy of Pgp substrates by inhibiting efflux and therefore enhancing drug delivery (217). Numerous studies have been conducted with tariquidar and various Pgp substrate drugs. For example, a 12-fold increase in distribution of verapamil was observed in the brain due to inhibition of Pgp at the BBB by tariquidar (218). Enhanced central nervous system (CNS) distribution was also observed when tariquidar was co-administered with diazepam, an anticonvulsant, and resulted in enhanced anti-seizure activity (219). Aside from increased CNS distribution, tariquidar may also increase oral absorption of Pgp substrates by

[2] Yae Eun Chong, Manting Chiang, Kiran Deshpande, Simon Haroutounian, Leonid Kagan, Jong Bong Lee (Published: Biomedical Chromatography

inhibiting efflux at the gut endothelium. One study found a 10-fold increase in oral bioavailability of paclitaxel by co-administering HM30181 (220), a third generation Pgp inhibitor that is structurally related to tariquidar (221).

Ondansetron is a Pgp substrate that may benefit from co-administration with tariquidar. Ondansetron is a competitive antagonist of the 5-HT_3 receptor and is used as an antiemetic for chemotherapy-induced nausea and vomiting, as well as having anxiolytic and neuroleptic properties (222). Because ondansetron is a Pgp substrate, distribution of ondansetron to the CNS was found to be enhanced 4-fold in mice deficient in Pgp expression (71). Increased distribution from co-administering ondansetron and tariquidar has also been reported, whereby decreased ondansetron levels from seizure-induced Pgp overexpression was revered with tariquidar co-administration (192). Further investigations would be required to elucidate the pharmacokinetic-pharmacodynamic relationships of the two drugs for translation of preclinical findings to clinical settings.

Several bioanalytical methods have been developed and validated for quantification of ondansetron in plasma samples (60, 157, 223-226). Methods that utilize mass spectrometry for detection could achieve good sensitivity with lower limit of quantification (LLOQ) of 0.2-0.5 ng/mL but narrow calibration curve ranges were reported (up to 20-60 ng/mL) (60, 224, 226). Validated HPLC-UV methods have reported LLOQ of 0.62-1.0 ng/mL, but large volumes of plasma (1-2 mL) were necessary for the analysis, which is not practically achievable in preclinical studies (60, 157, 225). For tariquidar, a few methods have been reported to be used in the literature but none of them have shown method validation (227-229). Furthermore, no bioanalytical method has been reported to simultaneously quantify ondansetron with tariquidar or any other third-generation Pgp inhibitors. Therefore, the aim of this study was to develop and validate a bioanalytical method for simultaneous quantification of ondansetron and tariquidar in rat and human plasma. The method was fully validated, and sample stability studies have been carried out. The utility of the method

was demonstrated by application to a preclinical pharmacokinetic study with co-administration of the two drugs.

A.1.2 Materials and methods

A.1.2.1 Chemicals and reagents

Ondansetron hydrochloride (CAS: 103639-04-9), tariquidar (CAS: 206873-63-4), and *N*-benzylbenzamide (CAS: 1485-70-7) were purchased from Sigma-Aldrich (St. Louis, MO). Human and rat plasma were obtained from BioIVT (Westbury, NY). All solvents used in the study were HPLC grade and were purchased from Fisher Scientific (Fair Lawn, NJ).

A.1.2.2 Analytical methods

A.1.2.2.1 Preparation of stock solutions and standard samples

Stock standard solutions of ondansetron, tariquidar and internal standard (IS, *N*-benzylbenzamide) were prepared in acetonitrile at 1.0, 0.5 and 1.0 mg/mL, respectively, and stored at -20 °C. Working standard solutions were diluted in acetonitrile and yielded concentrations of 0.1, 0.2, 0.5, 1, 5, 10, 50 and 100 µg/mL for ondansetron and 0.5, 1, 2, 3, 5, 10, 30 and 50 µg/mL for tariquidar. For calibration curves, 10 µL of the working standard solutions of each drug was spiked into 100 µL of plasma (1:10) to yield concentrations of 10, 20, 50, 100, 500, 1000, 5000 and 10000 ng/mL for ondansetron and 50, 100, 200, 300, 500, 1000, 3000 and 5000 ng/mL for tariquidar.

Working standard solutions for quality control samples were prepared in concentrations of 0.25, 4 and 80 µg/mL for ondansetron and 1.25, 4 and 40 µg/mL for tariquidar. By spiking 10 µL of working standard solutions into 100 µL of plasma, the low quality control (LQC), medium quality control (MQC) and high quality control (HQC) samples yielded concentrations of 25, 400 and 8000 ng/mL, respectively for ondansetron, and 125, 400 and 4000 ng/mL, respectively, for tariquidar.

A.1.2.2.2 Plasma sample preparation procedures

For liquid-liquid extraction, 10 µL of IS (100 µg/mL) was spiked into 100 µL of plasma. A volume (300 µL) of 0.1 M NaOH was added to modify the pH of the samples. Methyl-*tert*-butyl-ether (MTBE) (3 mL) was then added as the extraction solvent. The samples were vortexed for 10 min and centrifuged for 5 min at 1902 *g* at 4 °C (Eppendorf Centrifuge 5810R, Eppendorf, Hauppauge, NY). After transferring the organic layer, the samples were evaporated under a stream of N_2 gas (TurboVap, Biotage, Charlotte, NC). The samples were reconstituted in 100 µL of acetonitrile in water (3:7, v/v), vortexed for 5 minutes, and 40 µL was injected into the HPLC-UV machine for analysis.

A.1.2.2.3 Chromatographic conditions

The HPLC-UV system used in the study was an Agilent 1260 Infinity setup (1260 Quat Pump, 1260 HiP ALS and 1260 DAD). Separation was achieved using a Phenomenex Gemini column (3 µm C18, 150 × 2 mm), protected by a SecurityGuard pre-column. The column temperature was maintained at 45°C. The mobile phase consisted of acetonitrile and 5 mM ammonium acetate buffer (pH 4, modified with glacial acetic acid) operated with a gradient program (Table 1). The detection wavelengths were 310 nm for ondansetron and 240 nm for tariquidar and IS.

A.1.2.3 Method Validation

Full validation of the method was attained by following the US FDA Guidance for Bioanalytical Method Validation (230).

A.1.2.3.1 Selectivity

The selectivity was determined by comparing the chromatograms of blank plasma samples with the samples spiked with ondansetron and tariquidar at the LLOQ.

A.1.2.3.2 Intra- and inter-day precision and accuracy

Precision was expressed as the relative standard deviation (RSD) and the accepted values were within ±15%. Accuracy was expressed as relative error (RE) and the accepted values were ≤15%. The accepted criteria of RSD and RE for the LLOQ were within ±20% and ≤20%, respectively. The intra- and inter-day precision and accuracy were validated with rat and human plasma samples containing ondansetron at concentrations of 25 (LQC), 400 (MQC) and 8000 ng/mL (HQC) and tariquidar at concentrations of 125 (LQC), 400 (MQC) and 4000 ng/mL (HQC), respectively. The intra-day validation consisted of six replicates of rat and human plasma QC samples on the same day. The inter-day validation consisted of six replicates of QC samples on six separate days.

A.1.2.3.3 Sensitivity

The LLOQ was defined as the lowest tested concentration of spiked plasma sample which demonstrated precision within ±20% and accuracy within ≤20% from intra- and inter-day validation.

A.1.2.3.4 Extraction recovery

To determine the extraction recovery, the peak areas from extracted QC samples (n = 3) were compared with that of samples in the reconstitution solvent (acetonitrile in water (3:7, v/v)) without the extraction process.

A.1.2.3.5 Stability

The stability of ondansetron and tariquidar in plasma samples was determined by testing the freeze-thaw, benchtop, long-term, and autosampler stability in human plasma. For freeze-thaw stability, QC samples (n = 6) underwent three cycles of freeze-thaw (-80°C for 24 h and room temperature) and were analyzed after the third cycle with a freshly prepared calibration curve. For benchtop stability, samples were prepared and stored under room temperature for 6 h and

analyzed afterwards with a freshly prepared calibration curve. For long-term stability, samples were prepared and stored in -80°C for 1 month and analyzed afterwards with a freshly prepared calibration curve. For autosampler stability, the processed samples were stored in the autosampler of the HPLC (4°C) for 24 h and analyzed afterwards with a freshly prepared calibration curve. The precision and accuracy of stability tests were accepted at RSD ≤ 15% and RE within ±15%.

A.1.2.3.6 Linearity

Calibration curves ranged from 10–10000 ng/mL for ondansetron and 50–5000 ng/mL for tariquidar. The LLOQ was detected at 10 ng/mL for ondansetron and 50 ng/mL for tariquidar. For each calibration curve, a blank sample without any drug and a blank sample with only the IS were included. The accepted criteria for the calibration curve were a correlation coefficient $r^2 > 0.99$ and accuracy within ±15%, except for LLOQ (±20%).

A.1.2.4 Pharmacokinetic Study

The pharmacokinetic study protocol was approved by the Institutional Animal Care and Use Committee at Rutgers, The State University of New Jersey. Male Sprague Dawley rats (Envigo, Inc., NJ, USA) weighing 350-380 g were used for the experiment. The animals were housed in a temperature-controlled, 12 h light-dark cycle with free access to food and water. The animals were acclimatized for at least 6 days prior to experimental procedures. Afterwards, right jugular vein cannulation was performed to facilitate blood sample collection.

For ondansetron, dosing formulation was prepared at 10 mg/mL in normal saline, and dose of 5 mg/kg was administered. For tariquidar, dosing formulation was prepared at 5 mg/mL in 2.5% dextran in water, and was administered at dose of 15 mg/kg. Both ondansetron and tariquidar were administered intravenously as a bolus, and ondansetron was administered 1 h after

tariquidar administration. Blood samples (0.2 mL) were collected at pre-dose, 5, 15, 30, 60, 65, 75, 90, 120, 180, 240, 300 and 360 min following administration of tariquidar, and were separated by centrifugation to obtain plasma and stored at -80°C until analysis. Non-compartmental pharmacokinetic data analysis was conducted using Phoenix WinNonlin 7 software (Pharsight, a Certara Company).

A.1.3 Results and discussion

A.1.3.1 Method development

The development of the bioanalytical method was focused on simultaneously detecting two drugs with substantially different lipophilicity (cLog P: ondansetron, 2.35; tariquidar, 5.68). The gradient program applied in this method was sufficient for capturing both drugs in a single chromatogram with a reasonable run time (Table 1). The selection of reconstitution solvent was also heavily affected by the difference in lipophilicity. A higher percentage of acetonitrile in water was desired to increase extraction recovery of tariquidar. On the other hand, higher percentages of acetonitrile resulted in distorted peak shapes of ondansetron. At the end, acetonitrile in water (3:7, v/v) was selected which yielded a good peak shape for ondansetron. However, it was a limiting factor for the upper range of calibration for tariquidar as concentrations of >5000 ng/mL resulted in significantly reduced recovery.

A.1.3.2 Method validation

The developed method was fully validated for both ondansetron and tariquidar as per the US FDA guideline in matrices of human and rat plasma to demonstrate the utility of the method in preclinical and clinical studies (230-232). The sample stability studies were performed in human plasma.

A.1.3.2.1 Selectivity

The chromatographic conditions of this method were able to achieve appropriate separation of ondansetron, tariquidar and IS as well as other interfering peaks. At the retention times of ondansetron (2.5 min) and tariquidar (9.1 min), the blank samples were free of interfering peaks. The selective detection of both drugs is demonstrated in the chromatograms shown in Figures 1-4, as background peaks from blank rat and human plasma samples do not interfere with the peaks of interest.

A.1.3.2.2 Intra- and inter-day precision and accuracy

The precision and accuracy of intra- and inter-day validation were all within the accepted limits as shown in Table 2 for both ondansetron and tariquidar. These results indicate the validity of this method for simultaneous detection of ondansetron and tariquidar in both rat and human plasma with acceptable accuracy and precision.

A.1.3.2.3 Sensitivity and linearity

The LLOQs of ondansetron (10 ng/ml) and tariquidar (50 ng/mL) met the accepted criteria of RE within ±20% and RSD <20% from the intra- and inter-day validations (Table 2). The linearity of ondansetron and tariquidar, with concentrations ranging from 10–10000 ng/mL and 50–5000 ng/mL, respectively, were confirmed with RE and RSD values within the accepted criteria and the correlation coefficient r^2 >0.99.

A.1.3.2.4 Recovery

The extraction recovery of both ondansetron and tariquidar was shown to be comparable across the different concentration ranges tested. The recovery values were 110.5 ± 12.7, 98.0 ± 5.8 and 95.5 ± 6.5% for HQC, MQC and LQC levels of ondansetron, respectively. Those values for TQD were 84.4 ± 6.1, 79.6 ± 6.8 and 80.5 ± 8.1%, respectively. The recovery for IS was 97.6 ± 1.6%.

A.1.3.2.5 Stability

To ensure samples are stable under routine handling conditions and are not subject to degradation from effects of sample storage, stability tests were conducted in human plasma at various storage conditions. The stability results of ondansetron and tariquidar are reported in Table 3. The benchtop stability test kept samples at room temperature for 6 h and were analyzed afterwards with a freshly prepared calibration curve. This test was to ensure the plasma samples are stable during the sample preparation. To account for the time samples are kept in the autosampler for injection, autosampler stability test was performed up to 24 h to confirm sample stability. The QC samples underwent 3 cycles of freeze-thaw (-80° C) to show that samples are not affected by such conditions. The samples were kept in – 80° C for 1 month and analyzed afterwards to confirm stability during long-term storage. The stability tests were confirmed to be within the accepted RSD and RE criteria.

A.1.3.3 Pharmacokinetic study

Following validation of the method, it was applied to sample analysis in a preclinical pharmacokinetic study where ondansetron and tariquidar were administered concomitantly. Ondansetron exhibited significantly faster distribution and elimination compared with tariquidar (Figure 5). The prolonged half-life of tariquidar has also been observed in a previous study (229). The half-life (0.54 ± 0.02 h) and clearance (3.7 ± 0.4 L/h/kg) of ondansetron (Table 4) were comparable to a previously published study where they reported 0.47 ± 0.06 h and 3.0 ± 0.8 L/h/kg for half-life and clearance, respectively, following dose of 4 mg/kg (63). This study also confirmed dose-linearity of ondansetron at a dose range of 1-20 mg/kg. This indicates that plasma pharmacokinetics of ondansetron did not differ between with and without co-administration of tariquidar. Nevertheless, further investigation is warranted as the distribution pattern of ondansetron can potentially differ with the effect of Pgp inhibition.

A.1.4 Conclusion

The presented bioanalytical method has been developed and validated for the simultaneous quantification of ondansetron and tariquidar in rat and human plasma. This method is the first to be reported to simultaneously quantify ondansetron with a third-generation Pgp inhibitor. The utility of the method has been demonstrated with application to a preclinical pharmacokinetic study. The detection of both drugs in one assay will provide efficiency in time and cost related to bioanalytics.

Table A.1.1 Mobile phase gradient program applied to the HPLC method

Time (min)	Acetonitrile	Buffer[a]	Flow rate (mL/min)
0	20	80	0.6
2.5	20	80	0.6
9.6	59	41	0.6
9.7	20	80	0.6
13	20	80	0.6

[a] 5 mM ammonium acetate buffer with pH 4.0

Table A.1.2 Intra- and inter-day validation results of bioanalytical method for simultaneous quantification of ondansetron and tariquidar in rat and human plasma (n=6)

	Rat plasma				Human plasma			
	Intra-day		Inter-day		Intra-day		Inter-day	
	Accuracy (RE, %)	Precision (RSD, %)	Accuracy (RE, %)	Precision (RSD, %)	Accuracy (RE, %)	Precision (RSD, %)	Accuracy (RE, %)	Precision (RSD, %)
Ondansetron								
LLOQ (10 ng/mL)	-5.3	6.4	5.6	11.2	11.5	5.6	5.7	7.2
LQC (25 ng/mL)	1.0	2.8	-1.2	1.7	-0.8	3.1	-6.1	7.4
MQC (400 ng/mL)	-1.1	1.9	-1.1	2.1	-1.8	5.2	-2.3	5.2
HQC (8000 ng/mL)	2.6	4.1	0.9	4.6	-3.9	6.4	-3.1	14.1
Tariquidar								
LLOQ (50 ng/mL)	-1.2	11.9	8.2	7.5	6.7	7.0	4.8	9.0
LQC (125 ng/mL)	0.0	8.3	-0.2	6.7	14.3	14.6	-2.2	5.2
MQC (400 ng/mL)	0.8	5.6	-3.3	2.4	6.5	13.5	-4.3	5.9
HQC (4000 ng/mL)	-1.0	8.0	-0.2	2.8	-11.2	10.5	-2.5	1.5

RE, relative error; RSD, relative standard deviation; LLOQ, lower limit of quantification; LQC, low quality control; MQC, medium quality control; HQC, high quality control.

Table A.1.3 Stability assessment of human plasma samples spiked with ondansetron and tariquidar stored in various conditions (n=6)

	Benchtop stability (25 °C, 6 h)		Autosampler stability (4 °C, 24 h)		Freeze-thaw stability (-80 °C, 3 cycles)		Long-term stability (-80 °C, 1 month)	
	RE (%)	RSD (%)	RE (%)	RSD (%)	RE (%)	RSD (%)	RE (%)	RSD (%)
Ondansetron								
LQC (25 ng/mL)	5.40	6.10	-2.9	2.2	-3.3	1.3	-3.3	5.0
MQC (400 ng/mL)	11.47	1.19	-0.2	3.6	-6.4	1.5	7.8	3.8
HQC (8000 ng/mL)	14.20	2.03	-1.6	1.2	-5.5	2.0	8.4	2.8
Tariquidar								
LQC (125 ng/mL)	4.3	7.6	-11.9	9.8	-7.7	2.2	-9.0	5.3
MQC (400 ng/mL)	2.8	3.1	-7.0	3.0	-5.5	1.2	-6.7	6.3
HQC (4000 ng/mL)	6.6	5.5	4.2	7.1	-5.1	3.1	-7.5	7.5

Table A.1.4 Pharmacokinetic parameters obtained following intravenous coadministration of ondansetron 5 mg/kg) and tariquidar (15 mg/kg) in male Sprague Dawley rats (mean±SD, n=4)

	Ondansetron		**Tariquidar**	
Parameters	**Mean**	**SD**	**Mean**	**SD**
$AUC_{0\rightarrow t}$ (h·ng/mL)	2678	330	5678	1367
C_0 (ng/mL)	12942	4662	4157	1778
$t_{1/2}$ (h)	0.54	0.02	7.35	2.48
V_{ss} (L/kg)	1.86	0.54	10.69	1.49
CL (L/h/kg)	3.70	0.44	1.11	0.31

$AUC_{0\rightarrow t}$, area under the curve from time zero to the last sampling time point (AUC was not extrapolated to infinity due to the long half-life observed for tariquidar); C_0, concentration extrapolated to time zero; $t_{1/2}$, half-life; V_{ss}, volume of distribution at steady state; CL, clearance.

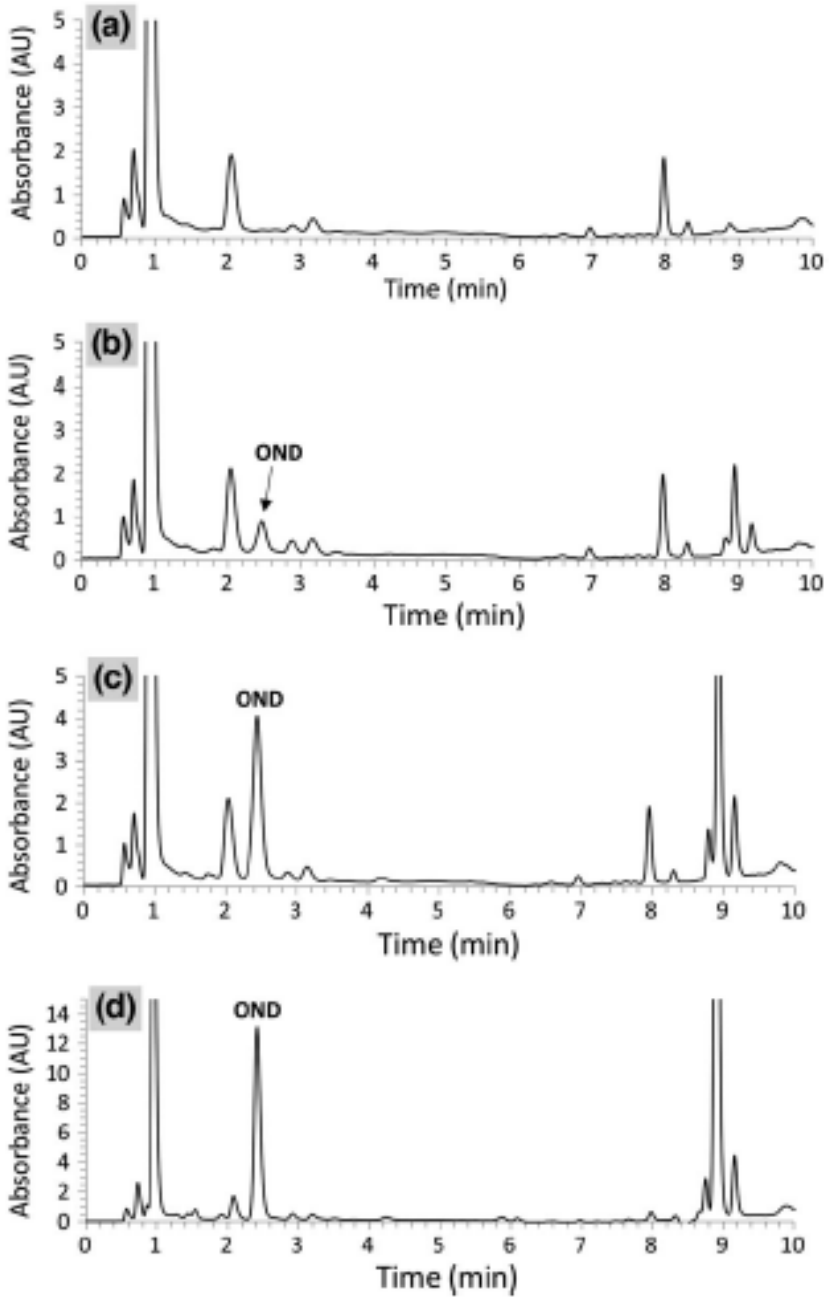

Figure A.1.1 Representative HPLC-UV chromatograms for ondansetron (OND) in rat plasma. **A**, blank rat plasma; **B**, rat plasma spiked with 10 ng/mL OND (LLOQ); **C**, rat plasma spiked with 50 ng/mL OND; **D**, rat plasma sample from pharmacokinetic study obtained 15 min following intravenous administration of OND (5 mg/kg). Chromatograms were observed at λ = 310 nm.

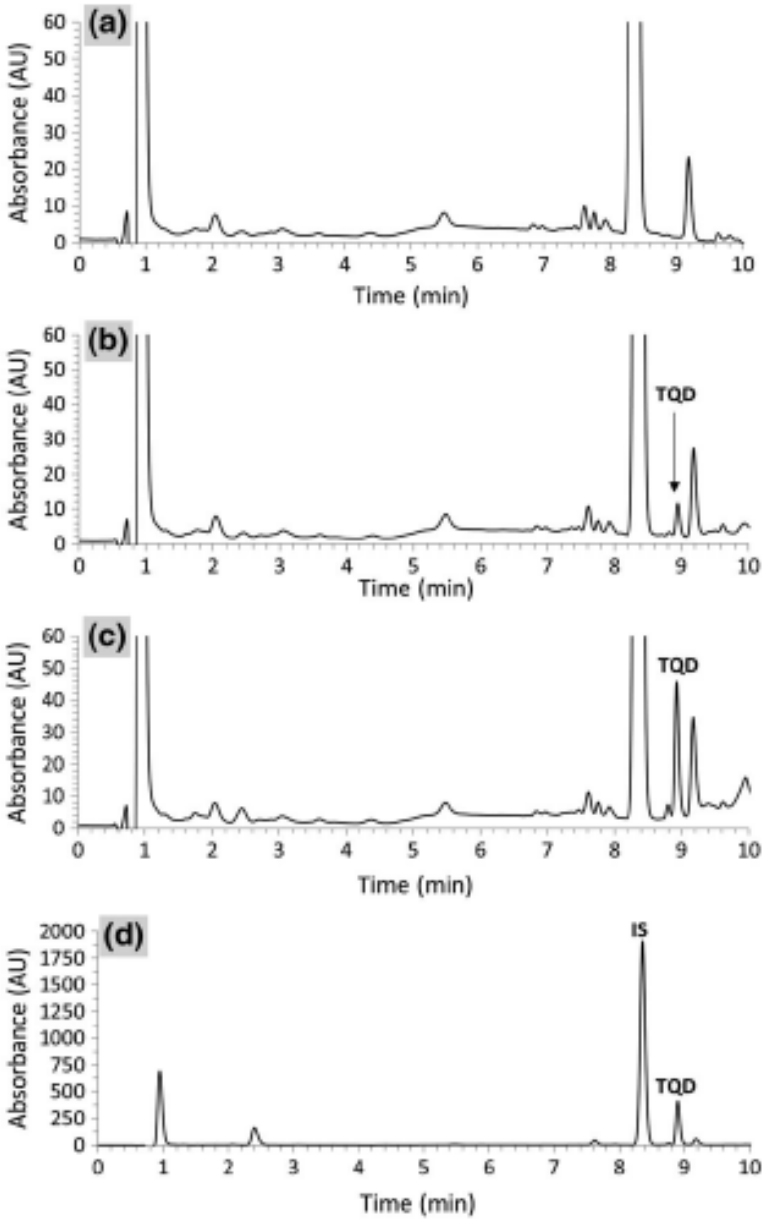

Figure A.1.2 Representative HPLC-UV chromatograms for tariquidar (TQD) and internal standard (IS) in rat plasma. **A**, blank rat plasma; **B**, rat plasma spiked with 50 ng/mL TQD (LLOQ); **C**, rat plasma spiked with 200 ng/mL TQD; **D**, rat plasma sample from pharmacokinetic study obtained 75 min following intravenous administration of TQD (15 mg/kg). Chromatograms were observed at λ = 240 nm.

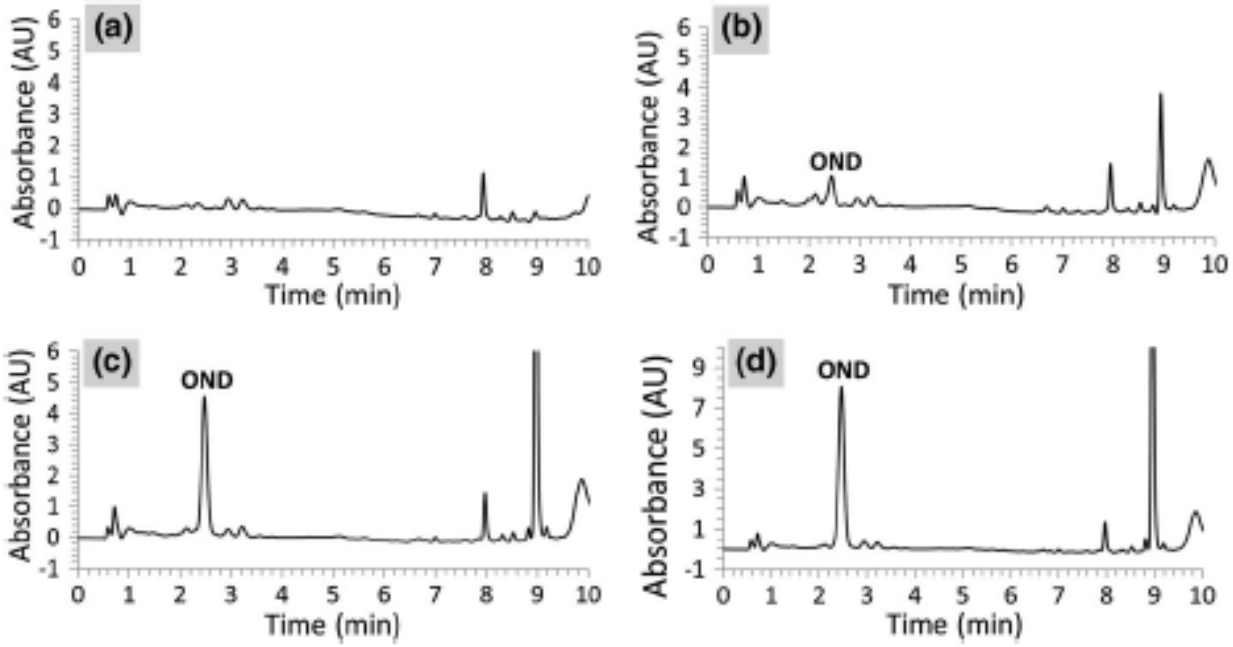

Figure A.1.3 Representative HPLC-UV chromatograms for ondansetron (OND) in human plasma. **A**, blank human plasma; **B**, human plasma spiked with 10 ng/mL OND (LLOQ); **C**, human plasma spiked with 50 ng/mL OND; **D**, human plasma spiked with 100 ng/mL OND. Chromatograms were observed at λ = 310 nm.

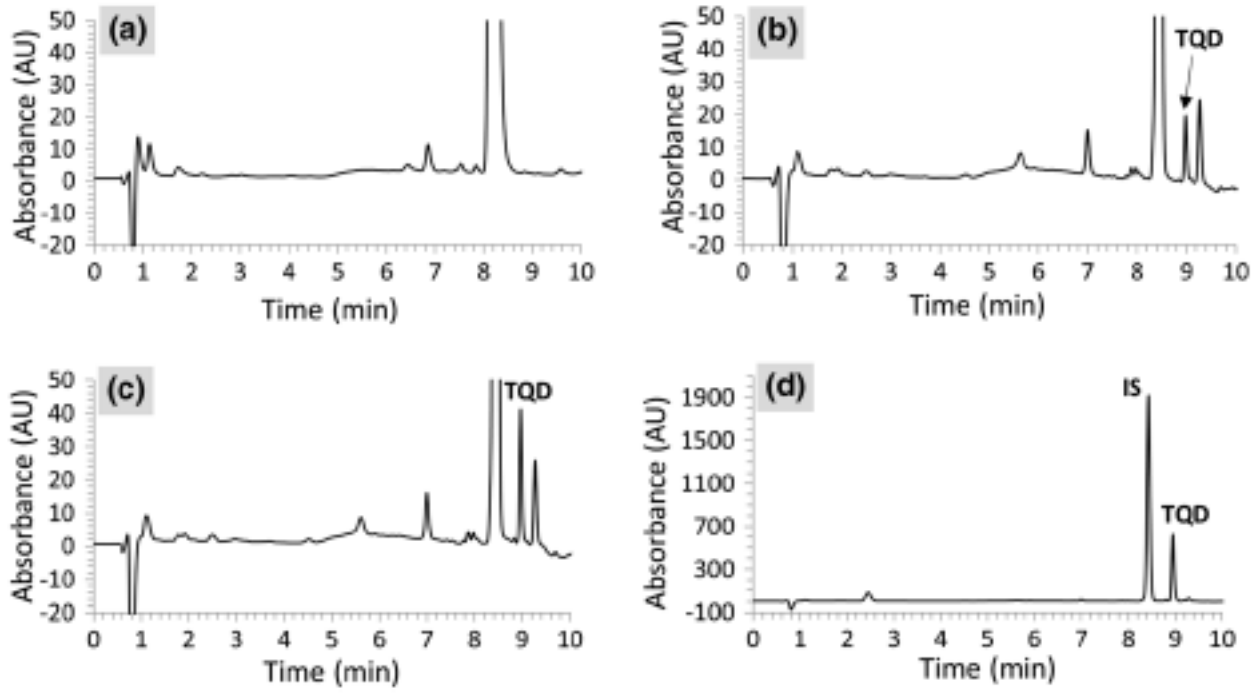

Figure A.1.4 Representative HPLC-UV chromatograms for tariquidar (TQD) and internal standard (IS) in human plasma. **A**, blank human plasma; **B**, human plasma spiked with 50 ng/mL TQD (LLOQ); **C**, human plasma spiked with 100 ng/mL TQD; **D**, human plasma spiked with 1000 ng/mL TQD. Chromatograms were observed at λ = 240 nm.

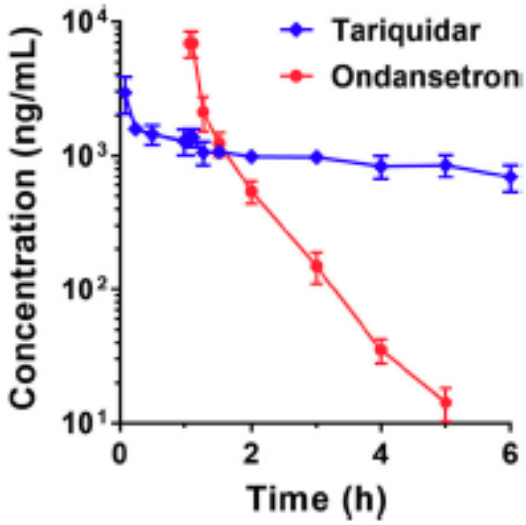

Figure A.1.5 Plasma concentration-time profiles following intravenous co-administration of ondansetron (5 mg/kg) and tariquidar (15 mg/kg) in male Sprague Dawley rats (mean ± SD, n = 4). Ondansetron was administered 1 h after administration of tariquidar.

Appendix 2 Is rat a good model for assessment of particulate-based taste-masked formulations?[3]

A.2.1 Introduction

The oral route is the most popular and convenient route for drug administration (233). For the prescription of medicinal products to patient populations such as pediatrics and geriatrics the acceptability of a solid oral dosage form can be paramount to the products success(234). There are several challenges to overcome when designing solid oral dosage forms for children and older adults. For example, children can have issues with conventional solid dosage forms due to poor palatability, limited dose flexibility, difficulty swallowing, recalcitrance, and differences in anatomy and physiology (234-236). Therefore, there can be a subsequent impact on therapeutic performance of the product. For pediatrics, there have been recent developments in European Union (EU) legislation (Reg 1901/2006/EU and Reg 1902/2006/EU) stating that new medicines coming to commercial markets must demonstrate pediatric suitability (237). Geriatrics also receiving a similar spotlight with calls for an update in legislation for geriatric drug development (238, 239). Consequently, there have been increased discussions on the development of patient-centric particulate-based oral dosage forms for these specific populations. Many Active Pharmaceutical Ingredients (APIs) and excipients are known to cause an aversive taste response (240). The unpleasant taste has been shown to greatly affect acceptability of a dosage form (241). Therefore, taste-masking strategies need to be utilized when these challenges occur. Particulate-based oral dosage forms can have a polymer coating applied to provide a physical barrier between the aversive tasting API and taste receptors within the oral cavity. The addition of coatings to particulates to prevent a taste response reports have shown a significant increase in

[3] Joseph Ali, Manting Chiang, Jong Bong Lee, Gregory O. Voronin, Joanne Bennett, Anne Cram, Leonid Kagan, Martin C. Garnett, Clive J. Roberts, Pavel Gershkovich (Published: European Journal of Pharmaceutics and Biopharmaceutics)

palatability of the dosage form when compared to API alone (242). This demonstrates the effectiveness of coatings in particulate-based formulations for taste-masking and increasing acceptability in pediatrics. Particulate-based oral dosage forms may be used for better acceptability in pediatrics due to enhanced palatability(243), flexible dosing, and improved swallowability (244). Particulate-based oral formulations such as multi-particulates, sprinkle capsules, suspensions, and granules are intended to be swallowed from the oral cavity intact. Appropriate preclinical assessment method is required to investigate the efficiency of taste-masking in coated particulate-based formulations.

Currently the most common method for taste evaluation for solid oral dosage forms is using human taste panels (245). However, target populations that require taste-masked formulations, such as pediatrics, may not be suitable for this assessment method due to ethical concerns, and the target population may have high inter-individual variability (245). *In vitro* drug release and dissolution studies can be used for the determination of drug released from particulate-based taste-masked formulations, to determine if the concentration is above the taste threshold. However, there is no general consensus on what parameters should be used in an oral cavity dissolution test (246). What is agreed on is that biorelevant dissolution testing is of great value and allows for a robust assessment method with better predictions of *in vivo* behavior for the formulations of interest (247-251).

Currently most common preclinical *in vivo* taste evaluation method for liquid dosage forms is the Brief-Access Taste Aversion (BATA) method. Often mice and rats are deprived of water for 16 – 24 hours for motivation to drink. Then the animal is placed into ‘lickometer’ apparatus which records the number of licks that the rodent makes for different concentrations of the drug presented in several sipper tubes. A high number of licks (relative to a suitable control) indicates an acceptable taste whilst those solutions with aversive taste will suppress the number of licks (252). It has been reported that the taste aversion data of model bitter tasting drugs in this rodent model has good correlation to human taste data (253-255). What needs to be explored is whether

the BATA method in rats could be adapted to also allow the assessment of particulate-based taste-masked formulations. As the taste response associated with particulate-based taste-masked formulations is dependent on the degree of drug release within the oral cavity, it is imperative to understand the characteristics of the rat oral cavity to investigate the applicability of the rat taste aversion model to particulate-based formulations.

The dissolution of solid dosage forms in the rat oral cavity is dependent on the physicochemical characteristics of rat saliva, the dissolution media of the rat oral cavity. Therefore, further investigation is needed to determine rat saliva physiochemical characteristics and to assess drug dissolution of model bitter tasting APIs in saliva. In this study two model bitter APIs (sildenafil citrate, and efavirenz) were used to compare dissolution of in human and rat saliva.

Sildenafil citrate acts as a selective inhibitor of cGMP-specific phosphodiesterase type 5 (PDE 5) and is used primarily in the treatment of erectile dysfunction. However, sildenafil citrate also has therapeutic applications in the management of pediatric pulmonary hypertension. Sildenafil citrate is a BCS Class I drug that is known to produce a bitter taste response (252). Efavirenz is in the non-nucleoside reverse-transcriptase inhibitor (NNRTI) family of anti-retroviral therapy that is used in the treatment of human immunodeficiency virus (HIV), including the treatment of pediatric HIV. It is a BCS Class II drug that is bitter tasting and gives burning mouth syndrome (256). Both these model drugs have clinical use for pediatric populations, and both have issues for solid oral administration due to aversive taste responses.

Therefore, the aim of the present work was to determine if rat saliva has appropriate physicochemical and drug dissolution properties for potential adaptation of a rat taste preclinical taste model to the assessment of particulate-based taste-masked formulations.

A.2.2 Materials and methods

Sildenafil citrate API powder was donated by Pfizer Ltd. (Sandwich, UK). Efavirenz API powder was purchased from ChemShuttle (Wuxi City, China). Pilocarpine hydrochloride was purchased from Sigma-Aldrich (UK). Methyl-tert-butyl ether (MTBE) was purchased from Fisher Scientific (UK). All solvents used in the study were HPLC grade or higher.

A.2.2.1 Collection of human saliva from healthy adult volunteers

Human saliva was collected in accordance with Ethics Reference Number: R12122013 from Faculty of Medicine and Health Sciences, Nottingham University Hospitals, as previously described (257, 258). Informed written consent was obtained from all volunteers. All data was held in agreement with the Data Protection Act. Exclusion criteria for the volunteers included chronic or acute illness in the past 3 months, cold or flu symptoms, oral health concerns, and taking medication (except contraceptives). Before collection of saliva (at least 2 hours prior) volunteers were asked to not eat, smoke, drink or use oral hygiene. To avoid differences in saliva composition due to circadian rhythms, all saliva was collected between 14:00 and 16:00 h. Participants were asked to chew on 5 cm × 5 cm square of Parafilm® for stimulated saliva (SS), which is a known inert material that is widely used for mechanical stimulation of saliva (259-262). To donate saliva, participants were asked to lean forward and drain saliva into sterile polypropylene graduated centrifuge tubes via sterile disposable funnels (Grenier Bio-One, UK). Saliva samples were then flash frozen in liquid nitrogen and stored at −80 °C. In total, four volunteers donated saliva. The donated saliva was pooled, characterized, and used in dissolution studies.

A.2.2.2 Collection of stimulated rat saliva

All procedures for rat saliva collection were reviewed and approved by the Rutgers University Institutional Animal Care and Use Committee. Male Sprague-Dawley rats (Envigo, USA) 8 – 12 weeks old were used for saliva collection. Animals were housed under controlled temperature, twelve-hour light/dark cycle and free access to food and water.

For the collection of rat saliva there are two main approaches described in literature. Firstly, intra-oral cannulation of salivary duct orifices to gather saliva from their respective glands (263-267). Secondly, an elevation collection method, that collects saliva passively from the mouth from anaesthetized animals (268, 269).

The saliva collection method used in this work was an optimization of the previously reported non-invasive, elevation sialometric method (268, 269). This sialometric method involves anaesthetizing animals, then administering a sialagogue agent, and orientating animals head in a downwards slope to which then saliva can passively flow into collection tubes. General anesthesia was induced with inhalation of 3% isoflurane, and anesthesia was maintained throughout collection with isoflurane via a nose cone. Specific 3D printed platforms were necessary for efficient saliva collection as the platform must hold a number of components at once: a nose cone for anesthesia, the collection tube, orientation of the animals' head downwards without impacting cardiovascular parameters, and engagement of the lower incisors to keep the mouth open during collection, as shown in Figure 1. These platforms were tapered in height from 50 mm to 10 mm, width 100 mm, depth 125 mm.

Immediately before saliva collection 2 mL saline was injected for fluid replacement by subcutaneous bolus. Saliva was then stimulated by intraperitoneal administration of 2 mg/kg pilocarpine hydrochloride. Immediately following the injection, the animals were positioned on top of the platforms for saliva collection. After collection, the animals were left to recover for 48 hours, and were given an additional 2 mL saline replacement 24 hours post collection. Immediately following collection, pH of individual saliva samples was measured with a Mettler Toledo S220 Seven Compact pH/ion meter, connected to an InLab Micro pH electrode (Mettler Toledo, Switzerland). Saliva samples were then flash frozen in liquid nitrogen and stored at -80 °C until further analysis.

A.2.2.3 Characterization of rat and human saliva

Pooled stimulated human saliva was characterized for: pH, buffer capacity, viscosity, and surface tension as previously described (257, 258). As stated previously, individual rat saliva samples were tested for pH immediately after collection. Pooled stimulated rat saliva was characterized for: buffer capacity, viscosity, and surface tension. Two hundred µL of rat saliva, and 4 mL of human saliva samples were brought to 37 °C in a water bath. Initial pH was determined using Mettler Toledo S220 Seven Compact pH/ion meter, connected to an InLab Micro pH electrode. Saliva samples were titrated with 0.01 M HCl until pH had decreased by 1 unit. Buffer capacity was then calculated in mmol H^+/L, by the amount of acid added. A Modular Compact Rheometer MCR 302 (Anton Paar GmbH, Germany) was used with a cone-plate set up to measure viscosity of saliva. The cone used was a CP50-2-SN30270, diameter 49.972 mm, angle 2.016 °, truncation 211 µm. Viscosity measurements were taken at 37 °C over three logarithmic decades for shear rate from 1 – 1000 s^{-1} with measurements taken at 8 points per decade. Data was recorded on Rheoplus software (Anton Paar GmbH, Germany) for analysis. A DSA 100 Drop Shape Analyser with DSA 4 software (Kruss GmbH, Germany) was used to measure surface tension of saliva by using the pendant drop method with Laplace-Young computational method. Temperature was set to 37 °C using an MB-5 heat circulator and water bath (Julabo GmbH, Germany).

A.2.2.4 Oral cavity dissolution studies of sildenafil citrate and efavirenz in pooled rat and human stimulated saliva

The volume of saliva used in the oral cavity dissolution method was based on resident saliva volumes reported for adult humans (270, 271). Multiple small-scale dissolution vessels were kept at 37 °C each with a magnetic stirrer in a setup as was previously described for human saliva dissolution studies (258). Separate dissolution vessels were used in parallel to measure the concentration of drug over different time points. At each time point pH of saliva was recorded. Pooled stimulated saliva (200 µL) was added to 10 mg of sildenafil citrate. Pooled stimulated saliva (250 µL) was added to 10 mg of efavirenz. A constant stirring speed of 200 rpm was used

to allow adequate mixing of solid material in relatively small volumes of media. Both rat and human stimulated saliva were used as dissolution media for the two drugs of interest. After each time point was reached, the entire contents of the dissolution vials were transferred to Costar Spin-X centrifuge tubes with 0.22 µm pore CA filters (Corning B.V. Life Sciences, UK), and centrifuged for 10 minutes at 17,000 x *g*.

A.2.2.5 Analytical procedures

Filtered dissolution sample (10 µL) was transferred to a glass test tube, to which the following was added: 10 µL of internal standard (IS), 90 µL of blank saliva (for further dilution of the drug to the range suitable for HPLC analysis), and 400 µL of 50:50 acetonitrile, methanol mixture (stored at -20 °C). After filter centrifugation of efavirenz samples, 180 µL of filtered dissolution sample was transferred to a glass test tube, to which 20 µL of internal standard (IS), and 400 µL of acetonitrile/methanol mixture (50:50, stored at -20 °C) was added. Then, the test tubes were vortex mixed for 2 minutes. Next, methyl-tert-butyl ether (MTBE) was added to each test tube (3 mL for sildenafil, 4 mL for efavirenz), and vortex mixed at 1200 min^{-1} for 10 minutes in a multi-tube vortexer (VWR VX-2500). Then, samples were centrifuged at 1690 x *g* for 10 minutes. Following centrifugation, the organic layer was transferred and evaporated to dryness under nitrogen. The dry residue was then reconstituted with 100 µL of mobile phase (44% ACN, 56% water). Reconstituted samples were then vortex mixed and centrifuged, before transferring the contents to HPLC vials. All calibration and quality control samples underwent the same sample preparation procedures as stated for the dissolution samples.

Waters (Milford, USA) 2695 separations module HPLC system equipped with Waters 996 PDA UV detector was used. Samples in the autosampler were maintained at 4 °C and the column oven was set to 40 °C. Empower 2 software was used for data processing. Separation of the extracted sildenafil citrate and efavirenz samples were achieved with Waters Xterra C18 2.1 x 100 mm, 3.5 µm particle size column, with Xterra MS C18 2.1 x 10 mm 3.5 µm guard column and pre-column filter including a 0.5 µm stainless steel frit. Mobile phase was 56% 0.2 M ammonium

acetate buffer (pH 7.0) and 44% ACN, eluted at isocratic conditions at 0.3 mL/min for sildenafil citrate, and 0.2 mL/min for efavirenz. Bifonazole was used as the internal standard (IS) for sildenafil. Sildenafil citrate was used as the internal standard (IS) for efavirenz. Sildenafil citrate and bifonazole were detected at 224 nm at 3.1 and 7.9 minutes respectively. Efavirenz and sildenafil were detected at 290 nm and 224 nm at 11.2 and 4.0 minutes respectively. Validation of both assays for these compounds was performed following FDA guidelines [40]. A summary of validation parameters is shown in Tables 1 & 2 for sildenafil and efavirenz respectively. Calibration curves were constructed in the concentration ranges expected from dissolution of the drug in saliva. Calibration curves all had correlation coefficient (r^2) values of >0.99.

A.2.2.6 Statistical Analysis

Results are expressed as mean ± standard deviation (SD). pH, buffer capacity and surface tension were analyzed with unpaired t test. Dissolution and viscosity results were analyzed with one-way ANOVA and Sidak's multiple comparisons test. A $p < 0.05$ was considered to represent a significant difference.

A.2.3 Results

A.2.3.1 Characterization of rat and human saliva

Stimulated rat (RS SS) and human saliva (HS SS) was characterized for: pH, buffer capacity, viscosity, and surface tension (Figure 2). The characterization results for human saliva were in agreement with our previously reported works [25,26]. However, all characterization parameters of stimulated rat saliva were substantially different from stimulated human saliva. Stimulated rat saliva had dramatically higher pH compared to stimulated human saliva (Figure 2A), but substantially lower buffer capacity (Figure 2B) and surface tension (Figure 2C). Stimulated rat saliva had also statistically significantly lower ($p < 0.05$) viscosity at shear rates from 1.33 – 10.0 s^{-1} compared to stimulated human saliva, whist no significant differences between rat and human saliva at 1 s^{-1} nor in the range of 13.33 – 1000 s^{-1} shear rates (Figure 2D).

Dissolution of sildenafil citrate (SC) API powder was assessed in pooled stimulated rat and human saliva. Concentrations of SC in human saliva were profoundly higher than the concentrations of SC in rat saliva, as shown in Figure 3. Changes in pH of saliva over SC dissolution time course are shown in Figure 4. In both HS and RS saliva pH was shown to drop to pH 4.5 within the first time point (1 min).

A.2.3.2 Dissolution of efavirenz in saliva

Dissolution of efavirenz (EFV) API powder was assessed in pooled stimulated rat and human saliva. Concentrations of EFV in human saliva were substantially lower than in rat saliva, as shown in Figure 5. Changes in saliva pH over EFV dissolution time course are shown in Figure 6. In both HS and RS saliva pH was shown to increase over 2 minutes with substantial differences between HS and RS throughout the dissolution time course.

A.2.4 Discussion

Most currently used taste assessment methods were designed for the assessment of liquid dosage forms (245). However, methods designed for the assessment of liquid dosage forms with taste-masking agents may not be optimal for particulate-based formulations. Particulate-based taste-masked formulations aim to prevent an aversive taste response by reducing the release of the poorly tasting drug into the oral cavity. Thus, the dissolution properties of the API in saliva become critical. There is a lack of *in vivo* preclinical models that take into account the interaction between particulate-based formulations and oral cavity saliva. To assess the applicability of rat as an *in vivo* taste evaluation model for particulate-based formulations, rat saliva was characterized in this work for parameters important for drug dissolution and compared to these parameters in human saliva. Moreover, dissolution of model bitter APIs were assessed in rat saliva and compared head to head to dissolution in human saliva. Rat saliva was found to be dramatically different to human saliva for all tested parameters. The pH of rat saliva was substantially more alkaline compared to human saliva, as shown in Figure 2A. The rat saliva pH

levels recorded in this study are also supported by similar findings in literature (272). The difference in pH between rat and human saliva can significantly affect the dissolution profile of drugs, especially of weakly acidic ionizable APIs and excipients due to higher aqueous solubility at higher pH. For example, acidic drugs clinically relevant for pediatric use and taste aversiveness such as efavirenz, diclofenac and chloral hydrate can achieve higher concentrations in rat oral cavity compared to the human oral cavity due to this pH effect on solubility. In addition, taste-masking strategies such as the use of weak base anion exchange resins will not function in a manner similar to human oral cavity at the higher pH of rat saliva (242). Therefore, this difference in pH between rat and human saliva could impact the extrapolation of particulate-based formulation rat taste studies to humans.

The buffer capacity of rat saliva was significantly lower than human saliva, as displayed in Figure 2B. As saliva is a buffered aqueous medium the dissolution rate of sparingly soluble weak acid or weak base drugs can be affected due to ionic interactions at the microenvironment solid-liquid interface (273). The impact the buffer has on drug dissolution is dependent on several factors, such as ionization constants of the buffer and drug, molar concentration of the buffer, buffer capacity, and the concentration of buffer species reacting with the drug (273). Therefore, the results suggest that it is likely that the dissolution of drugs could be affected by this difference in buffer capacity which could then impact the correlation between rat and human particulate-based formulation taste studies.

Previous studies have shown the effect of surface tension on drug dissolution (274, 275). The surface tension of rat saliva was dramatically lower than the surface tension of human saliva. The Washburn equation explains that the penetration of dissolution media is the rate limiting step to solid dosage form disintegration, and is directly influenced by media surface tension (276). Therefore, the disintegration of particulate-based formulations in the oral cavity will be affected by saliva surface tension.

From shear rates 1.33 – 10.0 s^{-1} rat saliva viscosity was significantly lower than the viscosity of human saliva. The relationship of viscosity on drug dissolution rate has shown to be inversely proportional (277). Using the Noyes-Witney dissolution model, an increase in dissolution media viscosity would increase the thickness of boundary layers and decrease the diffusion coefficient (278). On the other hand, the shear rate experienced in humans from the initial perception of solids within the oral cavity has shown to be around 50 s^{-1} (279). At 50 s^{-1} no significant differences in viscosity were observed between rat and human saliva. However, currently there are no reports of shear rates experienced in rats for initial perception of solids within the oral cavity, so it is impossible to determine how these viscosity differences could affect taste *in vivo*. Rheology is known to be a key element in the oral processing of solid oral dosage forms (279). Differences in rheology and potential differences in oral cavity shear could impact the correlation of particulate-based taste-masked formulations assessment in a rat model.

The substantial differences observed from the characterization data suggest that there could be differences in dissolution of drugs between human and rat saliva. Therefore, it was important to confirm this assumption by investigating the dissolution of model bitter APIs with distinct physicochemical properties.

The concentration of sildenafil citrate was found to be significantly lower in rat saliva compared to human saliva. Conversely, the concentration of efavirenz was shown to be significantly higher in rat saliva compared to human saliva. These differences in dissolution profiles between the two saliva sources are likely to be due to the differences in physicochemical properties of saliva. For sildenafil citrate dissolution, the measurements of dissolution chamber pH for both saliva types were shown to remain at pH 4.5 after the one-minute time point as shown in Figure 4. The immediate drop in saliva pH likely suggests that the introduction of sildenafil citrate into saliva had caused dissociation of the salt back into the sildenafil free base (280). The pH over the remaining time course in both rat and human saliva was maintained around pH 4.5, this suggests the differences seen in sildenafil concentrations over the time course between the two saliva sources

was not primarily due to pH. Instead, these differences in dissolution for sildenafil between the two saliva types may be caused by other saliva parameters mentioned previously. For efavirenz the difference in dissolution profile from rat and human saliva was likely due to the differences in saliva pH. Efavirenz is known to have a pH-dependent relationship with regards to solubility. Previous studies have shown that when media pH exceeds pH 8.0, the solubility of efavirenz increases 6-fold compared to the solubility at pH 7.4 (281). Figure 6 shows that the differences in saliva pH are likely to be a main contributing factor to the differences in EFV concentration. However, in this study the difference in efavirenz concentration was much greater than 6-fold, suggesting that other characteristics of rat saliva were also contributors to the dissolution profile observed.

In order to have a reliable rat taste model to assess particulate-based taste-masked formulations, and to have direct correlation to human taste procedures the characteristics of rat saliva should be to some extent similar to human saliva. The dissolution of drugs would have to be similar in both rat and human saliva as the media of the oral cavity would dictate the release of drug from taste-masked formulations. However, this study has shown that the physicochemical characteristics of rat saliva is very different from human saliva. Moreover, this was further confirmed by the dissolution of two model bitter drugs being completely different in rat versus human saliva. Therefore, the data suggest that a rat taste model for the assessment of particulate-based taste-masked formulations would not likely be representative of the taste response from human taste panels. This might have potential implications for the possibilities around the adaptation of currently existing BATA models used successfully for liquid taste masked formulations. Looking at other common laboratory animals, previous comparisons have also shown that canine saliva is also different to human saliva as it has higher pH, buffer capacity, and concentration of minerals (281). These considerable changes in saliva characteristics between species suggest that particulate-based taste-masked formulations should be for now assessed *in vivo* utilizing human taste panels. Further work is needed to hopefully find another suitable

species for a preclinical *in vivo* model with similar saliva characteristics to humans. Moreover, *in vitro* biorelevant oral cavity dissolution models, mimicking physicochemical parameters of human saliva and fluid dynamics of oral cavity could also provide useful alternative to human panels in the future.

A.2.5 Conclusion

In this study it has been found that stimulated rat saliva is significantly different from stimulated human saliva in terms of pH, buffer capacity, surface tension, and viscosity. In addition, the dissolution of two model bitter drugs, sildenafil citrate and efavirenz gave very different concentrations in stimulated rat saliva compared to stimulated human saliva. These differences suggest that the fate of the particulate-based dosage forms in the rat oral cavity could be quite different compared to human oral cavity. This discrepancy in saliva parameters and dissolution of model drugs suggests that a rat preclinical taste evaluation method of particulate-based taste-masked formulations could be not representative of the taste of these particulate-based taste-masked formulations in humans. Alternative preclinical *in vivo* models in other species, or improved biorelevant *in vitro* models should be considered instead.

Table A.2.1 Validation parameters measured for HPLC-UV assay of sildenafil citrate in stimulated human saliva (HS SS) and stimulated rat saliva (RS SS). Validation outputs include lowest limit of quantification (LLOQ), lower quality control (LQC), middle quality control (MQC), higher quality control (HQC), and recovery. Accuracy and precision of the assay gave acceptable values of relative error (RE), and relative standard deviation (RSD) respectively from both intra-day and inter-day analyses (282).

Sildenafil citrate		**LLOQ**			**LQC**					**MQC**					**HQC**					**Recovery ± SD (%)**
		Conc. (ng/mL)	**RSD (%)**	**RE (%)**	**Conc. (ng/mL)**	**Intra-day**		**Inter-day**		**Conc. (ng/mL)**	**Intra-day**		**Inter-day**		**Conc. (ng/mL)**	**Intra-day**		**Inter-day**		
	n					**RSD (%)**	**RE (%)**	**RSD (%)**	**RE (%)**		**RSD (%)**	**RE (%)**	**RSD (%)**	**RE (%)**		**RSD (%)**	**RE (%)**	**RSD (%)**	**RE (%)**	
HS SS	6	20	<20	<20	100	<15	<15	<15	<15	300	<15	<15	<15	<15	1200	<15	<15	<15	<15	100.11 ± 0.26
RS SS	6	20	<20	<20	100	<15	<15	<15	<15	300	<15	<15	<15	<15	1200	<15	<15	<15	<15	100.13 ± 0.07

Table A.2.2 Validation parameters measured for HPLC-UV assay of efavirenz in stimulated human saliva (HS SS) and stimulated rat saliva (RS SS). Validation outputs include lowest limit of quantification (LLOQ), lower quality control (LQC), middle quality control (MQC), higher quality control (HQC), and recovery. Accuracy and precision of the assay gave acceptable values of relative error (RE), and relative standard deviation (RSD) respectively from both intra-day and inter-day analyses (282).

Efavirenz		**LLOQ**			**LQC**					**MQC**					**HQC**					**Recovery ± SD (%)**
		Conc. (ng/mL)	**RSD (%)**	**RE (%)**	**Conc. (ng/mL)**	**Intra-day**		**Inter-day**		**Conc. (ng/mL)**	**Intra-day**		**Inter-day**		**Conc. (ng/mL)**	**Intra-day**		**Inter-day**		
	n					**RSD (%)**	**RE (%)**	**RSD (%)**	**RE (%)**		**RSD (%)**	**RE (%)**	**RSD (%)**	**RE (%)**		**RSD (%)**	**RE (%)**	**RSD (%)**	**RE (%)**	
HS SS	6	75	<20	<20	200	<15	<15	<15	<15	3000	<15	<15	<15	<15	15000	<15	<15	<15	<15	105.11 ± 0.18
RS SS	6	75	<20	<20	200	<15	<15	<15	<15	3000	<15	<15	<15	<15	15000	<15	<15	<15	<15	105.29 ± 0.01

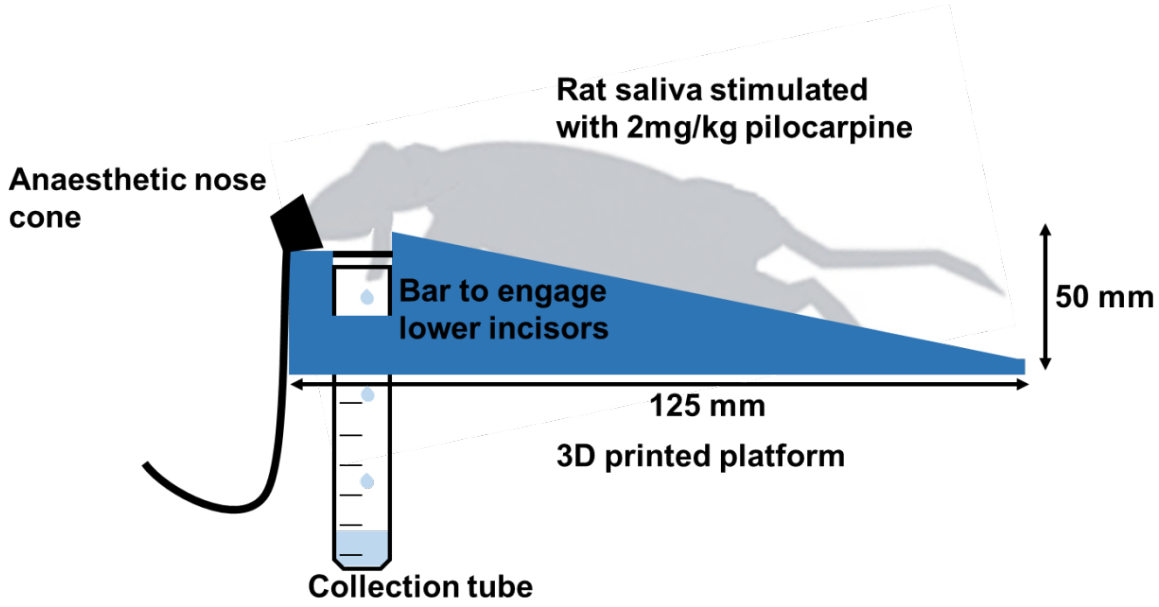

Figure A.2.1 Schematic description of the non-invasive sialometric method to collect stimulated saliva from anaesthetized rats.

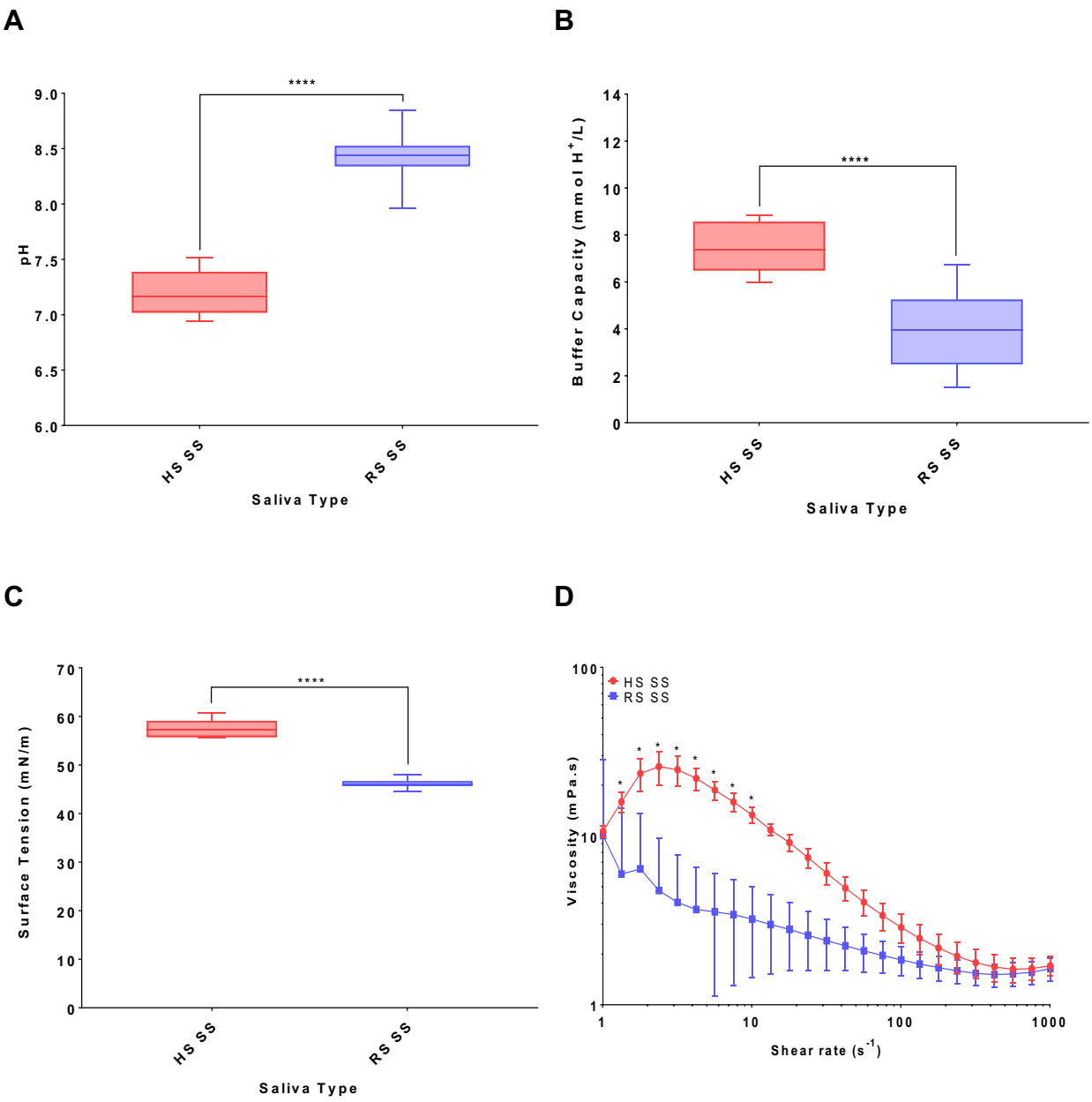

Figure A.2.2 Characterization of stimulated rat saliva (RS SS) and stimulated human saliva (HS SS). (A) pH of individual stimulated rat saliva samples and pooled stimulated human saliva (n= 24 rat, n= 12 human). (B) Buffer capacity of pooled stimulated rat and human saliva (n= 12 rat, n= 8 human). (C) Surface tension of pooled stimulated rat and human saliva (n= 12 rat, n=8

human). (D) Viscosity of pooled stimulated rat and human saliva at different shear rates (n= 12 rat, n= 3 human). Box represents median value, 25th and 75th percentile. Whiskers represent maximum and minimum values. Viscosity values are expressed as mean ± SD. Statistical analysis was performed using unpaired t-test for pH, buffer capacity, and surface tension. Statistical analysis was performed using one-way ANOVA and Sidak's multiple comparisons test for viscosity. Significant differences were observed for all parameters between rat and human saliva; **** $p < 0.0001$, * $p < 0.05$.

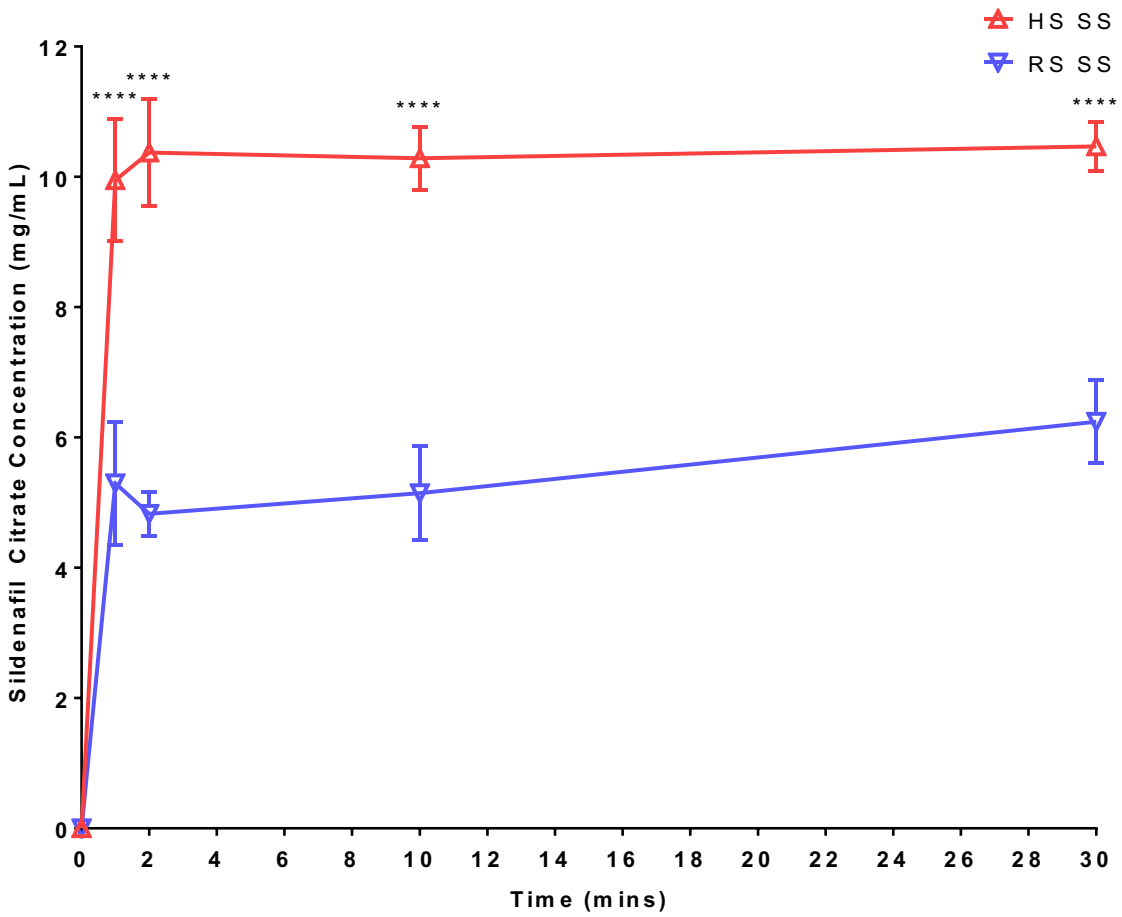

Figure A.2.3 Dissolution-time profile of sildenafil citrate (SC) API powder in pooled stimulated rat saliva (RS SS) and pooled stimulated human saliva (HS SS). Values are expressed as mean ± SD (n= 6). **** Significantly lower ($p < 0.0001$) concentration in rat compared to human saliva. Statistical analysis was performed using one-way ANOVA with Sidak's multiple comparisons test.

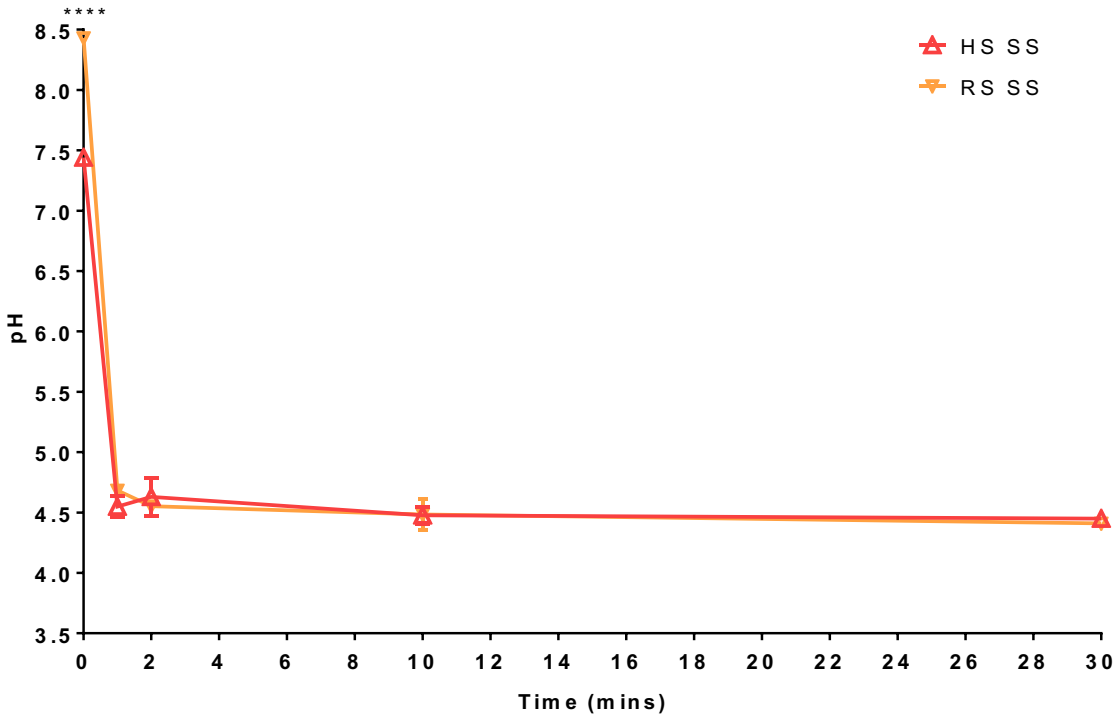

Figure A.2.4 pH of saliva over the course of sildenafil citrate dissolution in pooled stimulated human saliva (HS SS), and pooled stimulated rat saliva (RS SS). Values expressed as mean ± SD (n= 3). **** Significantly higher ($p < 0.0001$) pH in rat compared to human saliva. Statistical analysis was performed using one-way ANOVA with Sidak's multiple comparisons test.

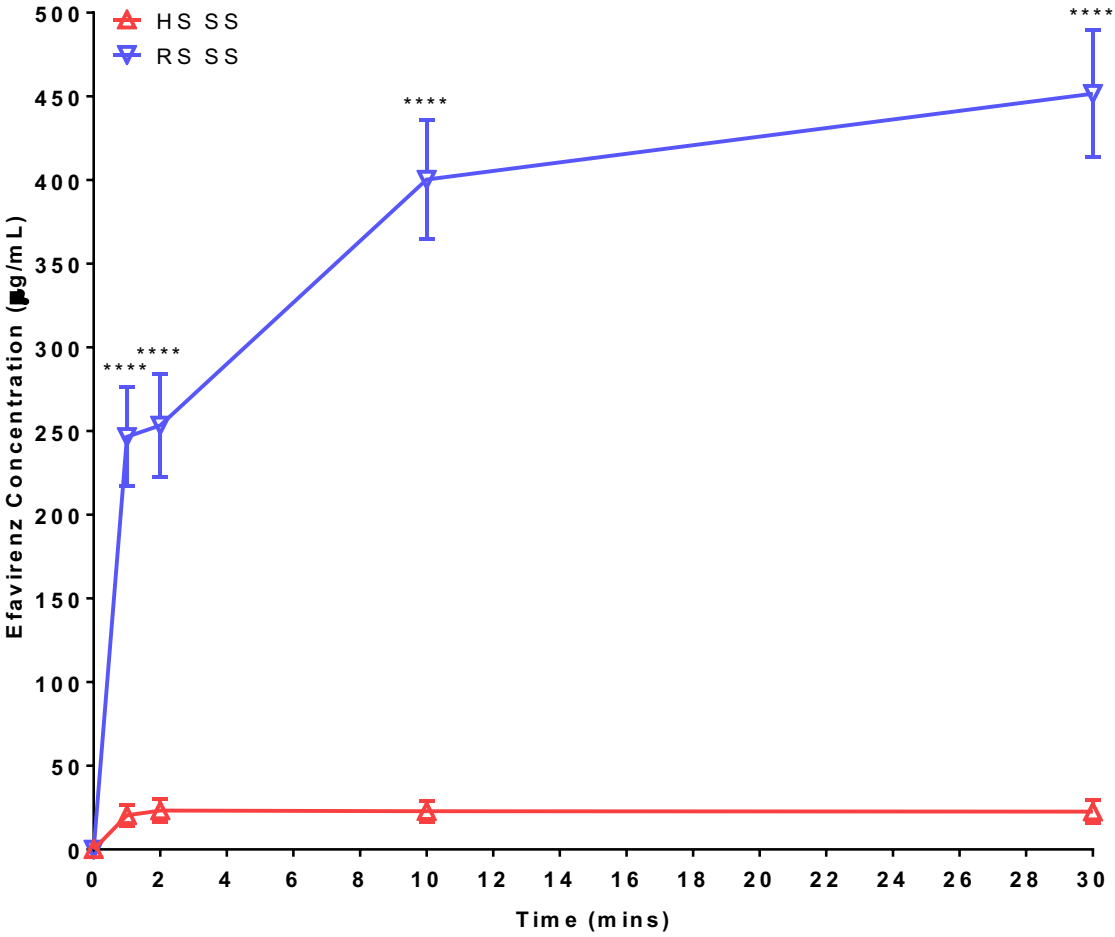

Figure A.2.5 Dissolution-time profile of efavirenz (EFV) API powder in pooled stimulated rat saliva (RS SS) and pooled stimulated human saliva (HS SS). Values are expressed as mean ± SD (n= 6). **** Significantly higher ($p < 0.0001$) concentration in pooled stimulated rat saliva compared to pooled stimulated human saliva. Statistical analysis was performed using one-way ANOVA with Sidak's multiple comparisons test.

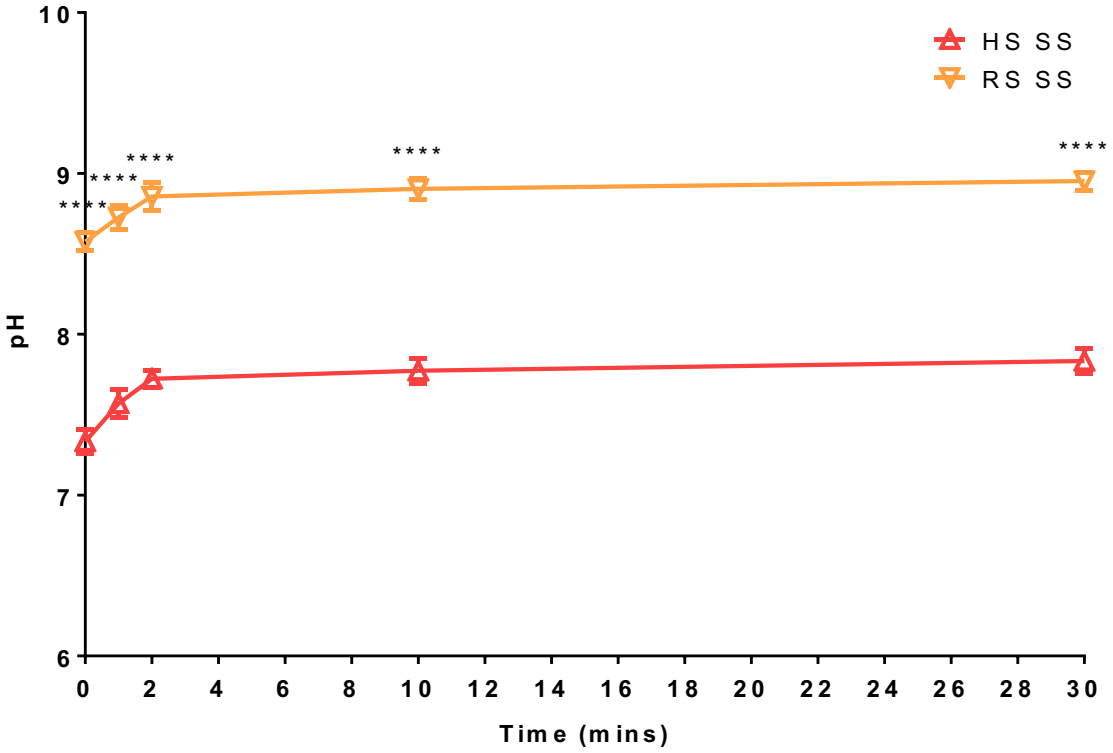

Figure A.2.6 pH measurements taken from saliva over the course of efavirenz dissolution in pooled stimulated human saliva (HS SS), and pooled stimulated rat saliva (RS SS). Values expressed as mean ± SD (n= 3). **** Significantly higher ($p < 0.0001$) pH in rat compared to human saliva. Statistical analysis was performed using one-way ANOVA with Sidak's multiple comparisons test.

References

1. Colloca L, Ludman T, Bouhassira D, Baron R, Dickenson AH, Yarnitsky D, et al. Neuropathic pain. Nat Rev Dis Primers. 2017;3:17002.
2. Merskey H BN, editor. Task Force on Taxonomy of the International Association for the Study of Pain: Classification of Chronic Pain. Description of Pain Syndromes and Definitions of Pain Terms.1994; Seattle, WA.
3. Cruccu G, Anand P, Attal N, Garcia-Larrea L, Haanpaa M, Jorum E, et al. EFNS guidelines on neuropathic pain assessment. Eur J Neurol. 2004;11(3):153-62.
4. Attal N, Bouhassira D, Baron R. Diagnosis and assessment of neuropathic pain through questionnaires. Lancet Neurol. 2018;17(5):456-66.
5. Klit H, Finnerup NB, Andersen G, Jensen TS. Central poststroke pain: a population-based study. Pain. 2011;152(4):818-24.
6. Rayment C, Hjermstad MJ, Aass N, Kaasa S, Caraceni A, Strasser F, et al. Neuropathic cancer pain: prevalence, severity, analgesics and impact from the European Palliative Care Research Collaborative-Computerised Symptom Assessment study. Palliat Med. 2013;27(8):714-21.
7. Bennett MI, Rayment C, Hjermstad M, Aass N, Caraceni A, Kaasa S. Prevalence and aetiology of neuropathic pain in cancer patients: a systematic review. Pain. 2012;153(2):359-65.
8. Clinic M. Available from: https://www.mayoclinic.org/diseases-conditions/diabetic-neuropathy/symptoms-causes/syc-20371580.
9. Dieleman JP, Kerklaan J, Huygen FJ, Bouma PA, Sturkenboom MC. Incidence rates and treatment of neuropathic pain conditions in the general population. Pain. 2008;137(3):681-8.
10. Clinic M.
11. Bouhassira D, Attal N, Alchaar H, Boureau F, Brochet B, Bruxelle J, et al. Comparison of pain syndromes associated with nervous or somatic lesions and development of a new neuropathic pain diagnostic questionnaire (DN4). Pain. 2005;114(1-2):29-36.
12. Health T. Available from: https://www.templehealth.org/services/conditions/atypical-facial-pain.
13. Nikolajsen L, Jensen TS. Phantom limb pain. Br J Anaesth. 2001;87(1):107-16.
14. Freynhagen R, Baron R, Tolle T, Stemmler E, Gockel U, Stevens M, et al. Screening of neuropathic pain components in patients with chronic back pain associated with nerve root compression: a prospective observational pilot study (MIPORT). Curr Med Res Opin. 2006;22(3):529-37.
15. Clinc M. Available from: https://www.mayoclinic.org/diseases-conditions/postherpetic-neuralgia/symptoms-causes/syc-20376588.
16. Finnerup NB, Haroutounian S, Kamerman P, Baron R, Bennett DL, Bouhassira D, et al. Neuropathic pain: an updated grading system for research and clinical practice. Pain. 2016;157(8):1599-606.
17. Borsook D. Neurological diseases and pain. Brain. 2012;135(Pt 2):320-44.
18. Watson JC, Sandroni P. Central Neuropathic Pain Syndromes. Mayo Clin Proc. 2016;91(3):372-85.
19. Yang Y, Wang Y, Li S, Xu Z, Li H, Ma L, et al. Mutations in SCN9A, encoding a sodium channel alpha subunit, in patients with primary erythermalgia. J Med Genet. 2004;41(3):171-4.
20. Baron R, Hans G, Dickenson AH. Peripheral input and its importance for central sensitization. Ann Neurol. 2013;74(5):630-6.

21. Patel R, Dickenson AH. Neuronal hyperexcitability in the ventral posterior thalamus of neuropathic rats: modality selective effects of pregabalin. J Neurophysiol. 2016;116(1):159-70.
22. Peyron R. Functional brain imaging: what has it brought to our understanding of neuropathic pain? A special focus on allodynic pain mechanisms. Pain. 2016;157 Suppl 1:S67-71.
23. van Hecke O, Austin SK, Khan RA, Smith BH, Torrance N. Neuropathic pain in the general population: a systematic review of epidemiological studies. Pain. 2014;155(4):654-62.
24. Attal N, Lanteri-Minet M, Laurent B, Fermanian J, Bouhassira D. The specific disease burden of neuropathic pain: results of a French nationwide survey. Pain. 2011;152(12):2836-43.
25. Torrance N, Smith BH, Bennett MI, Lee AJ. The epidemiology of chronic pain of predominantly neuropathic origin. Results from a general population survey. J Pain. 2006;7(4):281-9.
26. Finnerup NB, Attal N, Haroutounian S, McNicol E, Baron R, Dworkin RH, et al. Pharmacotherapy for neuropathic pain in adults: a systematic review and meta-analysis. Lancet Neurol. 2015;14(2):162-73.
27. Binder A, Bruxelle J, Rogers P, Hans G, Bosl I, Baron R. Topical 5% lidocaine (lignocaine) medicated plaster treatment for post-herpetic neuralgia: results of a double-blind, placebo-controlled, multinational efficacy and safety trial. Clin Drug Investig. 2009;29(6):393-408.
28. Demant DT, Lund K, Finnerup NB, Vollert J, Maier C, Segerdahl MS, et al. Pain relief with lidocaine 5% patch in localized peripheral neuropathic pain in relation to pain phenotype: a randomised, double-blind, and placebo-controlled, phenotype panel study. Pain. 2015;156(11):2234-44.
29. Backonja M, Wallace MS, Blonsky ER, Cutler BJ, Malan P, Jr., Rauck R, et al. NGX-4010, a high-concentration capsaicin patch, for the treatment of postherpetic neuralgia: a randomised, double-blind study. Lancet Neurol. 2008;7(12):1106-12.
30. Vinik AI, Perrot S, Vinik EJ, Pazdera L, Jacobs H, Stoker M, et al. Capsaicin 8% patch repeat treatment plus standard of care (SOC) versus SOC alone in painful diabetic peripheral neuropathy: a randomised, 52-week, open-label, safety study. BMC Neurol. 2016;16(1):251.
31. Burness CB, McCormack PL. Capsaicin 8 % Patch: A Review in Peripheral Neuropathic Pain. Drugs. 2016;76(1):123-34.
32. Attal N, de Andrade DC, Adam F, Ranoux D, Teixeira MJ, Galhardoni R, et al. Safety and efficacy of repeated injections of botulinum toxin A in peripheral neuropathic pain (BOTNEP): a randomised, double-blind, placebo-controlled trial. Lancet Neurol. 2016;15(6):555-65.
33. Shackleton T, Ram S, Black M, Ryder J, Clark GT, Enciso R. The efficacy of botulinum toxin for the treatment of trigeminal and postherpetic neuralgia: a systematic review with meta-analyses. Oral Surg Oral Med Oral Pathol Oral Radiol. 2016;122(1):61-71.
34. Lakhan SE, Velasco DN, Tepper D. Botulinum Toxin-A for Painful Diabetic Neuropathy: A Meta-Analysis. Pain Med. 2015;16(9):1773-80.
35. Yaksh TL. Central Pharmacology of Nociceptive Transmission. 4th Edision ed. Edinburgh: Churchill Livingston; 1999.
36. Fields HL, Basbaum, A.I. Central Nervous System Mechanisms of Pain Modulation. 4th Edision ed. Edinburgh: Churchill Livingston; 1999.
37. Willis WD, Coggeshall, R.E. Sensory Mechanisms of the Spinal Cord. 2nd Edition ed. New York: Plenum Press; 1991.
38. Millan MJ. The induction of pain: an integrative review. Prog Neurobiol. 1999;57(1):1-164.
39. Dolgin E. Fluctuating baseline pain implicated in failure of clinical trials. Nat Med. 2010;16(10):1053.

40. Bjorklund A, Skagerberg, G. Descending Monoaminergic Projections to the Spinal Cord. Amsterdam: Elsevier; 1982.
41. Bowker RM, Westlund KN, Sullivan MC, Wilber JF, Coulter JD. Descending serotonergic, peptidergic and cholinergic pathways from the raphe nuclei: a multiple transmitter complex. Brain Res. 1983;288(1-2):33-48.
42. Millan MJ. Descending control of pain. Prog Neurobiol. 2002;66(6):355-474.
43. Millan MJ. Endorphins and nociception: an overview. Methods Find Exp Clin Pharmacol. 1982;4(7):445-62.
44. Steinbusch HW. Distribution of serotonin-immunoreactivity in the central nervous system of the rat-cell bodies and terminals. Neuroscience. 1981;6(4):557-618.
45. Bowker RM, Abbott LC, Dilts RP. Peptidergic neurons in the nucleus raphe magnus and the nucleus gigantocellularis: their distributions, interrelationships, and projections to the spinal cord. Prog Brain Res. 1988;77:95-127.
46. Hokfelt T, Arvidsson U, Cullheim S, Millhorn D, Nicholas AP, Pieribone V, et al. Multiple messengers in descending serotonin neurons: localization and functional implications. J Chem Neuroanat. 2000;18(1-2):75-86.
47. Kwiat GC, Basbaum AI. The origin of brainstem noradrenergic and serotonergic projections to the spinal cord dorsal horn in the rat. Somatosens Mot Res. 1992;9(2):157-73.
48. Tuttle AH, Tohyama S, Ramsay T, Kimmelman J, Schweinhardt P, Bennett GJ, et al. Increasing placebo responses over time in U.S. clinical trials of neuropathic pain. Pain. 2015;156(12):2616-26.
49. Green GM, Scarth J, Dickenson A. An excitatory role for 5-HT in spinal inflammatory nociceptive transmission; state-dependent actions via dorsal horn 5-HT(3) receptors in the anaesthetized rat. Pain. 2000;89(1):81-8.
50. Svensson CI, Tran TK, Fitzsimmons B, Yaksh TL, Hua XY. Descending serotonergic facilitation of spinal ERK activation and pain behavior. FEBS Lett. 2006;580(28-29):6629-34.
51. Weil-Fugazza J, Godefroy F. Further evidence for the involvement of the diencephalo-dopaminergic system in pain modulation: a neurochemical study on the effect of morphine in the arthritic rat. Int J Tissue React. 1991;13(6):305-10.
52. Taguchi K, Suzuki Y. The response of the 5-hydroxyindole oxidation current to noxious stimuli in the spinal cord of anesthetized rats: modification by morphine. Brain Res. 1992;583(1-2):150-4.
53. Todd AJ. Anatomy of primary afferents and projection neurones in the rat spinal dorsal horn with particular emphasis on substance P and the neurokinin 1 receptor. Exp Physiol. 2002;87(2):245-9.
54. Tyce GM, Hammond, D.L., Rorie, D.K., and Yaksh, T.L. In vivo and in vitro efflux of conjugated amines into superfusates from discrete areas of central nervous system of cats and rats. London and Basingstoke: Macmillian Pub. Inc.,; 1981.
55. Ye JH, Ponnudurai R, Schaefer R. Ondansetron: a selective 5-HT(3) receptor antagonist and its applications in CNS-related disorders. CNS Drug Rev. 2001;7(2):199-213.
56. Zofran (ondansetron hydrochloride) Prescribing Information. Food and Drug Administration.
57. Pritchard JF. Ondansetron metabolism and pharmacokinetics. Semin Oncol. 1992;19(4 Suppl 10):9-15.
58. Gandhi M, Aweeka F, Greenblatt RM, Blaschke TF. Sex differences in pharmacokinetics and pharmacodynamics. Annu Rev Pharmacol Toxicol. 2004;44:499-523.
59. Roila F, Del Favero A. Ondansetron clinical pharmacokinetics. Clin Pharmacokinet. 1995;29(2):95-109.
60. Colthup PV, Felgate CC, Palmer JL, Scully NL. Determination of ondansetron in plasma and its pharmacokinetics in the young and elderly. J Pharm Sci. 1991;80(9):868-71.

61. VanDenBerg CM, Kazmi Y, Stewart J, Weidler DJ, Tenjarla SN, Ward ES, et al. Pharmacokinetics of three formulations of ondansetron hydrochloride in healthy volunteers: 24-mg oral tablet, rectal suppository, and i.v. infusion. Am J Health Syst Pharm. 2000;57(11):1046-50.
62. Hsyu PH, Pritchard JF, Bozigian HP, Lloyd TL, Griffin RH, Shamburek R, et al. Comparison of the pharmacokinetics of an ondansetron solution (8 mg) when administered intravenously, orally, to the colon, and to the rectum. Pharm Res. 1994;11(1):156-9.
63. Yang SH, Lee MG. Dose-independent pharmacokinetics of ondansetron in rats: contribution of hepatic and intestinal first-pass effects to low bioavailability. Biopharm Drug Dispos. 2008;29(7):414-26.
64. Probst RJ, Lim JM, Bird DN, Pole GL, Sato AK, Claybaugh JR. Gender differences in the blood volume of conscious Sprague-Dawley rats. J Am Assoc Lab Anim Sci. 2006;45(2):49-52.
65. Simpson KH, Murphy P, Colthup PV, Whelan P. Concentration of ondansetron in cerebrospinal fluid following oral dosing in volunteers. Psychopharmacology (Berl). 1992;109(4):497-8.
66. Nagaya Y, Nozaki Y, Kobayashi K, Takenaka O, Nakatani Y, Kusano K, et al. Utility of cerebrospinal fluid drug concentration as a surrogate for unbound brain concentration in nonhuman primates. Drug Metab Pharmacokinet. 2014;29(5):419-26.
67. Juliano RL, Ling V. A surface glycoprotein modulating drug permeability in Chinese hamster ovary cell mutants. Biochim Biophys Acta. 1976;455(1):152-62.
68. Gros P, Croop J, Housman D. Mammalian multidrug resistance gene: complete cDNA sequence indicates strong homology to bacterial transport proteins. Cell. 1986;47(3):371-80.
69. Chen CJ, Chin JE, Ueda K, Clark DP, Pastan I, Gottesman MM, et al. Internal duplication and homology with bacterial transport proteins in the mdr1 (P-glycoprotein) gene from multidrug-resistant human cells. Cell. 1986;47(3):381-9.
70. Endicott JA, Ling V. The biochemistry of P-glycoprotein-mediated multidrug resistance. Annu Rev Biochem. 1989;58:137-71.
71. Schinkel AH, Wagenaar E, Mol CA, van Deemter L. P-glycoprotein in the blood-brain barrier of mice influences the brain penetration and pharmacological activity of many drugs. J Clin Invest. 1996;97(11):2517-24.
72. Schinkel AH, Wagenaar E, van Deemter L, Mol CA, Borst P. Absence of the mdr1a P-Glycoprotein in mice affects tissue distribution and pharmacokinetics of dexamethasone, digoxin, and cyclosporin A. J Clin Invest. 1995;96(4):1698-705.
73. Schinkel AH, Smit JJ, van Tellingen O, Beijnen JH, Wagenaar E, van Deemter L, et al. Disruption of the mouse mdr1a P-glycoprotein gene leads to a deficiency in the blood-brain barrier and to increased sensitivity to drugs. Cell. 1994;77(4):491-502.
74. Yang SH, Yang KH, Lee MG. Gender differences in ondansetron pharmacokinetics in rats. Biopharm Drug Dispos. 2008;29(7):406-13.
75. Pritchard JF, Bryson JC, Kernodle AE, Benedetti TL, Powell JR. Age and gender effects on ondansetron pharmacokinetics: evaluation of healthy aged volunteers. Clin Pharmacol Ther. 1992;51(1):51-5.
76. Jann MW, ZumBrunnen TL, Tenjarla SN, Ward ES, Jr., Weidler DJ. Relative bioavailability of ondansetron 8-mg oral tablets versus two extemporaneous 16-mg suppositories: formulation and gender differences. Pharmacotherapy. 1998;18(2):288-94.
77. Badeaux J, Bonanno L, Au H. Effectiveness of ondansetron as an adjunct to lidocaine intravenous regional anesthesia on tourniquet pain and postoperative pain in patients undergoing elective hand surgery: a systematic review protocol. JBI Database System Rev Implement Rep. 2015;13(1):27-38.
78. Deegan R. Ondansetron: pharmacology of a specific 5HT3-receptor antagonist. Am J Med Sci. 1992;304(6):373-8.

79. Derbent A, Uyar M, Demirag K, Uyer M, Kurtoglu E, Goktay A. Can antiemetics really relieve pain? Adv Ther. 2005;22(4):307-12.
80. Arcioni R, della Rocca M, Romano S, Romano R, Pietropaoli P, Gasparetto A. Ondansetron inhibits the analgesic effects of tramadol: a possible 5-HT(3) spinal receptor involvement in acute pain in humans. Anesth Analg. 2002;94(6):1553-7, table of contents.
81. Ambesh SP, Dubey PK, Sinha PK. Ondansetron pretreatment to alleviate pain on propofol injection: a randomized, controlled, double-blinded study. Anesth Analg. 1999;89(1):197-9.
82. Reddy MS, Chen FG, Ng HP. Effect of ondansetron pretreatment on pain after rocuronium and propofol injection: a randomised, double-blind controlled comparison with lidocaine. Anaesthesia. 2001;56(9):902-5.
83. Ergene U, Pekdemir M, Canda E, Kirkali Z, Fowler J, Coskun F. Ondansetron versus diclofenac sodium in the treatment of acute ureteral colic: a double blind controlled trial. Int Urol Nephrol. 2001;33(2):315-9.
84. McCleane GJ, Suzuki R, Dickenson AH. Does a single intravenous injection of the 5HT3 receptor antagonist ondansetron have an analgesic effect in neuropathic pain? A double-blinded, placebo-controlled cross-over study. Anesth Analg. 2003;97(5):1474-8.
85. Tuveson B, Leffler AS, Hansson P. Ondansetron, a 5HT3-antagonist, does not alter dynamic mechanical allodynia or spontaneous ongoing pain in peripheral neuropathy. Clin J Pain. 2011;27(4):323-9.
86. Rivlin AS, Tator CH. Objective clinical assessment of motor function after experimental spinal cord injury in the rat. J Neurosurg. 1977;47(4):577-81.
87. Oatway MA, Chen Y, Weaver LC. The 5-HT3 receptor facilitates at-level mechanical allodynia following spinal cord injury. Pain. 2004;110(1-2):259-68.
88. Chen Y, Oatway MA, Weaver LC. Blockade of the 5-HT3 receptor for days causes sustained relief from mechanical allodynia following spinal cord injury. J Neurosci Res. 2009;87(2):418-24.
89. Tzvetkov MV, Saadatmand AR, Bokelmann K, Meineke I, Kaiser R, Brockmoller J. Effects of OCT1 polymorphisms on the cellular uptake, plasma concentrations and efficacy of the 5-HT(3) antagonists tropisetron and ondansetron. Pharmacogenomics J. 2012;12(1):22-9.
90. Li Q, Guo D, Dong Z, Zhang W, Zhang L, Huang SM, et al. Ondansetron can enhance cisplatin-induced nephrotoxicity via inhibition of multiple toxin and extrusion proteins (MATEs). Toxicol Appl Pharmacol. 2013;273(1):100-9.
91. Saynor DA, Dixon CM. The metabolism of ondansetron. Eur J Cancer Clin Oncol. 1989;25 Suppl 1:S75-7.
92. Hewitt W. The Gross Anatomy of the Brain. Philadelphia: Lippincott; 1967.
93. Sakka L, Coll G, Chazal J. Anatomy and physiology of cerebrospinal fluid. Eur Ann Otorhinolaryngol Head Neck Dis. 2011;128(6):309-16.
94. J. Gordon Betts TJC, Eddie Johnson, Central Oregon Communinty College, James A. Wise, Hampton University, Kelly A. Young, California State University, Long Beach. Anatomy and Physiology (OpenStax)2019.
95. Minn A, Ghersi-Egea JF, Perrin R, Leininger B, Siest G. Drug metabolizing enzymes in the brain and cerebral microvessels. Brain Res Brain Res Rev. 1991;16(1):65-82.
96. Kalvass JC, Maurer TS. Influence of nonspecific brain and plasma binding on CNS exposure: implications for rational drug discovery. Biopharm Drug Dispos. 2002;23(8):327-38.
97. Hammarlund-Udenaes M. Active-site concentrations of chemicals - are they a better predictor of effect than plasma/organ/tissue concentrations? Basic Clin Pharmacol Toxicol. 2010;106(3):215-20.
98. de Lange EC. The mastermind approach to CNS drug therapy: translational prediction of human brain distribution, target site kinetics, and therapeutic effects. Fluids Barriers CNS. 2013;10(1):12.

99. Abbott NJ. Evidence for bulk flow of brain interstitial fluid: significance for physiology and pathology. Neurochem Int. 2004;45(4):545-52.
100. Cserr HF, Depasquale M, Patlak CS, Pullen RG. Convection of cerebral interstitial fluid and its role in brain volume regulation. Ann N Y Acad Sci. 1986;481:123-34.
101. Nogradi A VG. Anatomy and Physiology of the Spinal Cord. In: 2000-2013.
102. Le T. First Aid for the USMLE Step 1 2014. 24 ed: McGraw-Hill Professional Publishing; 2014.
103. Waxenbaum JA FB. Anatomy, Back, Lumbar Vertebrae. In. StatPearls Publishing; 2019.
104. Biliouris K, Gaitonde P, Yin W, Norris DA, Wang Y, Henry S, et al. A Semi-Mechanistic Population Pharmacokinetic Model of Nusinersen: An Antisense Oligonucleotide for the Treatment of Spinal Muscular Atrophy. CPT Pharmacometrics Syst Pharmacol. 2018;7(9):581-92.
105. Kuttler A, Dimke T, Kern S, Helmlinger G, Stanski D, Finelli LA. Understanding pharmacokinetics using realistic computational models of fluid dynamics: biosimulation of drug distribution within the CSF space for intrathecal drugs. J Pharmacokinet Pharmacodyn. 2010;37(6):629-44.
106. Abbott NJ, Patabendige AA, Dolman DE, Yusof SR, Begley DJ. Structure and function of the blood-brain barrier. Neurobiol Dis. 2010;37(1):13-25.
107. Liu X, Tu M, Kelly RS, Chen C, Smith BJ. Development of a computational approach to predict blood-brain barrier permeability. Drug Metab Dispos. 2004;32(1):132-9.
108. Levin VA. Relationship of octanol/water partition coefficient and molecular weight to rat brain capillary permeability. J Med Chem. 1980;23(6):682-4.
109. Greig NH, Momma S, Sweeney DJ, Smith QR, Rapoport SI. Facilitated transport of melphalan at the rat blood-brain barrier by the large neutral amino acid carrier system. Cancer Res. 1987;47(6):1571-6.
110. Tsuji A, Tamai II. Carrier-mediated or specialized transport of drugs across the blood-brain barrier. Adv Drug Deliv Rev. 1999;36(2-3):277-90.
111. de Lange EC. The physiological characteristics and transcytosis mechanisms of the blood-brain barrier (BBB). Curr Pharm Biotechnol. 2012;13(12):2319-27.
112. Zhang EY, Knipp GT, Ekins S, Swaan PW. Structural biology and function of solute transporters: implications for identifying and designing substrates. Drug Metab Rev. 2002;34(4):709-50.
113. Guillot FL, Audus KL, Raub TJ. Fluid-phase endocytosis by primary cultures of bovine brain microvessel endothelial cell monolayers. Microvasc Res. 1990;39(1):1-14.
114. Gonatas J, Stieber A, Olsnes S, Gonatas NK. Pathways involved in fluid phase and adsorptive endocytosis in neuroblastoma. J Cell Biol. 1980;87(3 Pt 1):579-88.
115. Broadwell RD. Transcytosis of macromolecules through the blood-brain barrier: a cell biological perspective and critical appraisal. Acta Neuropathol. 1989;79(2):117-28.
116. Claudio L, Kress Y, Norton WT, Brosnan CF. Increased vesicular transport and decreased mitochondrial content in blood-brain barrier endothelial cells during experimental autoimmune encephalomyelitis. Am J Pathol. 1989;135(6):1157-68.
117. Schinkel AH. P-Glycoprotein, a gatekeeper in the blood-brain barrier. Adv Drug Deliv Rev. 1999;36(2-3):179-94.
118. Shen DD, Artru AA, Adkison KK. Principles and applicability of CSF sampling for the assessment of CNS drug delivery and pharmacodynamics. Adv Drug Deliv Rev. 2004;56(12):1825-57.
119. Nagaya Y, Nozaki Y, Takenaka O, Watari R, Kusano K, Yoshimura T, et al. Investigation of utility of cerebrospinal fluid drug concentration as a surrogate for interstitial fluid concentration using microdialysis coupled with cisternal cerebrospinal fluid sampling in wild-type and Mdr1a(-/-) rats. Drug Metab Pharmacokinet. 2016;31(1):57-66.

120. Westerhout J. Prediction of brain target site concentrations on the basis of CSF PK: Ipskamp Drukkers, Enschede; 2014.
121. Yamamoto Y, Valitalo PA, van den Berg DJ, Hartman R, van den Brink W, Wong YC, et al. A Generic Multi-Compartmental CNS Distribution Model Structure for 9 Drugs Allows Prediction of Human Brain Target Site Concentrations. Pharm Res. 2017;34(2):333-51.
122. Cserr H. Potassium exchange between cerebrospinal fluid, plasma, and brain. Am J Physiol. 1965;209(6):1219-26.
123. Bass NH, Lundborg P. Postnatal development of mechanisms for the elimination of organic acids from the brain and cerebrospinal fluid system of the rat: rapid efflux of (3 H)para-aminohippuric acid following intrathecal infusion. Brain Res. 1973;56:285-98.
124. Nilsson C, Stahlberg F, Thomsen C, Henriksen O, Herning M, Owman C. Circadian variation in human cerebrospinal fluid production measured by magnetic resonance imaging. Am J Physiol. 1992;262(1 Pt 2):R20-4.
125. Cserr HF, Cooper DN, Suri PK, Patlak CS. Efflux of radiolabeled polyethylene glycols and albumin from rat brain. Am J Physiol. 1981;240(4):F319-28.
126. Kimelberg HK. Water homeostasis in the brain: basic concepts. Neuroscience. 2004;129(4):851-60.
127. DJ B. Transport to the brain. In: D.J. Begley MWBaJK, editor. The blood-brain barrier and drug delivery to the CNS. New York: Dekker; 2000. p. 93-108.
128. Syvanen S, Lindhe O, Palner M, Kornum BR, Rahman O, Langstrom B, et al. Species differences in blood-brain barrier transport of three positron emission tomography radioligands with emphasis on P-glycoprotein transport. Drug Metab Dispos. 2009;37(3):635-43.
129. Yasuno F, Zoghbi SS, McCarron JA, Hong J, Ichise M, Brown AK, et al. Quantification of serotonin 5-HT1A receptors in monkey brain with [11C](R)-(-)-RWAY. Synapse. 2006;60(7):510-20.
130. Zhang XY, Yasuno F, Zoghbi SS, Liow JS, Hong J, McCarron JA, et al. Quantification of serotonin 5-HT1A receptors in humans with [11C](R)-(-)-RWAY: radiometabolite(s) likely confound brain measurements. Synapse. 2007;61(7):469-77.
131. Liow JS, Lu S, McCarron JA, Hong J, Musachio JL, Pike VW, et al. Effect of a P-glycoprotein inhibitor, Cyclosporin A, on the disposition in rodent brain and blood of the 5-HT1A receptor radioligand, [11C](R)-(-)-RWAY. Synapse. 2007;61(2):96-105.
132. Cutler L, Howes C, Deeks NJ, Buck TL, Jeffrey P. Development of a P-glycoprotein knockout model in rodents to define species differences in its functional effect at the blood-brain barrier. J Pharm Sci. 2006;95(9):1944-53.
133. Hsiao P, Sasongko L, Link JM, Mankoff DA, Muzi M, Collier AC, et al. Verapamil P-glycoprotein transport across the rat blood-brain barrier: cyclosporine, a concentration inhibition analysis, and comparison with human data. J Pharmacol Exp Ther. 2006;317(2):704-10.
134. Ball K, Bouzom F, Scherrmann JM, Walther B, Decleves X. Development of a physiologically based pharmacokinetic model for the rat central nervous system and determination of an in vitro-in vivo scaling methodology for the blood-brain barrier permeability of two transporter substrates, morphine and oxycodone. J Pharm Sci. 2012;101(11):4277-92.
135. Yamamoto Y, Danhof M, de Lange ECM. Microdialysis: the Key to Physiologically Based Model Prediction of Human CNS Target Site Concentrations. AAPS J. 2017;19(4):891-909.
136. Vertebral Column. Available from: https://www.britannica.com/science/vertebral-column.
137. Cyprotex. In vitro permeability and transporters. Available from: https://www.cyprotex.com/admepk/in-vitro-permeability.
138. Ederoth P, Tunblad K, Bouw R, Lundberg CJ, Ungerstedt U, Nordstrom CH, et al. Blood-brain barrier transport of morphine in patients with severe brain trauma. Br J Clin Pharmacol. 2004;57(4):427-35.

139. Bouw R, Ederoth P, Lundberg J, Ungerstedt U, Nordstrom CH, Hammarlund-Udenaes M. Increased blood-brain barrier permeability of morphine in a patient with severe brain lesions as determined by microdialysis. Acta Anaesthesiol Scand. 2001;45(3):390-2.
140. Gaohua L, Neuhoff S, Johnson TN, Rostami-Hodjegan A, Jamei M. Development of a permeability-limited model of the human brain and cerebrospinal fluid (CSF) to integrate known physiological and biological knowledge: Estimating time varying CSF drug concentrations and their variability using in vitro data. Drug Metab Pharmacokinet. 2016;31(3):224-33.
141. De Lange ECM, Vd Berg DJ, Bellanti F, Voskuyl RA, Syvanen S. P-glycoprotein protein expression versus functionality at the blood-brain barrier using immunohistochemistry, microdialysis and mathematical modeling. Eur J Pharm Sci. 2018;124:61-70.
142. Wang XX, Li YB, Feng MR, Smith DE. Semi-Mechanistic Population Pharmacokinetic Modeling of L-Histidine Disposition and Brain Uptake in Wildtype and Pht1 Null Mice. Pharm Res. 2018;35(1):19.
143. Cao Y, Jusko WJ. Applications of minimal physiologically-based pharmacokinetic models. J Pharmacokinet Pharmacodyn. 2012;39(6):711-23.
144. Boxenbaum H. Interspecies scaling, allometry, physiological time, and the ground plan of pharmacokinetics. J Pharmacokinet Biopharm. 1982;10(2):201-27.
145. Boxenbaum H, Fertig JB. Scaling of antipyrine intrinsic clearance of unbound drug in 15 mammalian species. Eur J Drug Metab Pharmacokinet. 1984;9(2):177-83.
146. Mahmood I, Balian JD. Interspecies scaling: predicting pharmacokinetic parameters of antiepileptic drugs in humans from animals with special emphasis on clearance. J Pharm Sci. 1996;85(4):411-4.
147. Lave T, Dupin S, Schmitt C, Chou RC, Jaeck D, Coassolo P. Integration of in vitro data into allometric scaling to predict hepatic metabolic clearance in man: application to 10 extensively metabolized drugs. J Pharm Sci. 1997;86(5):584-90.
148. Zilliox LA. Neuropathic Pain. Continuum (Minneap Minn). 2017;23(2, Selected Topics in Outpatient Neurology):512-32.
149. Finnerup NB, Attal N. Pharmacotherapy of neuropathic pain: time to rewrite the rulebook? Pain Manag. 2016;6(1):1-3.
150. Kulsoom Farhat MI, Shabana Ali, Anwar Kamal Pasha. Resistance to ondansetron: Role of pharmacogenetics in post-operative nausea and vomiting. Egyptian Journal of Medical Human GEnetics. 2013;14(4):331-6.
151. Perez EA. Review of the preclinical pharmacology and comparative efficacy of 5-hydroxytryptamine-3 receptor antagonists for chemotherapy-induced emesis. J Clin Oncol. 1995;13(4):1036-43.
152. Janelsins MC, Tejani MA, Kamen C, Peoples AR, Mustian KM, Morrow GR. Current pharmacotherapy for chemotherapy-induced nausea and vomiting in cancer patients. Expert Opin Pharmacother. 2013;14(6):757-66.
153. Chatterjee S, Rudra A, Sengupta S. Current concepts in the management of postoperative nausea and vomiting. Anesthesiol Res Pract. 2011;2011:748031.
154. MacDougall MR, Sharma S. Physiology, Chemoreceptor Trigger Zone. StatPearls. Treasure Island (FL)2019.
155. Lexicomp. Ondansetron - Pharmacology & Pharmacokinetics. Available from: https://online.lexi.com/lco/action/doc/retrieve/docid/patch_f/7399?cesid=1SZaHK51VNz&searchUrl=%2Flco%2Faction%2Fsearch%3Fq%3Dondansetron%26t%3Dname%26va%3Dondansetron#pha.
156. Chong YE, Chiang M, Deshpande K, Haroutounian S, Kagan L, Lee JB. Simultaneous quantification of ondansetron and tariquidar in rat and human plasma using a high performance liquid chromatography-ultraviolet method. Biomed Chromatogr. 2019:e4653.

157. Depot M, Leroux S, Caille G. High-resolution liquid chromatographic method using ultraviolet detection for determination of ondansetron in human plasma. J Chromatogr B Biomed Sci Appl. 1997;693(2):399-406.
158. NextAdvance. Brain - Bullet Blender Homogenization Protocol. Available from: https://www.nextadvance.us/scripts/public/bullet-blender/protocols/protocol_display/protocol.php?samplename=Brain&sample_id=10&protocol_id=15.
159. Hammarlund-Udenaes M, Friden M, Syvanen S, Gupta A. On the rate and extent of drug delivery to the brain. Pharm Res. 2008;25(8):1737-50.
160. Kawakami J, Yamamoto K, Sawada Y, Iga T. Prediction of brain delivery of ofloxacin, a new quinolone, in the human from animal data. J Pharmacokinet Biopharm. 1994;22(3):207-27.
161. Jablonski MR, Jacob DA, Campos C, Miller DS, Maragakis NJ, Pasinelli P, et al. Selective increase of two ABC drug efflux transporters at the blood-spinal cord barrier suggests induced pharmacoresistance in ALS. Neurobiol Dis. 2012;47(2):194-200.
162. Dulin JN, Moore ML, Grill RJ. The dual cyclooxygenase/5-lipoxygenase inhibitor licofelone attenuates p-glycoprotein-mediated drug resistance in the injured spinal cord. J Neurotrauma. 2013;30(3):211-26.
163. Harrold J. Available from: https://ubiquity.tools.
164. Hamidovic A, Hahn K, Kolesar J. Clinical significance of ABCB1 genotyping in oncology. J Oncol Pharm Pract. 2010;16(1):39-44.
165. Huang L, Li X, Roberts J, Janosky B, Lin MH. Differential role of P-glycoprotein and breast cancer resistance protein in drug distribution into brain, CSF and peripheral nerve tissues in rats. Xenobiotica. 2015;45(6):547-55.
166. Zamek-Gliszczynski MJ, Bedwell DW, Bao JQ, Higgins JW. Characterization of SAGE Mdr1a (P-gp), Bcrp, and Mrp2 knockout rats using loperamide, paclitaxel, sulfasalazine, and carboxydichlorofluorescein pharmacokinetics. Drug Metab Dispos. 2012;40(9):1825-33.
167. Bundgaard C, Jensen CJ, Garmer M. Species comparison of in vivo P-glycoprotein-mediated brain efflux using mdr1a-deficient rats and mice. Drug Metab Dispos. 2012;40(3):461-6.
168. Syvanen S, Hooker A, Rahman O, Wilking H, Blomquist G, Langstrom B, et al. Pharmacokinetics of P-glycoprotein inhibition in the rat blood-brain barrier. J Pharm Sci. 2008;97(12):5386-400.
169. Westerhout J, Ploeger B, Smeets J, Danhof M, de Lange EC. Physiologically based pharmacokinetic modeling to investigate regional brain distribution kinetics in rats. AAPS J. 2012;14(3):543-53.
170. Manting D. Chiang KF, Chris Lee, Evan D. Kharasch, Dani Tallchief, Christopher Sawyer, Jane Blood, Leonid Kagan, and Simon Haroutounian. Plasma and cerebrospinal fluid pharmacokinetics of ondansetron in humans. Under revision.
171. Geldof M, Freijer J, van Beijsterveldt L, Danhof M. Pharmacokinetic modeling of non-linear brain distribution of fluvoxamine in the rat. Pharm Res. 2008;25(4):792-804.
172. Tamaki A, Ierano C, Szakacs G, Robey RW, Bates SE. The controversial role of ABC transporters in clinical oncology. Essays Biochem. 2011;50(1):209-32.
173. Shaffer BC, Gillet JP, Patel C, Baer MR, Bates SE, Gottesman MM. Drug resistance: still a daunting challenge to the successful treatment of AML. Drug Resist Updat. 2012;15(1-2):62-9.
174. Weidner LD, Fung KL, Kannan P, Moen JK, Kumar JS, Mulder J, et al. Tariquidar Is an Inhibitor and Not a Substrate of Human and Mouse P-glycoprotein. Drug Metab Dispos. 2016;44(2):275-82.
175. Loo TW, Clarke DM. Tariquidar inhibits P-glycoprotein drug efflux but activates ATPase activity by blocking transition to an open conformation. Biochem Pharmacol. 2014;92(4):558-66.

176. Martin C, Berridge G, Mistry P, Higgins C, Charlton P, Callaghan R. The molecular interaction of the high affinity reversal agent XR9576 with P-glycoprotein. Br J Pharmacol. 1999;128(2):403-11.
177. Kuntner C, Bankstahl JP, Bankstahl M, Stanek J, Wanek T, Stundner G, et al. Dose-response assessment of tariquidar and elacridar and regional quantification of P-glycoprotein inhibition at the rat blood-brain barrier using (R)-[(11)C]verapamil PET. Eur J Nucl Med Mol Imaging. 2010;37(5):942-53.
178. Chong YE, Chiang M, Deshpande K, Haroutounian S, Kagan L, Lee JB. Simultaneous quantification of ondansetron and tariquidar in rat and human plasma using a high performance liquid chromatography-ultraviolet method. Biomed Chromatogr. 2019;33(11):e4653.
179. Zimmermann ES, de Miranda Silva C, Neris C, Torres B, Schmidt S, Dalla Costa T. Population pharmacokinetic modeling to establish the role of P-glycoprotein on ciprofloxacin distribution to lung and prostate following intravenous and intratracheal administration to Wistar rats. Eur J Pharm Sci. 2019;127:319-29.
180. Gardner ER, Smith NF, Figg WD, Sparreboom A. Influence of the dual ABCB1 and ABCG2 inhibitor tariquidar on the disposition of oral imatinib in mice. J Exp Clin Cancer Res. 2009;28:99.
181. Kong LL, Shen GL, Wang ZY, Zhuang XM, Xiao WB, Yuan M, et al. Inhibition of P-Glycoprotein and Multidrug Resistance-Associated Protein 2 Regulates the Hepatobiliary Excretion and Plasma Exposure of Thienorphine and Its Glucuronide Conjugate. Front Pharmacol. 2016;7:242.
182. Zimmermann ES, Laureano JV, Dos Santos CN, Schmidt S, Lagishetty CV, de Castro WV, et al. Simultaneous Semimechanistic Population Analyses of Levofloxacin in Plasma, Lung, and Prostate To Describe the Influence of Efflux Transporters on Drug Distribution following Intravenous and Intratracheal Administration. Antimicrob Agents Chemother. 2016;60(2):946-54.
183. Montesinos RN, Moulari B, Gromand J, Beduneau A, Lamprecht A, Pellequer Y. Coadministration of P-glycoprotein modulators on loperamide pharmacokinetics and brain distribution. Drug Metab Dispos. 2014;42(4):700-6.
184. Englund G, Lundquist P, Skogastierna C, Johansson J, Hoogstraate J, Afzelius L, et al. Cytochrome p450 inhibitory properties of common efflux transporter inhibitors. Drug Metab Dispos. 2014;42(3):441-7.
185. Torrance N, Ferguson JA, Afolabi E, Bennett MI, Serpell MG, Dunn KM, et al. Neuropathic pain in the community: more under-treated than refractory? Pain. 2013;154(5):690-9.
186. Chitour D, Dickenson AH, Le Bars D. Pharmacological evidence for the involvement of serotonergic mechanisms in diffuse noxious inhibitory controls (DNIC). Brain research. 1982;236(2):329-37.
187. Bardin L. The complex role of serotonin and 5-HT receptors in chronic pain. Behav Pharmacol. 2011;22(5-6):390-404.
188. Bannister K, Patel R, Goncalves L, Townson L, Dickenson AH. Diffuse noxious inhibitory controls and nerve injury: restoring an imbalance between descending monoamine inhibitions and facilitations. Pain. 2015;156(9):1803-11.
189. Kimura M, Obata H, Saito S. Peripheral nerve injury reduces analgesic effects of systemic morphine via spinal 5-hydroxytryptamine 3 receptors. Anesthesiology. 2014;121(2):362-71.
190. Dogrul A, Ossipov MH, Porreca F. Differential mediation of descending pain facilitation and inhibition by spinal 5HT-3 and 5HT-7 receptors. Brain research. 2009;1280:52-9.
191. Suzuki R, Rahman W, Rygh LJ, Webber M, Hunt SP, Dickenson AH. Spinal-supraspinal serotonergic circuits regulating neuropathic pain and its treatment with gabapentin. Pain. 2005;117(3):292-303.

192. Marchi N, Guiso G, Caccia S, Rizzi M, Gagliardi B, Noe F, et al. Determinants of drug brain uptake in a rat model of seizure-associated malformations of cortical development. Neurobiology of disease. 2006;24(3):429-42.
193. Choi EM, Lee MG, Lee SH, Choi KW, Choi SH. Association of ABCB1 polymorphisms with the efficacy of ondansetron for postoperative nausea and vomiting. Anaesthesia. 2010;65(10):996-1000.
194. Collins JM, Dedrick RL. Distributed model for drug delivery to CSF and brain tissue. Am J Physiol. 1983;245(3):R303-10.
195. Yang SH, Lee MG. Dose-independent pharmacokinetics of clindamycin after intravenous and oral administration to rats: contribution of gastric first-pass effect to low bioavailability. Int J Pharm. 2007;332(1-2):17-23.
196. Tzvetkov MV, Vormfelde SV, Balen D, Meineke I, Schmidt T, Sehrt D, et al. The effects of genetic polymorphisms in the organic cation transporters OCT1, OCT2, and OCT3 on the renal clearance of metformin. Clinical pharmacology and therapeutics. 2009;86(3):299-306.
197. Thompson AJ, Lummis SC. 5-HT3 receptors. Curr Pharm Des. 2006;12(28):3615-30.
198. Patel R, Dickenson AH. Modality selective roles of pro-nociceptive spinal 5-HT2A and 5-HT3 receptors in normal and neuropathic states. Neuropharmacology. 2018;143:29-37.
199. de Lange EC. Utility of CSF in translational neuroscience. J Pharmacokinet Pharmacodyn. 2013;40(3):315-26.
200. Westerhout J, Danhof M, De Lange EC. Preclinical prediction of human brain target site concentrations: considerations in extrapolating to the clinical setting. J Pharm Sci. 2011;100(9):3577-93.
201. Brown RP, Delp MD, Lindstedt SL, Rhomberg LR, Beliles RP. Physiological parameter values for physiologically based pharmacokinetic models. Toxicol Ind Health. 1997;13(4):407-84.
202. Davies B, Morris T. Physiological parameters in laboratory animals and humans. Pharm Res. 1993;10(7):1093-5.
203. Quimby JM, Lake RC, Hansen RJ, Lunghofer PJ, Gustafson DL. Oral, subcutaneous, and intravenous pharmacokinetics of ondansetron in healthy cats. J Vet Pharmacol Ther. 2014;37(4):348-53.
204. Blake JC, Palmer JL, Minton NA, Burroughs AK. The pharmacokinetics of intravenous ondansetron in patients with hepatic impairment. Br J Clin Pharmacol. 1993;35(4):441-3.
205. Rodgers T, Leahy D, Rowland M. Physiologically based pharmacokinetic modeling 1: predicting the tissue distribution of moderate-to-strong bases. J Pharm Sci. 2005;94(6):1259-76.
206. Rodgers T, Rowland M. Physiologically based pharmacokinetic modelling 2: predicting the tissue distribution of acids, very weak bases, neutrals and zwitterions. J Pharm Sci. 2006;95(6):1238-57.
207. Li J, Wu J, Bao X, Honea N, Xie Y, Kim S, et al. Quantitative and Mechanistic Understanding of AZD1775 Penetration across Human Blood-Brain Barrier in Glioblastoma Patients Using an IVIVE-PBPK Modeling Approach. Clin Cancer Res. 2017;23(24):7454-66.
208. Hakkarainen JJ, Jalkanen AJ, Kaariainen TM, Keski-Rahkonen P, Venalainen T, Hokkanen J, et al. Comparison of in vitro cell models in predicting in vivo brain entry of drugs. Int J Pharm. 2010;402(1-2):27-36.
209. Scientists S. Personal correspondence - CNS Parameterizations. 2018.
210. Worboys PD, Brennan B, Bradbury A, Houston JB. Metabolite kinetics of ondansetron in rat. Comparison of hepatic microsomes, isolated hepatocytes and liver slices, with in vivo disposition. Xenobiotica. 1996;26(9):897-907.
211. O'Brien FE, Dinan TG, Griffin BT, Cryan JF. Interactions between antidepressants and P-glycoprotein at the blood-brain barrier: clinical significance of in vitro and in vivo findings. Br J Pharmacol. 2012;165(2):289-312.

212. Fromm MF. P-glycoprotein: a defense mechanism limiting oral bioavailability and CNS accumulation of drugs. Int J Clin Pharmacol Ther. 2000;38(2):69-74.
213. Leslie EM, Deeley RG, Cole SP. Multidrug resistance proteins: role of P-glycoprotein, MRP1, MRP2, and BCRP (ABCG2) in tissue defense. Toxicol Appl Pharmacol. 2005;204(3):216-37.
214. Thanki K, Gangwal RP, Sangamwar AT, Jain S. Oral delivery of anticancer drugs: challenges and opportunities. Journal of controlled release : official journal of the Controlled Release Society. 2013;170(1):15-40.
215. Thomas H, Coley HM. Overcoming multidrug resistance in cancer: an update on the clinical strategy of inhibiting p-glycoprotein. Cancer Control. 2003;10(2):159-65.
216. Breedveld P, Beijnen JH, Schellens JH. Use of P-glycoprotein and BCRP inhibitors to improve oral bioavailability and CNS penetration of anticancer drugs. Trends Pharmacol Sci. 2006;27(1):17-24.
217. Fox E, Bates SE. Tariquidar (XR9576): a P-glycoprotein drug efflux pump inhibitor. Expert Rev Anticancer Ther. 2007;7(4):447-59.
218. Bankstahl JP, Kuntner C, Abrahim A, Karch R, Stanek J, Wanek T, et al. Tariquidar-induced P-glycoprotein inhibition at the rat blood-brain barrier studied with (R)-11C-verapamil and PET. J Nucl Med. 2008;49(8):1328-35.
219. Meerhoff GF, Vester SM, Hesseling P, Klaassen SD, Cornelissen AS, Lucassen PJ, et al. Potentiation of antiseizure and neuroprotective efficacy of standard nerve agent treatment by addition of tariquidar. Neurotoxicology. 2018;68:167-76.
220. Amin ML. P-glycoprotein Inhibition for Optimal Drug Delivery. Drug Target Insights. 2013;7:27-34.
221. Kohler SC, Wiese M. HM30181 Derivatives as Novel Potent and Selective Inhibitors of the Breast Cancer Resistance Protein (BCRP/ABCG2). J Med Chem. 2015;58(9):3910-21.
222. Christofaki M, Papaioannou A. Ondansetron: a review of pharmacokinetics and clinical experience in postoperative nausea and vomiting. Expert Opin Drug Metab Toxicol. 2014;10(3):437-44.
223. Dotsikas Y, Kousoulos C, Tsatsou G, Loukas YL. Development and validation of a rapid 96-well format based liquid-liquid extraction and liquid chromatography-tandem mass spectrometry analysis method for ondansetron in human plasma. J Chromatogr B Analyt Technol Biomed Life Sci. 2006;836(1-2):79-82.
224. Moreira RF, Salvadori MC, Azevedo CP, Oliveira-Silva D, Borges DC, Moreno RA, et al. Development and validation of a rapid and sensitive LC-ESI-MS/MS method for ondansetron quantification in human plasma and its application in comparative bioavailability study. Biomed Chromatogr. 2010;24(11):1220-7.
225. Bauer S, Stormer E, Kaiser R, Tremblay PB, Brockmoller J, Roots I. Simultaneous determination of ondansetron and tropisetron in human plasma using HPLC with UV detection. Biomed Chromatogr. 2002;16(3):187-90.
226. Alvarez JC, Charbit B, Grassin-Delyle S, Demolis JL, Funck-Brentano C, Abe E. Human plasma quantification of droperidol and ondansetron used in preventing postoperative nausea and vomiting with a LC/ESI/MS/MS method. J Chromatogr B Analyt Technol Biomed Life Sci. 2011;879(2):186-90.
227. Bauer M, Zeitlinger M, Todorut D, Bohmdorfer M, Muller M, Langer O, et al. Pharmacokinetics of single ascending doses of the P-glycoprotein inhibitor tariquidar in healthy subjects. Pharmacology. 2013;91(1-2):12-9.
228. Wagner CC, Bauer M, Karch R, Feurstein T, Kopp S, Chiba P, et al. A pilot study to assess the efficacy of tariquidar to inhibit P-glycoprotein at the human blood-brain barrier with (R)-11C-verapamil and PET. Journal of nuclear medicine : official publication, Society of Nuclear Medicine. 2009;50(12):1954-61.

229. Matzneller P, Kussmann M, Eberl S, Maier-Salamon A, Jager W, Bauer M, et al. Pharmacokinetics of the P-gp Inhibitor Tariquidar in Rats After Intravenous, Oral, and Intraperitoneal Administration. European journal of drug metabolism and pharmacokinetics. 2018;43(5):599-606.
230. Administration USDoHaHSFaD. Bioanalytical Method Validation Guidance for Industry. 2018:41.
231. Kaza M, Karazniewicz-Lada M, Kosicka K, Siemiatkowska A, Rudzki PJ. Bioanalytical method validation: new FDA guidance vs. EMA guideline. Better or worse? J Pharm Biomed Anal. 2019;165:381-5.
232. Lee JB, Zgair A, Kim TH, Kim MG, Yoo SD, Fischer PM, et al. Simple and sensitive HPLC-UV method for determination of bexarotene in rat plasma. Journal of chromatography B, Analytical technologies in the biomedical and life sciences. 2017;1040:73-80.
233. M A. Aulton's Pharmaceutical. Churchill LIvingstone: Elsevier; 2007.
234. Liu F, Ranmal S, Batchelor HK, Orlu-Gul M, Ernest TB, Thomas IW, et al. Patient-centred pharmaceutical design to improve acceptability of medicines: similarities and differences in paediatric and geriatric populations. Drugs. 2014;74(16):1871-89.
235. Batchelor HK, Marriott JF. Formulations for children: problems and solutions. Br J Clin Pharmacol. 2015;79(3):405-18.
236. Schlatter AF, Deathe AR, Vreeman RC. The Need for Pediatric Formulations to Treat Children with HIV. AIDS Res Treat. 2016;2016:1654938.
237. E. Commission, Regulation (EC) No 1901/2006 of the European Parliament and of the Council of 12 December 2006 on medicinal products for paediatric use and amending Regulation (EEC) No 1768/92, Directive 2001/20/EC, Directive 2001/83/EC and Regulation (EC) No 726/2004 2006. https://ec.europa.eu/health//sites/health/files/files/eudralex/vol-1/reg_2006_1901/reg_2006_1901_en.pdf.
238. Concept paper on the need for a reflection paper on quality aspects of medicines for older people, 44 2013. https://www.ema.europa.eu/en/documents/scientific-guideline/concept-paper-need-reflection-paper-quality-aspects-medicines-older-people-first-version_en.pdf.
239. van Riet-Nales DA, Hussain N, Sundberg KA, Eggenschwyler D, Ferris C, Robert JL, et al. Regulatory incentives to ensure better medicines for older people: From ICH E7 to the EMA reflection paper on quality aspects. Int J Pharm. 2016;512(2):343-51.
240. Cram A, Breitkreutz J, Desset-Brethes S, Nunn T, Tuleu C, European Paediatric Formulation I. Challenges of developing palatable oral paediatric formulations. Int J Pharm. 2009;365(1-2):1-3.
241. Matsui D. Current issues in pediatric medication adherence. Paediatr Drugs. 2007;9(5):283-8.
242. Sohi H, Sultana Y, Khar RK. Taste masking technologies in oral pharmaceuticals: recent developments and approaches. Drug Dev Ind Pharm. 2004;30(5):429-48.
243. Mistry P, Batchelor H, project SP-U. Evidence of acceptability of oral paediatric medicines: a review. J Pharm Pharmacol. 2017;69(4):361-76.
244. Walsh J, Ranmal SR, Ernest TB, Liu F. Patient acceptability, safety and access: A balancing act for selecting age-appropriate oral dosage forms for paediatric and geriatric populations. Int J Pharm. 2018;536(2):547-62.
245. Anand V, Kataria M, Kukkar V, Saharan V, Choudhury PK. The latest trends in the taste assessment of pharmaceuticals. Drug Discov Today. 2007;12(5-6):257-65.
246. Gittings S, Turnbull N, Roberts CJ, Gershkovich P. Dissolution methodology for taste masked oral dosage forms. J Control Release. 2014;173:32-42.
247. Dressman JB, Reppas C. In vitro-in vivo correlations for lipophilic, poorly water-soluble drugs. Eur J Pharm Sci. 2000;11 Suppl 2:S73-80.

248. Kostewicz ES, Brauns U, Becker R, Dressman JB. Forecasting the oral absorption behavior of poorly soluble weak bases using solubility and dissolution studies in biorelevant media. Pharm Res. 2002;19(3):345-9.
249. Sunesen VH, Pedersen BL, Kristensen HG, Mullertz A. In vivo in vitro correlations for a poorly soluble drug, danazol, using the flow-through dissolution method with biorelevant dissolution media. Eur J Pharm Sci. 2005;24(4):305-13.
250. Vertzoni M, Dressman J, Butler J, Hempenstall J, Reppas C. Simulation of fasting gastric conditions and its importance for the in vivo dissolution of lipophilic compounds. Eur J Pharm Biopharm. 2005;60(3):413-7.
251. Okumu A, DiMaso M, Lobenberg R. Dynamic dissolution testing to establish in vitro/in vivo correlations for montelukast sodium, a poorly soluble drug. Pharm Res. 2008;25(12):2778-85.
252. Mohamed-Ahmed AH, Soto J, Ernest T, Tuleu C. Non-human tools for the evaluation of bitter taste in the design and development of medicines: a systematic review. Drug Discov Today. 2016;21(7):1170-80.
253. J. Soto AK, A. V Keating, A.H.A. Mohamed-ahmed, Y. Sheng, G. Winzenburg, R. Turner, S. Desset-brèthes, M. Orlu, C. Tuleu. Assessing the bitter taste of medicines: A comparison between rat taste panels (via the brief-access taste aversion (BATA) model) and human taste panels,. Int J Pharm. 2016;511:1127-8.
254. Soto J, Keeley A, Keating AV, Mohamed-Ahmed AHA, Sheng Y, Winzenburg G, et al. Rats can predict aversiveness of Active Pharmaceutical Ingredients. Eur J Pharm Biopharm. 2018;133:77-84.
255. Keeley A, Teo M, Ali Z, Frost J, Ghimire M, Rajabi-Siahboomi A, et al. In Vitro Dissolution Model Can Predict the in Vivo Taste Masking Performance of Coated Multiparticulates. Mol Pharm. 2019;16(5):2095-105.
256. Chiappetta DA, Hocht C, Sosnik A. A highly concentrated and taste-improved aqueous formulation of efavirenz for a more appropriate pediatric management of the anti-HIV therapy. Curr HIV Res. 2010;8(3):223-31.
257. Gittings S, Turnbull N, Henry B, Roberts CJ, Gershkovich P. Characterisation of human saliva as a platform for oral dissolution medium development. Eur J Pharm Biopharm. 2015;91:16-24.
258. Ali J, Zgair A, Hameed GS, Garnett MC, Roberts CJ, Burley JC, et al. Application of biorelevant saliva-based dissolution for optimisation of orally disintegrating formulations of felodipine. Int J Pharm. 2019;555:228-36.
259. Aiuchi H, Kitasako Y, Fukuda Y, Nakashima S, Burrow MF, Tagami J. Relationship between quantitative assessments of salivary buffering capacity and ion activity product for hydroxyapatite in relation to cariogenic potential. Aust Dent J. 2008;53(2):167-71.
260. Bardow A, Moe D, Nyvad B, Nauntofte B. The buffer capacity and buffer systems of human whole saliva measured without loss of CO2. Arch Oral Biol. 2000;45(1):1-12.
261. Christersson CE, Lindh L, Arnebrant T. Film-forming properties and viscosities of saliva substitutes and human whole saliva. Eur J Oral Sci. 2000;108(5):418-25.
262. H. Inoue KO, W. Masuda, T. Inagaki, M. Yokota, K. Inenaga. Rheological Properties of Human Saliva and Salivary Mucins. OJ Oral Biosci. 2008;50:134-41.
263. Omnell KA, Quarnstrom EE. A technique for intraoral cannulation and infusion of the rat submandibular gland. Dentomaxillofac Radiol. 1983;12(1):13-5.
264. Katsukawa H, Ninomiya Y. Capsaicin induces cystatin S-like substances in submandibular saliva of the rat. J Dent Res. 1999;78(10):1609-16.
265. Kopach O, Vats J, Netsyk O, Voitenko N, Irving A, Fedirko N. Cannabinoid receptors in submandibular acinar cells: functional coupling between saliva fluid and electrolytes secretion and Ca2+ signalling. J Cell Sci. 2012;125(Pt 8):1884-95.

266. Nezu A, Morita T, Tojyo Y, Nagai T, Tanimura A. Partial agonistic effects of pilocarpine on Ca(2+) responses and salivary secretion in the submandibular glands of live animals. Exp Physiol. 2015;100(6):640-51.
267. Ulmansky M, Sela J, Dishon T, Rosenmann E, Boss JH. A technique for the intubation of the parotid duct in rats. Arch Oral Biol. 1972;17(3):609-12.
268. Benarde MA, Fabian FW, Rosen S, Hoppert CA, Hunt HR. A method for the collection of large quantities of rat saliva. J Dent Res. 1956;35(2):326-7.
269. Kopittke L, Gomez R, Barros HM. Opposite effects of antidepressants on unstimulated and stimulated salivary flow. Arch Oral Biol. 2005;50(1):17-21.
270. Lagerlof F, Dawes C. The volume of saliva in the mouth before and after swallowing. J Dent Res. 1984;63(5):618-21.
271. Rudney JD, Ji Z, Larson CJ. The prediction of saliva swallowing frequency in humans from estimates of salivary flow rate and the volume of saliva swallowed. Arch Oral Biol. 1995;40(6):507-12.
272. Tatevossian A, Wright WG. The collection and analysis of resting rat saliva. Arch Oral Biol. 1974;19(9):825-7.
273. A. Tatevossian WW. The collection and analysis of resting rat saliva. Arch Oral Biol. 1974;19:825-7.
274. Finholt P, Solvang S. Dissolution kinetics of drugs in human gastric juice--the role of surface tension. J Pharm Sci. 1968;57(8):1322-6.
275. Efentakis M, Dressman JB. Gastric juice as a dissolution medium: surface tension and pH. Eur J Drug Metab Pharmacokinet. 1998;23(2):97-102.
276. Fathi Azarbayjani A, Jouyban A, Chan SY. Impact of surface tension in pharmaceutical sciences. J Pharm Pharm Sci. 2009;12(2):218-28.
277. Braun RJ, Parrott EL. Influence of viscosity and solubilization on dissolution rate. J Pharm Sci. 1972;61(2):175-8.
278. Banakar UV. Pharmaceutical Dissolution Testing. In: Group TF, editor.1991.
279. J.R. Stokes MWB, S.K. Baier. Current Opinion in Colloid & Interface Science Oral processing , texture and mouthfeel : From rheology to tribology and beyond. Curr Opin Colloid Interface Sci. 2013;18:349-59.
280. Serajuddin AT. Salt formation to improve drug solubility. Adv Drug Deliv Rev. 2007;59(7):603-16.
281. Pasha S, Inui T, Chapple I, Harris S, Holcombe L, Grant MM. The Saliva Proteome of Dogs: Variations Within and Between Breeds and Between Species. Proteomics. 2018;18(3-4).
282. Administration UFaD. Guidance for Industry: Bioanalytical Method Validation. 2001:4-10.